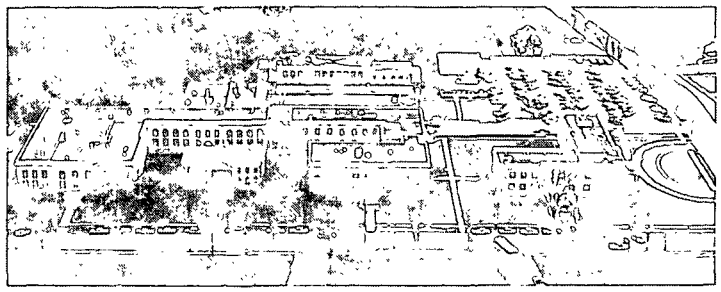

THE INSTITUTE OF PAPER CHEMISTRY, APPLETON, WISCONSIN

STATUS REPORTS

To The

PAPER PROPERTIES AND USES

PROJECT ADVISORY COMMITTEE

October 21-22, 1986
The Institute of Paper Chemistry
Continuing Education Center
Appleton, Wisconsin

NOTICE & DISCLAIMER

The Institute of Paper Chemistry (IPC) has provided a high standard of professional service and has exerted its best efforts within the time and funds available for this project. The information and conclusions are advisory and are intended only for the internal use by any company who may receive this report. Each company must decide for itself the best approach to solving any problems it may have and how, or whether, this reported information should be considered in its approach.

IPC does not recommend particular products, procedures, materials, or services. These are included only in the interest of completeness within a laboratory context and budgetary constraint. Actual products, procedures, materials, and services used may differ and are peculiar to the operations of each company.

In no event shall IPC or its employees and agents have any obligation or liability for damages, including, but not limited to, consequential damages, arising out of or in connection with any company's use of, or inability to use, the reported information. IPC provides no warranty or guaranty of results.

This information represents a review of on-going research for use by the Project Advisory Committees. The information is not intended to be a definitive progress report on any of the projects and should not be cited or referenced in any paper or correspondence external to your company.

Your advice and suggestions on any of the projects will be most welcome.

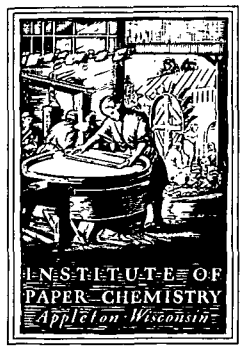

THE INSTITUTE OF PAPER CHEMISTRY
Post Office Box 1039
Appleton, Wisconsin 54912
Phone: 414/734-9251
Telex: 469289

October 3, 1986

TO: MEMBERS OF PAPER PROPERTIES AND USES PROJECT ADVISORY COMMITTEE

Attached for your review are the Status Reports for the Projects to be discussed at the Paper Properties and Uses PAC meeting scheduled for October 21-22, 1986, in Appleton. A meeting agenda can be found inside the booklet.

For those of you staying at the Continuing Education Center, the attached pink card gives the combination to the front door so that you can gain entrance if you arrive after the doors are locked. Room schedules are posted in the lobby. A room has been reserved for you for the nights of October 20 and 21. If you do not need accommodations for both nights, will be staying elsewhere, or not attending the meeting, please advise Sheila Burton at 414/738-3259.

We look forward to seeing you on October 21. Best regards.

Sincerely yours,

Gary

Gary A. Baum
Director
Paper Materials Division

GAB/sb
Enclosure

TABLE OF CONTENTS

	Page
AGENDA	ii
COMMITTEE ROSTER	iv
Project 3469 -- Strength Improvement and Failure Mechanisms	2
Project 3467 -- Process, Properties and Product Relationships	33
Project 3526 -- Internal Strength Enhancement	130
Project 3571 -- Board Properties and Performance	167
Project 3332 -- On-Line Measurement of Paper Mechanical Properties	207
Glossary	222

MEETING AGENDA

PAPER PROPERTIES AND USES
PROJECT ADVISORY COMMITTEE

October 21-22, 1986
The Institute of Paper Chemistry
Continuing Education Center
Appleton, WI

Tuesday -- October 21

8:30 a.m.	Welcome/Introductions	Van Liew/Baum
8:45	OVERVIEW OF PROJECTS	Baum
9:15	PROJECT REVIEWS	
	Strength Improvement and Failure Mechanisms	Waterhouse
	Student Presentation	Franke
10:15	COFFEE BREAK	
10:45	PROJECT REVIEWS	
	Process, Properties, Product Relationships	Baum/Habeger
12:00 noon	LUNCH (CEC Dining Room)	
1:00	TOUR OF PAPER MATERIALS DIVISION LABORATORIES	
2:15	PROJECT REVIEWS	
	Internal Strength Enhancement	Stratton/Hardacker
	Student Presentation	Berger, B. F.
3:00	COFFEE BREAK	
3:15	PROJECT REVIEWS	
	Board Properties and Performance	Whitsitt/Halcomb/ Dees
	On-Line Measurement of Paper Mechanical Properties	Habeger/Baum
5:15	SOCIAL TIME	
6:00	DINNER (CEC Dining Room)	
7:30	Committee Discussion: Graphics Arts Research	

Wednesday -- October 22

7:15 a.m.	BREAKFAST (CEC Dining Room)	
8:00	DISCUSSION OF PROJECTS (Krannert 108/109)	Committee
9:30	COFFEE BREAK	
10:00	DISCUSSION OF PROJECTS (continued)	
11:00	CLOSING COMMENTS	
	NEXT MEETING - March 25-26, 1987	
11:30	ADJOURNMENT/LUNCH (CEC Dining Room)	

PAPER PROPERTIES AND USES
PROJECT ADVISORY COMMITTEE

Dr. Gary Van Liew, Chairman -- 6/87*
Department Manager, Shipping
Container & Containerboard R&D
Weyerhaeuser Company
WTC 2h42
Tacoma, WA 98477
(206) 924-6464

Mr. James E. Beatty -- 6/89
Technical Director
Amricon Corporation
800 South Lawe
Appleton, WI 54915
(414) 733-3070

Dr. Robert L. Beran -- 6/89
Research Director
Westvaco Corporation
Covington Research Center
Covington, VA 24426
(703) 962-2111

Mr. Dennis Betz -- 6/89
Assistant Research Director
P. H. Glatfelter Co.
228 S. Main Street
Spring Grove, PA 17362
(717) 225-4711

Mr. Marvin D. Cooper -- 6/89
Resident Manager
Western Kraft Paper Group
Red River Mill
Willamette Industries, Inc.
P.O. Box 377
Campti, LA 71411
(318) 476-3392

Dr. John L. Firkins -- 6/88
Director of Product Development
Thilmany Pulp and Paper Company
P.O. Box 600
Kaukauna, WI 54130
(414) 766-4611

Mr. Richard P. Grant -- 6/89
Senior Engineer
Eastman Kodak Company
1669 Lake Avenue
Rochester, NY 14650
(716) 477-6537

Dr. Peter F. Lee -- 6/88
Director, Pulp and Paper Technology
Mead Corporation
Central Research
8th and Hickory St.
Chillicothe, OH 45601
(614) 772-3528

Dr. R. Heath Reeves -- 6/89
Sr. Research Associate
James River Corporation
Neenah Technical Center
1915 Marathon Avenue
Neenah, WI 54956
(414) 729-8148

Mr. Lowell Schleicher -- 6/89
Director of Basic Research
Appleton Papers Inc.
P.O. Box 359
Appleton, WI 54912
(414) 735-8857

Mr. Robert L. Smathers -- 6/89
Manager of Technical Services
MacMillan Bloedel Inc.
P.O. Box 336
Pine Hill, AL 36769
(205) 963-4391

Mr. David South -- 6/89
Technical Director
Chesapeake Corporation
P.O. Box 311
West Point, VA 23181
(804) 843-5252

Mr. Roger W. Youngs -- 6/89
Manager of Materials Science
Container Corporation of America
450 East North Avenue
Carol Stream, IL 60188
(312) 655-8825

Mr. Gary White -- 6/89
Supervisor, Materials Development
Owens-Illinois, Inc.
P.O. Box 1035
Toledo, OH 43666
(419) 247-5786

*Date of retirement from committee
9/86

THE INSTITUTE OF PAPER CHEMISTRY

Appleton, Wisconsin

Status Report

to the

PAPER PROPERTIES AND USES

PROJECT ADVISORY COMMITTEE

Project 3469

STRENGTH IMPROVEMENT AND FAILURE MECHANISMS

September 10, 1986

PROJECT SUMMARY

PROJECT NO. 3469: STRENGTH IMPROVEMENT AND FAILURE MECHANISMS

STAFF: J. Waterhouse, W. Whitsitt September 10, 1986

PROGRAM GOAL:

Identify critical parameters which describe converting and end-use performance and promote improvements in cost/performance ratios.

PROJECT OBJECTIVE:
Establish practical methods for enhancing strength properties (especially compressive strength) during paper manufacture and to evaluate deformation behavior as it relates to sheet composition and structure.

PROJECT RATIONALE, PREVIOUS ACTIVITY and PLANNED ACTIVITY FOR FISCAL 1986-87 are on the attached 1986-87 Project Form.

SUMMARY OF RESULTS LAST PERIOD: (October 1985 - March 1986)

(1) The compressive strengths of small pulped wood samples were measured and compared with compressive strengths measured on paper samples made from the separated wood fibers. The values for the handsheets (of the same nominal density as the wood specimens) were typically one-half the values obtained for the wood samples.

(2) Work has begun in characterizing small wood coupons, differing in lignin content, using non-destructive measurements. The purpose is to elucidate, if possible, the maximum strength and/or stiffness potential of pulped unseparated fibers.

(3) In student related work L. Charles has determined the effects of supercalendering on strength and other physical properties of uncoated Formette handsheets made with various levels of wet pressing and fiber orientation.

(4) In student related work T. Bither has started work on determining the factors responsible for differences in strength development which occur by refining and wet pressing.

(5) In student related work M. Kemps has started work on the measurement of internal stresses in paper and board using the layer removal technique.

SUMMARY OF RESULTS THIS PERIOD: (March 1986 - September 1986)

(1) In an attempt to determine the compressive strength potential of pulped unseparated fibers, wood coupons, 16 mm x 16 mm of white spruce have been ultrasonically characterized after 8 hrs and 12 hrs of acid chlorite treatment. Half of the wood coupons were given a mild caustic treatment to facilitate fiber separation and 19 mm diameter handsheets were made. Ultrasonic characterization and compressive strength measurements were also made on these handsheets.

(2) In student related work B. Allender has completed his research project "Morphological Factors in the Refining of Eucalypt and Pinus Radiata Fibers". A paper has been accepted for the PIRA, Paper and Board Division International Conference "Advances in Refining Technologies" Birmingham England, December 1986.

(3) In student related work Tom Bither's doctoral research is entitled, "Strength development through Internal Fibrillation and Wet Pressing" Tom has been evaluating a device for ensuring restrained drying after wet pressing. In addition the response of three different pulps to wet pressing and refining is being determined.

(4) In student related work M. Franke (formerly M. Kemps) master's research is entitled, "Z-direction variation of internal stress and paper properties". Marypat is evaluating the layer removal technique using commercial board and Formette handsheets to determine their Z-direction variation of residual stress and properties.

(5) A progress report is being prepared on our experience with the Formette Dynamique. Results for the effects of furnish, differences in jet-wire speed, consistency, basis weight, refining, wet pressing, drying, synthetic fibers and additives on fiber orientation and sheet anisotropy are included.

PROJECT TITLE: Strength Improvement and Failure Mechanisms

PROJECT STAFF: J. Waterhouse/W. Whitsitt

PRIMARY AREA OF INDUSTRY NEED: Properties related to end use

Date:	6/1/86
Budget:	$100,000
Period Ends:	6/30/87
Project No.:	3469

PROGRAM AREA: Improved converting processes and converted products

PROGRAM GOAL:

Identify critical parameters which describe converting and end-use performance and promote improvements in cost/performance ratios.

PROJECT OBJECTIVE:

Establish practical methods for enhancing strength properties (especially compressive strength) during paper manufacture and to evaluate deformation behavior as it relates to sheet composition and structure.

PROJECT RATIONALE:

Strength properties are important in predicting end use performance. An improved understanding of failure mechanisms and ways to improve certain strength properties are important to nearly all grades. The recognized importance of compressive strength in linerboard and corrugating medium and likely changes in shipping regulations provide impetus for research on compressive strength. Research to date suggests that there are ways to approach the objective through new papermaking strategies.

RESULTS TO DATE:

We have shown that compressive strength is highly related to a product of in-plane and out-of-plane elastic stiffnesses of paper. The relationship holds for commercial and experimental sheets made under a variety of conditions. This development suggests it will be possible to monitor compressive strength in the mill using ultrasonic techniques.

Compressive strength is enhanced by high densification, which increases bonding, and high fiber compressive stiffness. Our results on oriented sheets indicate that compressive strength increases with refining, and further increases can be obtained by wet pressing to increase density. Within a practical range, higher CD compressive strength can be achieved by decreased fiber orientation and/or increased CD restraint during drying. Where limitations to increased refining and wet pressing exist, low levels of polymer addition could be used as a viable means to improve compressive strength.

We have developed a torsion mode technique for measuring the out-of-plane shear stress-strain behavior, and studied ZD shear straining on compressive strength. Internal stress variations have been determined in the thickness direction together with the variation of in-plane and out-of-plane properties.

PLANNED ACTIVITY FOR THE PERIOD:

We will continue investigations of the compressive behavior of board as a function of composition, structure, and process variables. For the coming period this will include the effects of HW/SW furnish blends on compressive strength and a study of the compressive strength potential of pulped wood chips.

STUDENT RELATED RESEARCH:

T. Bither, Ph.D.-1988; L. Charles, M.S.-1986; M. Kemps, M.S.-1987.

Status Report

STRENGTH IMPROVEMENT AND FAILURE MECHANISMS

Project 3469

INTRODUCTION

In order to improve the strength of paper and board there is a need to assess the strength potential of the raw materials from which they are made and to determine how this potential is modified by papermaking and other process variables. In addition there is an underlying need to understand the causes of failure. By strength we not only refer to compressive strength, a major consideration in this project, but also for example, combined stress situations which paper experiences during converting and end use.

These needs form the basis of our investigations carried out during this period. The major effort has been directed towards determining the compressive strength potential of white spruce as outlined in section 1 below. Section 2 is concerned with student related work involving refining and the development of techniques for mini-handsheet making and characterization which were also utilized in the work outlined in Section 1. Sections 3 and 4 outline our activity and proposals for future work in the area of formation and combined stress measurements, respectively.

1. COMPRESSIVE STRENGTH IMPROVEMENT

In past work we have explored a number of pathways towards the goal of improving compressive strength and these include:

1. Raw Materials
    - furnish improvement by species selection
    - high yield pulps with chemical treatment
    - polymer addition

2. Papermaking Process Variables
   - formation and fiber orientation
   - wet pressing and drying restraint

Work is expected to continue in these and other areas as fresh opportunities present themselves. Currently we are trying to determine more precisely the compressive strength potential of certain species as a function of yield. We would also like to determine the losses incurred, if any, in the fiber separation process, and the appropriate measures which might be taken to reduce anticipated strength losses with increasing yield. A flow diagram for determining how the compressive strength potential of wood coupons is related to handsheet performance is shown in Fig. 1.

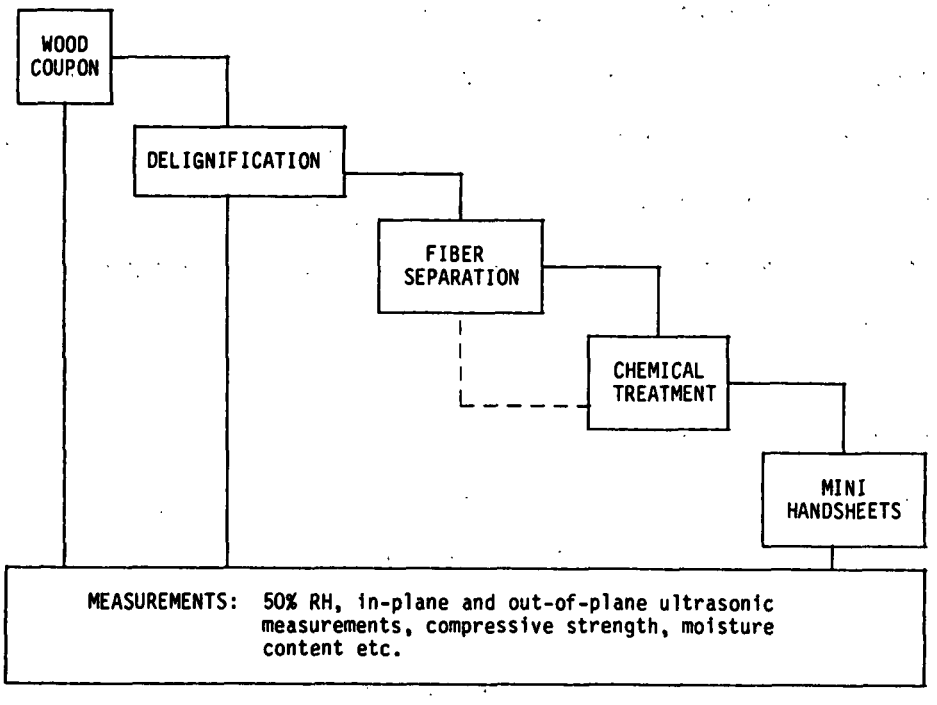

Figure 1. Flow diagram for determining strength potentials.

Based on the empirical/theoretical model developed for compressive strength by Habeger and Whitsitt[1], we now appreciate that compressive strength is strongly dependent on both in-plane and out-of-plane elastic constants. It is appropriate therefore that we should be able to measure these elastic constants on the raw material i.e., wood chip (coupon) and monitor the changes in them due to delignification, fiber separation, chemical treatment and handsheet preparation. With the development of instrumentation for measuring the out-of-plane properties of paper and board in both the longitudinal and shear mode, it is now possible in principle to use this equipment to measure the in-plane and out-of-plane elastic constants of small wood coupons (16 mm x 16 mm) and handsheets (19 mm dia).

For this study radial sections 3, 4, 5 and 8 of a 36-year-old white spruce log were selected see Fig. 2. A substantial data base on the performance of this log is available (Chemical Sciences Division). To determine the feasibility of this approach it was decided to use acid-chlorite delignification to determine the effects of lignin content on handsheet compressive strength performance. Preliminary experiments were made on wood coupon samples to determine the time required for achieving different levels of delignification in acid-chlorite solutions, the results are given in Table 1 below:

Table 1. Delignification trials.

Time	Yield*	Wood Section
1 hr	--	-
2 hr	98.0	5
4 hr	92.3	5
8 hr	82.1	3, 5, 8
12 hr	71.1	4

*Coupons were air dried to approximately 93-95% solids and then treated with acid-chlorite solution and then oven dried. Yield = oven dried weight/air dry weight.

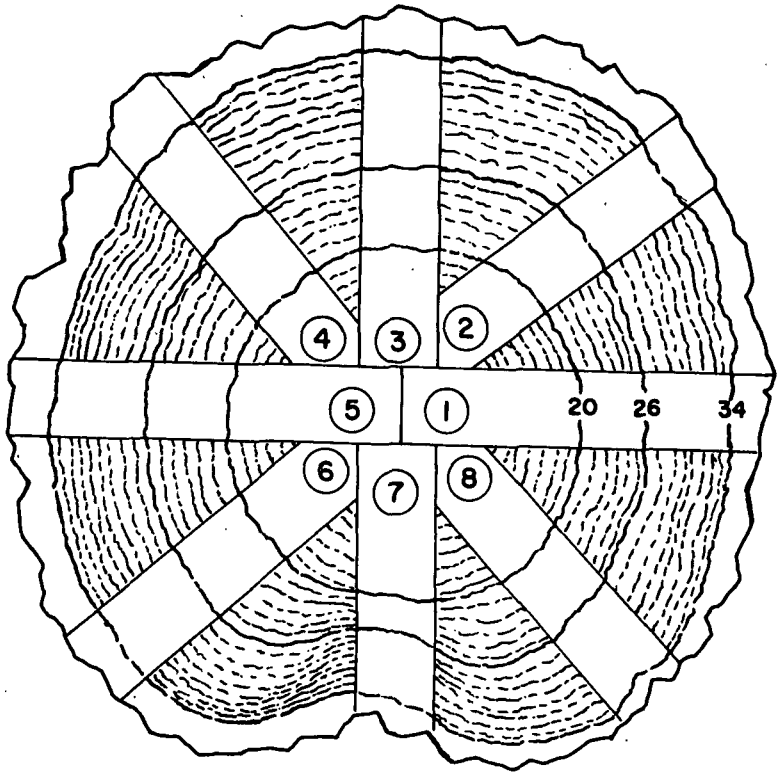

Figure 2. Location of wood coupon sections in white spruce.

On the basis of these results, a series of wood coupons were prepared and individually labeled. The density of the coupons with excess water removed was measured and ranged from 0.900 g/cm^3 to 1.050 g/cm^3, two groups were then subjected to acid chlorite delignification for 8 hrs and 12 hrs.

Following acid-chlorite treatment half of the wood coupons were washed and then placed between glass slides and clamped in order to minimize shrinkage, the remainder were used to make mini handsheets. A mild caustic treatment was required to produce fiber separation which was accomplished using a magnetic stirring unit. The separation occurred it is believed with minimal fiber damage although more careful observation of the fibers will be required to verify this.

The technique for making mini handsheets was developed by B. Allender which he also utilized in his project concerned with the effects of fiber morphology on the development of internal fibrillation (see later section in this report). The handsheets are formed from a dilute suspension of fibers onto a 200 mesh wire screen located in the end of a 19 mm ID centrifuge tube used to obtain water retention values. A number of mini handsheets so formed were wet pressed and dried between blotters using the IPC press and drum dryer combination to ensure restrained drying. Both the wood coupons and mini handsheets were conditioned to 50% RH 23°C.

The variation of in-plane and out-of-plane elastic constants for 0, 8, and 12 hrs acid chlorite treatment are shown in Figs. 3-5. A reasonable correlation is obtained with the apparent density of the wood coupon. The increase in in-plane constants C_{11}/ρ and C_{22}/ρ with increasing wood coupon density and delignification is respectively attributed to the expected higher moduli of latewood fibers and reduced lignin content (i.e., by the law of mixtures and E/ρ cellulose >> E/ρ lignin, a reduced lignin content would result in a higher fiber modulus). It is interesting to note the corresponding, albeit small, reduction in the out-of-plane constant C_{33}/ρ with increasing wood coupon density and delignification.

The correlation between conditioned wood coupon density and initial wet wood density is shown in Fig. 6. One purpose of this correlation is to estimate the conditioned density of the wood coupons from which the mini handsheets were made. Shown in Fig. 7 is the variation of mini handsheet apparent density with conditioned wood coupon apparent density for 12 hrs acid chlorite delignification based on the data shownin Fig. 6. The reduction in

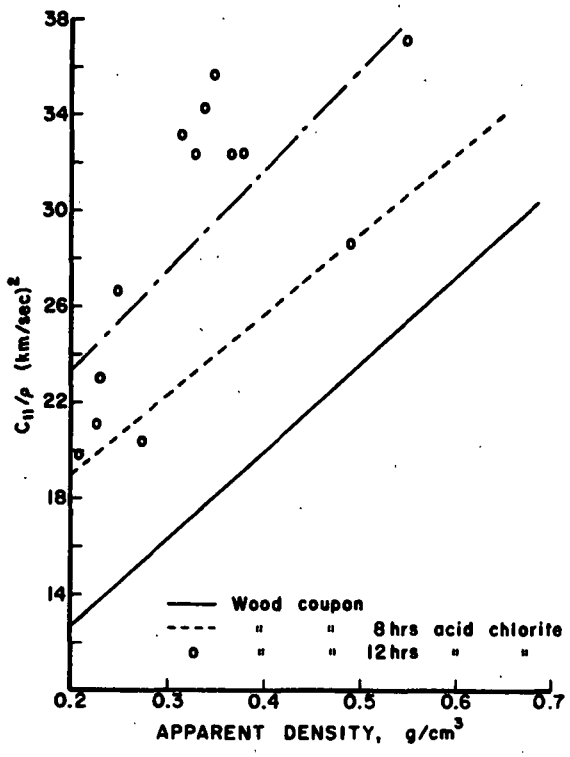

Figure 3. Variation of specific elastic constant with apparent density.

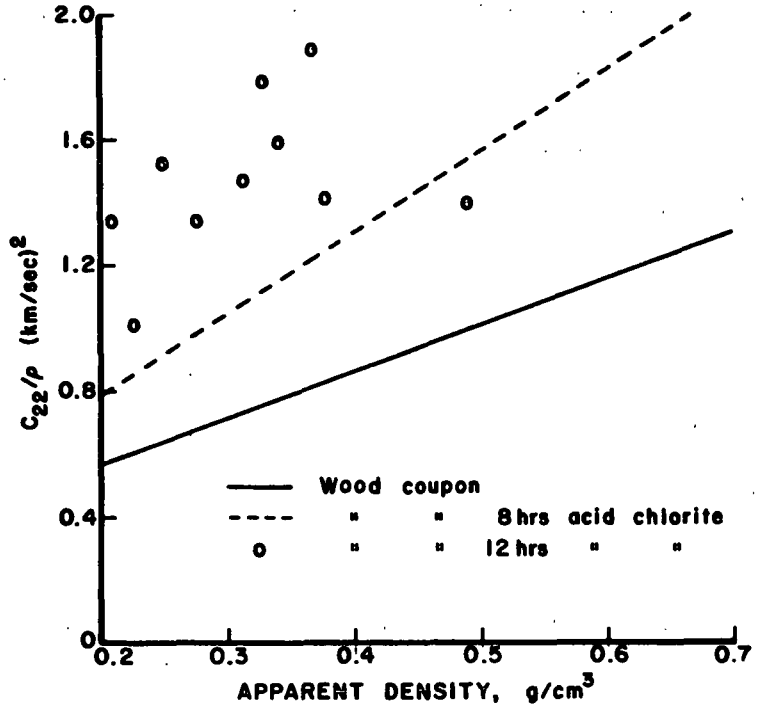

Figure 4. Variation of specific elastic constant with apparent density.

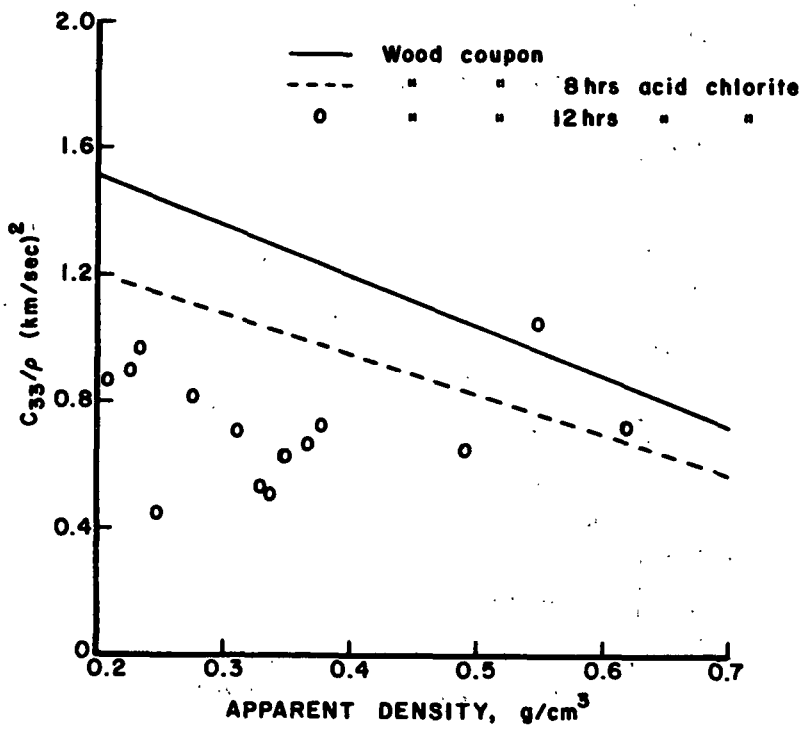

Figure 5. Variation of specific elastic constant with apparent density.

handsheet density with increasing wood coupon density is in part attributed to the greater proportion of latewood fibers present i.e., latewood fibers are less conformable than earlywood fibers.

Variation of the mean in-plane specific elastic constant with apparent density for the mini handsheets is shown in Fig. 8, for two levels of delignification. No significant difference is shown, however there is an increase in the elastic constant with handsheet densification. Using the results and correlations shown in Fig. 3 and 6 the elastic constant (for an ideal fiber network) has been calculated i.e., $\overline{C}/\rho$ ideal = 1/3 C_{11}/ρ wood coupon and is also shown in Fig. 8. We see that the ideal constant based on wood coupon elastic constant measurements is below that for the measured handsheet data i.e., the wood coupon potential underpredicts the handsheet performance at least for this limited

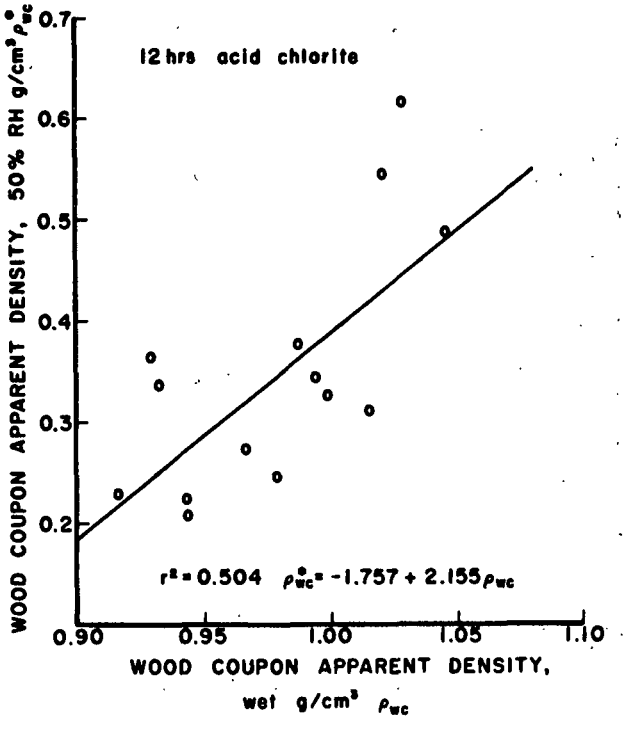

Figure 6. Correlation of conditioned and wet wood coupon densities.

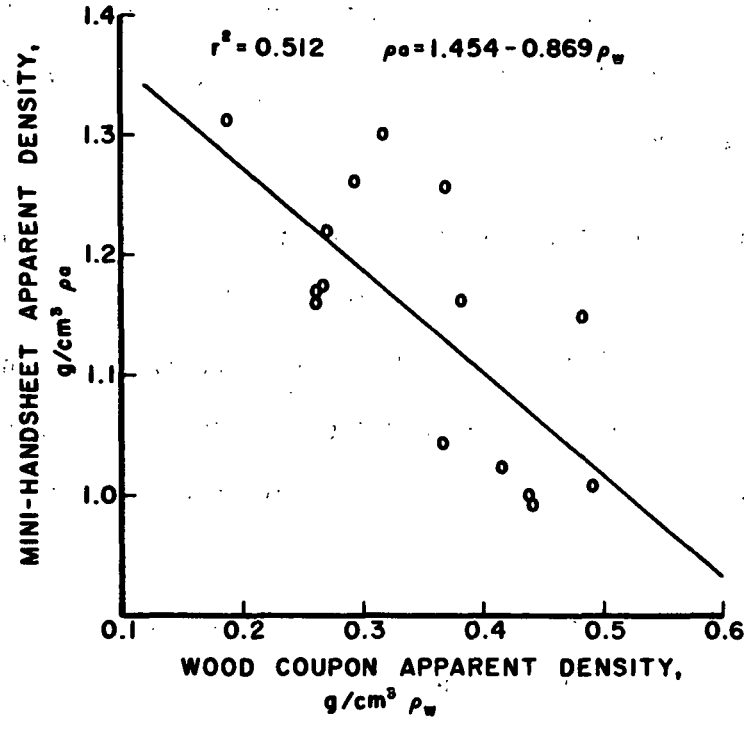

Figure 7. Correlation of mini-handsheet and conditioned wood coupon densities.

amount of data. The reduction in modulus with increasing handsheet density is in accordance with Fig. 7. The 19 mm diameter mini handsheets were carefully squared to approximately 16 mm x 16 mm and STFI compression strength measurements were made on them. Unfortunately for quite a number of the samples the span to caliper ratio was greater than 7 and the compressive strength for these samples is less than the intrinsic or plateau compressive strength. Using the simplified form of the Habeger/Whitsitt compressive strength relationship and the appropriate measured values, the compressive strength correlation with span/caliper ratio is shown in Fig. 9. The variation of compressive strength with apparent density for span/caliper ratios of less than 8 is shown in Fig. 10. It is seen that (intrinsic) specific compressive strength for a well bonded sheet of white spruce fibers is 37.1 Nm/g.

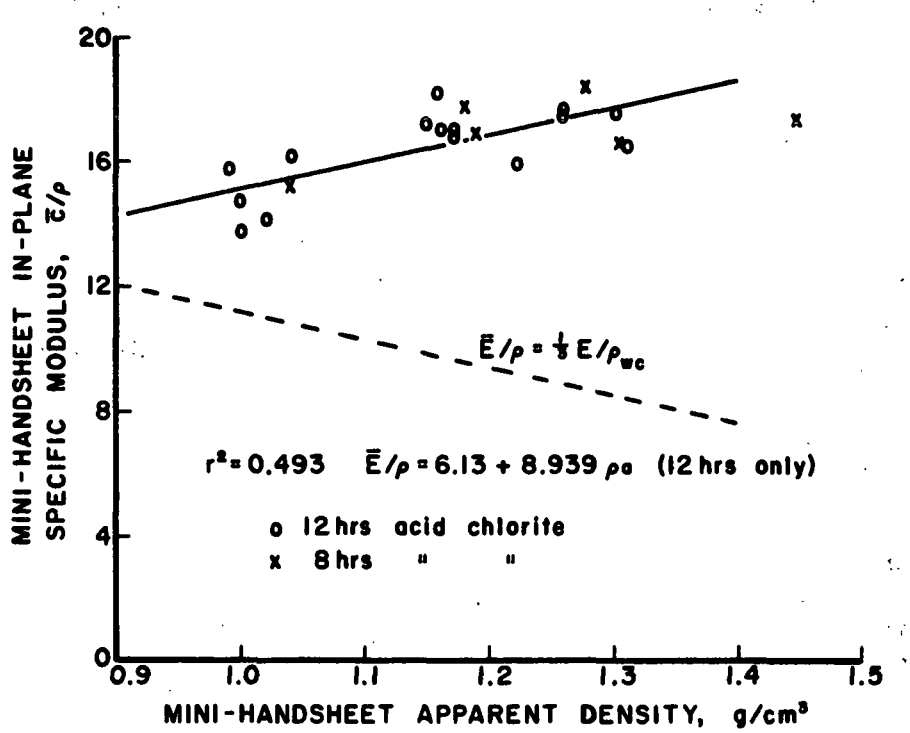

Figure 8. Variation of specific elastic constant with handsheet density.

Prediction of Compressive Strength

At a recent "Progress in Paper Physics Seminar" held at the Minnowbrook Center, New York, August 10-13, 1986, Page[2] presented a simple equation for the prediction of compressive strength as follows.

$$\sigma_c/\rho = - \sigma_y/\rho$$

where σ_c/ρ and σ_y/ρ are the specific compressive strength and yield strength respectively. The mechanism of failure is suggested to be one of shear between the microfibrils and the hemicellulose lignin matrix. This flow process is supposed to occur at the yield point in tension hence, the rationale for Eq. (1). Handsheet evidence was provided to substantiate the equation, however, because a precise measurement of yield stress was not available, a reasonable one-to-one correlation was obtained by using the arithmetic mean of stresses measured at 0.1% strain and the estimated yield point.

There are a number of interesting points raised by Eq. (1) which we hope to address in due course. In view of our own work on compressive strength modeling it is clear that both in-plane and out-of-plane elastic constants are important in determining compressive strength. It is possible therefore, that if indeed Eq. (1) has some validity, then we can predict the yield stress using ultrasonic measurements. Furthermore if we accept the findings of Htun[3], i.e., that drying stress is equal to the yield stress, then we also have a prediction of the drying stress levels in paper and board.

2. MORPHOLOGICAL FACTORS IN THE REFINING OF PINUS RADIATA AND EUCALYPT PULPS - BRUCE ALLENDER.

Some highlights of the investigation recently completed by Bruce Allender, a special student from APM, Australia, are given below. The specific

refining effect which we sought to induce and measure, as well as determine its effects on paper properties, was internal fibrillation. Unbleached kraft Pinus radiata and bleached kraft eucalypt pulps were subjected to different levels of refining in a PFI mill. In addition to internal fibrillation, fiber length reduction, external fibrillation and fines generation are also likely to be present as a result of PFI refining.

A number of methods have been suggested for measuring the extent to which fibers have been internally fibrillated and include: 1) water uptake in the cell wall, 2) direct observation of cell wall delamination, 3) increased fiber flexibility, 4) changes in cell wall dimensions, 5) crystallinity and crystallite size, 6) fiber collapse, 7) paper properties. In this work we have used methods 1, 2, and 7.

1) Direct Observation of Cell Wall Delamination.

In this technique unrefined and refined pulp samples were solvent exchanged using an ethanol/water series and then subjected to critical point drying using CO_2 to preserve the swollen state of the fiber. The fibers were then freeze fractured in liquid nitrogen and after coating with gold-palladium were examined in the SEM. Recognizing that freeze fracturing could damage the cell wall we nevertheless feel that there is evidence of increasing cell wall delamination with increased levels of refining as shown in Figs. 11 and 12.

We believe this is the first time cell wall delamination in hardwoods has been demonstrated. In both the Pinus radiata and eucalypt pulp samples about 20% of the unrefined fibers showed some evidence of delamination while at the highest levels of refining this increased to 95%.

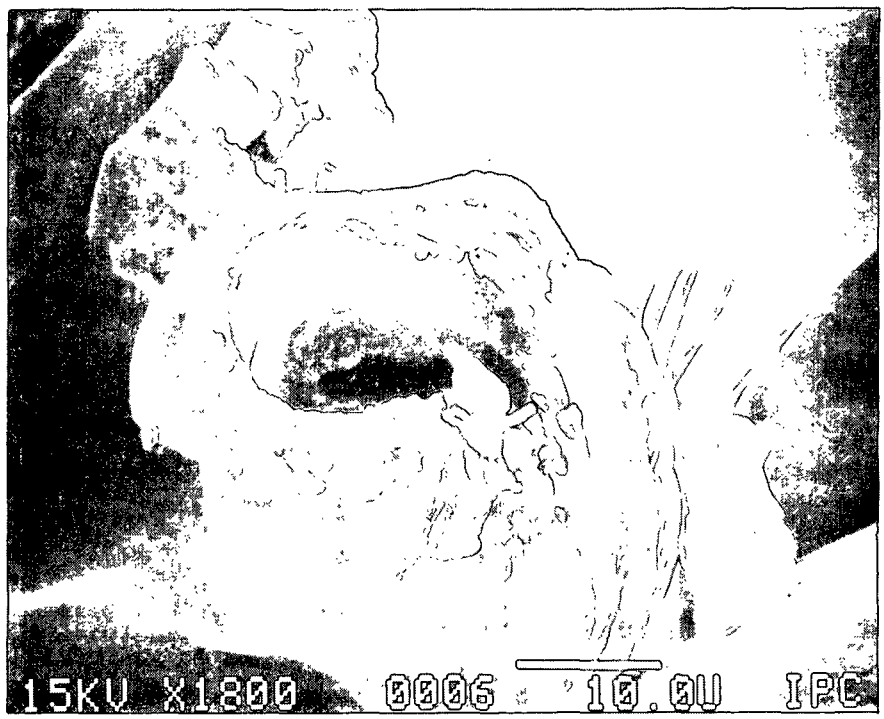

Figure 11a. Unrefined latewood fiber Pinus radiata, x 1800.

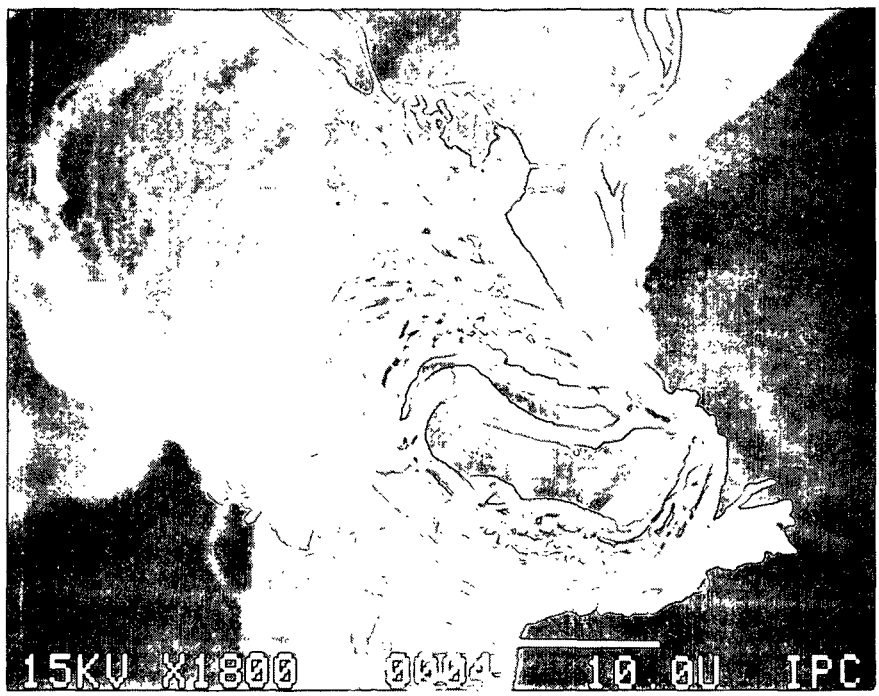

Figure 11b. Refined 7000 revolutions PFI latewood Pinus radiata, x 1800.

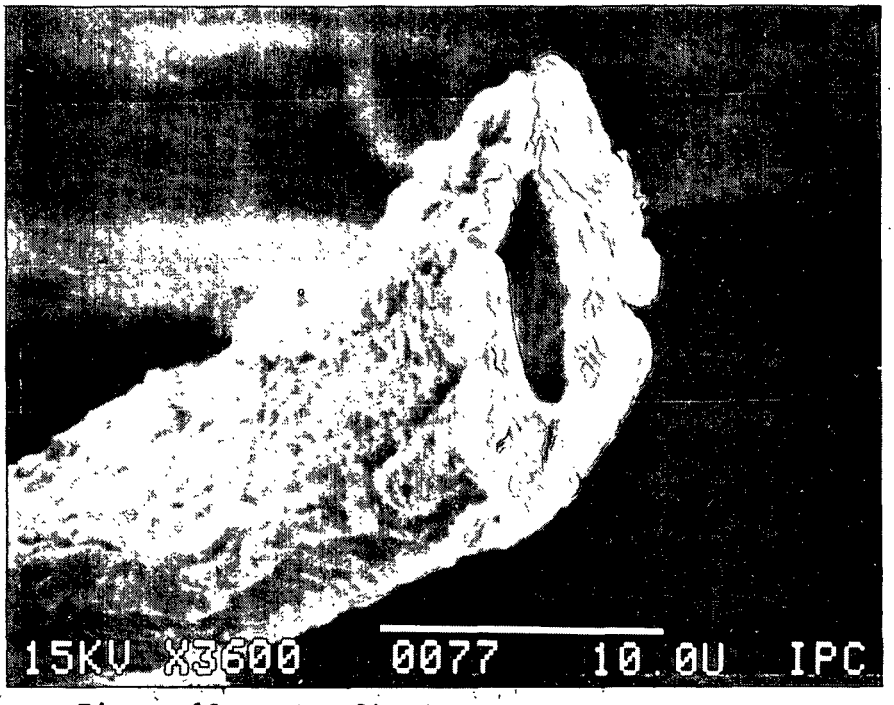

Figure 12a. Unrefined fiber eucalypt, x 3600.

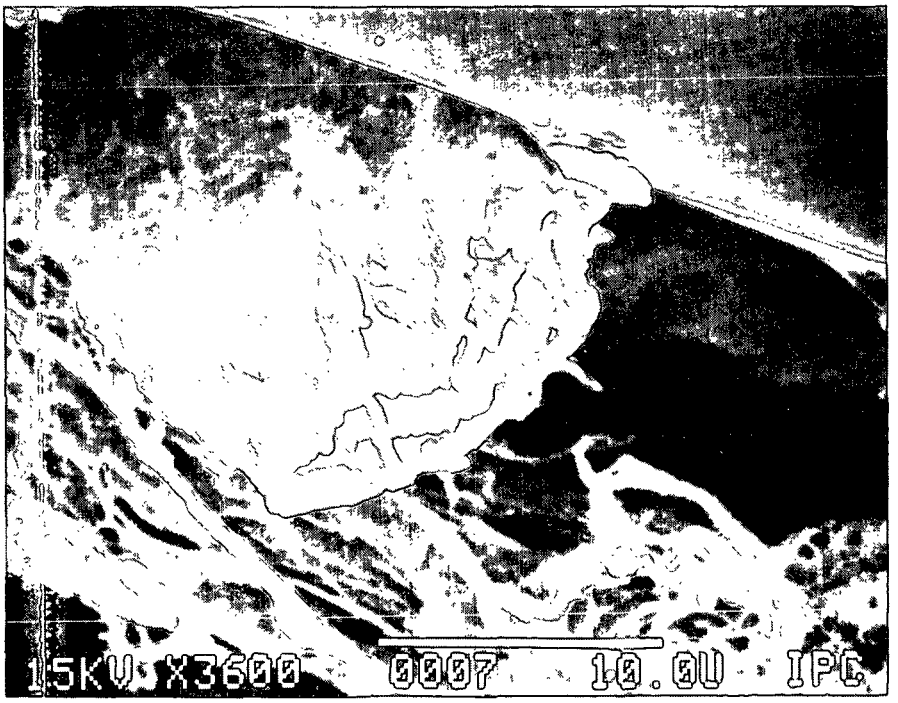

Figure 12b. Refined 3500 revolutions PFI eucalypt, x 3600.

2) Water uptake in the cell wall.

The variation of water retention value W.R.V. (expressed as the ratio of the weight of water to the weight of fibers) with centrifugal force (i.e., g) was used to determine if changes in fiber structure in the wet state could be measured. A typical WRV curve is shown in Fig. 13 for the unbleached radiata pine (whole pulp).

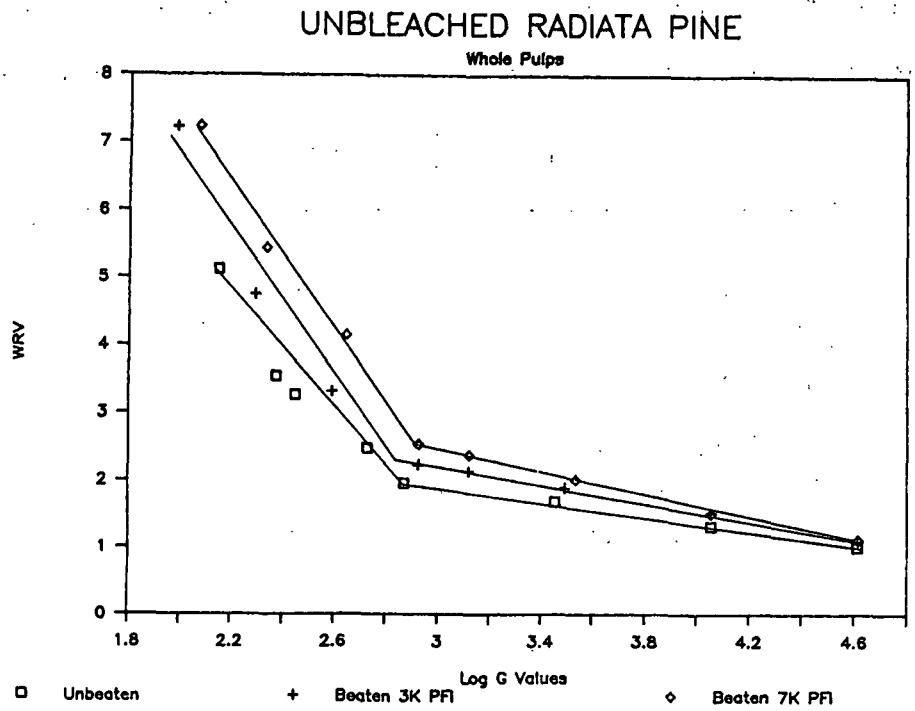

Figure 13. Variation of water retention values with centrifugal force.

Two distinct regions are observed. In the first region with the highest slope it can be argued that mainly interfiber water is being expelled from the mat while the lower slope region denotes loss of intrafiber water (i.e., from the cell wall). We note that refining affects both regions. The WRV curves shown in Figs. 14 and 15 are for the unbleached Pinus radiata and

bleached eucalypt pulps respectively with fines removed (i.e., fines/passing 200 mesh). The differences in the curves due to refining are now greatly diminished. WRV's at 3000 g are shown in Figs. 16 and 17 as a function of PFI revolutions. It is assumed that at 3000 g the changes in WRV are mainly affected by changes in cell wall structure which could include external fibrillation. A small but significant change in WRV for both pulps with increased refining is seen i.e., 9.05% for the Pinus radiata and 5.44% for the eucalypt. The effect of air drying on WRV is also shown for both pulps. A large drop in the WRV value for both pulps with virtually no change with refining was found.

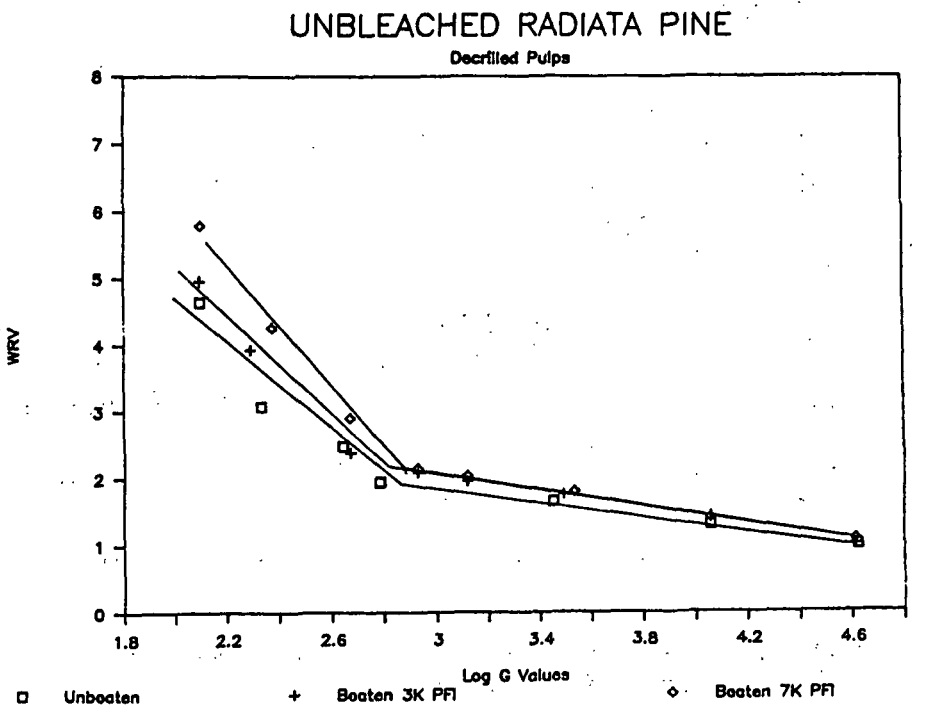

Figure 14. Variation of water retention values with centrifugal force.

3) Paper Properties

In view of the limited quantities of pulp and the needs of other project areas (e.g. wood coupon work reported on earlier in this section) it was decided to evaluate paper properties using mini handsheets. Mini handsheets

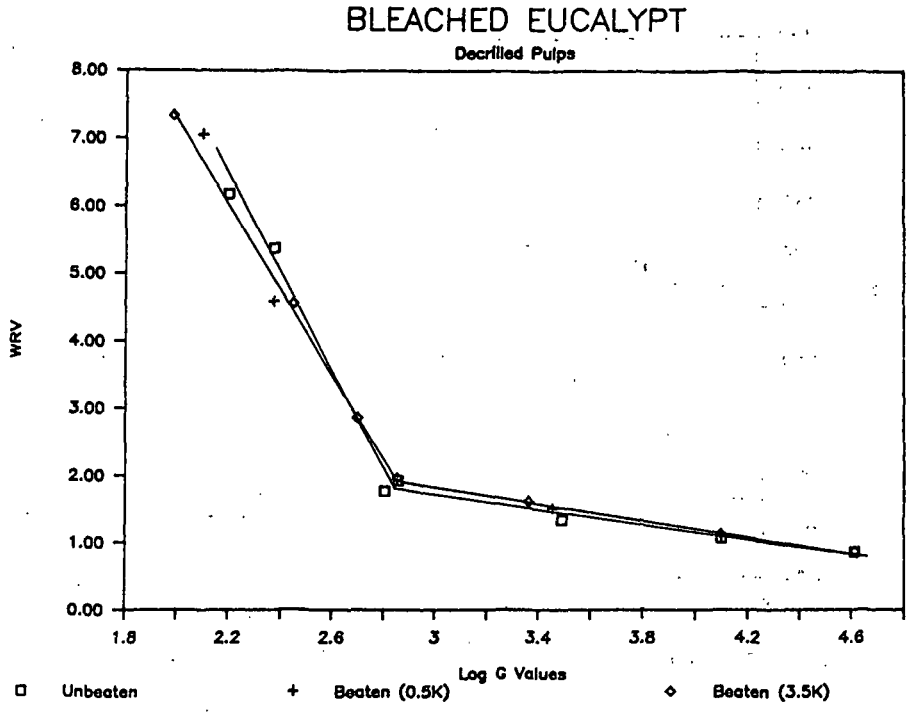

Figure 15. Variation of water retention values with centrifugal force.

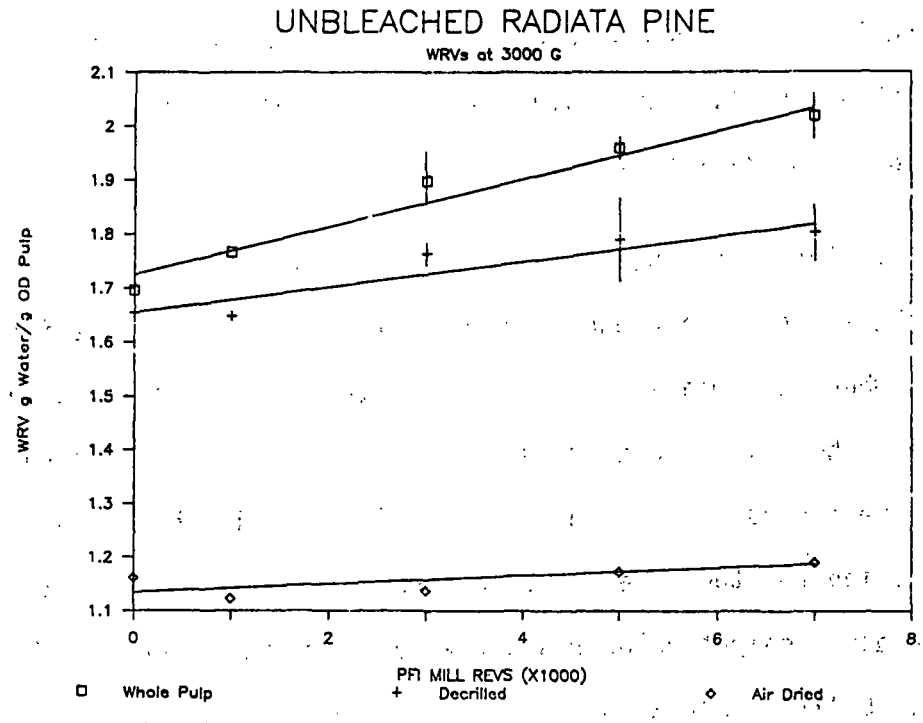

Figure 16. Variation of water retention value with PFI revolutions.

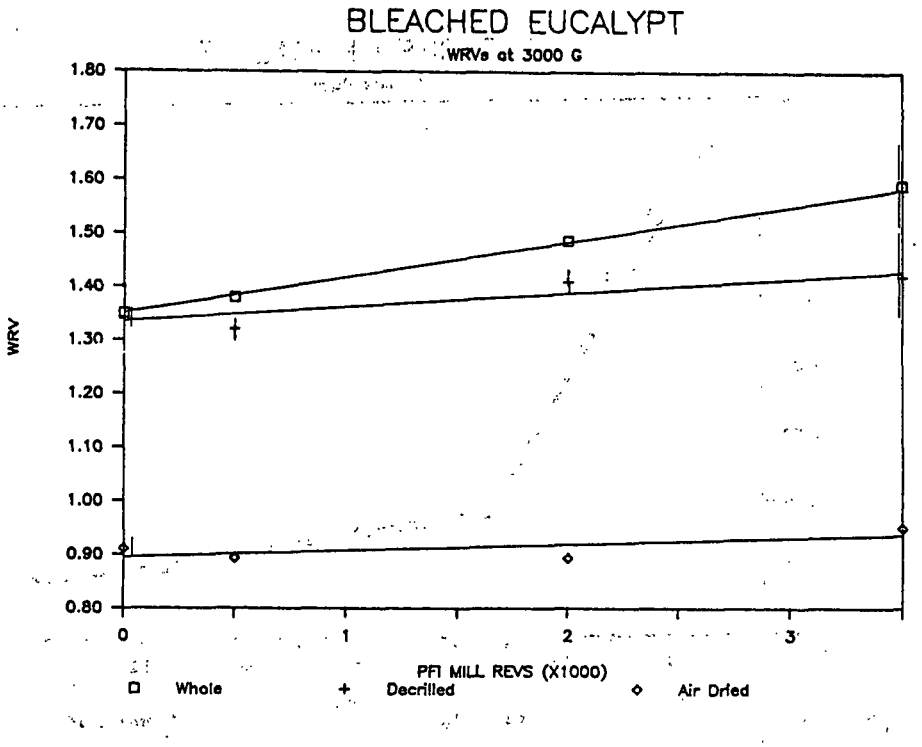

Figure 17. Variation of water retention value with PFI revolutions.

(19 mm diameter) having a basis weight of 250 g/m^2 were made, as described in section 1 of this report, from whole pulp, fines free and air dry pulp samples. Handsheet properties are summarized in Table 2.

The variation of sheet apparent density with WRV at 3000 g is shown in Fig. 18 for the Pinus radiata and eucalypt pulps. The dominant effect of fines is again seen when we compare the whole and fines free curves. At the highest refining levels there is a large reduction in WRV, however the corresponding change in apparent density is much smaller. The overall change in apparent density with refining for the fines free handsheets is 23.4% and 24.2% for the Pinus radiata and eucalypt pulps respectively which correspond to changes of only 9.05% and 5.44% in WRV as noted above. We might therefore conclude that

Table 2. WRV and mini-handsheet properties.

Pulp	CSF	WRV 3000 g	Basis Wt. g/m^2	Density g/cc	$\bar{C}/\rho$ $(km/sec)^2$	C_{33}/ρ $(km/sec)^2$	STFI c/ρ Nm/g
Bleached Kraft Eucalypt							
E0	612	1.347	260	0.808	9.14	0.097	24.9
E0.5	555	1.376	258	0.840	10.44	0.193	31.6
E1	520	1.537	253	0.886	11.34	0.231	35.3
E2	460	1.486	248	0.889	11.78	0.280	36.1
E3.5	345	1.586	271	0.923	12.13	0.349	37.4
EA0.5	---	0.893	223	0.737	7.65	0.0655	18.4
EA2	---	0.894	223	0.773	7.92	0.0751	21.1
ED0	---	1.342	207	0.744	8.80	0.0729	23.7
ED3.5	---	1.415	221	0.924	12.78	0.235	36.5
Unbleached Kraft Pinus Radiata							
P0	737	1.696	212	0.849	10.63	0.068	31.0
P1	694	1.766	250	0.908	12.43	0.144	35.4
P3	610	1.897	246	0.941	13.78	0.181	42.6
P5	526	1.958	268	0.957	14.17	0.181	42.9
P7	420	2.018	243	0.994	14.38	0.189	43.9
PWA0	---	1.160	255	0.695	6.99	0.018	17.8
PWA7	---	1.190	230	0.869	9.43	0.106	29.1
PD0	---	1.655	228	0.788	9.57	0.044	28.7
PD7	---	1.804	212	0.972	13.21	0.123	43.1

apparent density is a more sensitive indicator of changes in cell wall structure (internal fibrillation).

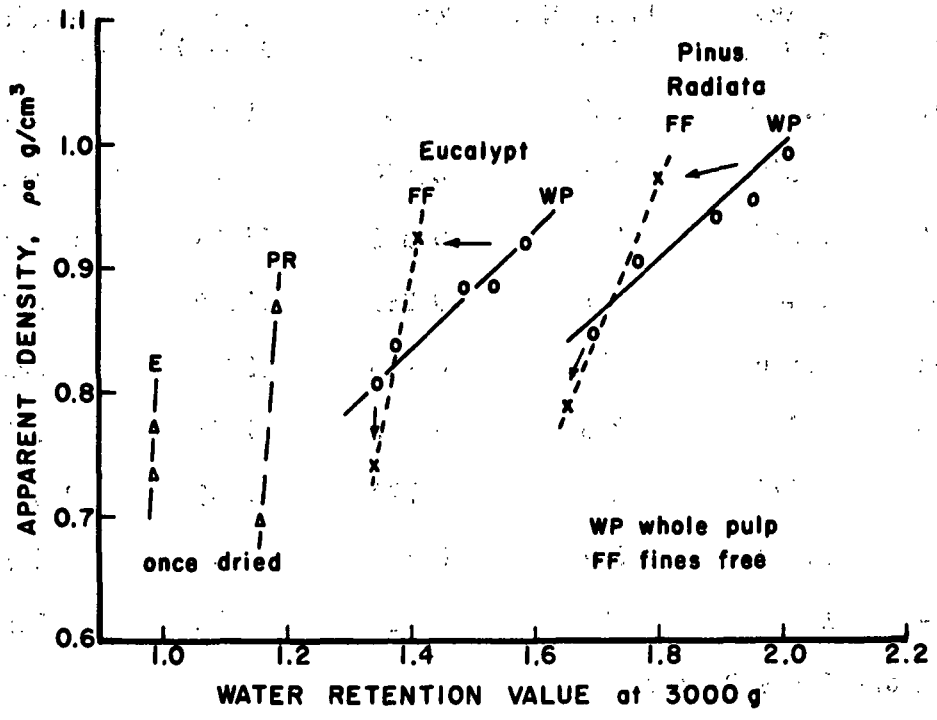

Figure 18. Variation of sheet density with water retention value.

The compressive strength correlation using the Habeger/Whitsitt model is shown in Fig. 19 for the Pinus radiata and eucalypt mini handsheets.

3. Formation Measurements

It has long been appreciated that certain aspects of formation: namely, small scale basis weight variation (or distribution of mass density) play an important role in failure properties. Small scale basis weight variations are also recognized as being important in such converting operations as corrugating, calendering, supercalendering and printing. Until recently the

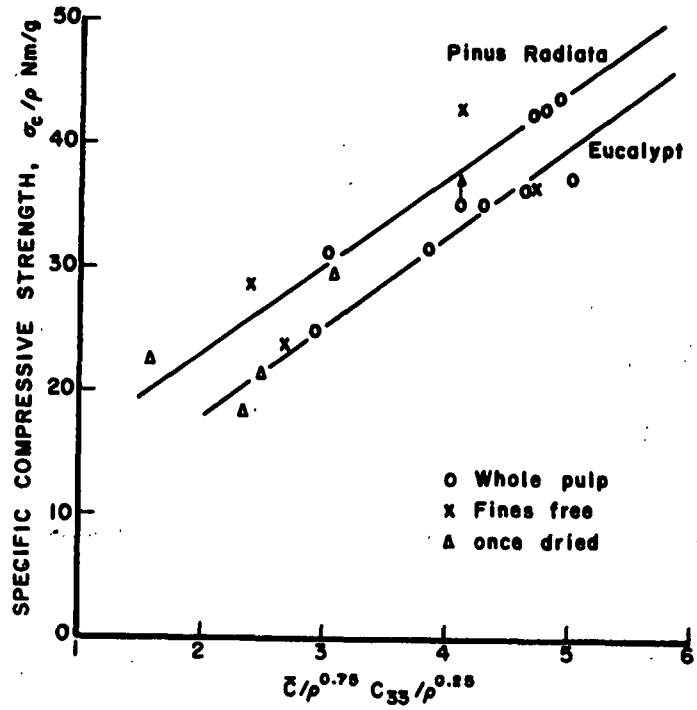

Figure 19. Compressive strength correlation.

only means available for studying formation at the Institute was a Thwing Albert Formation tester (its operating principle is based on light transmission). In conjunction with an API sponsored evaluation of formation instruments, an MK systems microformation tester has been donated to the Institute. An outline of the API and joint API/IPC formation studies are outlined in Table 3. As part of the joint API/IPC project a proposal has also been made for the design of a formation tester as shown in Fig. 20. This has the capability of making light transmission and reflectance measurements as well as beta particle absorption measurements. The latter being a true measure of mass density. Further progress on this proposal is awaiting appropriate funding. A new technology which is being applied to the measurement of formation is soft x-rays. This is

Table 3. Planned formation studies at IPC.

API-IPC FORMATION MEASUREMENT SYSTEM: Joint Development

- Mass density measurements-beta radiation
  - Pm147 source - approx. 0.6 mm aperture
  - Solid state detection
- Optical density measurements-400 to 700 nm
  - Reflectance measurements
  - Transmission measurements
- Measurement Positioning - precision x-y table
  - Eight inch square specimens
  - Table positioning and precision - 0.01 mm
- Data acquisition and control system - IBM-XT

API-IRC: EVALUATION OF FORMATION MEASURING INSTRUMENTS

- Two commercial instruments
  - Accuray Optipak - on-line
  - MKS Microformation - off-line and on-line
- Papermaking factors
  - Furnish - each at 5 "formation" levels
    - Tissue
    - Newsprint
    - Fine paper
  - Color (of sheet) at two formation levels
  - Basis weight - three levels at two formations
  - Fiber orientation - two levels
  - Commercial vs handsheets
- Instrumental factors
  - Quality of measurements
    - Reproducibility
    - Sensitivity
    - Calibration and/or standardization
  - Instrument stability
    - Instrument drift
    - Line voltage fluctuations
    - Response time and warm-up
  - Environmental effects
    - Relative humidity
    - Ambient light level
    - Mechanical vibrations
    - Dust or other pollutants
  - Ease of use and maintenance
- Effects due to measurement parameters
  - Paper web velocity
  - Optical properties
    - Measurement wavelength
    - Diffuse vs collimated illumination

Table 3 continued.....

API-IRC EVALUATION STUDIES (cont.)

- **Comparison between commercial instruments and test instrument**

IPC FORMATION STUDY - Areas of Interest

- **Effect of papermaking variables on formation**
  - **Furnish**
    - **Pulping method - fiber type**
    - **Bleaching**
    - **Refining**
    - **Chemical additives**
  - **Forming methods - fiber orientation and ZD variations**
    - **Laboratory handsheets**
    - **Formette sheets**
    - **Fourdrinier papers**
    - **Twin wire formers**
  - **Sheet properties**
    - **Basis weight**
    - **Density**
    - **Surface roughness**
  - **Formation changes with process changes**
    - **Wet straining**
    - **Restraint during drying**
    - **Wet pressing**
    - **ZD variation**

- **Effects of measurement variables**
  - **Beta measurements**
    - **Aperture size**
    - **Environmental effects**
  - **Light measurements - transmission and reflectance**
    - **Diffuse vs collimated illumination**
    - **Measurement wavelength (into ir)**
    - **Aperture size**
    - **Environmental effects**

- **Relationships between mass density and optical density variations**

- **Relationships between formation and optical properties**

- **Relationships between formation and mechanical properties**

- **Relationships between formation and end-use performance**

currently being evaluated by Dr. Ted Farrington of the Engineering Division. At least two publications on the application of soft x-rays to paper formation measurements have appeared in Japanese literature from researchers at the Faculty of Agriculture, Kyoto University.

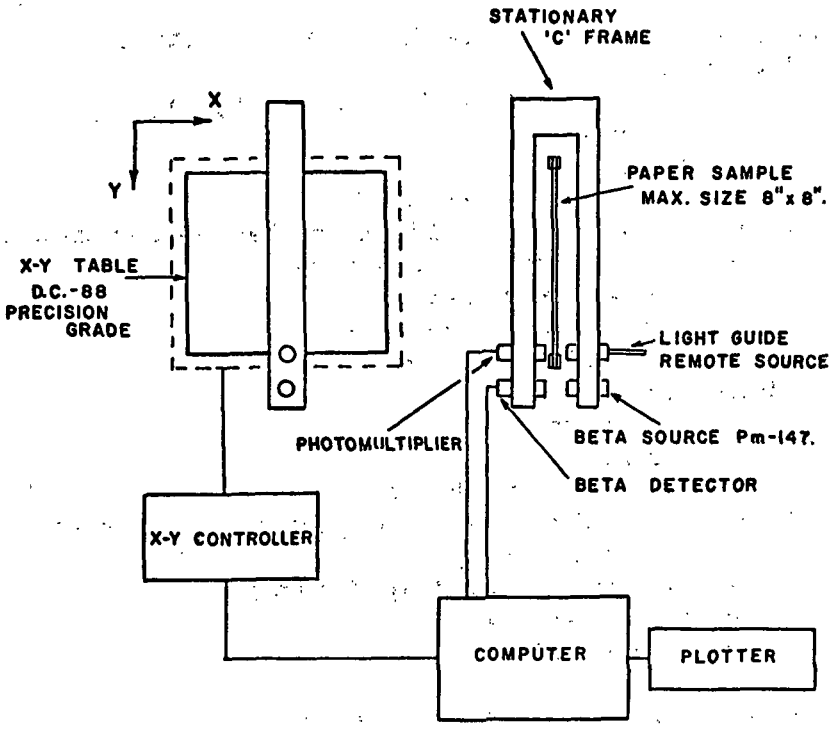

Figure 20. Schematic of API/IPC formation tester.

Therefore as the need arises in our current and future projects for mass density distribution measurements we hope that capability will be available.

4. COMBINED STRESS MEASUREMENTS

In many converting processes paper is subjected to various combined stress situations. In supercalendering for example, paper is subjected to nor-

mal and out-of-plane cyclic shear stresses. Shear and normal stresses are also important in corrugating.

In order to study the effects of out-of-plane combined stresses on paper and board deformation behavior, it is proposed that the device conceived by Arcan[4] and shown in Fig. 21 for shear measurements be modified for such purposes.

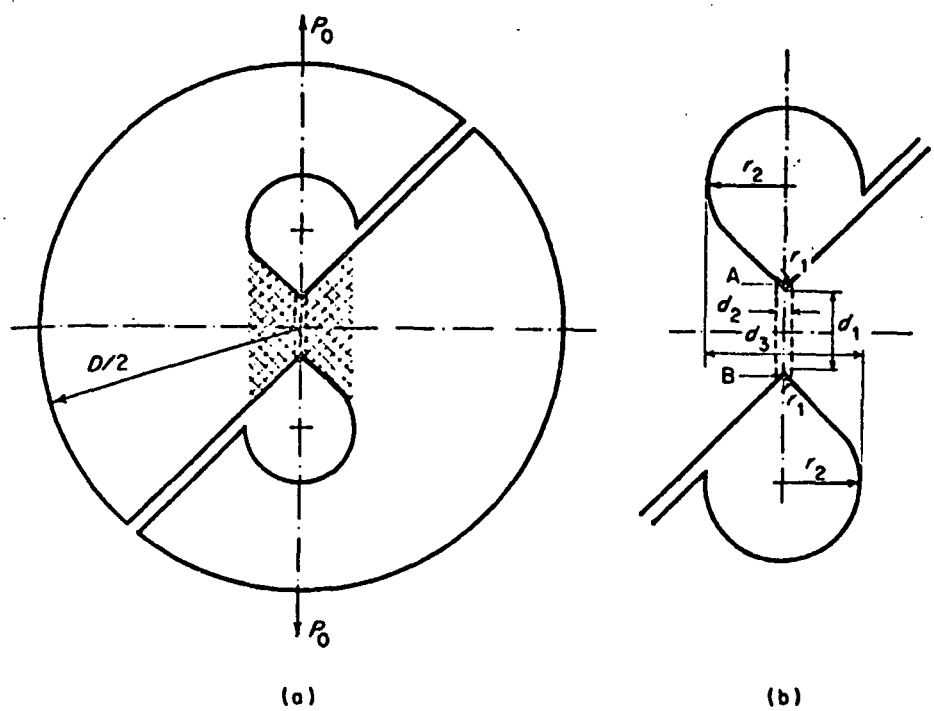

Figure 21. The two constitutive parts of the sample: the significant sample (between dashed lines) and the exterior one with the zone governing (a) isostatics, (b) dimensions.

STUDENT RELATED WORK

1. "Strength Development through Internal Fibrillation and Wet Pressing". This is the title of Tom Bither's doctoral research and we hope that Tom will report on his work to the committee at some future meeting.

2. "Z-direction Variation of Residual Stress and Paper Properties". This is the title of Marypat Franke's masters research project. She will make a short presentation on the objectives and progress of the work at the forthcoming PAC meeting.

Literature Cited

1. Habeger, C., Whitsitt, W. Fiber Science and Technology 19(1983) 215-239.

2. Page, D. "The Mechanism of Compressive Failure", Extended Abstract International Paper Physics Seminar Minnowbrook Conference Center. New York August 10-12, 1986.

3. Htun, M. "The Influence of Drying Strategies on The Mechanical Properties of Paper", Doctoral Dissertation, The Royal Institute of Technology.

4. Arcan, M., Hashin, Z., Voloshin, A. Experimental Mechanics 18:141-146(1978).

THE INSTITUTE OF PAPER CHEMISTRY

Appleton, Wisconsin

Status Report

to the

PAPER PROPERTIES AND USES

PROJECT ADVISORY COMMITTEE

Project 3467

PROCESS, PROPERTIES, PRODUCT RELATIONSHIPS

September 10, 1986

PROJECT SUMMARY

PROJECT NO. 3467: PROCESS, PROPERTIES, PRODUCT RELATIONSHIPS

PROJECT STAFF: G. A. Baum, C. C. Habeger September 10, 1986

PROGRAM GOAL:

Develop relationships between the critical paper and board property parameters and how they are achieved in terms of raw material selection, principles of sheet design, and processing conditions.

PROJECT OBJECTIVE:

(1) To improve our capability of characterizing paper and board materials,
(2) to relate measured parameters to end-use performance (especially in the case of Z-direction measurements), and
(3) to relate measured parameters to machine and process variables.

PROJECT RATIONALE, PREVIOUS ACTIVITY, AND PLANNED ACTIVITY FOR FISCAL 1986-87 are on the attached 1986-87 Project Form.

SUMMARY OF RESULTS LAST PERIOD: (October 1985 - March 1986)

(1) The anisotropy of an in-plane elastic property vs. angle from the MD is being studied. The area and general geometry of the polar graphs is being investigated relative to process variables such as refining, wet pressing, and yield.

(2) For machine made papers the envelope of elastic properties vs. angle from the MD is usually elliptical. The angular displacement of the major axis from the MD is indicative of flows from the paper machine headbox. These vary from point to point in the cross machine direction.

(3) Elastic properties have been examined at intermediate to high moisture contents (up to 65%). Generally the water in the sheet dominates the results at moisture contents over 40 to 50%.

(4) The new broadband plastic (PVDF) ZD transducers have been perfected and are in use in the longitudinal ZD apparatus. Automation of the laboratory ZD measurement equipment is underway.

(5) Work on the effects of refining and yield on the ZD properties is continuing. Oriented sheets have been made from the laboratory pulps described earlier.

(6) The effects of non-uniform drying restraints on local sheet properties have been investigated. The results are more complicated than anticipated. Analysis is underway.

(7) Surface roughness measurements have been made using a stylus type instrument. The results were compared with standard air leak methods for

estimating smoothness. The effects of some papermaking variable on roughness were also examined.

(8) A new automatic in-plane elastic property measurement system is under development. Improvements in both hardware and software are planned, including a computer interface to the IBM family of 8088 machines.

SUMMARY OF RESULTS THIS PERIOD: (April 1986 - September 1986)

(1) The automatic device for measuring the in-plane elastic stiffnesses of paper has been improved mechanically in several ways. Plans are underway for the third generation device which will use the latest technology and "off-the-shelf" components.

(2) The carriage translation on the in-plane robotic system is now driven by a magnetic linear motor resulting in a great reduction in maintenance.

(3) There also have been a number of software changes in the automatic device. These include specific software for testing handsheets and changes in the reporting format for the polar data results.

(4) The apparatus for measuring the out-of-plane specific stiffness has been automated, significantly reducing operator time. There have been other improvements in transducer design.

(5) A Fourier analysis capability was added to the automated ZD system.

(6) A study of rubber to sample coupling was undertaken. This could lead to loss tangent measurements on paper at high loading pressures.

(7) Work is underway to elucidate those papermaking variables that affect the shape and size of the polar graphs of specific stiffness vs. angle. During the past period we have been studying (1) CD profiles, (2) the affects of drying restraints, and (3) stress relaxation of the sheets by rewetting.

(8) Work on the impact of refining and yield on the ZD properties is continuing. Recent work has involved measurements of single fiber transverse modulus.

(9) A device which will be able to measure specific scattering coefficients in heavy board materials is being designed and constructed.

(10) A paper "Automatic Determination of Ultrasound Velocities in Planar Materials" (Technical Paper Series 181) was submitted to Ultrasonics for publication. It is attached as Appendix A.

(11) A paper "Elastic Properties, Paper Quality, and Process Control" (Technical Paper Series 186) was written for publication in Tappi. It is attached as Appendix B.

(12) A paper "Roughness Anisotropy in Paper" (IPC Technical Paper Series 190) has been submitted to J. Pulp and Paper Science. It is attached as Appendix C.

PROJECT TITLE: Process, Properties, Product Relationships

PROJECT STAFF: G. Baum, C. Habeger, J. Waterhouse

PRIMARY AREA OF INDUSTRY NEED: Properties related to end uses

PROGRAM AREA: Performance and Properties of Paper and Board

Date: 6/1/86

Budget: $180,000

Period Ends: 6/30/87

Project No: 3467

PROGRAM GOAL:

Develop relationships between the critical paper and board property parameters and how they are achieved in terms of raw material selection, principles of sheet design, and processing conditions.

PROJECT OBJECTIVE:

(1) To improve our capability of characterizing paper and board materials,
(2) to relate measured parameters to end-use performance (especially in the case of Z-direction measurements), and
(3) to relate measured parameters to machine and process variables.

PROJECT RATIONALE:

It is important to understand the relationships between end-use performance and properties in order to improve paper and board products or maintain performance within close tolerances while effectively utilizing available raw materials, minimizing energy requirements, and minimizing environmental impacts.

RESULTS TO DATE:

Ultrasonic techniques for measuring in-plane and out-of-plane elastic properties of paper have been developed. Instruments for measuring these properties have been designed, constructed and tested. These include separate instruments for out-of-plane shear and out-of-plane Youngs modulus, and a robotic tester for measuring the four in-plane elastic properties. A soft platen caliper gage which gives values comparable or superior to existing caliper gages has been designed and constructed. The effects of fiber orientation, wet straining, and wet pressing on elastic properties have been extensively studied using softwood kraft furnishes. The in-plane and out-of-plane elastic parameters have been related to end use tests and converting operations in a number of cases. A microwave technique for determining fiber orientation has been developed.

PLANNED ACTIVITY FOR THE PERIOD:

1. In-plane and out-of-plane elastic constants will be measured on a representative group of samples differing in composition and structure (yield and refining) in different ambient environments. These data will be compared with use-oriented test results, where possible.

2. A device to measure specific scattering coefficients in heavy board materials has been designed and is undergoing construction. This will be used to test boards differing in composition and structure.

3. Work on automation of the ZD velocity measurements is underway. Improvements in the existing apparatus are anticipated.

4. The effort to establish relationships between properties and end-use performance will continue.

5. A fundamental study of formation is planned. This effort will be complementary to an existing contract research program with the API Instrumentation Research Program.

6. A licensing agreement has been prepared concerning the laboratory ultrasonic equipment. Negotiations are underway with several instrument manufacturers.

STUDENT RELATED RESEARCH:

B. Berger, Ph.D.-1987; B. Berger, M.S.-1984; D. Waterman, M.S.-1986; W. Westerveldt, M.S.-1986.

Status Report

PROCESS, PROPERTIES, PRODUCT RELATIONSHIPS

Project 3467

INTRODUCTION

This project has been going forward on several fronts. Accordingly, this report is divided into different sections. Section 1 deals with the continuing work related to polar diagrams and how they are impacted by paper machine process variables. Section 2 deals with improvements in the laboratory equipment for measuring both in-plane and out-of-plane elastic stiffnesses. Section 3 deals with fundamental studies which may lead to improved or new measurements in the future. Related student work is not described in this report but, in some instances, will be reported at the next meeting.

SECTION 1

Polar Diagrams

The in-plane robotic tester can measure the specific longitudinal or shear stiffnesses in the plane of the paper at various angles to the MD. The shape and areas enclosed by the resultant polar diagrams are related to paper machine process variables. In the last Paper Properties and Uses PAC report, dated April 1-2, 1986, we discussed the affects of yield, refining, and wet pressing on the polar diagrams. In general, a decrease in yield or an increase in refining or wet pressing increased the area of the polar diagram, but did not change its shape from the usual elliptical pattern. Data on commercial papers was also presented that indicated that oftentimes the major axis of the ellipse is tipped away from the machine direction. This behavior has been attributed to cross flows coming from the headbox which cause some preferential alignment of fibers at an angle to the MD.

Work carried out in this area since April has been focused in three areas: (1) verification that the angular displacement is not related to wet straining or restraints during drying; (2) a study of how wet straining or drying restraints affect the general shape and area of the polar diagrams, and (3) a study of a commercial paper to determine how parameters taken from the polar diagrams relate to other commonly used parameters. Each of these are described in some detail below.

Rewetting Experiments

Polar diagrams of specific stiffness were obtained for a number of paper samples which were then immersed in water for 24 hours, dried, and remeasured. The results shown here are for samples which had been air dried for 24 hours in a 20% relative humidity (low moisture content) environment, and then conditioned and tested at Tappi standard conditions of 50% RH and 23 degrees Celsius. The rewetting of the paper would be expected to release any stresses dried into the paper and generally result in lower values of specific stiffness. No changes in fiber orientation, however, would be expected, whether along or at some angle to the MD.

Figure 1 shows polar diagrams for a linerboard (top) and fine paper (bottom) before and after rewetting. The linerboard diagram has a slight clockwise angular displacement from the MD of 3.8 degrees with an enclosed area of 315 $(km/s)^4$. After wetting and freely drying the angular displacement is about the same, 4.4 degrees, but the enclosed area is only 210 $(km/s)^4$, a 33% decrease. For the fine paper the "before" diagram shows an angular displacement of 8.4 degrees counter clockwise from the MD with an area of 214 $(km/s)^4$. After rewetting these two values are 8.2 degrees and 181 $(km/s)^4$, respectively.

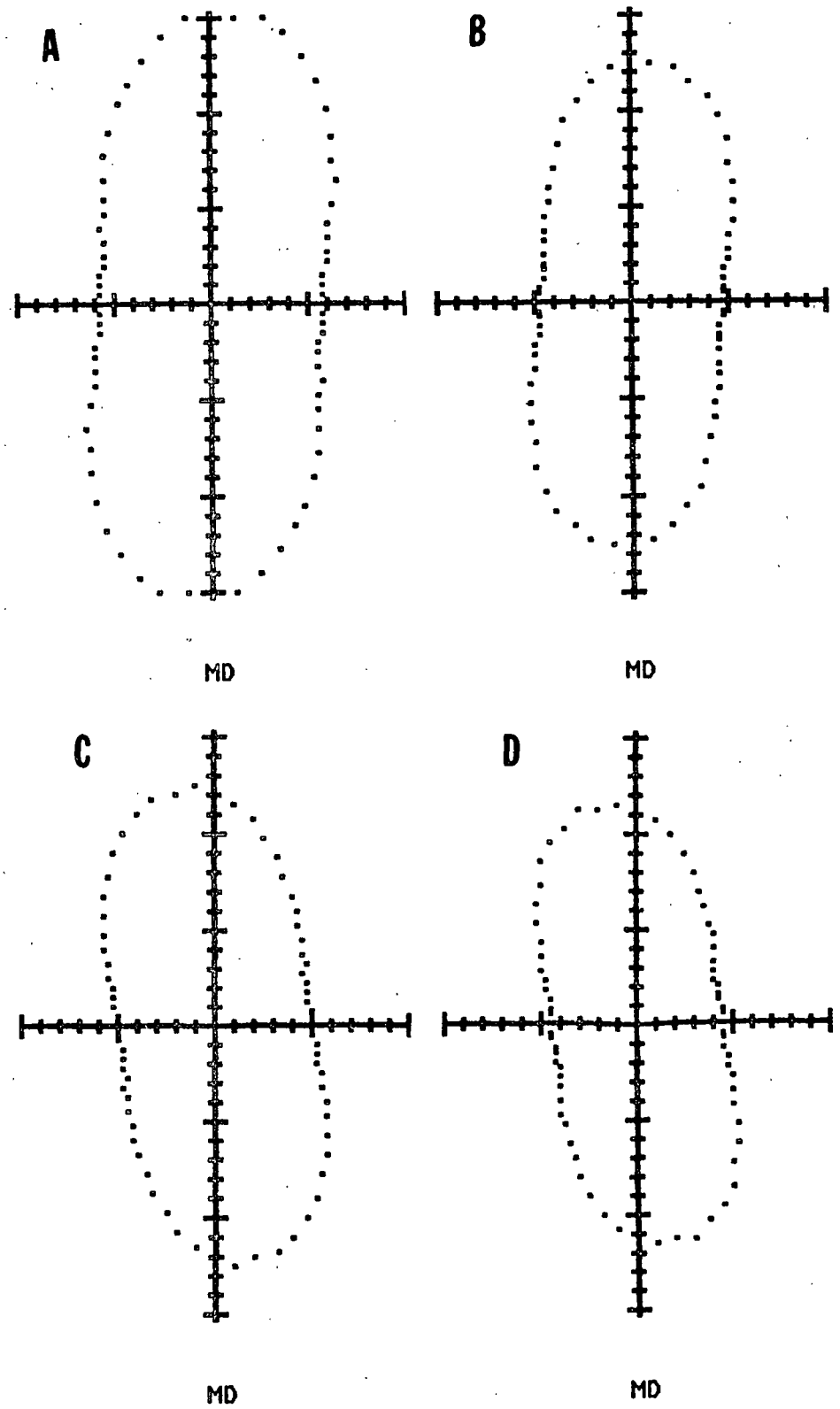

Figure 1. Top: Linerboard before (A) and after (B) rewetting.
Bottom: Fine paper before (C) and after (D) rewetting.

Figure 2 shows four fine paper samples having different angular displacements ranging from about -8 degrees to +4 degrees. (These samples were from the same CD specimen and were shown in Figure 6 in the last Status Report.) Figure 2 reveals that rewetting the paper does not change the angular displacement of the major axis of the ellipse from the MD, consistent with the notion that the angular displacement is related to fiber orientation in the paper.

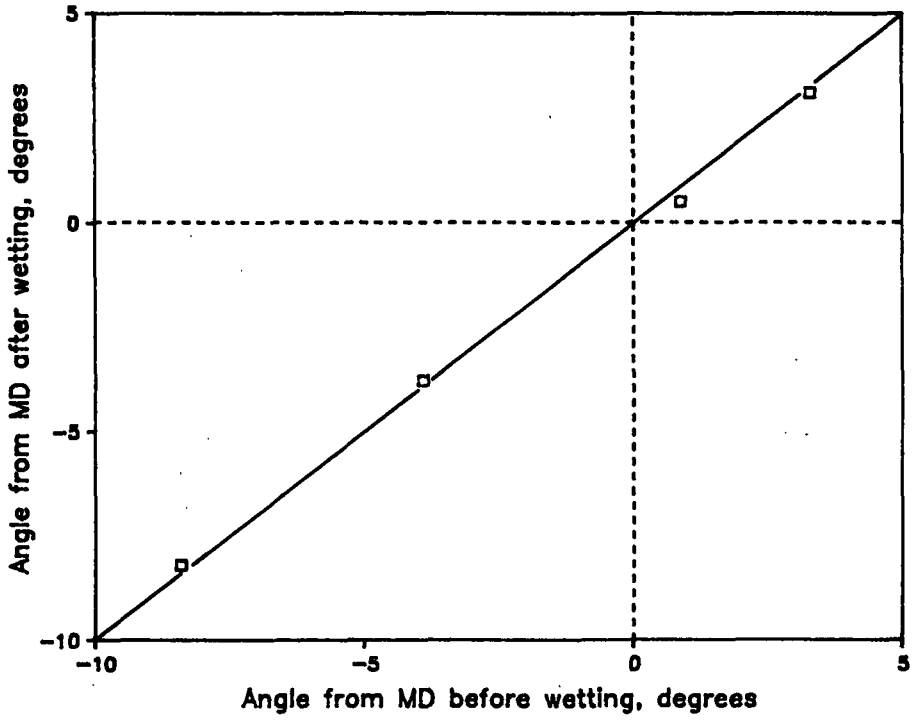

Figure 2. Angle from MD after wetting vs. angle from MD before wetting.

During the above experiments the question arose as to how accurately the operator could position the test sample on the rotating platform from test to test. For anisotropic handsheets, which are typically smaller than the test platform, it would be possible to misalign the MD of the specimen with the "MD" of the instrument. Subsequent testing, however, indicated that a skilled operator can easily position within about one half of a degree.

Figure 3 compares the MD/CD stiffness ratios before and after wetting (and drying). The effect is small, if real, and would be expected if MD and CD dimensional changes upon rewetting and drying were similar. Figure 4 depicts the areas enclosed by the polar diagrams for the same four fine paper samples. The areas enclosed after wetting are considerably less than the initial areas. The numbers next to each datum are the angular displacement from the MD. They suggest that there is no relationship between angle and area loss.

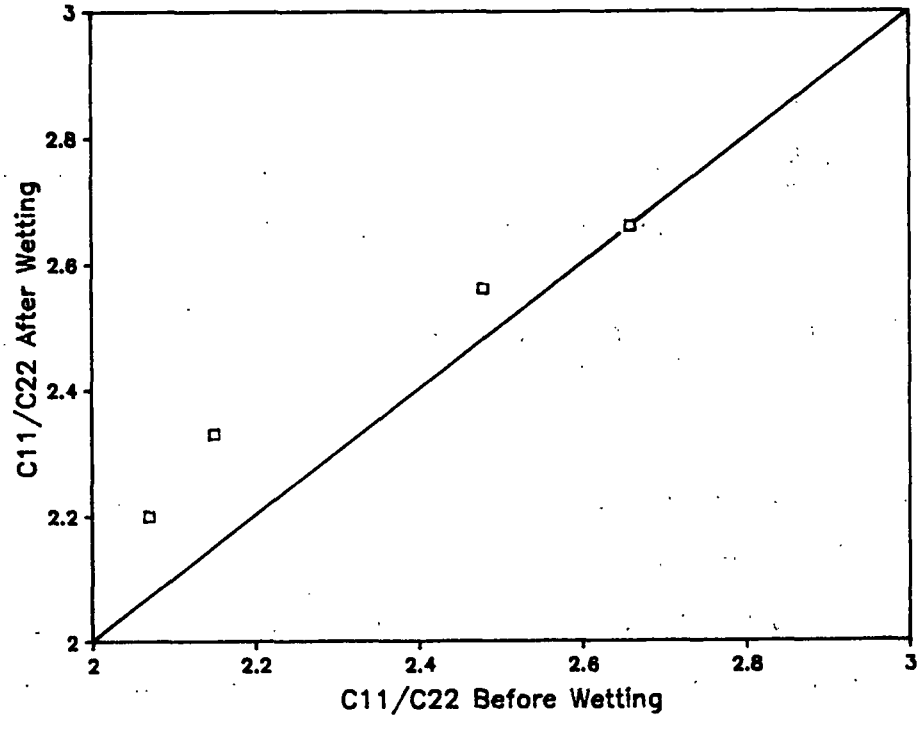

Figure 3. C_{11}/C_{22} after wetting vs. C_{11}/C_{22} before wetting.

The area enclosed by a polar diagram appears to be a useful quantity but the information perhaps may be expressed in a more meaningful way. By finding the radius of a circle having the same area, we can define an effective radius, or an "effective stiffness". That is, effective stiffness equals $(Area_{ellipse}/pi)^{1/2}$. At first glance the effective stiffness would appear to be similar to the geometric mean stiffness, defined as $(C_{11}*C_{22})^{1/2}$, but this

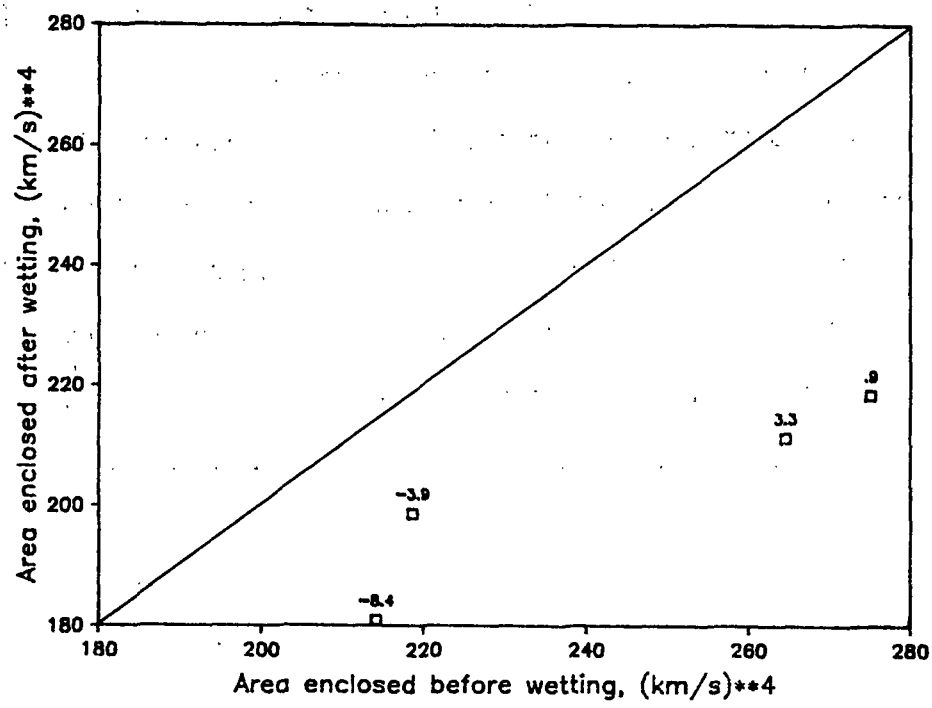

Figure 4. Area enclosed after wetting vs. area enclosed before wetting.

is not the case as shown in Fig. 5. The specific effective stiffness is larger than the specific geometric mean stiffness, which only takes into account the properties along the MD and CD directions. Later, in Fig. 21, we will see that the difference between the two quantities becomes larger as the polar diagram becomes more "peanut" shaped.

Fiber Orientation/Wet Straining Studies

In attempt to elucidate the effects of fiber orientation, wet straining, and drying restraints on the shape of the polar diagrams, sheets were prepared under various conditions and constructions. Two layer composite papers were made by wet pressing together Formette sheets having a nominal basis weight of about 100 g/m^2 and an elastic anisotropy of 1.62. The resultant 200 g/m^2 sheets were wet strained or dried under several conditions. Figure 6 shows the polar

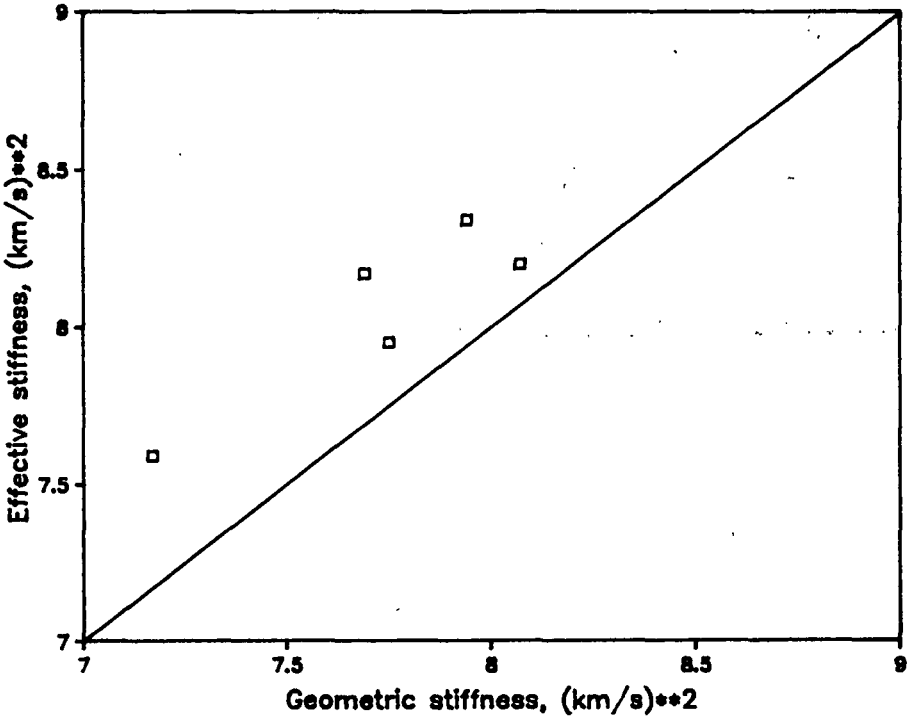

Figure 5. Effective stiffness vs. geometric stiffness.

diagrams from the four constructions and drying conditions. In sample A the two plies had their MD directions parallel and the sheet was dried under both MD and CD restraint. Sample B also had parallel plies, but the sheet was dried only under MD restraint. It was free to shrink in the CD. Sample C had parallel construction, but after wet pressing was strained about 2% in the MD, and then dried under both MD and CD restraint. In sample D the two plies were perpendicular to each other and the sheet was dried under both MD and CD restraint.

The shapes of the polar diagrams in Fig. 6 reflect the different constructions and drying situations. In A the elliptical shape is due to the anisotropy of the two layers (the C_{11}/C_{22} ratio is 1.54). Sample B, however, which was allowed to contract in CD while drying is starting to show a "peanut" shape similar to that observed in some commercial papers. In C the wet straining changes C_{11}/C_{22} to 2.05, but the elliptical shape is preserved. In D

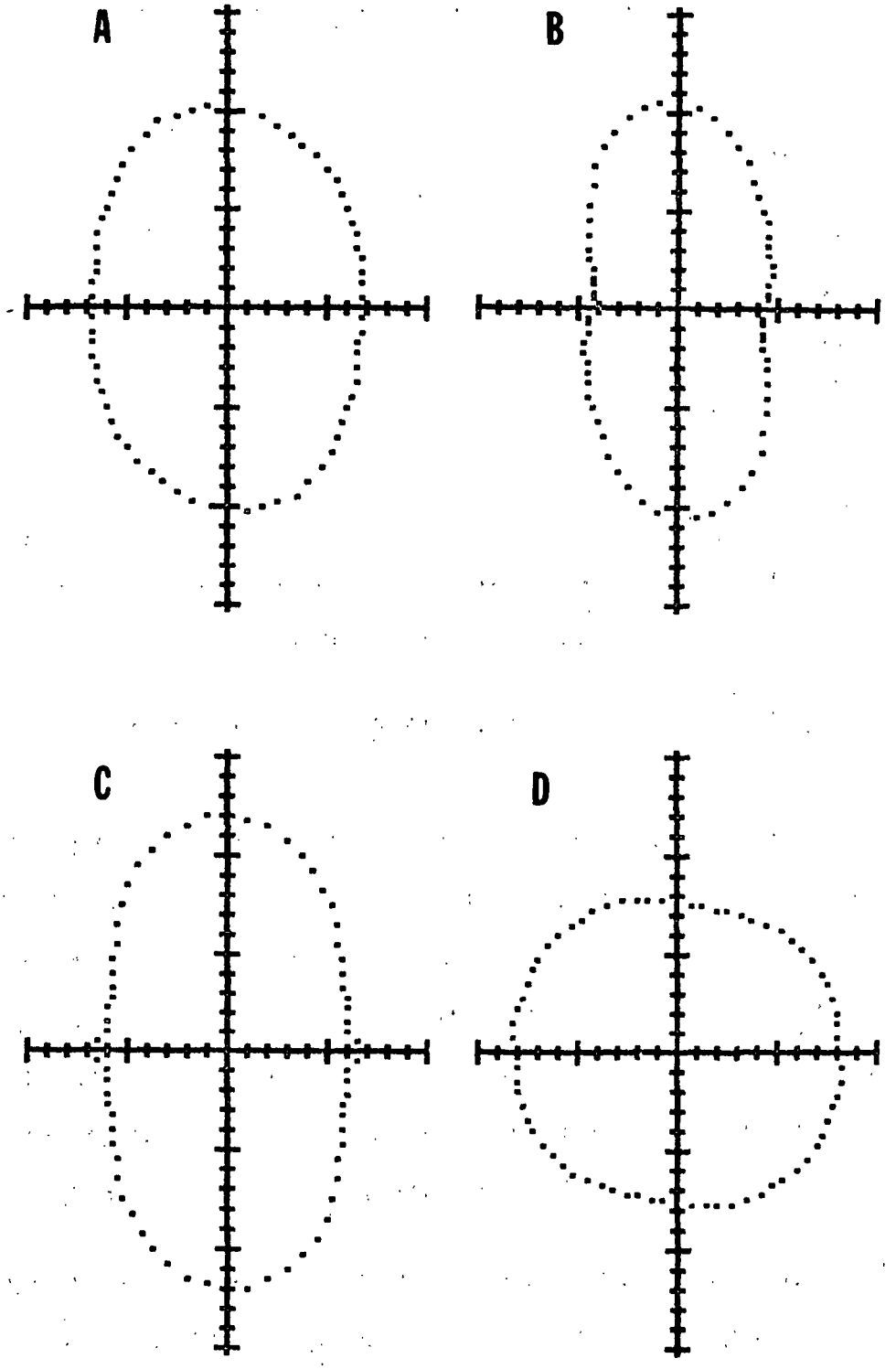

Figure 6. Polar diagrams of sheets made from 2 plies of oriented paper pressed together while wet. (A) Parallel plies dried under MD and CD restraint. (B) Parallel plies dried under restraint in MD only. (C) Parallel plies, strained about 2% in MD while wet and dried under MD and CD restraint. (D) Perpendicular plies dried under MD and CD restraint.

the crossed plies approach the circular shape which would be expected if there were no fiber orientation at all (C_{11}/C_{22} = 0.98).

Figures 7 and 8 plot MD specific stiffness or CD specific stiffness versus the MD dimensional change or CD dimensional change, respectively. As expected, MD stiffness increases with increasing dimensional change (caused by wet straining) and CD stiffness decreases with increasing shrinkage (negative dimensional change). The ZD specific stiffnesses were also measured for these sheets. Figure 9 shows this quantity plotted against MD specific stiffness. In these experiments, where MD stiffness is increased only by wet straining or the prevention of MD shrinkage, the ZD stiffness is seen to decrease with increasing MD stiffness. The results would be different in the case of increasing MD stiffness by increased wet pressing or refining. Figure 10 depicts ZD specific stiffness vs. the average dimensional change. The latter is simply the average of the MD and CD dimensional changes for each sample. Figure 10 again shows a decrease in the ZD stiffness as shrinkage decreases or for positive dimensional changes. As expected, the areas enclosed by the polar diagrams increase as one moves toward positive dimensional changes as shown in Fig. 11. The effective radius or effective stiffness, defined earlier, would behave in a similar way as shown in Fig. 12.

Figure 13 plots ZD specific stiffness versus effective thickness. For the wet straining and drying restraints used here, ZD specific stiffness decreases over 40% while MD stiffness is increasing about 20%. Figure 14 shows specific effective stiffness plotted against the geometric mean of the MD and CD specific stiffnesses. Again, as in Fig. 5, the effective value determined from the area of the polar diagrams is larger than the geometric mean value.

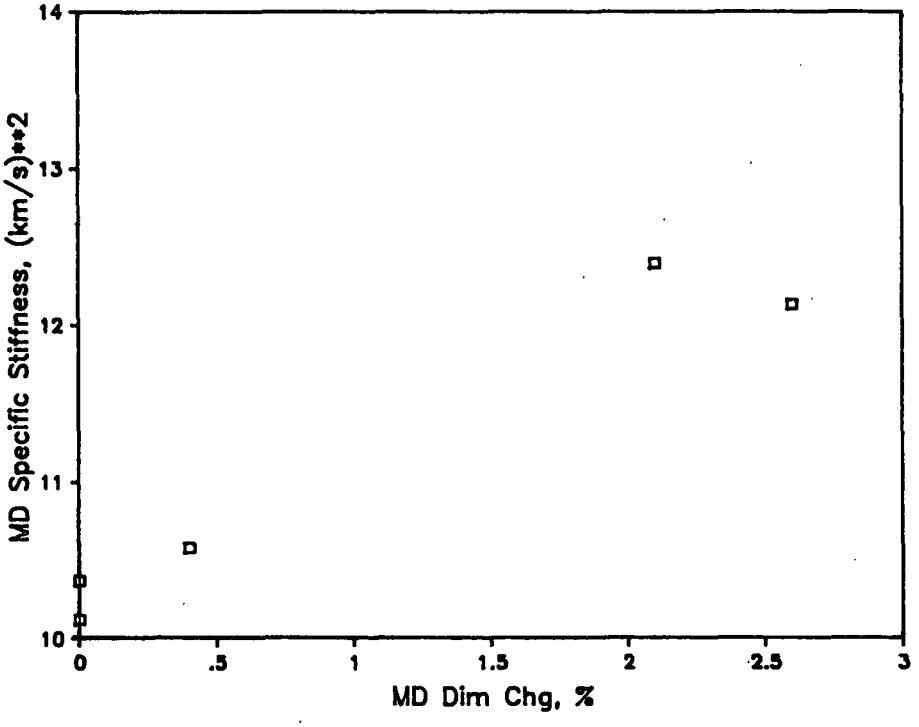

Figure 7. MD specific stiffness vs. MD dimensional change.

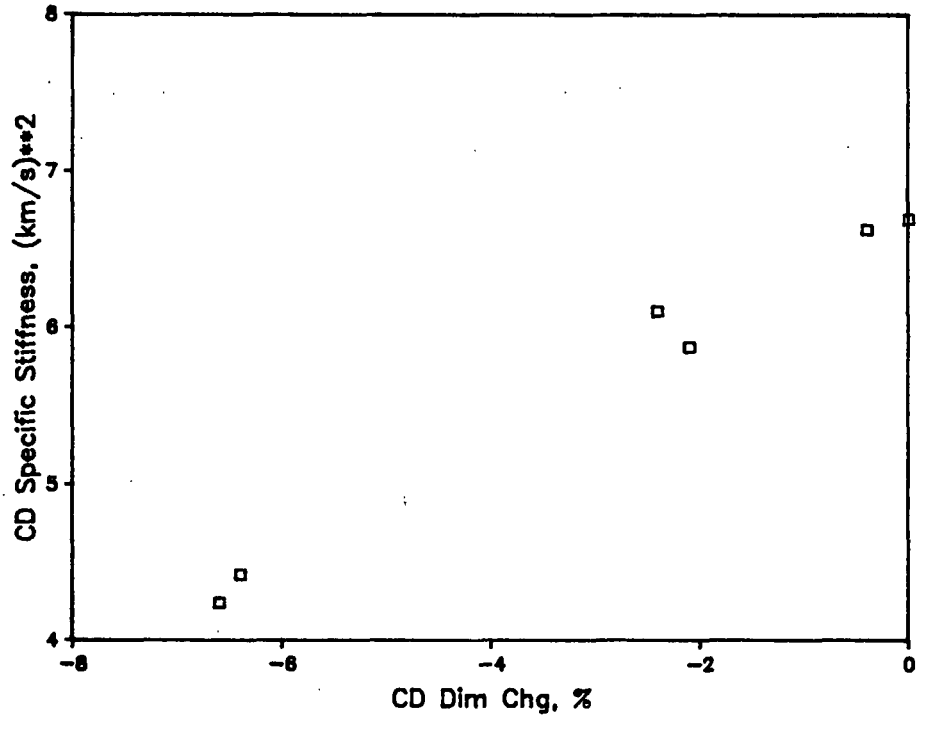

Figure 8. CD specific stiffness vs. CD dimensional change.

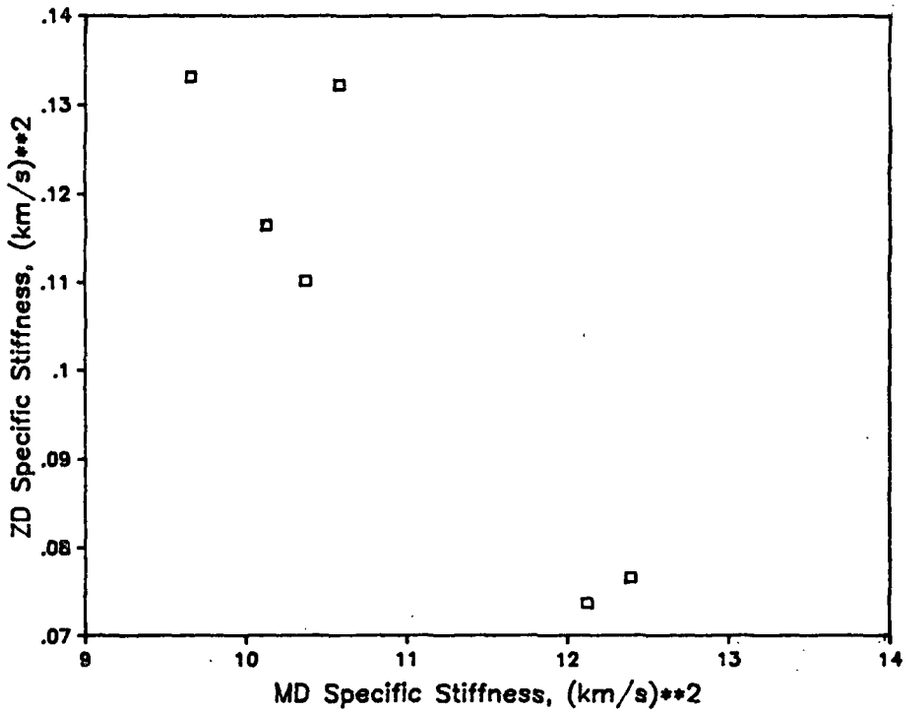

Figure 9. ZD specific stiffness vs. MD specific stiffness.

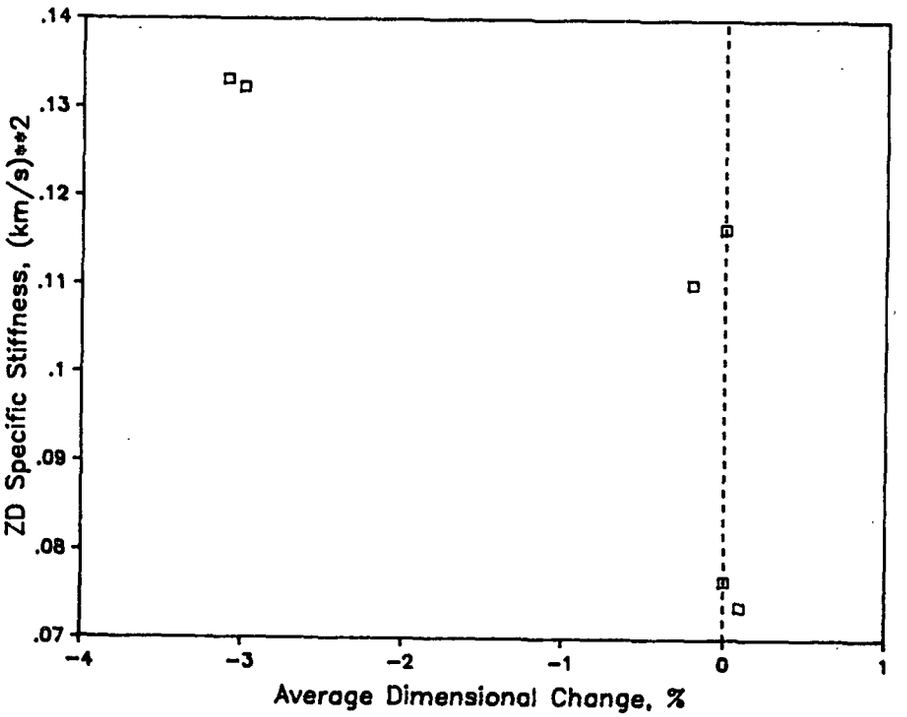

Figure 10. ZD specific stiffnes vs. average dimensional change.

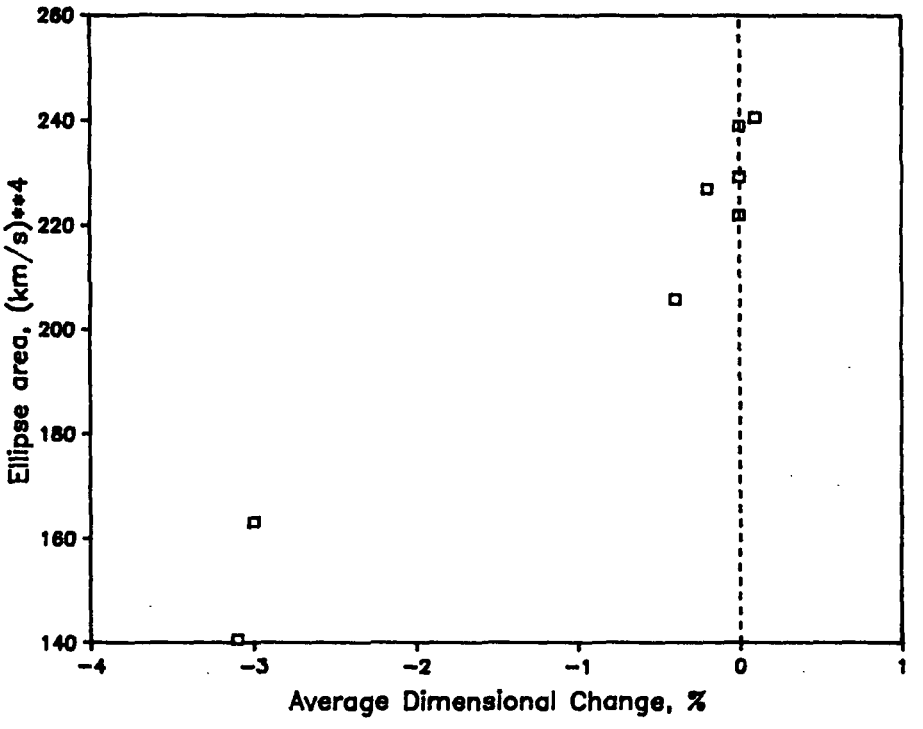

Figure 11. Ellipse area vs. average dimensional change.

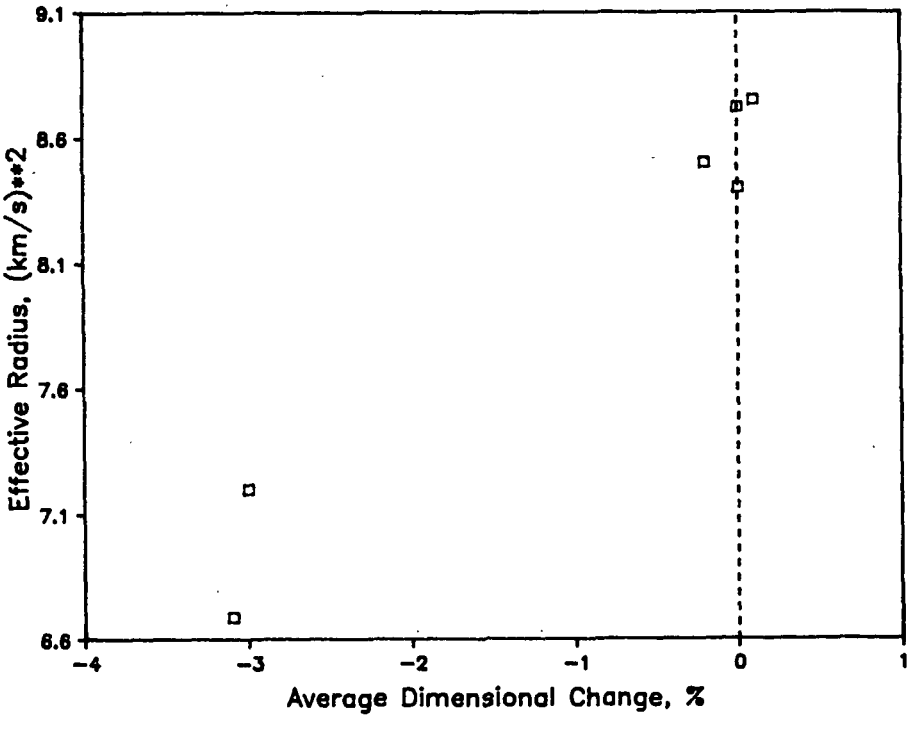

Figure 12. Effective radius vs. average dimensional change.

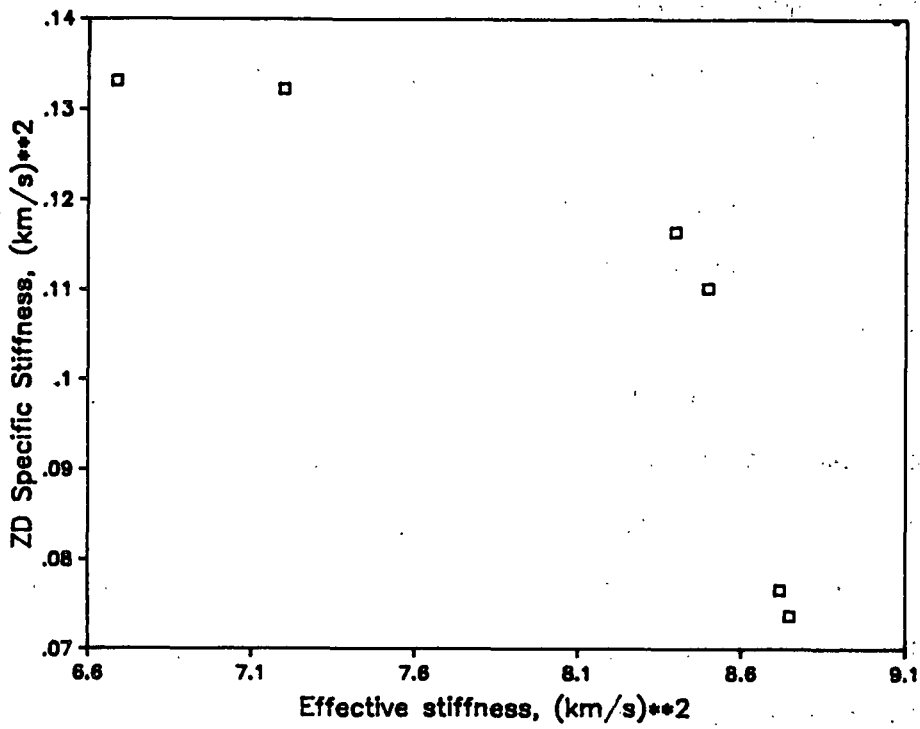

Fiugre 13. ZD specific stiffness vs. effective stiffness.

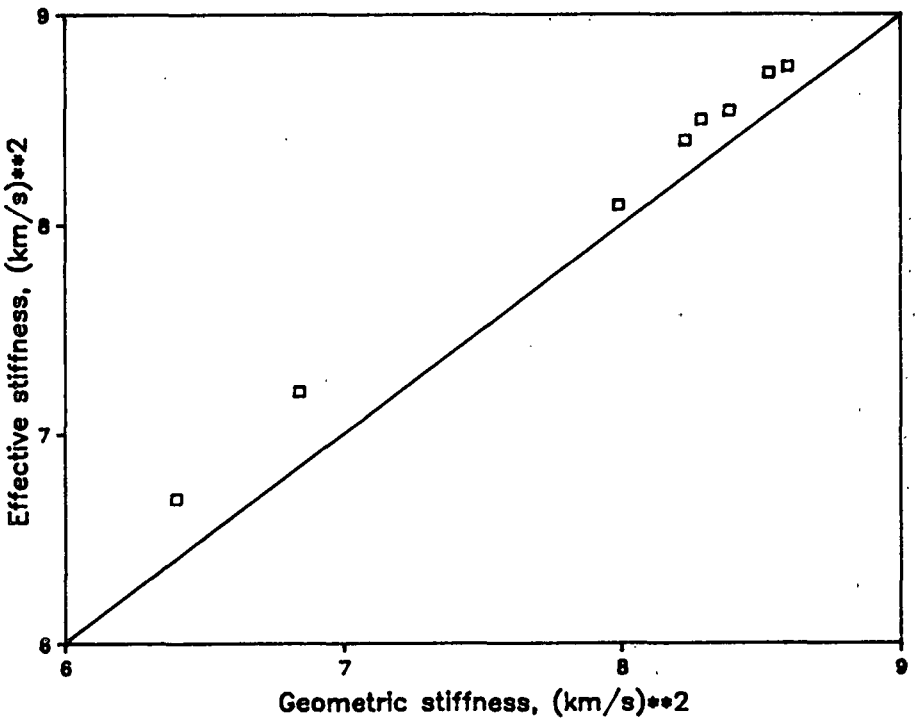

Figure 14. Effective stiffness vs. geometric stiffness.

Commercial Paper Samples

A large number of commercial samples have been tested. Most of these have been CD strips in which information about the nature of cross flows from the headbox was sought. Figure 15 shows one fine paper sample in which polar data was obtained every eight inches across the width of the machine. In this case the angular displacement is a maximum on the front side of the machine (about six degrees) and decreases gradually until it approaches zero on the back side. Such behavior is somewhat unusual in our experience. Figure 16 shows polar diagrams taken near the front side, near the center, and near the back side. In addition to the changing angle from the the MD, the area of the polar diagram at the center of the machine is noticeably larger than near the edges. This is depicted perhaps more clearly in Fig. 17 which plots area versus CD position. Together Figs. 15 and 17 again imply that no relationship exists between the area and angle of lean, consistent with the earlier conclusion based on the rewetting work.

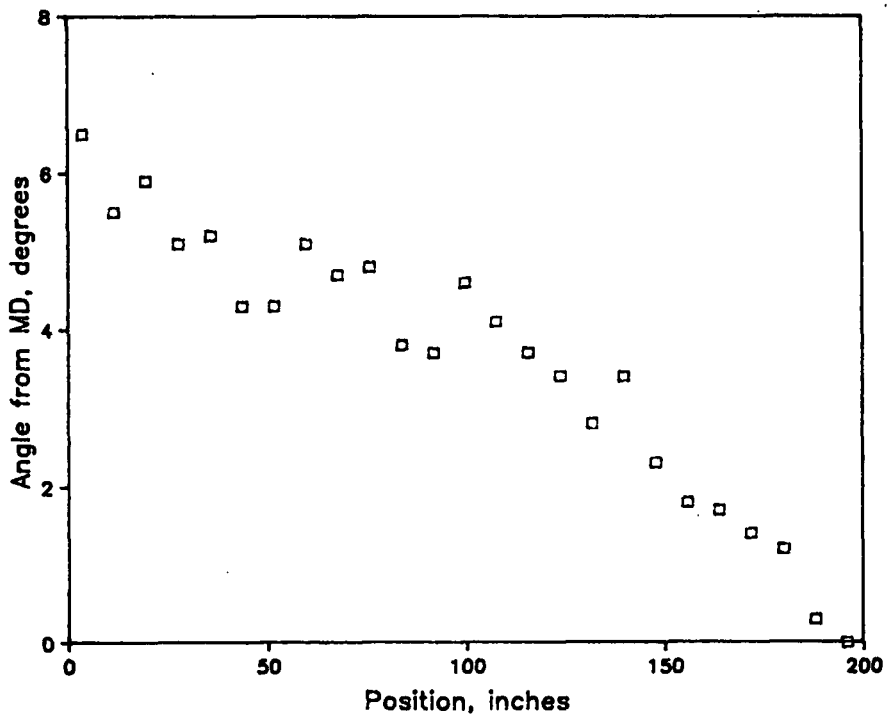

Figure 15. Angle from MD vs. position.

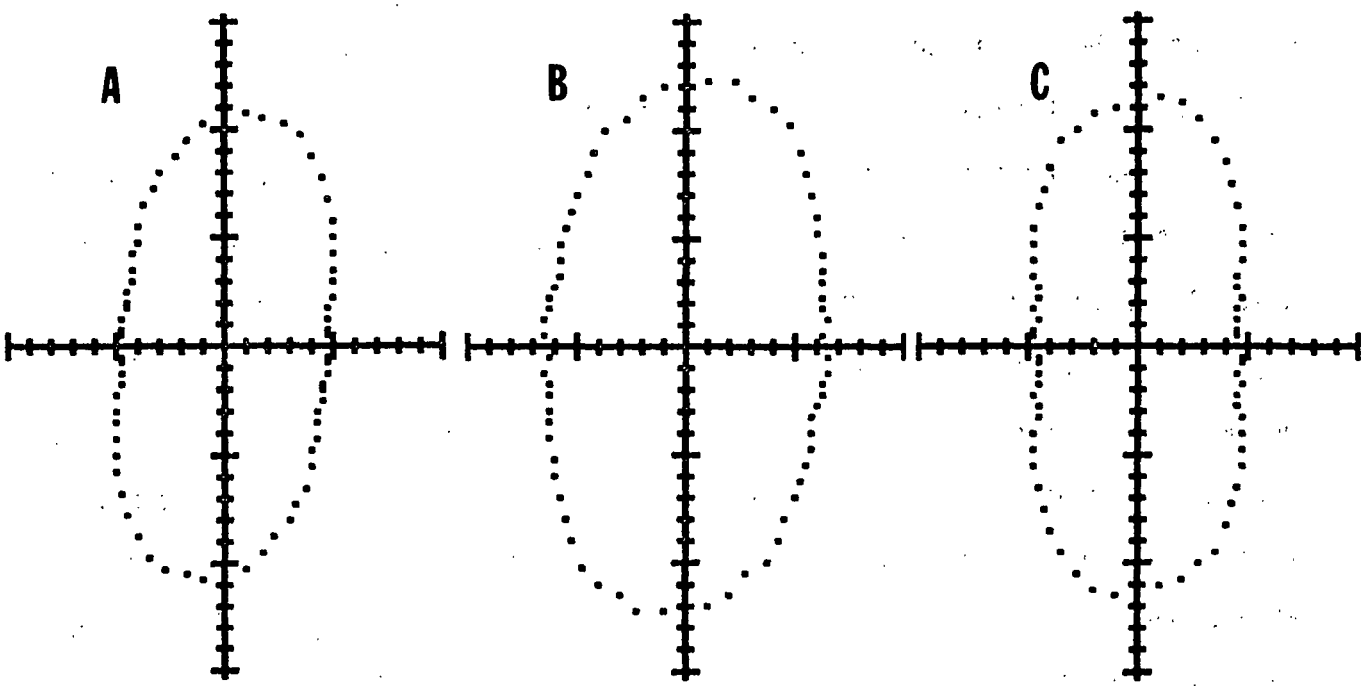

Figure 16. Polar diagrams taken from different CD web positions. (A) Near front side, (B) near center, (C) near back side.

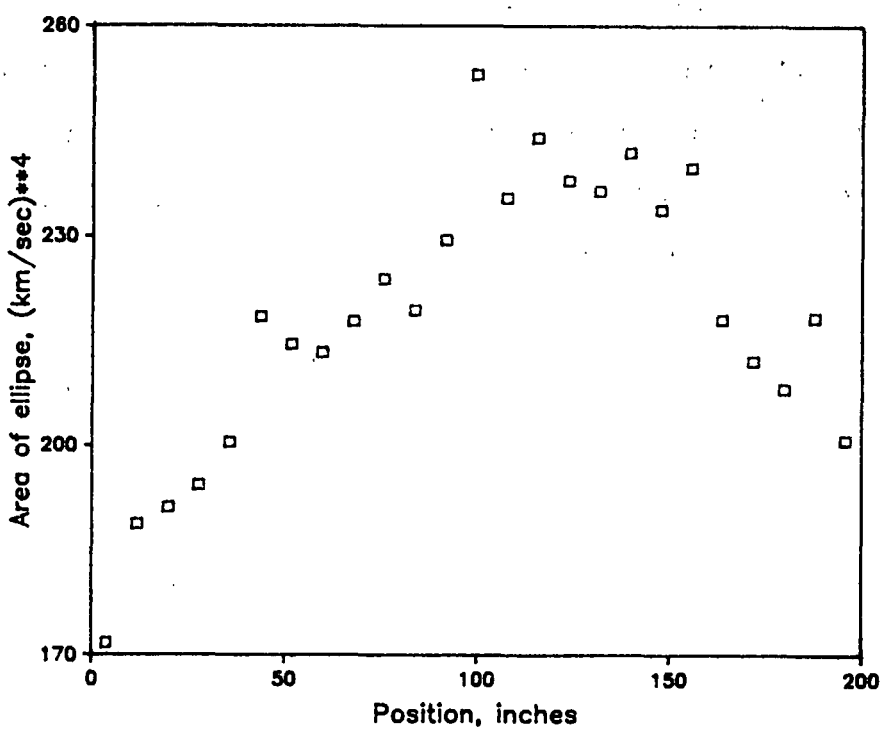

Figure 17. Area of ellipse vs. position.

Figure 18 shows the MD specific stiffness (top), the CD specific stiffness (bottom), and the geometric mean stiffness (center) as a function of CD position. The slight convex curvature is similar to that observed in many CD profiles of mechanical properties. Figure 19 compares the geometric mean specific stiffness and the effective specific stiffness as functions of position in the cross machine direction. As expected, in general, the latter quantity is slightly larger than the former all across the width of the paper machine. Figure 20, however, which shows effective specific stiffness plotted against the geometric mean specific stiffness, reveals that the differences between the two become larger at the lower stiffness levels. This probably just reflects the fact that, for the paper studied, using the geometric mean value for a "peanut" shaped profile or a "tipped" profile gives a value that is too low, while the effective stiffness value is independent of the profile shape or angle of inclination. In this respect the effective stiffness parameter may be a more meaningful quantity than the geometric mean. The observation that MD and particularly CD stiffness values may be misleading under certain conditions (leaning or "peanut" shaped polar diagrams) can also be seen in Fig. 21 which depicts C_{11}/C_{22} as a function of position. The increases in anisotropy ratio seen at the sides of the web would appear to arise because of low C_{22} values near the edges (see also Fig. 18).

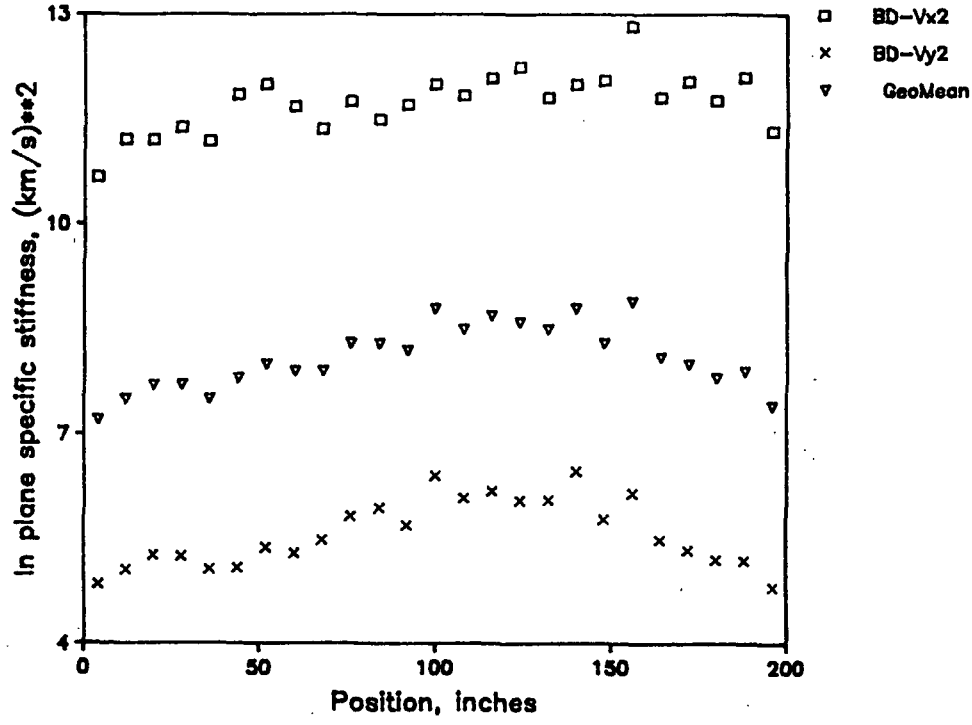

Figure 18. In-plane specific stiffness vs. position.

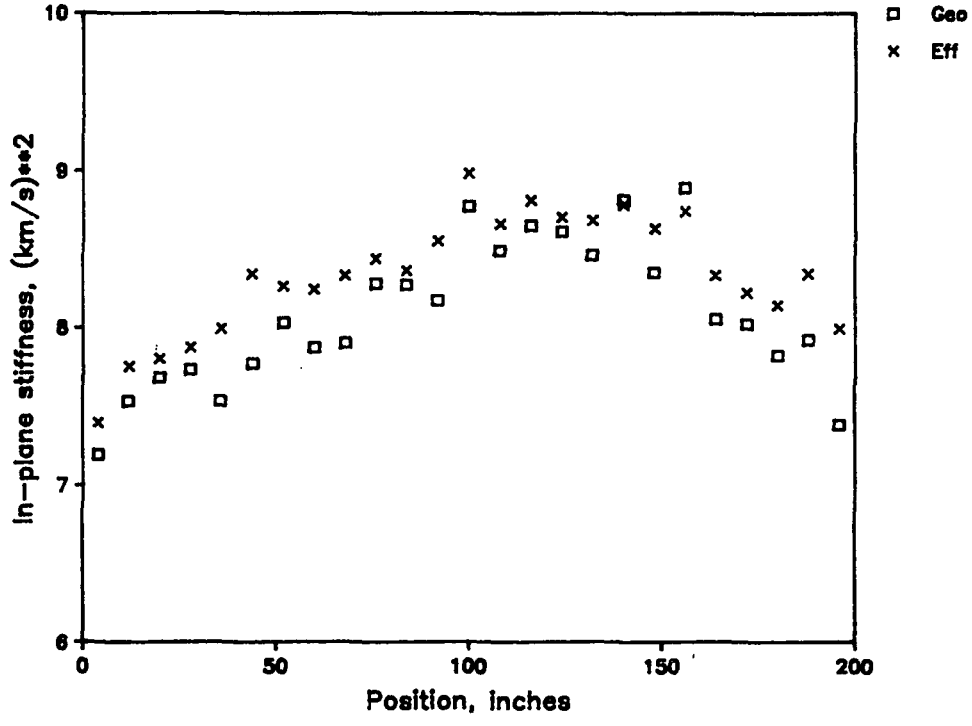

Figure 19. In-plane stiffness vs. position.

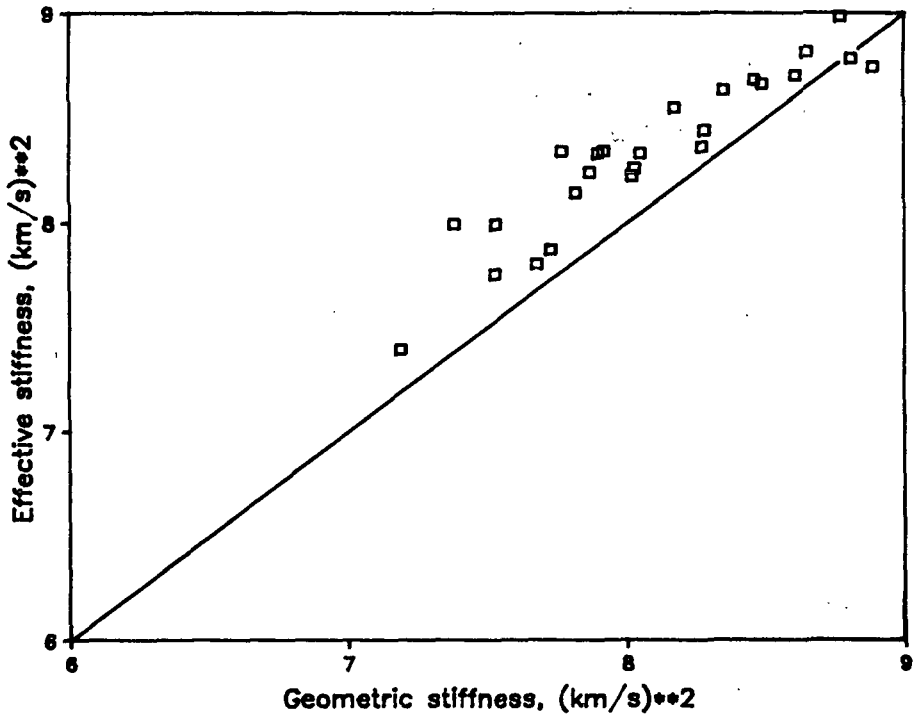

Figure 20. Effective stiffness vs. geometric stiffness.

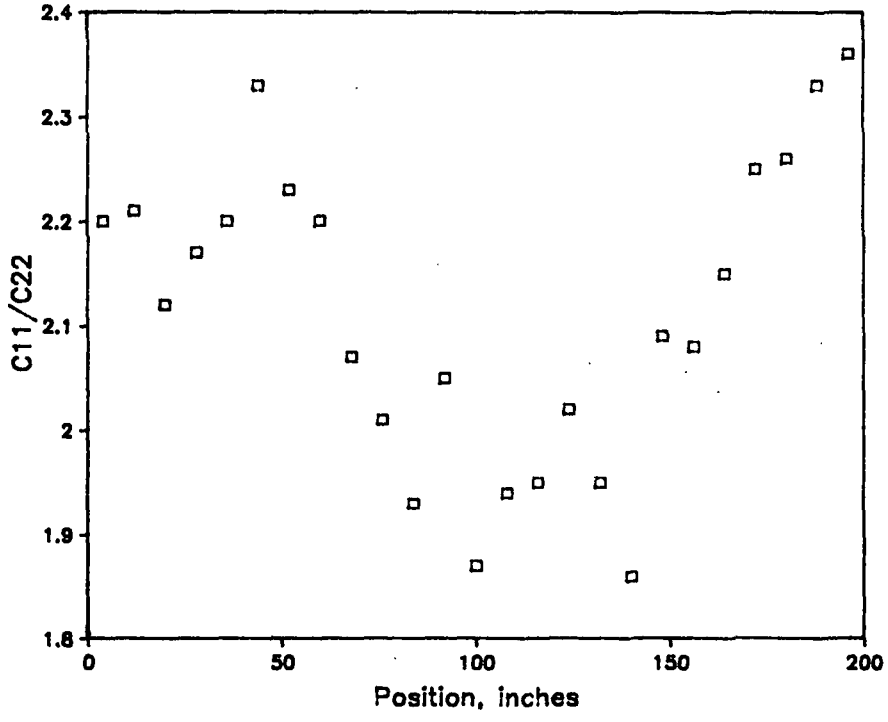

Figure 21. C_{11}/C_{22} vs. position.

SECTION 2

Improvements to the Automated In-Plane Ultrasonic Gage

Over the last six months we have made some changes to the robotic system that have increased its versatility and reliability. The most significant improvement is the use of a magnetic, linear motor to translate the transducer carriage. Originally we drove the carriage with a double-action air cylinder. Air driven stops engaged rachets to interrupt the carriage translation at prescribed locations. The timing of the stops was computer calibrated by translating the carriage and observing the motion through the turning of a potentiometer coupled to the translation. Maintaining proper timing required periodic (~ weekly) software and/or hardware adjustments. In addition the ratchet and stop translation scheme was the source of about 90% of our runnability problems. A major improvement in system reliability was achieved when we switched the translation drive to a linear motor. A linear motor is a magnetic driver head, mounted through rollers on a metallic platen. The driver translates 1/12000 of an inch each time an electrical pulse is sent to an electronic control module. We have removed the air cylinder drive mechanism and mounted the magnetic driver through ball joints to the transducer carriage. The platen is fixed so that pulsing the linear motor translates the carriage. Microswitches are used to detect the extremes of the permitted carriage translation. The computer "homes" the carriage by moving until a microswitch engages. The linear motor has performed flawlessly for about three months and eliminated the maintenance headache in operating the robotic gage.

Another improvement is the addition of a micrometer adjustment for the transducer drop. This allows rapid optimization of the transducer to the sheet coupling when non-standard thickness or modulus samples are tested.

We have also made a number of software enhancements. The most important is the development of a handsheet test. Here, the sample is assumed to be isotropic in-plane, and the sheet is sampled by platter rotation rather than carriage translation. Only two velocities (one shear and one longitudinal) are measured. The positioning of the transducer for the near spacing is maintained in the middle of the sample as the platter rotates. This means smaller samples (~6" in diameter) can be tested with no boundary reflection problems and with a complete sampling of the specimen.

Our immediate plans are to construct a second generation robotic system. We are now designing a few mechanical changes. The transducers will be dead-weighted and mounted in linear bearings. This will allow the transducer-to-sample coupling to be constant regardless of the caliper of the sample and will eliminate alignment adjustments. A manual adjustment for the platter rotation home setting will be added. A more compact design of the air cylinder relays is planned, and a cheaper, more powerful linear motor will be used. Off the shelf instruments will replace most of custom built electronics. Also, to speed operation and ease software development, the present Apple 2-E computer will be replaced by an IBM PC XT.

Figure 22, 23 and 24 show the current reporting forms for in-plane measurements on commercial sheets, handsheets, and polar diagrams, respectively.

Attached to this report as Appendix A is a paper which describes the automatic in-plane system.

Automation of Out-of-Plane Ultrasonic Velocity Measurements

In the last six months we have completed the development of our automated caliper and out-of-plane longitudinal velocity gage. This is a computer

THE INSTITUTE OF PAPER CHEMISTRY
TWO TRANSDUCER VELOCITY MEASUREMENT

OPERATOR :D BRENNAN
DATE :9 16 86
PROJECT: TEST 1

SAMPLE : H-600

MODE	TESTS	VELOCITY KM/SEC	ST DEV KM/SEC	V SQR KM2/SEC2	ST DEV KM2/SEC2	SIG AV
MD LONG	16	3.015	.087	9.10	.53	5
CD LONG	16	2.950	.076	8.71	.45	5
SHEAR	16	1.845	.043	3.40	.16	5
45 SHEAR	16	1.852	.026	3.43	.09	5

MODULI CALCULATIONS

MD-CD G. MEAN V SQR = 8.90 KM2/SEC2

STIFFNESS RATIO = 1.04
NUXY = .22
NUYX = .23

G. MEAN NU = .22

DENSITY = .622 GM/CM3

EX = 5.36 GPA EX/RHO = 8.62 KM2/SEC2
EY = 5.13 GPA EY/RHO = 8.25 KM2/SEC2
G = 2.12 GPA G/RHO = 3.40 KM2/SEC2

THE MD-CD G. MEAN E/RHO = 8.43 KM2/SEC2

Figure 22. Typical modulus printout from in-plane robotic system.

THE INSTITUTE OF PAPER CHEMISTRY
TWO TRANSDUCER VELOCITY MEASUREMENT

OPERATOR :D BRENNAN
DATE :9 11 86
PROJECT: HANDSHEET TEST

SAMPLE : Sa 2-1500

MODE	TESTS	VELOCITY KM/SEC	ST DEV KM/SEC	V SQR KM2/SEC2	ST DEV KM2/SEC2	SIG AV
LONG.	18	3.137	.057	9.85	.36	6
SHEAR	18	1.911	.014	3.65	.05	6

MODULI CALCULATIONS

NU = .26

DENSITY = .706 GM/CM3

E	=	6.49	GPA	E/RHO	=	9.19	KM2/SEC2
G	=	2.58	GPA	G/RHO	=	3.65	KM2/SEC2

Figure 23. Typical handsheet modulus printout from in-plane robotic system.

THE INSTITUTE OF PAPER CHEMISTRY
LONGITUDINAL SPECIFIC STIFFNESS (VEL SQR) VS ANGLE TO MD

OPERATOR: D BRENNAN
PROJECT : FREE DRYING TEST

DATE :9 17 86
SAMPLE : LB1 (11)

ANGLE DEGREES	VEL SQR KM2 / SEC2	STD DEV	ANGLE DEGREES	VEL SQR KM2 / SEC2	STD DEV
0	11.84	.67	90	4.04	.35
5	11.70	.53	95	4.03	.46
10	11.59	.56	100	4.06	.45
15	11.35	.70	105	4.02	.43
20	10.88	.76	110	4.08	.40
25	9.82	.53	115	4.21	.33
30	9.10	.60	120	4.41	.36
35	8.19	.49	125	4.66	.37
40	7.33	.39	130	5.03	.39
45	6.59	.39	135	5.49	.39
50	5.97	.48	140	5.99	.43
55	5.45	.46	145	6.66	.43
60	5.03	.44	150	7.36	.51
65	4.66	.37	155	8.14	.61
70	4.34	.31	160	9.04	.69
75	4.25	.31	165	9.96	.43
80	4.14	.31	170	10.71	.51
85	4.01	.30	175	11.38	.48

TEST PER 5 DEGREE INCREMENT = 16
THE ANGLE TO MAJOR PRINCIPAL AXIS = 5.0
AREA (KM^4/SEC^4) = 174.4

SIGNALS AVERAGED = 6
STIFFNESS RATIO = 2.93

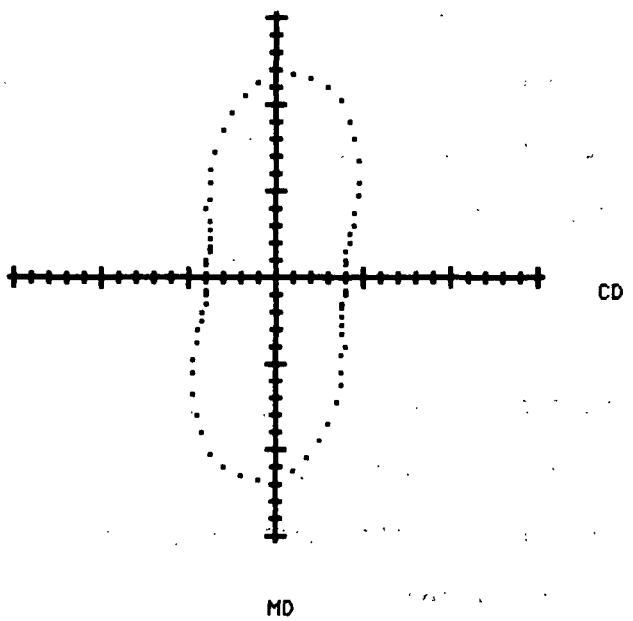

PLOT OF VEL SQR VS ANGLE AS SEEN FROM FELT SIDE

Figure 24. Typical in-plane polar plot.

(IBM PC XT) controlled instrument which allows rapid and repeatable characterization of ZD longitudinal velocity and soft platen caliper on paper samples.

The automated system is an extension of the manually operated gage which is composed of a caliper gage with neoprene faced, PVDF transducers attached to each jaw. When the jaws are manually closed, a caliper reading can be taken from an LED display and an ultrasonic pulse is passed through the sample. This signal is displayed on a Hewlett Packard 1980A digital oscilloscope. A signal, when thin aluminum foil was inserted, is stored by the oscilloscope. The signal through sample is manually offset to align a zero crossing with the foil signal zero crossing. The time translation necessary for alignment is taken as the time-of-flight differential. Longitudinal, ZD velocity is operator calculated as the caliper divided by the time-of-flight. This requires the operator to activate jaw movement, record caliper, adjust signal alignment, and record time-of-flight at a fixed time after jaw closure.

The idea of the automated system is to eliminate the majority of the operator functions. This is done by 1) interfacing the digital oscilloscope to a computer; 2) introducing the electronics to open and close the jaws on computer command; 3) interfacing the digital voltmeter, monitoring the LVDT on the caliper gage, to the computer; and 4) programming the computer to perform the necessary calculations. The finished system provides computer calibration of the caliper readings, a cross correlation velocity calculation, a reproduceable delay between jaw closure and sampling, and a printed report of all the results. The operator only needs to move the sheet to the sampling locations when the jaws are automatically separated.

A principal function of the system is the caliper measurement. In fact, the instrument can be operated (without the velocity measurement) simply as a caliper gage. In order to make accurate caliper measurements the instrument must be periodically calibrated. This is done by initiating a calibrate routine through the computer keyboard. The jaws are opened, and a thin shim of known thickness is inserted. The jaws are closed and after a prescribed delay the output of the digital voltmeter is read by the computer. The jaws open. A thick shim is inserted, and the digital voltmeter is read after the same delay. Assuming a linear relationship between voltage and caliper, the computer is now able to prescribe a caliper value to subsequent samples. Even though the loading time is constant, there is a small dependence of the neoprene conformability on the long-time loading history of the neoprene. To reduce this variability, a "warm-up" routine is provided. This merely cycles the jaws at the same rate encountered in testing. If the "warm-up" routine is run for about 15 minutes before testing and in intervals between tests, the neoprene deformation history is repeatable between cycles. Once "warmed-up" and calibrated, samples are simply moved to selected sampling locations as the jaws cycles. A major advantage of computer control is that sampling can be done at shorter delays from jaw closure. Initially the neoprene conforms rapidly and jaw separation changes relatively quickly. In manual operation, to get repeatable results, it was necessary to wait (~30 sec) until the voltage is changing very slowly to take a reading. With the more reproduceable timing of readings provided by computer control, it was possible to decrease the delay (to 5 sec) without sacrificing repeatability. This obviously reduces measurement time significantly.

To determine time-of-flight, the signal through the sample is compared to a signal through a thin (8 μm) aluminum foil. A reference signal through

the foil is recorded before starting velocity measurements and periodically during testing to reduce the effects of any electronic or mechanical drift. To do this, the "foil reference" routine is initiated. Here, the foil is inserted and the resulting signal is recorded after the proper loading delay.

After the caliper calibration is done and the reference signal is taken, sampling can begin. Since signal level and delay times vary greatly between samples, the first reading on a specimen must be used to adjust oscilloscope gain and predelay for subsequent testing. The first signal is taken with no predelay and at a low digitalization rate to assure that any reasonable signal will be recorded. The gain is adjusted so that the first peak is around 80% of full scale. The time of "zero-crossing" after the first peak is determined. The predelay for testing of this sample is adjusted until the first crossing will appear near the foil first crossing when the testing digitization rate of 125×10^6 samples/sec is instituted. Now testing begins in earnest. The jaws separate and close; so that, the first sample is tested after the correct delay. Both reference and sample signals are displayed on the oscilloscope and on the computer CRT with the different predelays. The two signals are multiplied together word-by-word and the result is summed. This is repeated at different sample signal delays until a maximum in the sum is located. The difference in reference and sample signal delays at sum maximum is the time-of-flight difference. Actually, the three largest sums are fit to a quadratic function, and the peak time of the quadratic is calculated in order to extrapolate between digitization points. The calculated delay time through the foil, 10 μsec, is added to the time-of-flight difference to get the time-of-flight. The predelay on the oscilloscope is now changed to align the reference and sample as determined by the above cross-correlation technique. This allows

the operator to monitor the computer's alignment procedure. After the first time-of-flight is calculated, the jaws open allowing the operator to test the rest of the sheet. After the set number of samplings are complete, the caliper and velocity results are printed. Figure 25 is a typical example.

The system has been checked out and evaluated. The results are very repeatable, and over a series of quite different samples the results differ from the manual technique (aligning zero crossings) no more than 2%. As the automated system does a full cross correlation on the entire pulses, it is insensitive to phase adjustments of the excitation pulse, and it is taken as the more exact definition of time-of-flight.

Fourier Analysis

A fundamental problem in time-of-flight measurements arises because the shape of the transmitted purpose is different through the foil than through the sample. The sample signal is dispersed since the higher frequency Fourier components of the pulse are preferably attenuated by the sample. This means that time-of-flight determination are somewhat arbitrary as there is no absolute way to line up the signals. The cross-correlation maximum is a good choice because it is sensitive to the total pulse. In fact it can be shown that, if attenuation varies linearly with frequency, the cross correlation velocity equals the average of the phase velocities of the Fourier components of the sample signal. However, the relative magnitudes of Fourier components depend on sample thickness and loss tangent and different samples are being effectively tested at different average frequencies. It would be better to compare the phase shift of each Fourier component and measure frequency dependent velocity directly. Amplitude measurements could also lead to frequency dependent loss tangent.

THE INSTITUTE OF PAPER CHEMISTRY
OUT OF PLANE LONGITUDINAL VELOCITY MEASUREMENT

OPERATOR: M Van Zummeren
DATE: August 15, 1986

PROJECT: 3332
SAMPLE: Liner sample

TEST NUMBER	CALIPER (microns)	DELAY (micro sec)	VELOCITY (km/sec)	V SQR (km^2/sec^2)
1	266.90	1.1352	0.2351	0.0553
2	272.10	1.2491	0.2178	0.0475
3	263.00	1.1470	0.2293	0.0526
4	266.70	1.1558	0.2307	0.0532
5	271.50	1.2089	0.2246	0.0504
6	269.80	1.1915	0.2264	0.0513
7	272.40	1.2007	0.2269	0.0515
8	259.01	1.0269	0.2522	0.0636
9	267.60	1.1413	0.2345	0.0550
10	261.61	1.0843	0.2413	0.0582
AVERAGE	267.1	1.1541	0.2319	0.0539
STD DEV	4.6	0.0643	0.0096	0.0045

GRAMMAGE (g/m^2) = 209.50
DENSITY (g/cm^3) = 0.784
C33 (GPa) = 0.042

STABILIZATION DELAY (secs) = 5
CALIBRATION VALUE (microns/volt) = 999.24
THIN SHIM THICKNESS (microns) = 8.0
THICK SHIM THICKNESS (microns) = 1576.0

FOIL CALIPER (microns) = 8.31
INTEGRATION WINDOW = 330

THE LARGE PROBES WERE USED

Figure 25. A typical printout for automated out-of-plane longitudinal velocity gage.

A fast Fourier transform routine has been added to software in the PC. We are just beginning to make frequency dependent phase velocity measurements and compare them with the cross correlation velocities. Preliminary results are very good and some data will be presented at the October meeting.

We are also hopeful of making loss tangent measurements at high loading pressures. To achieve this without over stressing the motor which raises the upper jaw, we have constructed disc transducers with a 0.25 inch instead of a 1.0 inch diameter. This allows the necessary pressures to be reached with the automated system. Some software modifications are being made to accommodate the new transducers. When this is complete, we will attempt to make loss tangent measurements and eventually try to correlate them with other physical properties.

SECTION 3

Loss Tangent Measurements

The elastic modulus of paper, like any viscoelastic polymeric material, has imaginary as well as a real part. Loss tangent is the ratio of the imaginary to real part. To date, our ultrasonic analysis of paper has dealt only with the real part. A valid characterization of loss processes in the paper by measuring loss tangent is yet to be developed. This would add a second dimension to our non-destructive characterization, and give parameters which might correlate with things like stretch, TEA, and lack of ply bonding in multi-layer sheets. At first, it seems that loss measurements are straight forward; simply measure the amplitude of the transmitted signal; correct for signal reflection at the transducer to sample interfaces; and calculate the loss per unit length in the sample. However, in practice the transmitted signal level is

strongly effected by the quality of coupling between sample and transducer, and signal level is more a measure of coupling than of loss processes in the paper.

Since the transducer to sample coupling has a profound effect on signal transmission, it is necessary to study this phenomena in detail. This might allow the coupling effect to be eliminated or accounted for, and the loss tangent might be measured. The following discussion is an effort to do this. It presents the results of a study of the ultrasonic coupling properties of soft rubber as a function of sample surface roughness and coupling pressure. It demonstrates that the rubber is a less than perfect coupling agent at pressures under a few atmospheres. This leads to small errors in time-of-flight velocity measurements and very large errors in sample attenuation characterizations. The coupling quality is shown to increase dramatically with pressure and to degrade when the sample surface is roughened. Large pressures (>500 kPa) will be necessary to obtain attenuation measurements, that characterize only bulk properties, on paper samples. A mathematical description which leads a single complex parameter for characterizing coupling quality, is presented.

Determination of the bulk acoustic properties of materials requires the coupling of piezoelectric transducers to a sample and the measurement of the resulting time and amplitude changes in a signal. To relate these measurements to the properties of the sample, the coupling at the transducer-sample interface must be characterized. The normal procedure is to assume "perfect" coupling. That is: (1) stress is continuous at the interface; and (2) the two surfaces are so well united that there is no slippage (deformation and velocities are continuous at the interface). From these two boundary conditions, the stress

reflection and stress transmission coefficients for a disturbance incident on the interface can be derived. The results are

$$T = 2Z_{TR}/(Z_I + Z_{TR}) \quad \text{and} \tag{1}$$

$$R = (Z_{TR}-Z_I)/(Z_I+Z_{TR}), \tag{2}$$

where Z_I and Z_{TR} are the mechanical impedances ($Z=\rho v=\rho\omega/k$) of the materials in which the sound is incident and transmitted respectively.

Consider the problem of finding the amplitude and phase changes in the Fourier components of a pulse transmitted through a sample coupled between identical transducers. If the acoustic properties of the sample and sample thickness are known, Eq. (1) and (2) can be used to find the amplitude change and time shift in the transmitted pulse in two special cases. The first case is when the duration of the pulse is smaller than the time-of-flight through the sample and only the first transmitted pulse is of interest. For each Fourier component of the incoming pulse, the transmitted signal is the product of the transmission coefficients at the two interface and the propagation coefficient through the sample:

$$S = T_T \rightarrow_S e^{-ik_s l_s} \; T_S \rightarrow_T = \frac{4e^{-ik_s l_s}}{(2 + Z_S/Z_T + Z_T/Z_S)} \tag{3}$$

where $k_S = \omega\rho_S/Z_S$, l_S is sample thickness, and ρ_S is sample density. The other situation, which leads to a simple result arises when the pulse duration is much greater than a single sample transit time. Here the partial waves from all possible multiple reflection paths contribute to the final phase and amplitude of the Fourier components in the transmitted pulse. Now

$$S = T_T \longrightarrow_S T_S \longrightarrow_T (e^{-ik_s l_s} + R_S^2 \longrightarrow_T e^{-3ik_s l_s} + R_S^4 \longrightarrow_T e^{-5ik_s l_s} \ldots$$

$$= T_T \rightarrow_S T_S \longrightarrow_T e^{-ik_s l_s}/ (1-R_S^2 \longrightarrow_T e^{-2ik_s l_s}) \tag{4}$$

Taking $T_T \longrightarrow_S$, $T_S \longrightarrow_T$, and $R_S \longrightarrow_T$ from equations (1) and (2), this becomes

$$S = 4Z_S Z_T / [(Z_S+Z_T)^2 e^{ik_s l_s} - (Z_S-Z_T)^2 e^{-ik_s l_s}] \quad (5)$$

For the special case of sample much thinner than one wavelength [$k_s l_s (Z_T/Z_S + Z_S/Z_T) \ll 1$], Eq. (5) reduces to

$$S = e^{-ik_s l_s}(Z_T/2Z_S + Z_S/2Z_T). \quad (6)$$

If the front plate of the transducer is sufficiently thick and its impedance, Z_T, is known, Eq. (3) or (5) could be used to calculate the complex impedance of the sample from phase and amplitude measurements on samples of appropriate thicknesses. Of course, all this relies on Eq. (1) and (2), i.e., the perfect coupling assumption.

The standard techniques to couple transducers and samples for acoustic characterization requires the use of adhesives or fluid coupling layers. These provide excellent acoustic bonds, making Eqs. (1) and (2) valid approximations. Once corrections are made for the couplant; the acoustic impedances of flat samples, which are impervious to fluids, can be determined. These approaches are, however, unacceptable for thin porous samples which imbibe fluids. The fluids change the effective acoustic properties of the sample by filling voids. They can also penetrate the matrix material, altering its bulk properties. In addition, the use of fluid couplants or adhesives often makes the test time consuming and destroys the sample. Therefore, there is need for alternate coupling techniques which will yield fundamental parameters for porous media and which are rapid and nondestructive.

Soft neoprene rubber is an alternative coupling agent. It conforms to rough surfaces and effectively transfers longitudinal motion into porous media. It does not damage the sample and is easily applied and released. However, it

is not obvious that it provides perfect coupling. Deviations from Eq. (1) and (2) could lead to errors when Eq. (3) or (5) are used to calculate the impedance. What are the extent of the errors; how are they effected by coupling pressure and surface roughness; and can imperfect coupling be characterized? These are the questions addressed below.

The purpose of the experiments is to measure the acoustic transmission through samples coupled to soft neoprene. The results are compared to those calculated using the perfect coupling assumption (Eq. (3) or (5)). Surface roughness and coupling pressure are varied and their effects on coupling are calculated.

The samples are placed between very broad banded piezoelectric transducers. The front face of the transducer is 0.125" thick neoprene ("super soft neoprene" of 5-10 durometer from Crane Packing Co.). The top transducer can be loaded to achieve variable coupling pressures, one transducer is excited with a single cycle, 1 MHz pulse. A disturbance passes through the sample and is detected by the second transducer. The received pulse is amplified and displayed on a digital oscilloscope. Transmissions through samples of different composition and thickness are compared by recording one signal and overlaying the other. The gain and time delay of the oscilloscope is adjusted until the two signals align. The oscilloscope has a one nanosecond time delay resolution and a 0.2% gain resolution. The amplitude ratio of the two signal is taken as one over the gain ratio and the 1 MHz phase difference is 2π times the delay difference divided by 1.0 μsec. A better procedure is to compare the amplitude and phase of the Fourier components of the two pulses. We have added Fast Fourier Transforms to our signal analysis capability, and we will soon be

repeating this experiment with a comparison of frequency dependent phase differences and amplitude ratios. For this study, however, we ignore dispersion assuming phase velocity and attenuation are frequency independent. On rough samples at low pressure the received signals can be significantly distorted, but in most cases the sample causes little distortion in the received pulse.

In order to study the efficiency of soft rubber coupling, samples of known thickness and acoustic impedance must be available. In addition, the acoustic impedance of the neoprene must be measured.

Aluminum foils comprise one set of samples. Textbook values for density and sound velocity are used to calculate an impedance of 17.3×10^6 kg/m^2sec (losses are assumed negligible). The thicknesses (7.95 μm, 15.5 μm, and 40.3 μm) were calculated from the textbook density and sample weights. For all thickness the pulse duration is much greater than the once through transit time and Eq. (5) is valid.

Plastic samples were also studied. They were made of polystyrene and Kynar. Polystyrene is an example of a plastic with little acoustic attenuation, while significant losses arise in the Kynar. The densities were calculated from the weights of regular shaped specimens. Phase velocities and attenuation coefficients came from transmission time and amplitude comparisions of samples about 1/8" and 1/4" thick. This is well into the thickness range where Eq. (3) applies. The phase shifts and signal losses due to poor coupling are independent of sample thickness and coupling effects should cancel in the measured time differences and amplitude ratios. These measurements, made as a function of loading pressure, are used to calculate the impedances in Table 1.

Table 1. Impedance as a function of loading pressure.

Loading Pressure (kpA)	Polystrene Impedance 10^6 kgm^2/sec	Kynar Impedance 10^6kgm^2/sec	Neoprene Impedance 10^6kgm^2/sec
50	2.392 (1+0.0168i)	3.388 (1+0.0248i)	1.585
95.7	2.399 (1+0.0109i)	3.405 (1+0.0301i)	1.609
137.6	2.402 (1+0.0089i)	3.400 (1+0.0313i)	1.625
226.4	2.404 (1+0.0048i)	3.404 (1+0.0302i)	1.639
318.2	2.408 (1+0.0045i)	3.409 (1+0.0311i)	1.643
405.7	2.410 (1+0.0034i)	3.419 (1+0.0309i)	1.648

The measured absolute values of the impedance increase slightly with pressure. This is taken as real and the later calculations of coupling efficiency accept this pressure dependence in the absolute value of impedance. Except for the lowest pressure reading the loss ratio is nearly constant for Kynar. The average value of the last six readings is used in all future calculations. The losses in the polystyrene appear to decrease with pressure. The higher pressure values are very low and are consistent with the known characteristics of polystyrene. I think that the large low pressure values are due to diffraction (beam broadening), and I will investigate this further in the future. At any rate the high pressure values are too small to have a significant effect on any later calculation, and for simplicity the imaginary part of the impedance of polystyrene is taken as zero at all pressures.

Neoprene density measurement were found by weighing a sample and finding its volume as a function of pressure in a mercury porosimeter. Measurements made to 2.7 x 10^4 kPa demonstrated that the rubber was almost incompressible: Density was 1108 kg/m^3 at atmospheric pressure and 1110 kg/m^3

at the top pressure. The neoprene density is taken to be 1108 kg/m^3 for these experiments. Velocity of sound measurement were made on the neoprene to complete the impedance calculation. The time-of-flight difference between a single 7.95 μm aluminum foil sample and an 0.125" neoprene sample sandwiched between foils were measured. A small correction for the extra foil transit time in the sandwich was made. Thickness measurements were made as the sample was tested. The velocity increased a few percent between 50 and 500 kPa leading to the rise in impedance with pressure reported in Table 1.

As will be shown, poor coupling generally leads to large decreases in transit signal amplitude and small changes in transit time. However, in the case of thin films this situation can be reversed. Consider Eq. (6) (the thin sample limit of Eq. (5)). The total phase shift is $\frac{1}{2}(Z_T/Z_S + Z_S/Z_T)$ multiplied by the once through propagation phase shift, $k_S l_S$. The transmitted pulse is the combination of multiple reflections back and forth through the sample, and the signal effectively goes through the sample $\frac{1}{2}(Z_T/Z_S + Z_S/Z_T)$ times. This number increases and with impedance mismatch and would be expected to be larger in the case of poor coupling. In the limit of Eq. (6), the foil causes no amplitude change and poor coupling should not greatly alter this.

As a test of rubber coupling, amplitude and time delay differences were measured for the 7.95 μm, the 15.5 μm and the 40.3 μm films. The mismatch between aluminum and the neoprene is large ($\frac{1}{2}(Z_T/Z_S + Z_S/Z_T) \approx 5$), therefore, the perfect coupling delay is about five times greater than the once through propagation time, $k_S l_S/2\pi$(1μsec). In Tables 2 and 3 experimental and perfect coupling theoretical (Eq. (5)) amplitude ratios and time differences between the thicker foils and the thin foil are tabulated. The results are the average of three runs. The standard deviations in the time differences are

Table 2. Time difference and amplitude ratio for 40.3 and 7.95 μm aluminum foils.

Pressure kPA	Time Theory nsec	Time Theory nsec	Amplitude Ratio Theory	Amplitude Ratio Exp.
50	27.23	46.3	0.9788	1.003
95.7	26.84	31.7	0.9795	1.011
137.6	26.59	31.3	0.9799	1.002
226.4	26.38	28.0	0.9802	0.992
318.2	26.32	28.0	0.9803	0.987
405.7	26.24	27.0	0.9804	0.986
494.6	26.21	26.7	0.9805	0.978

Table 3. Time differences and amplitude ratios for 15.5 and 7.95 μm aluminum foils.

Pressure kPA	Time Theory nsec	Time Theory nsec	Amplitude Ratio Theory	Amplitude Ratio Exp.
50	6.45	13.0	0.9975	1.002
95.7	6.35	8.0	0.9979	1.013
137.6	6.29	8.0	0.9917	1.003
226.4	6.24	7.3	0.9977	1.002
318.2	6.22	7.3	0.9977	0.999
405.7	6.21	7.1	0.9977	0.997
494.6	6.20	7.0	0.9977	0.997

about 2 nsec and those of the amplitude ratio are about 0.005. Notice that the experimental times are much greater than perfect coupling theory at low pressure, but approach agreement at higher pressures. Amplitudes are approximately equal to theory; however, they exhibit a significant decrease with pressure and are greater than 1.0 at low pressures. Agreement in both time and amplitude are excellent at the highest pressures, an indication that good acoustic coupling is possible without expoxies or fluids. Figure 26 is a log-log plot of the experimental time difference less the theoretical time difference all divided by the theoretical time difference vs. loading pressure for the 40.3 μm and 7.95 μm foils. The data approximates a single straight line with a slope of -3/2. Loading pressure appears to be an efficient method to improve coupling quality.

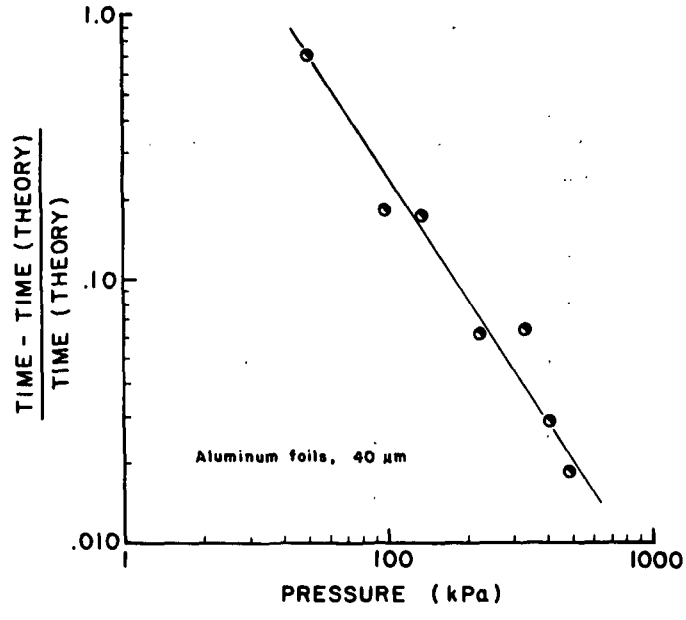

Figure 26. Pressure effects on aluminum-neoprene coupling (time).

The rest of the results are a comparison between plastic samples, thick enough to safely apply Eq. (3), and the 7.95 μm aluminum foil. Since time-of-flight measurements are typically done on samples greater than one wavelength long, these tests will directly relate to cases of most interest. The comparison is made to the thinnest aluminum since its effects on delay times and amplitude changes are minimal. (The comparison can not be made to a no sample condition, as the rubber edges deform less when a rigid sample is in between.) These results reflect primarily transmission through the plastic sample and are used to assess the consequences of pour coupling on time-of-flight velocity and attenuation measurements.

Five different plastic samples where tested. The surfaces of two, one of Kynar and one polystyrene, were flat. The other three were polystyrene samples with rough faces. Helical grooves covering about 50% of the two surfaces were machined into each sample. The depths of the grooves on the three rough samples were 0.001", 0.002" and 0.004" respectively. All samples were about 1/8" thick.

Theoretical (perfect coupling) time differences and amplitude ratios where calculated using Eq. (3) for the plastic and Eq. (5) for the aluminum foil. Comparisons of experimental and theoretical time differences and amplitude ratios are presented in Fig. 27 and 28.

There is little difference between experimental and theoretical time differences on smooth samples. Significant differences do arise on the rough samples but they appear to decrease at the higher pressures. The level of the high pressure plateaus on the rough samples depends on thicknesses measurements. These are done between soft rubber platens at 50

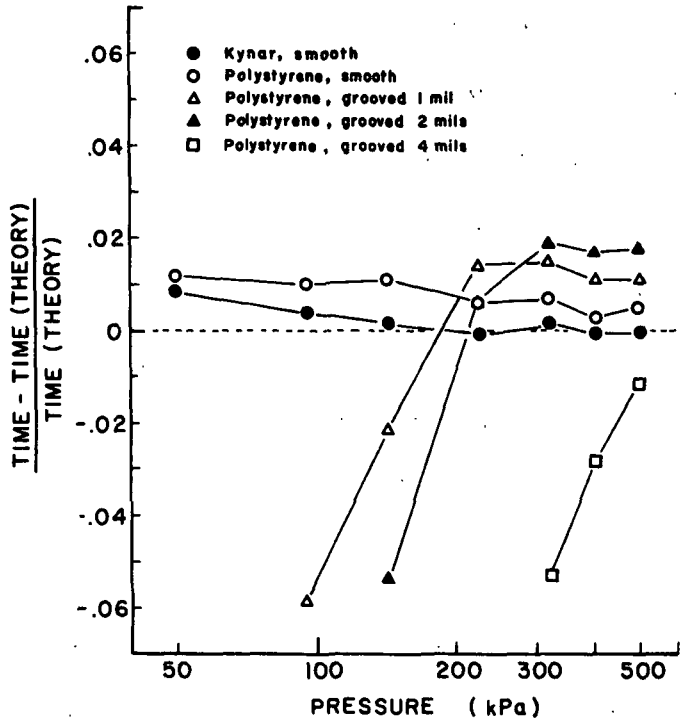

Figure 27. Pressure effects on plastic-neoprene coupling (time).

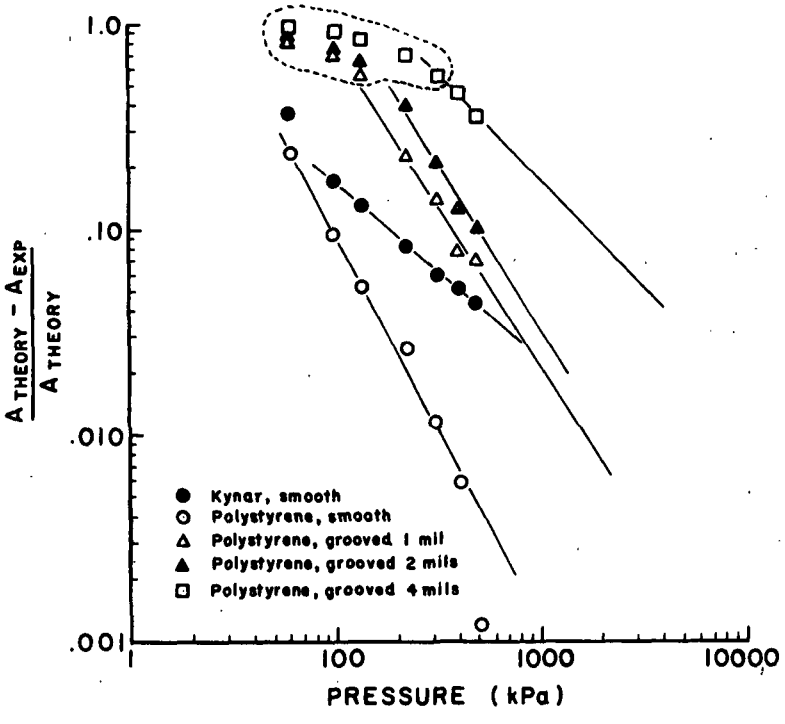

Figure 28. Pressure effects on plastic-neoprene coupling (amplitude).

kPa loading pressure. This is somewhat arbitrary; therefore, too much significance is not placed on high the pressure discrepancies between theory and experimental time differences. The coupling on rough samples seems to become satisfactory for time delay measurements at a threshold pressure that depends on roughness. The threshold is about 225 kPa for the 1 mil grooves, about 300 kPa for the 2 mil grooves, and maybe about 700 kPa for 4 mil grooves.

Amplitude difference between theory and experiment are much greater than time differences; however, they decrease rapidly with loading pressure. Notice that the plots for the polystyrene samples have approximately the same slope (Fig. 27) but are displaced to higher pressures with increased roughness. The circled data in Fig. 28 comes from distorted waveforms on rough samples at low pressure and should not be taken too seriously. As in the case of time delays on aluminum foil, increasing loading pressure appears to rapidly improve coupling efficiency. Roughing the surfaces causes large amplitude decreases which require large pressures for compensation. All this is taken to mean that time delay measurements and therefore phase velocity determinations are only slightly tainted by poor rubber coupling except at low pressures an for very rough surfaces, while amplitude measurements (and therefore loss calculations) are suspect except for smooth surfaces at high pressure.

Our ultimate concern is of course, to achieve valid measurements of phase velocity and loss angles in paper samples. Other materials were used here since their properties could be determined independently and coupling effects could be quantified. Direct determinations of the influence of rubber coupling are particularly difficult on paper for these reasons:

(1) Different thicknesses of paper samples with the same properties are not available and acoustic properties can not be determined independent of coupling, as they were for the plastics;

(2) paper properties change significantly with loading pressure, and a leveling off in a property vs. pressure plot can not be taken as a criterion for good coupling; and

(3) surface roughness is hard to characterize and to measure independently.

At this point I can only speculate on the errors introduced by poor coupling in paper samples.

For paper samples thick enough (>120 μm) for Eq. (3) to be valid, poor coupling probably causes little error in time-of-flight velocity measurements. Since fiber diameters are the order of 0.001 inch and the paper surface is more compliable than the plastic surface, I would think that the coupling quality of the 1 mil ridged polysytrene would be a conservative lower limit for paper. Typical paper samples have about one half the time delay of the polystyrene samples leading to larger percentage effect for the paper. None the less, if coupling pressure is over 100 kPa, I expect less than a one percent effect from poor coupling.

The conclusions are not so favorable for attenuation measurements. Assuming a loss tangent 0.04 in a paper sample 250 m thick having a phase velocity of 0.3 mm/μsec, the signal decreases by about 10% due to loss processes at 1 MHz. Notice that on the 1 mil ridged polystyrene there is a 7% effect at 500 kPa. This is of the order the total effect due to losses in a typical sample. If the sample were smooth the coupling error could be much less. However, remaining conservative, I conclude that pressures over 1000 kPa would be necessary to make reasonable loss measurements on paper.

In the past we have stated that increasing the pressure for out-of-plane measurements leads to a characterization of fiber properties and is less of an indication of the network structure. This conclusion comes from the observation that out-of-plane velocities become independent of process variables at high loading pressure. Therefore, it may be feasible to obtain a loss measurement on paper, that is independent of surface characteristics, but it will probably relate to the bulk properties of the fiber and not the fiberous structure.

In order to achieve the necessary pressures without excessively weighting the instrument, we are preparing to build transducers with smaller active areas. This, along with the Fast Fourier Analysis, will improve the quality and range of our longitudinal out-of-plane apparatus.

The main consequence of less than perfect coupling is to increase interface reflection coefficients and decrease transmission coefficients. To first order, this causes a decrease in signal amplitude on thick samples and an increase in delay time on thin samples. A natural thing to do at this point is to try characterize coupling in terms of a fundamental parameter. This requires a modeling of the less than perfect interface between rubber and sample. Two fundamentally different ways of doing this are apparent to me. One is imagine and interfacial region with a finite thickness and distinct acoustic properties. The other is to play around the boundary conditions. I pursued both of these. However, the second approach was the most fruitful; therefore, it will be discussed in detail, and I will only mention the limitations of the first.

The continuous stress and velocity boundary conditions lead directly to the perfect coupling formulae. Therefore, without interposing an interface,

the only way to develop different results is to the relax these boundary conditions. The continuity of stress boundary condition comes straight from Newton's second law, and without interfacial inertia it can not be altered. The continuity of velocity equation, however, does present possibilities. In fact slippage at the boundary is intuitively comfortable. Therefore, I make the following assumptions: (1) when an incident wave encounters a poorly coupled boundary, the velocity in the incident material will be larger by a factor, β, at the boundary than in the receiving material, and (2) the parameter, β, depends only on the coupling quality (surface characteristics and loading pressure) not on relative acoustic properties of the two media.

The transmission coefficient, T, and reflection coefficient, R, will now be found as a functions of β, Z_T, and Z_R under these assumption. Let a stress wave $P_I = e^{i(wt-kx)}$, be incident from material R to material T. The origin of the x-axis is taken at the boundary. The incident wave produces a reflected wave $Re^{i(wt+kx)}$, and a transmitted wave, $Te^{i(wt-kx)}$. The boundary conditions are:

$$1 + R = T \quad \text{and} \tag{7}$$

$$\beta[1/Z_T - R/Z_T] = T/Z_I \tag{8}$$

Solving these for R and T, gives

$$R = (Z_T - \beta Z_I)/(Z_T + \beta Z_I) \text{ and} \tag{9}$$

$$T = 2Z_T/(Z_T + \beta Z_I). \tag{10}$$

Comparing these with Eq. (1) and (2), the impedance of the incident material is effectively increased by a factor, β.

Now the poor coupling analogues of Eq. (3) and (5) are developed. For the thick sample limit, as before

$$S = T_R \longrightarrow_S T_S \longrightarrow_R e^{-ik_s l_s} \quad . \tag{11}$$

Substituting Eq. (10) into Eq. (11) gives the poor coupling version of Eq. (3),

$$S = \frac{4e^{-ik_s l_s}}{1 + \beta^2 + \beta(Z_S/Z_R + Z_R/Z_S)} \quad . \tag{12}$$

For a thin sample,

$$S = \frac{T_{R \longrightarrow S}\, T_{S \longrightarrow R}\, e^{-ik_s l_s}}{1 + R_S^2{}_{\longrightarrow R}\, e^{-2ik_s l_s}} \quad , \tag{13}$$

or

$$S = \frac{4Z_S Z_R(\beta Z_S + Z_R)}{(\beta Z_R + Z_S)[(Z_R + \beta Z_S)^2\, e^{ik_s l_s} - (\beta Z_S - Z_R)^2\, e^{-ik_s l_s}]} \tag{14}$$

in the limit of very thin samples, Eq. (14) reduces to

$$S = \frac{(\beta Z_S + Z_R)e}{(\beta Z_S + Z_S)\beta} \frac{ik_s l_s}{2}\left(\frac{Z_R}{\beta Z_S} + \frac{\beta Z_S}{Z_R}\right) \quad . \tag{15}$$

Physical intuition leads me to expect that the absolute value of β is greater than one. That is, slippage should lead to relatively less motion in the transmitted material. Also I wouldn't be surprised to see a phase lag from the incident to the transmitted material. This would give a positive (probably small) phase angle to β.

The differences between Eq. (3) and (12) and between equations (6) and (15) are qualitatively consistent with the experiments. For thick samples, the major effect of poor coupling (Eq. (12)) is to reduce the amplitude of the transmitted signal. This, of course, is exactly the conclusion from the experiments. For thin samples, using Eq. (15) we find that transit time is most sensitive to coupling, again agreeing with experiment. For the case tested (Z_S much larger than Z_R), the transit time is increased by poor coupling and the ampli-

tude is changed little (both theoretically and experimentally). Notice that when $Z_R > Z_S$ (the paper situation), Eq. (15) predicts that poor coupling would decrease the transit time.

Physical limitations can be placed on β by requiring that the acoustic power into the boundary be greater than or equal to the power out. For the case of real Z_I and Z_T, and unit input stress amplitude. The average power per unit area in less the average power out is

$$D = P_{IN} - P_T - P_R = \frac{1}{Z_I} - \frac{RR^*}{Z_I} - \frac{TT^*}{Z_T} \quad . \tag{16}$$

Substituting in R and T from Eq. (9) and (10) gives

$$D = \frac{1}{Z_I \left| Z_T + \beta Z_I \right|^2} [Z_T^2 + (\beta+\beta^*) Z_I Z_T + \beta\beta^* Z_I^2 + (\beta+\beta^*) Z_I Z_T - \beta\beta^* Z_T^2 - 4Z_I Z_T - Z_T^2]$$

$$D = \frac{2Z_T (\beta+\beta^*-2)}{\left| Z_T + \beta Z_I \right|^2} = \frac{4Z_T \beta (\mathrm{Re}(\beta) - 1)}{\left| Z_T + \beta Z_I \right|^2}$$

For the model to be physicaly acceptable the power in must be greater than or equal to power out, i.e., $D \geq 0$., Therefore, it is necessary that the real part of β be greater than or equal to 1. It seems reasonable that poor coupling (slippage) would lead to energy dissipatation and this is guaranteed if Re (β) >1. In fact, the ratio of energy lost to energy in, $4Z_T$ (Re(β)-1)/($Z_I \left| Z_T + \beta Z_I \right|^2$) is proportional to Re (β)-1.

The next step is to see if the slippage model is quantitatively consistent with the experiments. That is, are there values of β which yield the experimental phase shifts and amplitude ratios; do these values of β depend on coupling conditions (surface roughness, loading pressure, and rubber conform-

ability) and not on bulk acoustic properties; and are the calculated values of β physically reasonable?

The calculation of β from the two thicknesses of aluminum foil comparison is made by taking a ratio of two Eq. (14) signals (with different l_s's) and equating it to the experimental complex signal ratios. This reduces to a quadratic equation in β. One of the roots has Re (β) >1 and the absolute value and phase angle of the pressure dependence of these roots (for the 40.3 μm to 7.95 μm results) are plotted in Fig. 29 and 30 respectively. Notice particularly that by giving β a small positive phase angle which increases with poor coupling, its possible to explain the rather strange experimental amplitude ratios. That is, amplitude ratios may be greater than one at low pressures and decrease, dropping below 1, with better coupling. Physically, it seems reasonable that poor coupling should lead to a small phase lag in the transmitted medium.

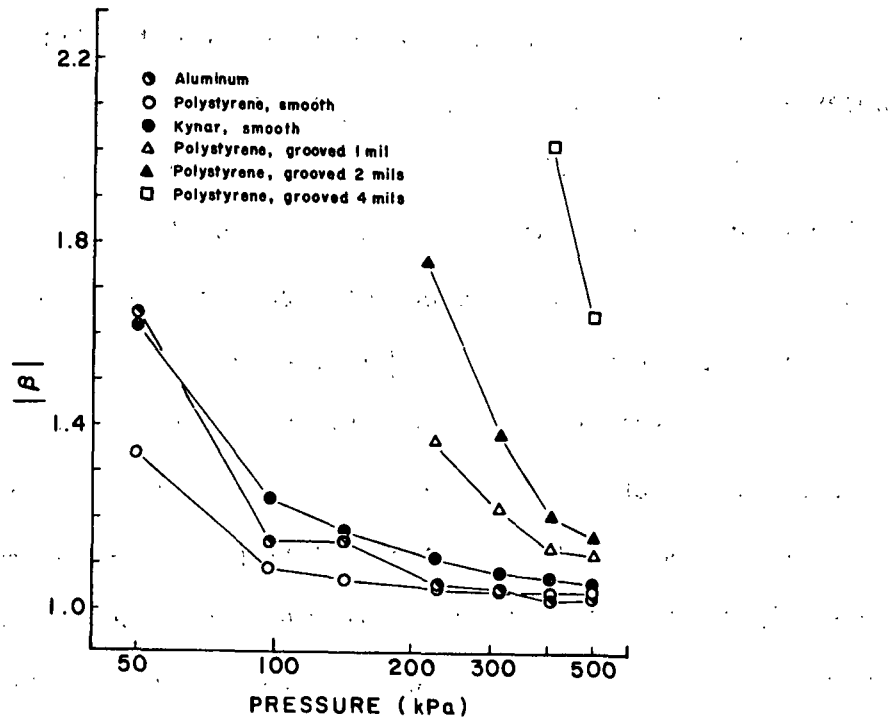

Figure 29. The absolute value of the coupling coefficient, β, as a function of loading pressure.

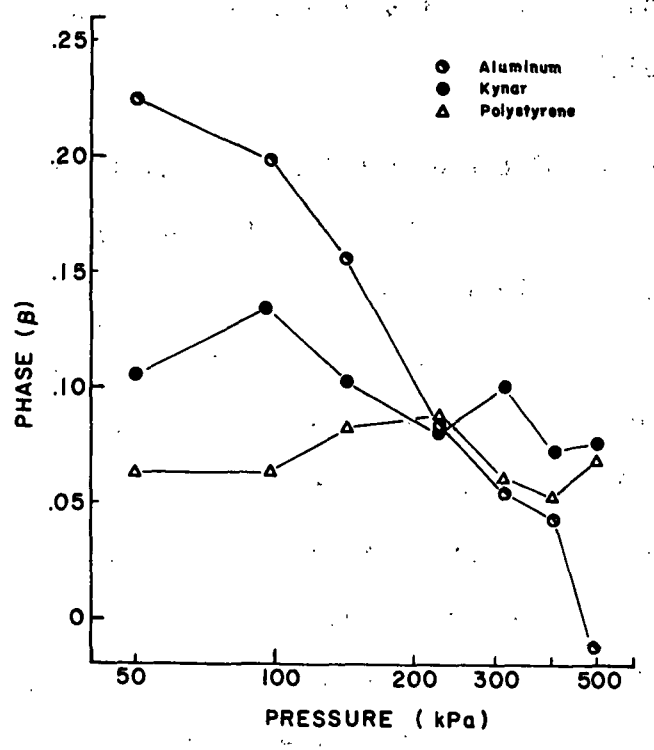

Figure 30. The phase of the coupling coefficient, β, as a function of loading pressure.

Values of β are also calculated from the thick plastic to thin foil comparison. This time the ratio of an Eq. (12) to Eq. (14) signal is set equal to the experimental ratio. The result is a cubic equation in β, but only one root has Re (β) >1. These results are also plotted in Fig. 29 and 30. It is encouraging that, regardless of the wide range in absolute value and phase angle of the sample impedances, the $|\beta|$ is the same, within experimental error, for all the smooth samples. The results of surface roughness is, of course, to increase $|\beta|$. For the thick plastic samples, the calculated phase angle is very sensitive to small absolute errors in sample thickness and time delay measurements. When determined from the aluminum foil comparison, β depends mostly on the amplitude ratio. I feel that the foil amplitude ratio is the more certain

measurement and conclude that the tendencies of the phase angle to increase with poor coupling (as shown for the foils) is the correct description of what is happening.

Even though it is a based on an arbitrary assumption, I feel that slippage model just presented is a particularly simple and effective way of describing poor coupling. With a physically reasonable choice of β, it is capable of predicting the amplitude and phase changes due to poor coupling in both thick and thin samples. It requires no artificial introduction of interfacial components, but merely a minor adjustment to a boundary condition.

I played with some other coupling models that gave less satisfying results. Variations from the perfect coupling equations can be achieved by mathematically introducing an interface with acoustic properties different from either material. In fact, there are two ways of producing interfaces: A thin section with uniform acoustic properties could be inserted; or a combination of lumped mechanical elements (masses, springs, dashpots) could perform the coupling. An example of a first case model is to think of a rough surface as a region partially of one material and partially void. The phase velocity in this region would be unchanged, but the mass density would be decreased. By adjusting the width and void ratio of the interface, equations analogous to Eq. (12) and (14) can be derived. These turn out to be unsatisfactory for two reasons. If it is assumed that the interface is much shorter than one wavelength, the only effect of this interface (or other first case assumptions) is to change the phase shift. This is obviously unappropriate in the thick sample case where amplitude decrease is the main experimental result of poor coupling. This model leads to no energy losses in the coupling process, a picture I believe is physically unacceptable. With sufficient patience, the approach of

inserting lumped parameters is capable of predicting any linear behavior. However, the resulting equations are much more complex and require more adjustable parameters. The parameters depend not only on coupling conditions but also on the bulk properties or the coupled media, and, finally, the use of springs, dashpots, and masses adds no physical insight into the coupling mechanisms.

APPENDIX A
IPC Technical Paper Series - Number 181
June, 1986

AUTOMATIC DETERMINATION OF ULTRASOUND VELOCITIES IN PLANAR MATERIALS

M. Van Zummeren, D. Young, C. Habeger, G. Baum and R. Treleven

Abstract

A computer-controlled, full-automated instrument which measures ultrasound velocities in planar materials is presented. By finding two longitudinal and two transverse velocities, it can completely characterize the in-plane elastic properties of an orthoropic sheet. Even though it is specifically designed to analyze paper and paperboard samples, other sheet materials can also be tested.

The authors are at The Institute of Paper Chemistry, P.O. Box 1039, Appleton, Wisconsin 54912, U.S.A.

Introduction

Paper and paperboard are orthotropic sheets whose mechanical properties are subject to paper machine process changes and variations in the furnished pulp. In-plane mechanical integrity (usually determined by strength testing) is important to end-use performance, and strength measurements are often used for quality control and to guide adjustments in manufacture. Even though failure testing is contrived to emulate the critical conditions which the final product must withstand, there are serious drawbacks to the standard practice of assigning strength tests as the indicators of mechanical quality. First of all, it is not feasible to test strength during manufacture; therefore, quality checks can be made only after samples are cut from a finished reel. For some grades, it requires about thirty minutes or more to make a reel of paper which weighs tens of tons and is worth tens of thousands of dollars. Since samples are only taken from the end of the reel, a very small portion of the product is characterized. Fifteen minutes can elapse before tests are completed and results are reported. Large quantities of product, which may be either substandard or needlessly over-built, are produced before any feedback is received. In addition, paper is non-homogeneous, and its strength properties have large variations. The number of tests performed in the allotted time is far too small to assign a reasonable level of confidence to the test average. This situation is greatly compounded if the papermaker needs to determine variations in strength profiles across the machine. Here is a clear case of too little testing coming too late, which can only be remedied with a computer-controlled, on-line measurement.

Before the principles of computer directed quality assurance and process control can be effectively utilized in the manufacture of paper, the standards for mechanical performance must be shifted from the traditional failure criteria

to other standards which can be applied nondestructively, rapidly, and on-line. The most fundamental and straightforward method to nondestructively assess mechanical behavior is to look at the relationships between stress and strain at small strains. The elastic parameters are the common representation of mechanical behavior in this linear regime, where on-line testing must be done. Therefore, elastic parameters are the natural choice to replace failure criteria as the standards for mechanical integrity during manufacture. Fortunately, this will not mean that the concept of strength prediction must be abandoned. In many cases paper strength is highly correlated to elastic parameters. This is particularly true for the less complex measurements, such as tensile strength[1] and compressive strength[2], in which elastic behavior is an important aspect of the failure mechanism. In fact, the prediction of strength from continuous, on-line elastic measurements may well be a better predictor of the strength properties of the entire reel than a few direct tests on sample from the reel end.

An effective way to determine elastic parameters of paper is to find the phase velocity of mechanical plate waves.[3,4,5] This technique is nondestructive, rapid, and has been demonstrated on-line.[6] As this technology is applied at the paper machine, a great need will arise for laboratory instruments which also measure ultrasonic velocities. These devices will provide the basis for on-line testing by allowing papermakers to understand the performance of their product in terms of elastic parameters. Aside from supporting on-line instrumentation, ultrasonic laboratory testing is important in its own right. It yields rapid, repeatable mechanical information without damaging the sample. It provides a complete set of in-plane elastic parameters including shear modulus and Poisson ratios, which are difficult to obtain in other ways.

The purpose of this paper is to describe an instrument which makes extensive laboratory testing feasible. It is fully automated and systematically determines the four independent in-plane elastic parameters of a sheet. It does the large number of repetitions necessary on inhomogeneous samples without being labor intensive. It is computer controlled, making it versatile and easily adapted to special needs.

Background

The measurement of ultrasound velocities is a powerful technique for nondestructive analysis of the mechanical properties of polymeric and other materials. Often, the phase velocity of plane wave propagation of sound through a material is equal to the square root of an elastic stiffness divided by the mass density. Therefore, the value of a mass specific elastic stiffness can be obtained from velocity calculations. Of particular interest here are planar materials. These are defined as plates whose lateral dimensions are large compared to the wavelength of bulk sound waves propagating in-plane and whose thickness is small compared to the wavelength of out-of-plane bulk waves. If the lateral dimensions of a sheet are much greater than the thickness, it is usually possible to find a frequency range in which the plate can be approximated as a planar material. Because of asymmetry in fabrication, the mechanical properties of paper (and many other polymeric sheets) are different along the direction of manufacture (the MD) than perpendicular to the direction of manufacture (the CD). Often, these sheets have orthotropic symmetry. That is, there are two orthogonal principal directions (the MD and CD) and the material has reflectional symmetry about planes determined by a principal axis and the sheet normal. If the frequency is low enough to consider the plate to be planar, symmetric plate waves are nondispersive.[7] The motions constituting these disturbances have a small

out-of-plane component, but they are mainly along the direction of propagation when traveling in a principal direction. Such modes will be called longitudinal. The velocity of a longitudinal wave in a principal direction is the square root of a planar stiffness divided by the density, i.e., in the MD, $V^2_{Lmd} = C'_{11}/\rho$, and in the CD, $V^2_{Lcd} = C'_{22}/\rho$. A planar stiffness is defined as the small strain limit of the ratio of the normal stress to the normal strain when there is no out-of-plane stress and no strain in the other principal direction. Transverse plane waves also propagate along the principal axes of the plate. Their motion has no out-of-plane component and is entirely along the principal axis perpendicular to the propagation direction. These modes are nondispersive at all frequencies, and the velocity squared in both principal directions is the shear stiffness, C_{66}, divided by density.[7] If desired, engineering elastic parameters can be calculated from planar stiffnesses.

Since the longitudinal and transverse modes in planar materials are nondispersive, time-of-flight velocity measurements can be used to characterize the elastic properties of the material. An orthotropic planar material has four independent elastic parameters, and four independent velocities must be measured to completely define the elastic behavior of the planar material. Three of these are the longitudinal in the MD, longitudinal in the CD, and transverse in the MD or CD. These comprise all the modes along principal axes. The fourth velocity measurement cannot be along the MD or CD. Plane waves which are not in a principal direction have in-plane components along and perpendicular to the propagation direction. If the sheet is not overly anisotropic, there is a plane wave, the quasitransverse mode, that displaces nearly perpendicular to the direction of propagation at all angles to the MD. Its velocity at 45 degrees to the MD can be the fourth measurement. However, there is a complication and this selection

needs justification. Even though off-axes normal modes in orthotropic materials are nondispersive (phase velocity and group velocity are equal and frequency independent), the time-of-flight velocity measured between point sources does not equal the phase velocity.[8] Roughly, this is because the path of least delay is not along the straight line from transmitter to receiver. There can be significant differences between the time of flight velocity and the plane wave phase velocity for quasilongitudinal waves. This is because quasilongitudinal phase velocity can vary rapidly with angle in highly anisotropic sheets. Fortunately, quasitransverse velocities change only a few percent between MD and CD. Thus, assuming that the measured velocity is related to elastic properties by the phase velocity equation leads to only small errors. The relationships between the engineering elastic parameters and the phase velocities are[3]

$$G/\rho = V_S^2 \tag{1}$$

$$\nu_{12} = \left(\left\{\left[2V_S^2(45°) - 1/2(V_{Lmd}^2 + V_{Lcd}^2) - V_S^2\right]^2 - \left[1/2(V_{Lmd}^2 - V_{Lcd}^2)\right]^2\right\}^{1/2} - V_S^2\right) / V_{Lmd}^2, \tag{2}$$

$$\nu_{21} = \nu_{12}\, V_{Lmd}^2 / V_{Lcd}^2, \tag{3}$$

$$E_{md}/\rho = V_{Lmd}^2/(1-\nu_{12}\nu_{21}), \tag{4}$$

$$\text{and } E_{cd}/\rho = V_{Lcd}^2/(1-\nu_{12}\nu_{21}). \tag{5}$$

Here, V_{Lmd} and V_{Lcd} are longitudinal velocities in the MD and CD, V_S and $V_S(45)$ are the transverse velocities in the principal directions and at 45°, respectively, ν's are Poisson ratios, E's are Young's moduli, and G is the shear modulus.

General description

This section provides an overview of the operation of the instrument. The specific details, organized by function (acoustic, mechanical, electronic, and programming), are discussed later.

The purpose of the instrument is to find the time-of-flight velocities of transverse and longitudinal plate waves in sheets. Fig. 1 is a schematic diagram of the apparatus, and Fig. 2 is a photograph of the system. Ceramic piezoelectric transducers placed on the surface of the sheet are used to couple mechanical energy into and out of the sample. A sinusoidal voltage pulse is applied to one transducer, the transmitter, which oscillates and sets up wave motion in the sample. A second transducer, the receiver, responds as the disturbance reaches it a short time later. The receiver signal is amplified, digitized, and transferred to a computer, which displays it as a function of time on a CRT. The computer analyzes the signal and adjusts the gain of the amplifier so that the full range of the A/D is used without saturation. This transmitter pulse and receiver signal analysis sequence is repeated for the number of times selected by the operator. Each receiver pulse is superimposed on the original CRT display. Under computer control, the transducers are lifted off the sheet, their separation distance is increased, and they are lowered back on to the sample. The signal analysis routine is repeated and the "far" signals are also superimposed and displayed on the CRT but below the "near" signals. The computer averages both the near and far sequences and replaces them with averaged signals. The computer then cross-correlates the two signals and finds the time shift which has a maximum in the cross-correlation function. The time-of-flight velocity is calculated by dividing the difference in transducer separations by this time shift.

The transducers are then lifted and returned to the near separation, completing one velocity measurement.

(Fig. 1 and 2 here)

The transducers oscillate in the plane of the sample, and it is possible to detect transverse or longitudinal waves by aligning the direction of oscillation perpendicular to or parallel with the transducer separations. The computer can initiate a rotation of the transducers by 90 degrees to alternate the mode of propagation detected. The computer can also translate the carriage holding the transducers laterally across the sheet. By moving the carriage, the sheet can be tested at a number of locations, and average values and variances can be calculated. Finally, the sample is attached to a rotating base driven by a stepping motor. The computer activates the stepping motor, permitting wave propagation velocities along different sheet axes to be measured. In all, the computer can (1) raise and lower the transducers, (2) choose between two transducer separations, (3) move the transducer carriage over the sample, (4) rotate the sample holder, and (5) rotate the transducers by 90 degrees.

The most common test determines the four independent in-plane elastic parameters. Before testing begins, the operator selects the number of received signals to be averaged and the number of locations, N, on the sheet, over which each velocity is to be averaged. A sample is cut with its edges parallel to the principal axes and placed in the rotating sample holder. When the operator initiates testing, the instrument first determines the machine- and cross-machine directions in the sample. It does this by orienting the transducers to study longitudinal motions and by making a velocity measurement in both principal directions. The direction with the largest velocity is designated as the MD, while the other is

the CD. The MD longitudinal velocities are now measured at N/2 translations of the carriage. The sample then rotates 180 degrees and another N/2 MD longitudinal tests are conducted on the other half of the sample. The N velocities are averaged and standard deviations are calculated. The sample then rotates 90 degrees and the CD longitudinal motion is analyzed in a like manner. Next, the transducers are rotated about their vertical axes for transverse wave propagation. Transverse velocity measurements are made N/4 times at each 90° increment from the MD. The average velocity and standard deviation of the shear mode in the principal directions are calculated. This measurement series is repeated for transverse waves at orientations 45° to the principal axes.

The four average velocities and their standard deviations and the average velocities squared and their standard deviations are printed out. The squared velocities of the first three modes are planar stiffnesses divided by density. These mass specific elastic parameters are appropriate for irregular materials like paper, whose thickness (and therefore density) are hard to define. However, if the operator chooses, a value for density is entered, and the engineering elastic parameters are calculated. The report generated afer testing a typical sample is presented in Fig. 3.

(Fig. 3 here)

Acoustics

The purpose of the acoustic portion of the apparatus is to generate and receive plate waves which have phase velocities that are directly related to mass specific elastic parameters. If the frequency is low enough so that the out-of-plane wavelengths are long compared to the sample thickness, the plate waves are nondispersive. In a nondispersive frequency range, the time-of-flight velocity equals the phase velocity, and time-of-flight measurements can determine elastic

disturbance and reflections from the boundaries. If CW methods are to be applied, the direct propagation must be separated from reflections. In other applications, time delay spectrometry has been used for this purpose. Here, the transmitter frequency is swept, the receiver signal is mixed with the transmitter signal, and the mixed signal is Fourier analyzed. Each transmitter to receiver path is represented by a low frequency peak in the Fourier transform. In fact, the transit time is proportional to the Fourier transform peak. This approach was rejected for our application, since the 100kHz upper frequency limit resulted in very poor time resolution. Continuous wave techniques are conceptually attractive, but no practical scheme is apparent. Time-of-flight measurements seem to be the only viable approach.

Even for time-of-flight measurements on short pulses, care must be taken to avoid reflectional interference. In this system, a single cycle, 60kHz pulse is used to excite the transmitter. The transducers ring for many cycles, but only the first half cycle of the received signals are used in the cross-correlation time delay determination. This permits testing to within about 3 cm of the sample edge without concern over errors from reflectional interference. Since attenuation increases with frequency, the pulse shape is distorted by propagation through the sample. Therefore, using only the front end of the pulse to calculate time-of-flight causes an overestimate of the phase velocity. However, the absolute error amounts to around one percent and is insensitive to changes in paper variables. This is small compared with differences between samples, and it can be neglected.

As noted earlier, the apparatus uses only two transducers. In order to measure a time-of-flight velocity, their separation distance is changed, and the two recorded

signals are compared. The mechanical apparatus necessary to implement this approach is more complex than one using two receivers (or two transmitters) unequally spaced from a transmitter (or a receiver). The three-transducer method, however, requires that the response of the two receiving transducers be closely matched. Our experience with three transducer systems has demonstrated that it is unrealistic to expect a pair of transducers to maintain the same interaction with the sample overtime. Two-transducer systems are repeatable over long periods of time, while three-transducer systems demand periodic calibration. Here, simplicity of design and speed of operation have been sacrificed for consistency of results.

The piezoelectric material in the transducers is lead zirconate titanate (PZT 5H). This is a dense ceramic with a large mechanical impedance. In order to impedance match the piezoelectrics to the samples, a parallel biomorph construction is used. To build a biomorph, two thin (~ 0.25 mm) plates of the PZT are bonded together with their polarities in the same out-of-plane direction. When a voltage is applied at the center electrode relative to the outside surfaces, one plate expands while the other contracts, causing the biomorph to bend. The bending yields greater motion per unit force than bulk waves in PZT and better coupling of energy into the sample. Biomorphs with a width of 6 mm are procured from Vernitron Inc. The edge which contacts the sample is rounded by pressing it between brass discs, 5 inches in diameter, and sanding off the excess. In the transducer mount, the biomorph is clamped with a set screw between two brass half moons. The length of biomorph from the clamp to the rounded free end determines the transducer's resonant frequency. The length of these transducers is 8 mm, making the resonant frequency 60kHz. Another advantage of the biomorph design is that transverse and longitudinal plate waves are generated with the

same transducers. If the transducer separation is parallel to the biomorph polarization direction, longitudinal waves propagate between the transducers. If the separation is perpendicular to the direction of propagation, transverse waves are propagated. The modal purity of the transducers can be confirmed by noting the small signal when one transducer is set for transverse propagation and the other for longitudinal. This is not the first time that biomorph transducers have been used to generate plate waves in polymeric sheets.[1] Suitable commercial transducers are available from the H.M. Morgan Co., but our design enhances performance. The use of parallel (as opposed to series) biomorphs leads to electrical isolation of the active electrodes and better signal to noise ratios. Sensitivity is increased by using wider elements. In all, the signal to noise ratio is about twice that of the commercial transducers.

Mechanics

The stepping motor driven, rotating plate which holds the sample is called the platter. Its base is a 13-inch pitch-diameter chain sprocket which is spindle mounted. It revolves in a bearing attached to the instrument frame. A thin teflon spacer separates the frame from the platter. A stepping motor, which turns a one-inch pitch-diameter chain sprocket, is also attached to the frame. This sprocket drives the platter through a stranded wire reinforced cable chain. Since the stepping motor increments 1.8 degrees per step, the platter requires 2600 steps for a revolution. A magnet is mounted on the circumference of the platter, and a pulse is generated as the magnet passes a Hall effect detector secured to the frame. This provides the reference for aligning the principal axes of the sample at a chosen angle to the transducer separation.

The upper portion of the platter is the sample holder. A square metal plate with a lip on three sides is screwed to the platter base. A grooved Delrin slat is attached to each lip, producing a slot on three sides of the plate. A rectangular tray is machined to slide into the slotted plate from the open side. A sheet sample, which is nominally 8 inches square, is placed on the tray, and the tray is inserted into the platter slot. A layer of soft rubber separates the metal tray from the sample. This acoustically isolates the sample from the platter.

The transducers are suspended on a carriage above the platter. The carriage rides on two hardened steel shafts, mounted on either side of the frame, through ball bushings. Translation of the carriage allows the transducers to span the sample. The carriage is driven by a double acting air cylinder; it can be pulled back to the rear of the sample or pushed toward the front. In order to position the carriage at discrete, intermediate positions, a serrated aluminum rack is fastened along each side of the carriage. Stops mounted on the frame are pushed into the rack to interrupt the translation of the carriage at the proper time. The stops are driven by single-acting, spring-extend air cylinders.

The location of the carriage is sensed with a potentiometer fixed to the carriage. A chain sprocket is attached to the shaft of the potentiometer. The ends of a cable chain are held by clamps on the frame. The chain threads around the potentiometer wheel and back around another sprocket mounted to the carriage, as shown in Fig. 1. As the carriage translates, the potentiometer shaft rotates, and the voltage at the wiper of the potentiometer changes.

In order to alternate transducer separations, a second carriage is mounted on the translation carriage. One of the transducers is attached to this carriage, which rides on hardened steel shafts through ball bushings. Since the axis of

these shafts is perpendicular to the axes of the translation shafts, the motion separating the transducers is perpendicular to translation. This carriage is driven by a double-acting air cylinder fixed to the translation carriage. Rigid stops insure that the difference in the two transducer spacings, achieved by pulling or pushing the air cylinder, is constant.

Rotation of the transducers about vertical axes for transverse and longitudinal operation is also achieved by double-acting air cylinders. A collar with a slotted lever arm controls the angular orientation of each transducer. The lineal motion of an air cylinder is converted to a rotation of a transducer by putting a yoke in the slot of a collar and applying the air cylinder drive to the yoke. Extension of the air cylinder results in a 90° rotation of the transducers.

A final pair of air cylinders are used to raise and lower the transducers. They are mounted on the carriages above the transducers. When air is applied, these double-acting cylinders elevate the transducers by pulling up on caps on the end of the transducer tubes. When released, the transducers descend until they are riding on springs inside the transducer tube. The tension of the springs and the extent of the fall can be manually adjusted. When unusually thin or thick samples are tested, it is necessary to use these adjustments to guarantee that there is sufficient transducer contact with no sample damage.

Electronics

The instrument electronics can be divided into three parts: the computer; commercial instruments; and custom wired circuitry. The computer which oversees the measurements is an Apple IIe with 64K of memory. Its functions are to initiate

an acoustic pulse, analyze the received signal, activate the air cylinders and stepping motor, monitor platter rotation and carriage translation, calculate velocities and moduli, and display the results. The commercial instruments are a Wavetek model 143 function generator to drive the transmitter and a 5050AE Panametrics amplifier to preamplify the receiver signal. Home-made electronics include a 10 MHz analog to digital converter for the received signal, a buffer memory to store the digitized signal, a hardware multiply circuit to speed the cross-correlation calculation, a variable gain amplifier which adjusts the input signal level to match the range of the A/D, stepping motor and air cylinder drive circuitry, and an A/D for the translation carriage potentiometer.

An ultrasonic pulse sequence begins with a TTL level signal from the computer triggering the function generator to emit a 60kHz, single-cycle pulse (see Fig. 1). The pulse amplitude can be adjusted to 30 volts peak-to-peak, but it is normally set at about 15 volts peak to peak. The initial phase of the sinusoidal output can also be altered. A one-time adjustment of the phase was conducted so that, when a typical sample is tested, the received signal has a pronounced, positive first response. This signal is used to excite the transmitter. The resulting electrical signal at the receiver goes to the Panametrics preamp. This is a battery-powered, 20kHz to 2MHz band pass amplifier which can be switched to a 40 dB or 60 dB gain. It has been modified to run off line power to avoid the nuisance of changing batteries. The signal now goes to a line receiver in the custom electronics box. From there, it is fed to a MC3340 variable attenuator. The analog attenuation input of this chip comes from a digital to analog convertor. The computer sends digital inputs to the D/A through a parallel output port. In this manner, the computer can adjust the receiver signal level. After this selectable attenuation, the signal is amplified and passed by a line driver to the A/D board.

The measurement stategy depends on a digital analysis of the receiver signals. In order to resolve the 60kHz signals, a high speed analog to digital conversion is required. This is achieved with an A/D card made by TRW, built around their TDC1007 flash A/D chip which can do conversions at up to 30 MHz. In this application, it is run at 10 MHz, giving a 0.1 μsec time resolution of the received signal.

The outputs from the A/D are stored in a specially built high-speed buffer memory. It is made from two each 4k x 4 IMS1421 NMOS static RAM's built by Inmos. The address and data lines of this memory are normally connected through tristate buffers to the Apple buses. However, when an A/D conversion is triggered (off the same pulse that fired the function generator), these lines are controlled for a time by the A/D circuitry. To be specific, a set of counters sequence the address lines. Starting from zero when the transmitter is triggered, the counters increment the following 2048 A/D conversions, which are now gated to the RAM I/O lines, into consecutive address locations. Before starting a pulse at the "far" spacing, the signal from the "near" spacing is moved from the buffer memory, to other locations in memory. A 20 MHz crystal oscillator generates the clock which runs the counters and provides the timing for the convert signals to the flash A/D. The trigger pulse, which fires the function generator and starts the A/D, is synchronized with this clock to preclude any jitter in the received signal.

The computer keeps track of the location of the translation carriage by monitoring the voltage at the wiper of the carriage potentiometer. This voltage is digitized using a D/A and a comparator. The outputs of an Apple parallel port are connected to the digital inputs of the D/A. The analog output of the D/A and the wiper voltage are inputs to the comparator. The computer sequences the

D/A inputs and monitors the output of the comparator. The value of the digital input when the comparator switches states is taken as the wiper voltage.

The time-of-flight determination comes from a cross-correlation calculation. This requires many multiplications and additions of the data representing the "near" and "far" signals. Calculation time is decreased by using a TRW TDC1008 8 bit multiplier-accumulator chip. When the proper code is on the address bus, inputs from the Apple data bus are latched into this chip. After the calculations are complete, the chip drives the data bus, and the results are available to the central processor.

There are also drive circuits for the air cylinders and the stepping motor. The solenoids that control flow to the air cylinders are activated by AC line voltage. The TTL level signals from parallel ports on the computer are buffered in order to drive the relays that channel power to the solenoids. The stepping motor is controlled by two TTL lines off a computer parallel port. A commercial driver board interfaces the parallel port to the stepping motor. Pulsing one of the TTL lines increments the motor, while the state of the other line determines the direction of rotation.

Software

The central function of the computerized data analysis is to determine a time-of-flight by performing a cross-correlation calculation on the "near" and "far" signals. This operation was outlined in the General Description and is now discussed in more detail. The main executive programs operating the instrument are written in Basic. However, Basic is too slow for the many repetitive calculations needed in the signal analysis routines, and these are done in assembly language.

One assembly language signal analysis routine defines the first peak in the "near" signal. This begins with a "baseline" analysis which is a characterization of the signal before the arrival of the acoustic pulse. Its purpose is to determine the average value and maximum deviation from the average of the initial segment of the received signal. The length of the baseline, which is about 50 data points, is adjusted by the software, depending on the anticipated velocity of the mode being propagated. After the baseline analysis, the computer starts from the end of the baseline interval and sequentially examines the data representing the signal. The point at which the signal exceeds the baseline average plus four times the maximum deviation is designated as the beginning of the first peak. Subsequent data are examined until a baseline crossing is detected. This is the end of the first peak and the limit of the "near" signal data in the cross-correlation calculations.

The automatic gain control is also an assembly language routine. When a new acoustic mode is initiated, the gain on the input amplifier defaults to a value that puts typical signals in the proper range for the A/D. If the first peak saturates the A/D, the gain, which has 256 discrete levels, is reduced by eight, and a new receiver signal is tested. This continues until an unsaturated first peak is generated. If the operator decides that this beginning gain is too low, the program can be interrupted, and the gain adjusted manually. After the carriage translates to a new sample location, the gain increments by eight and is reduced only if the first peak saturates. The signals taken during the gain control adjustments are plotted on the CRT display. If more than one pulse was necessary, the signals are superimposed and the progress of analysis can be observed.

Signal averaging is performed after the gain is fixed in the correct range. Five signals are digitally averaged to generate a composite signal, which has an improved signal to noise ratio. If the operator intercedes, the number of signals averaged can be changed. As they are received, the signals are superimposed on the CRT display. When the gain adjustment and the signal averaging are complete on the "near" and the "far" signals, all of the earlier signals are removed from the display, and the composite signals are exhibited. Fig. 4 is a print-out of the CRT display showing typical composite signals. Notice in the top figures the vertical line that designates the limit of the first peak on the "near" signals and the shorter lines that are the limits of the baselines on the "near" and "far" signals.

(Fig. 4 here)

The time-of-flight calculation is accomplished with an assembly language cross-correlation algorithm and an optimization routine written in basic. The first step in the cross-correlation program is to shift the "far" signal back by a number of data points called the "offset". Each "near" data point, acquired before the end of the first peak, is multiplied by the "far" data point which it corresponds to after the offset. These numbers are added together to give the value of the cross-correlation function for this offset. Unless an operator overrides normal procedure, the optimization routine defaults to a beginning offset that is typical for the mode being studied. After the first cross-correlation calculation is complete, the offset is incremented by one, and the process is repeated. If the second summation is larger than the first, the offset continues to increment until a maximum is reached. If the first summation is larger, the offset decrements until a maximum occurs. In either case, a quadratic equation is fit to the maximum and the sums on both sides of the maximum. The displacement offset value which gives a peak in the quadratic equation is

taken as the displacement of the "far" signal from the "near" signal. The time-of-flight is 100 nsec times this displacement, and the velocity is the separation difference divided by the time-of-flight. The CRT now displays the "far" signal shifted to the left by the offset at the maximum summation. See the lower curves on Fig. 4. If the initial offset is grossly in error, the "far" and the "near" signals could misalign by a wavelength. The operator would observe this, interrupt the program, and enter a different starting offset. When the carriage translates to a new position on the sample, the starting offset is the offset at the maximum of the previous position. After a velocity is calculated it is displayed on CRT along with the test number, the running average, and standard deviation.

The elastic characterization routine most commonly used was described in the general description section. Another useful program measures the time-of-flight velocity of the quasilongitudinal waves as a function of angle from the MD. The operator sets the number of signals to be averaged and the number of test locations for each angle. The testing begins with an MD determination as performed in the elastic characterization program. Velocities are then measured at each five degree rotation of the platter. The average velocity squared values (specific stiffnesses) and standard deviations are printed out along with a polar plot of the results. A typical report is presented in Fig. 5.

(Fig. 5 here)

The operator can enter an instrument check-out routine from the elastic characterization or the orientation program. This allows the basic operations of instrument to be selected and performed individually. The platter can be rotated, the carriage translated, or the transducers rotated. "Near" and "far"

signals can be taken and displayed, and the operator can set the preamplifier gain and the function generator output accordingly.

The major basic programs begin with an initialization procedure for platter rotation and carriage translation. First, the platter rotates to its "home" position. This leaves the sample holder square with the front of the instrument, and allows the sample to be placed on the slide tray and inserted into the instrument. The computer identifies home as a specific number of steps past the first detection of the magnet by the Hall effect transducer. The carriage initialization begins by retracting the translation stops, then pushing the carriage full forward, and pulling it all the way back. The potentiometer readings at the two extremes are noted. The locations of the intermediate locations are calculated by extrapolation. The potentiometer voltages that trigger release of the stops in later carriage translations are determined by this calculation. The carriage then moves to its starting point.

References

1. **Craver, J. K., Taylor D. L.** Tappi 48 (1965) 142.
2. **Habeger, C. C., Whitsitt, W. T.** Fibre Science and Technology 19 (1983) 215.
3. **Baum, G. A., Bornhoeft, L. R.,** Tappi 62 (1979) 87.
4. **Habeger, C. C., Mann, R. W., Baum, G. A.** Ultrasonics 17 (1979) 57.
5. **Baum, G. A., Brennan, D. C., Habeger, C. C.** Tappi 64 (1981) 97.
6. **Habeger, C. C., Baum, G. A.** Tappi (1986).
7. **Graff, D. F.,** Wave Motion in Elastic Solids, Ohio State University Press (1975).
8. **Musgrave, M. J. P.,** Proc. Royal Soc. A226 (1954) 339.

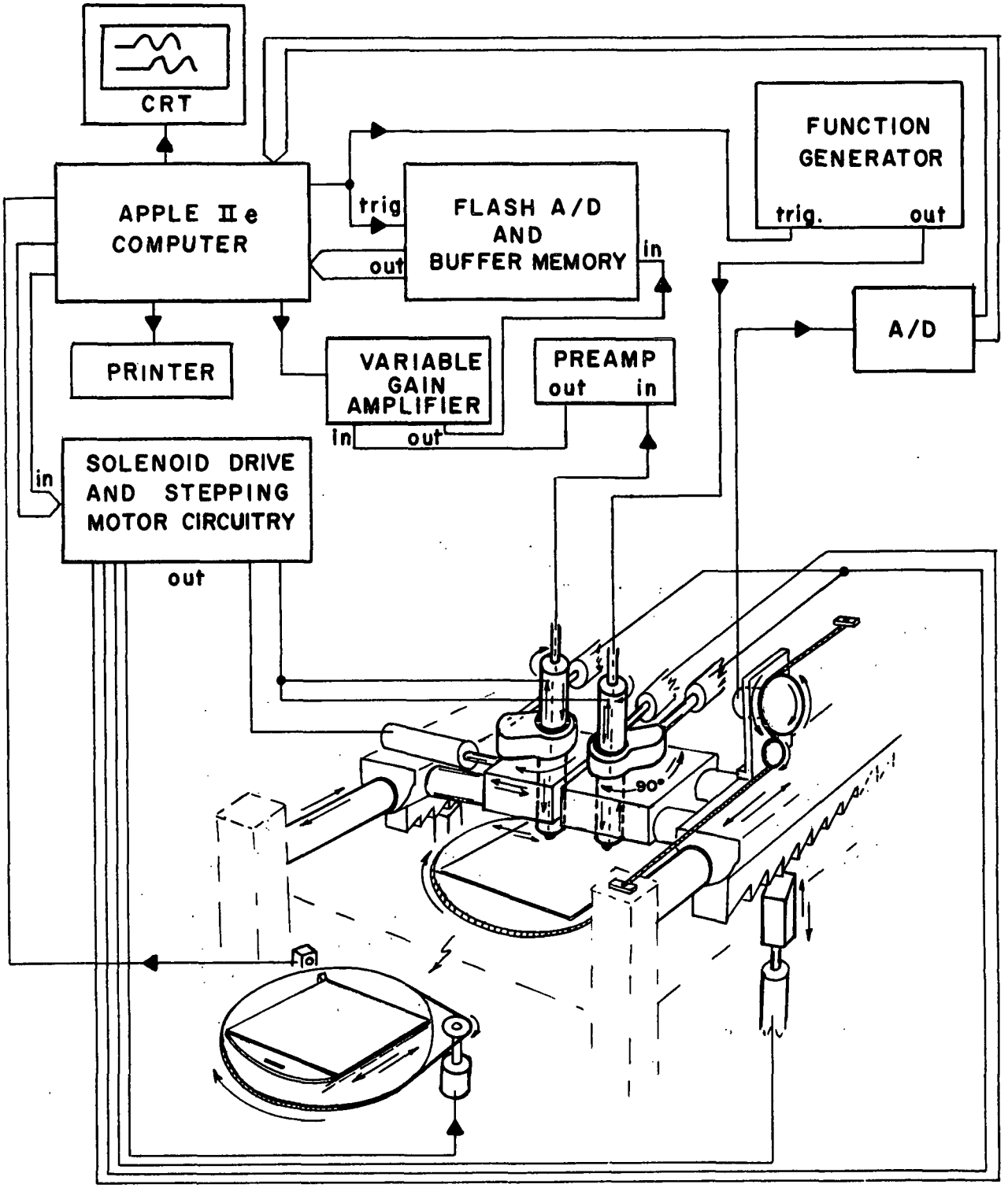

1. Mechanical and electronic schematic of the automated ultrasonic velocity apparatus.

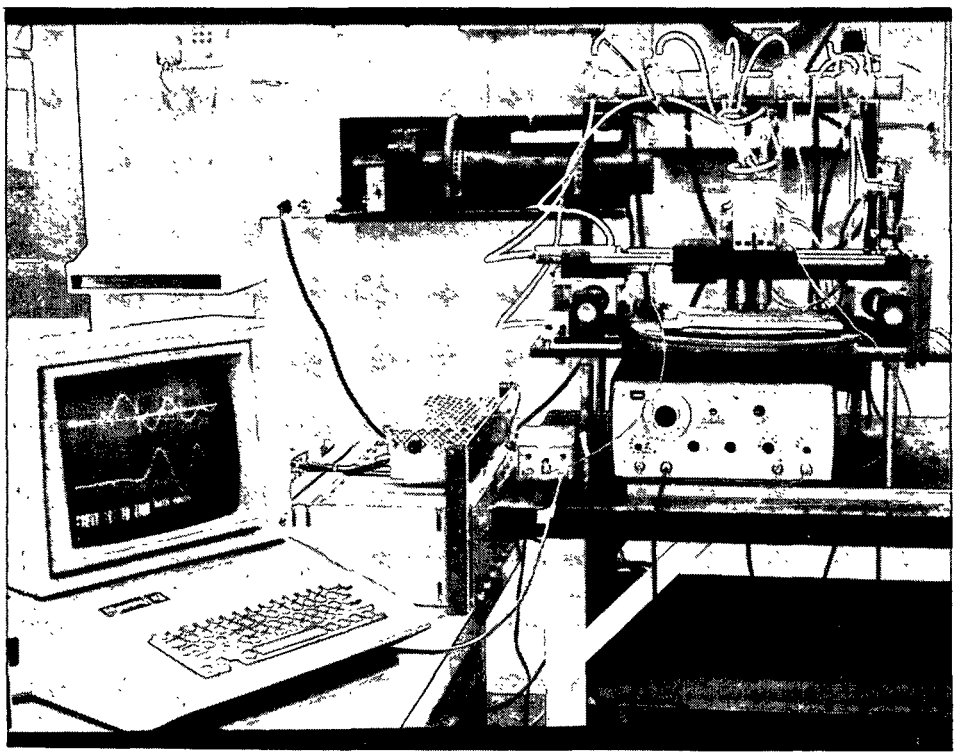

2. Photograph of the apparatus.

THE INSTITUTE OF PAPER CHEMISTRY
TWO TRANSDUCER VELOCITY MEASUREMENT

OPERATOR :C HABEGER
DATE :2 25 86
PROJECT: 86-4

SAMPLE : JR 1 SPECIMEN 5

LONGITUDINAL TRANSDUCER SEPARATION = 35.2 MM
SHEAR TRANSDUCER SEPARATION = 35.2 MM

SAMPLE TIME = .1 MICRO SEC

MODE	TESTS	VELOCITY KM/SEC	ST DEV KM/SEC	V SQR KM2/SEC2	ST DEV KM2/SEC2	SIG AV
MD LONG	16	3.101	.059	9.62	.36	6
CD LONG	16	2.464	.019	6.07	.09	6
SHEAR	16	1.669	.016	2.79	.05	6
45 SHEAR	16	1.668	.015	2.78	.05	6

MODULI CALCULATIONS

MD-CD G. MEAN V SQR = 7.64 KM2/SEC2

STIFFNESS RATIO = 1.58
NUXY = .20
NUYX = .32

G. MEAN NU = .25

DENSITY = .682 GM/CM3

EX = 6.13 GPA EX/RHO = 8.98 KM2/SEC2
EY = 3.87 GPA EY/RHO = 5.67 KM2/SEC2
G = 1.90 GPA G/RHO = 2.79 KM2/SEC2

THE MD-CD G. MEAN E/RHO = 7.14 KM2/SEC2

3. Printout for the in-plane moduli test.

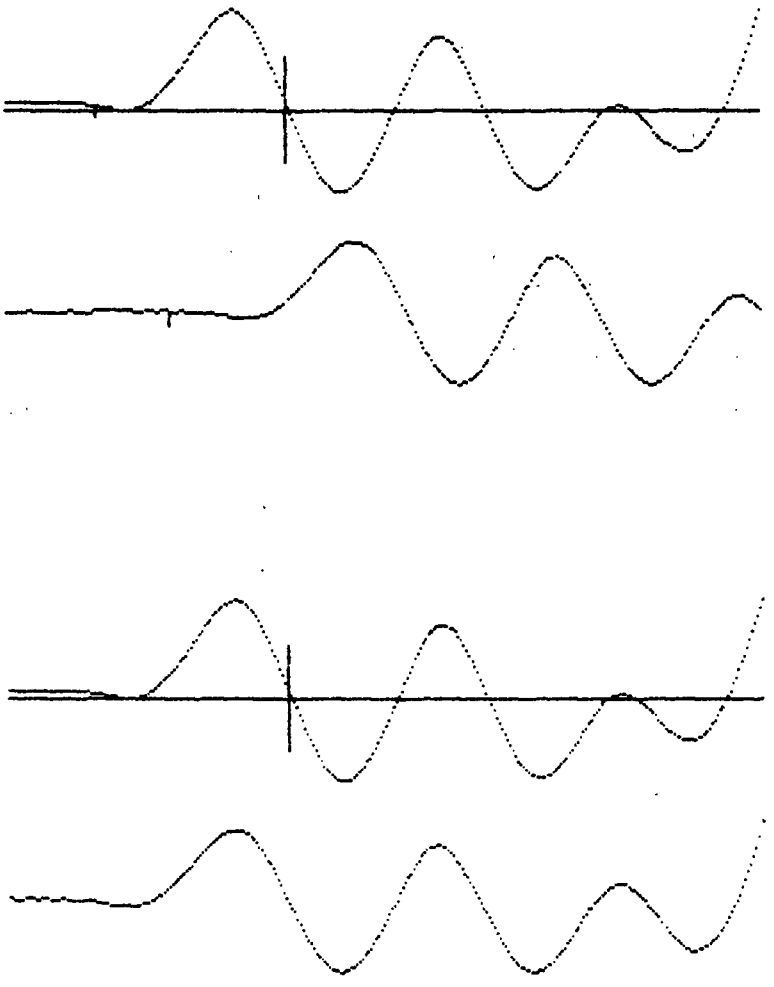

4. Composite "near" and "far" signals as displayed by the CRT before (top) and after (bottom) cross-correlation. Every other digitized point is shown up to the capacity of the display.

THE INSTITUTE OF PAPER CHEMISTRY
LONGITUDINAL SPECIFIC STIFFNESS (VEL SQR) VS ANGLE TO MD

OPERATOR: CHUCK
PROJECT : 3467

DATE :APRIL 21 1986
SAMPLE : A 31

ANGLE DEGREES	VEL SQR KM2 / SEC2	STD DEV	ANGLE DEGREES	VEL SQR KM2 / SEC2	STD DEV
0	13.22	.32	90	3.18	.14
5	13.21	.25	95	3.26	.15
10	12.65	.58	100	3.47	.17
15	11.62	.52	105	3.74	.11
20	10.80	.36	110	3.95	.15
25	9.47	.32	115	4.16	.07
30	8.59	.34	120	4.51	.09
35	7.60	.31	125	4.86	.03
40	6.78	.25	130	5.30	.16
45	5.98	.35	135	5.86	.18
50	5.41	.27	140	6.58	.19
55	4.92	.27	145	7.24	.22
60	4.50	.23	150	8.31	.04
65	4.18	.26	155	9.39	.22
70	3.92	.20	160	10.46	.11
75	3.73	.07	165	11.42	.11
80	3.47	.20	170	12.37	.27
85	3.24	.16	175	13.03	.39

TEST PER 5 DEGREE INCREMENT = 16 SIGNALS AVERAGED = 6
THE ANGLE TO MAJOR PRINCIPAL AXIS = .6

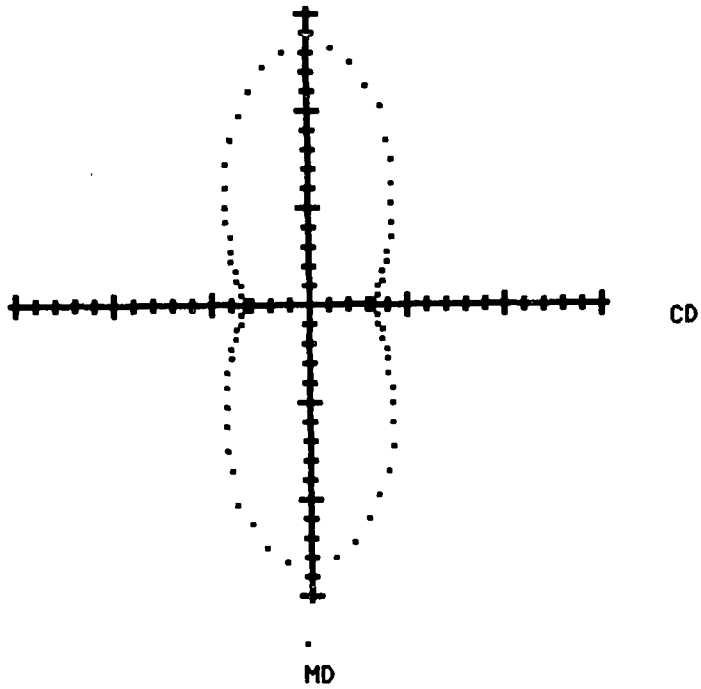

PLOT OF VEL SQR VS ANGLE AS SEEN FROM FELT SIDE

5. Printout for the square of the longitudinal velocity as a function of orientation.

APPENDIX B
IPC Technical Paper Series - Number 186
June, 1986

ELASTIC PROPERTIES, PAPER QUALITY, AND PROCESS CONTROL

G. A. Baum
Director, Paper Materials Division
The Institute of Paper Chemistry
P.O. Box 1039
Appleton, WI 54912

ABSTRACT

The elastic properties of paper are fundamental parameters that describe the small strain mechanical response in three dimensions. It is now possible to routinely measure seven of the nine elastic stiffnesses associated with paper, all on a single specimen. The elastic stiffnesses are sensitive to paper manufacturing conditions, allowing one to study the affects of a change in any machine operating variable on the three dimensional elastic behavior of the paper. The elastic stiffnesses can be related to a number of (destructive) end-use tests, making them useful indicators of product quality. Some of the elastic stiffnesses can be measured on the paper machine, providing both continuous monitoring of product quality and, eventually, control of the paper machine itself.

INTRODUCTION

The elastic properties of a material describe its deformation when a stress or combination of stresses are applied to it. For an isotropic material, one which has no directionality, there would be three elastic properties: a Young's modulus, E, relating axial stress and strain; a shear modulus, G, relating shear stress and shear strain; and a Poisson ratio, v, the ratio of the lateral contraction to the axial extension during uniaxial stressing. Only two of the three elastic properties for an isotropic material are independent. If any two are known, the third can be computed according to $G = E/2(1+v)$.

For paper, the manufacturing process results in symmetry conditions which require nine elastic properties (1,2). These include three Young's moduli (one in each principal direction), three shear moduli, and three Poisson ratios. Six of these parameters are defined in Fig. 1 and 2. The three Poisson ratios also could be determined from the three experiments shown in Fig. 1. If the nine elastic properties of paper are known, the three dimensional response of the paper to applied stresses is known. Such information is valuable in characterizing the end-use behavior of paper and for use in modeling containers or other structures.

Procedures have been developed at The Institute of Paper Chemistry for measuring the nine elastic properties of paper or other sheet materials (3-5). Seven of these are measured routinely in the laboratory. Measurements have been made on essentially all grades of paper and board, nonwovens, wood, and some plastics. There are limitations, however. The minimum sample size is around 6 by 6 inches, although measurements of elastic properties in the thickness direction can be made on smaller specimens. There is a minimum thickness for the z-direction measurements, however, of about 0.004 to 0.008 inch, depending on the surface roughness. There is no minimum thickness for elastic property measurements made in the (MD-CD) plane of the paper. As a consequence of these physical limitations on sample size, most of the three dimensional work has been carried out on board samples. The in-plane elastic properties measured on thin samples, however, are also useful in understanding the effect of process variables on properties and providing improved characterization of end-use performance.

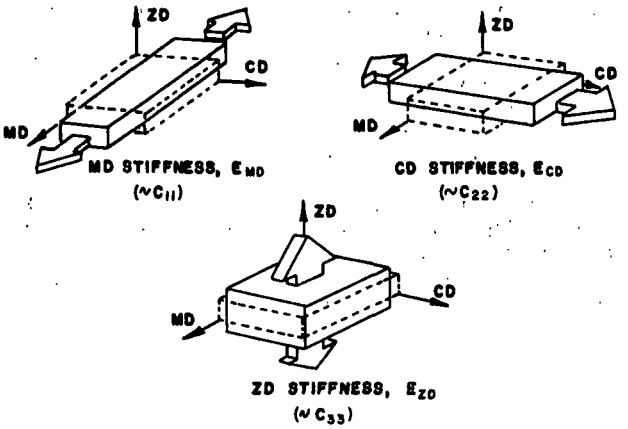

Fig. 1 Three modes of deformation in uniaxial tension.

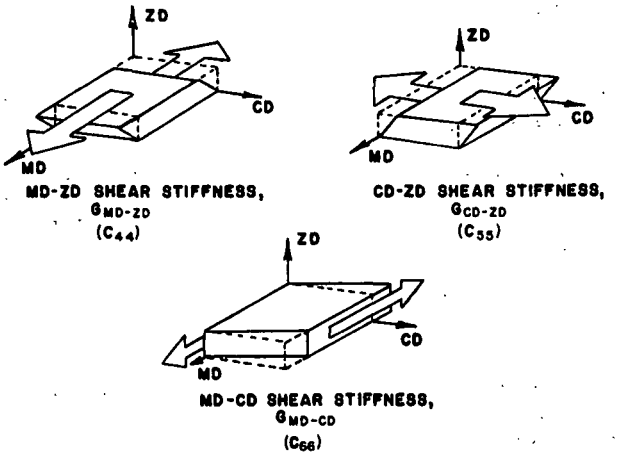

Fig. 2 Three modes of deformation in shear.

THEORY

The elastic properties are determined by measuring the velocity of ultrasound in the paper. The theory has been described in detail elsewhere (2-5), and only a brief overview will be given here. The generalized Hooke's Law for a three dimensional material is

$$\sigma_i = \sum_{j=1}^{6} C_{ij}\, e_j,$$

where i and j have values from one to six and where σ_i is the stress, e_j is the strain, and the C_{ij} are

the elastic stiffnesses. The nine elastic stiffnesses are related to the "engineering elastic constants" viz. Young's moduli, shear moduli, and Poisson ratios, see, for example, Ref. 3.

Three of the stiffnesses are easily determined by measuring z-direction bulk wave velocities:

$$C_{33} = \rho V^2_{Lz}$$

$$C_{44} = \rho V^2_{Sy-z}$$

$$C_{55} = \rho V^2_{Sx-z}$$

where

V_{Lz} = velocity of bulk longitudinal wave in the z-direction
V_{Sy-z} = velocity of bulk shear wave polarized in the y direction
V_{Sx-z} = velocity of bulk shear wave polarized in the x direction
ρ = apparent density

The constants C_{11} and C_{22} can be determined by propagating longitudinal waves in the machine (x) and cross-machine (y) directions, respectively. The velocities of V_{Lx} and V_{Ly} may then be used to compute C_{11} and C_{22} from:

$$C_{11} = \rho V^2_{Lx}$$

$$C_{22} = \rho V^2_{Ly}$$

The coefficient C_{66} is easily determined by measuring the velocity of a shear wave propagated in either the x or y direction with polarization in the y or x direction, respectively. The expression for C_{66} is:

$$C_{66} = \rho V^2_{Sx-y}$$

This shear velocity can be measured on either plate or bulk materials.

The constant C_{12} is obtained by propagating a shear wave, polarized in the x-y plane, at a direction 45° to both the x and y axes. The expression for C_{12} in this case is:

$$C_{12} = \{[2\rho V^2_S(45°) - 1/2(C_{11} + C_{22}) - C_{66}]^2 - [(C_{11} - C_{22})/2]^2\}^{1/2} - C_{66}$$

where V_S (45°) = velocity of the in-plane shear wave propagated in a direction 45° to the x and y directions.

The stiffnesses C_{13} and C_{23} are more difficult to obtain, and are not measured routinely at present. The following discussions will relate only to the seven stiffnesses mentioned above.

The experimental techniques for determining V_{Lz}, V_{Sy-z}, and V_{Sx-z}, have been previously described (4). These velocities are determined by measuring the transit time of a short burst of sine waves (pulse) through the specimen. Two piezoelectric transducers are used as depicted in Fig. 3. These transducers were specially designed by IPC staff for this purpose. The output pulse from the function generator is amplified and fed to the sending transducer and coincidently triggers the oscilloscope and starts a time interval counter. The mechanical disturbance transmitted through the specimen is detected by the receiving transducer and is converted back to an electrical signal, which is amplified and displayed on the oscilloscope. By adjusting a delay-time multiplier knob on the scope, the instant of triggering of a second delayed time base is controlled by the operator. The scope provides visualization of the precise point of triggering. Coincident with the triggering of the delayed time base is the delayed GATE OUT which stops the counter. Delay time intervals are averaged by the digital display counter. The measurements are corrected for delays in the transducers and electronics. By time-averaging the time intervals, delay times can be measured to the nearest nanosecond.

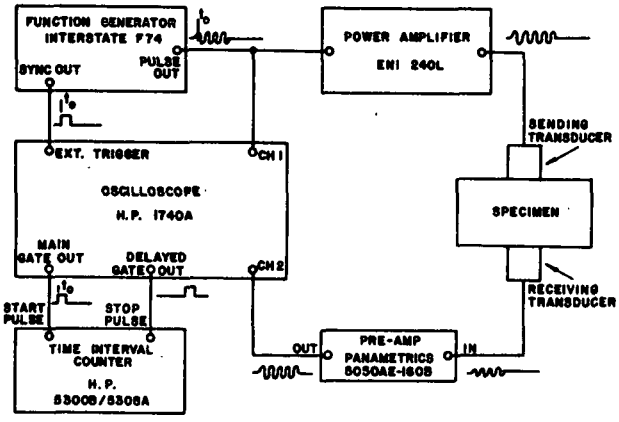

Fig. 3 System for making out-of-plane velocity measurements.

The type of system used for measuring V_{Lx}, V_{Ly}, V_{Sx-y}, and $V_S(45)$ is shown in Fig. 4. These measurement techniques also have been discussed in detail previously (3,4). There are two major changes in the in-plane measuring equipment, however. The first involves the use of a cross correlation method to improve the measurements. Briefly, the idea is to use a linear array of three transducers with the outer two transducers transmitters, and the inner one a receiver. The receiver is placed closer to one transmitter than the other. When the transmitters are alternately fired, signals with two different delay times are received by the middle transducer. These signals are digitized and their cross correlation function is calculated. The first maximum in the cross-correlation function gives the time difference, Δt, between the arrival of the two signals. The velocity is then calculated as the difference in the transducer spacing divided by Δt. Variations in sheet structure are accounted for by sampling over the sheet.

A schematic of the overall operation is presented in Fig. 5. The transmitter signals are initiated by a pulse generator, which fires a short pulse of sine waves from a signal generator and triggers the analog to digital conversion of the receiver signal. In normal operation, the signal generator output is a one to five cycle pulsed RF

signal at 30 to 80 kHz, adjusted to give a 500 Hz repetition rate.

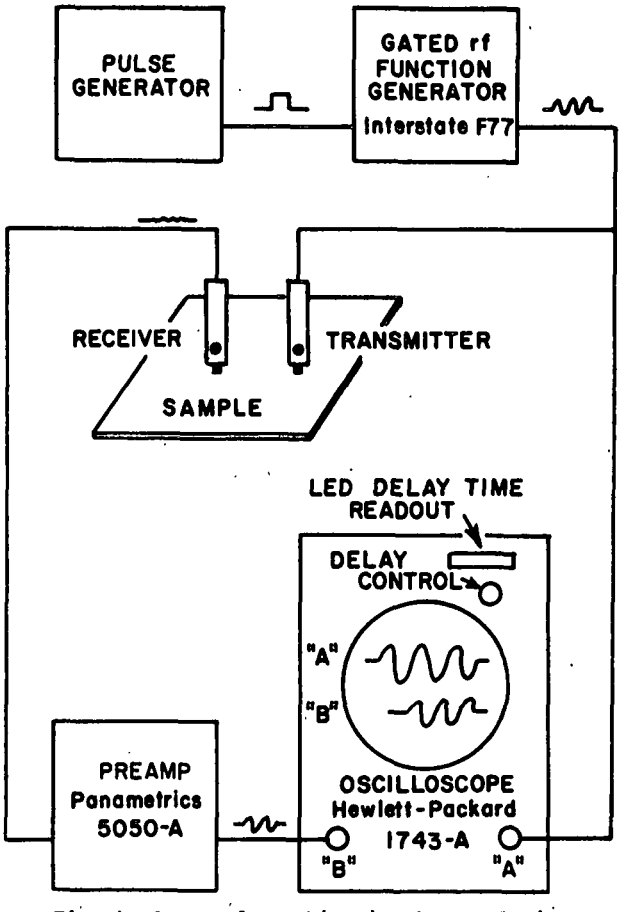

Fig. 4 System for making in-plane velocity measurements.

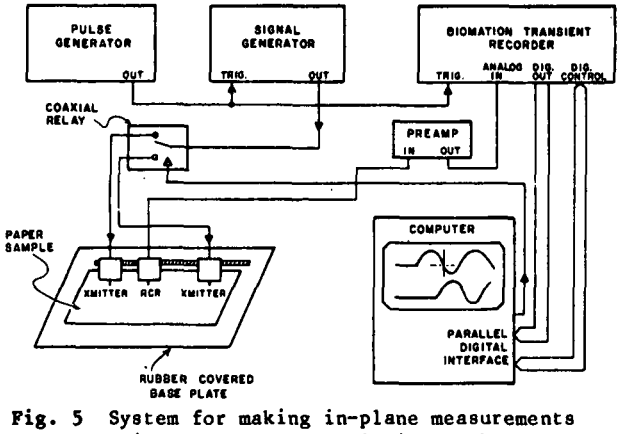

Fig. 5 System for making in-plane measurements using the cross correlation method.

The ultrasonic transducers are piezoelectric "bender" transducers, mounted on a ruled scale such that their separation can be adjusted and measured. Spring steel regulates the transducer pressure against the paper and allows the transducers to be pivoted vertically off the sheet without changing their spacing. The base plate is covered with soft rubber so the samples are acoustically isolated from the base. The sample is centered under the transducers, in order to avoid the problems caused by interference from reflections off the sample edges.

When activated by the pulsed RF signal, the bender transducers oscillate in the plane of the sheet. If the transducers are placed so that their direction of motion is parallel to their separation, a longitudinal plate wave is generated in the sheet and detected at the receiver after a time delay. Alternatively, the polarization can be perpendicular to the transducer separation, and a shear wave is generated and detected. In either case the receiver signal is amplified by a preamplifier and sent to a Biomation analog to digital recorder.

The digital output of the Biomation is then transferred to an Apple II Plus computer. For rapid data acquisition, the Apple is programmed in assembly language to control the input signals from both transducer pairs. The computer can do signal averaging on the received input signals.

The two received signals appear roughly as in the computer display shown in Fig. 5. After a dead time (flat portion) which is greatest for the long transducer setting (shown on the bottom), the sinusoidal signal is received. To avoid interference from waves reflected off the sample edges, only the first peak of the received signal is used in the analysis. The signal analysis limit, controlled from the keyboard by the operator, is indicated by a vertical line on the top CRT curve. The difference in delay time between the two signals is calculated using the cross-correlation technique mentioned above. This program is written in assembly language to obtain fast operation. The velocity of sound in the sheet is then found by dividing the difference in transducer separations by the time difference.

Paper is quite heterogeneous and the measured sound velocity can vary with transducer position on the sheet. To get an estimate of the average velocity and velocity variation in the sheet, a number of tests are performed. The operator inputs the number of tests to be averaged and places the transducers at the first position. The cross-correlation calculation is done, and the velocity calculated and displayed. The operator now raises the transducers off the sheet, the sheet is moved to a new position, and the test is repeated. The CRT displays the latest velocity, the average velocity, and the standard deviation. The process is repeated until the prescribed number of tests is complete, at which time the final velocity average and standard deviation are displayed on the CRT and printed. The cross-correlation calculations are carried out so fast that they are done while the operator moves the sheet, so data can be taken as fast as the operator can reposition the sheet and tap the appropriate key.

The second major change is the automation of the in-plane measurement system. A description, together with the details of the cross-correlation method, will be published elsewhere (6). A schematic of the device is shown in Fig. 6. This system automatically determines MD and CD directions in the sheet, measures the four velocities and their

standard deviations, and computes and outputs the specific elastic stiffnesses (elastic stiffness/density), or the engineering parameters if a density value is inputted. The device is also programmed to measure the elastic stiffnesses as a function of angle to the MD. Such measurements have proven useful in studying transverse headbox flows and other machine operating variables. Figure 7 depicts polar graphs of specific longitudinal stiffness where there is a transverse flow from the headbox, as evidenced by the lean of the elliptical envelope away from the MD.

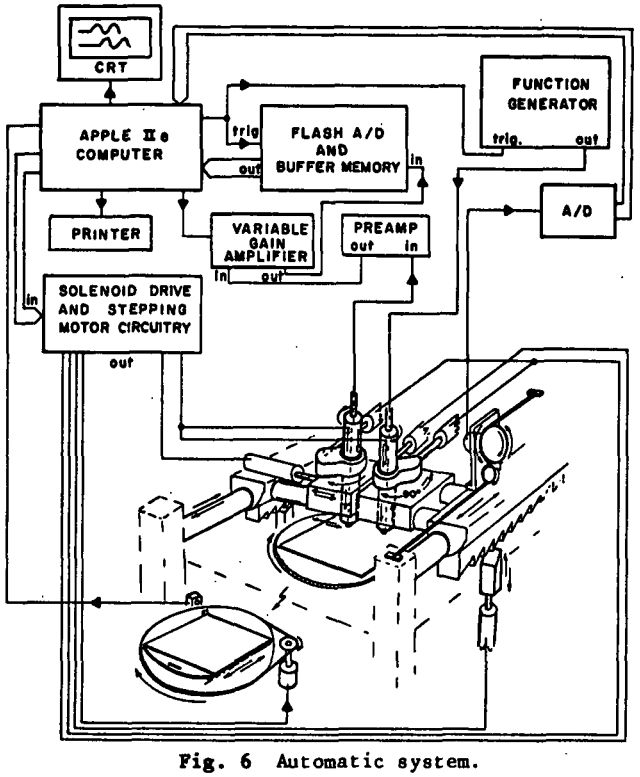

Fig. 6 Automatic system.

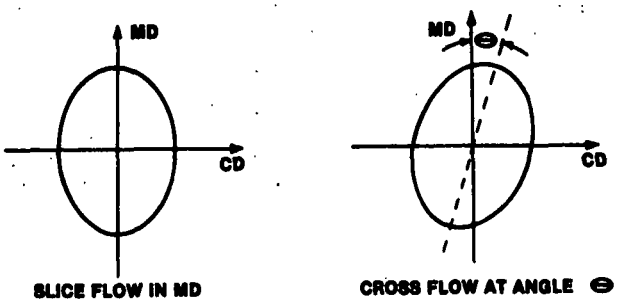

Fig. 7 Polar graphs.

The automatic system takes about 7 to 9 minutes to measure the four in-plane elastic stiffnesses. An operator can measure the three-out-of-plane specific stiffnesses in typically less than one-half hour. Thus in less than an hour, seven of the nine elastic stiffnesses can be measured, all on a single specimen of paper. Table 1 gives some typical values. The following sections describe how these elastic stiffnesses may be used.

Elastic Properties and Machine Variables

The relationships between paper machine variables and the in-plane (MD-CD) elastic properties have been studied by a number of authors (7-18). Relationships between process variables and both in-plane and out-of-plane parameters have received less attention. Figures 8-10 illustrate how the three longitudinal stiffnesses depend on fiber orientation, wet pressing (density), and wet straining (19) for a bleached softwood commercial kraft pulp refined to about 500 CSF. The fiber orientation was varied by changing the relative speeds of the pulp slurry and wire in a Formette Dynamique anisotropic sheet former, and the density was changed by wet pressing. After wet pressing, the sheets were strained in the MD while wet (35 to 40% solids) to levels of 1.2 and 2.4%. The sheets were then restrained in both the MD and CD (but not the ZD) during drying.

Table 1. Elastic properties.

	Apparent Density, ρ, kg/m^3	Stiffness[a] (GPa)									Engineering constants[b] (GPa)								
		C_{11}	C_{22}	C_{33}	C_{12}	C_{13}	C_{23}	C_{44}	C_{55}	C_{66}	E_x	E_y	E_z	ν_{xy}	ν_{xz}	ν_{yz}	G_{yz}	G_{xz}	G_{xy}
Carton stock	780	8.01	3.84	0.042	1.36	0.092	0.91	0.099	0.137	2.04	7.44	3.47	0.040	0.15	0.008	0.021	0.099	0.137	2.04
Linerboard 42 lb	752			0.059				0.050	0.060	2.08	9.98	3.39					0.050	0.060	2.08
Linerboard 90 lb	691	8.12	3.32	0.032	1.19	0.113	0.082	0.104	0.129	1.80	7.46	3.01	0.029	0.117	0.109	0.021	0.104	0.129	1.80
Boxboard	775			0.043				0.083	0.099	1.36	6.03	2.32		0.119			0.083	0.099	1.36
Laboratory BKSW[c]	721	10.9	6.40	0.172				0.290	0.343	3.09	10.3	6.04		0.182			0.290	0.343	2.97
Corrugating medium	682			0.103				0.046	0.053	1.58	6.89	2.68		0.167			0.046	0.053	1.58

[a]Three dimensional bulk stiffness.
[b]Poisson ratios are dimensionless.
[c]BKSW, bleached kraft softwood.

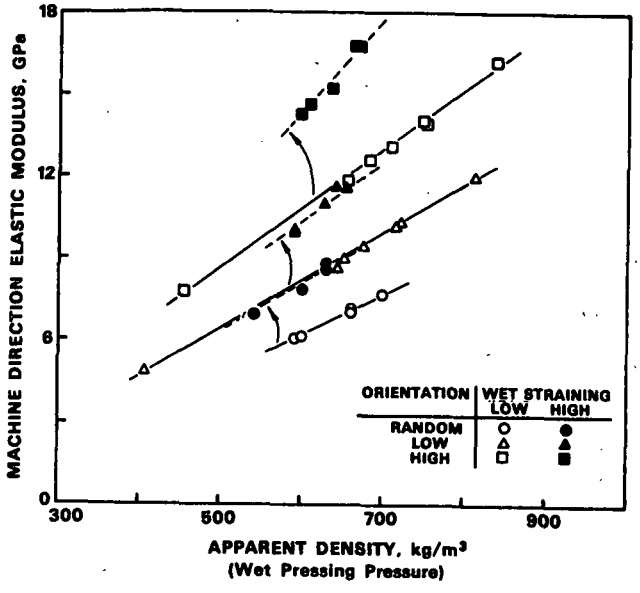

Fig. 8 E_{MD} vs. density with changing fiber orientation and wet straining.

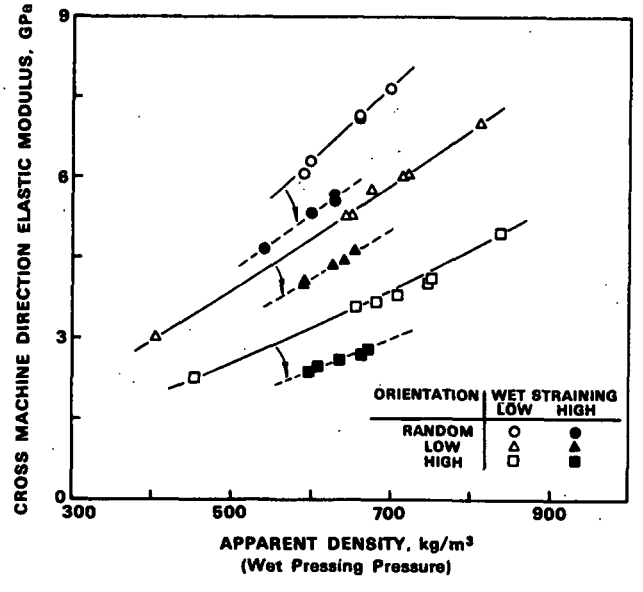

Fig. 9 E_{CD} vs. density with changing fiber orientation and wet straining.

In genetal, the elastic stiffness in the direction of fiber orientation or the direction of wet straining increases, while the properties in both the CD and ZD tend to decrease. The restraint in both MD and CD directions after wet stretching is thought to represent the situation existing near the center of the paper web in a modern, wide, paper machine. Near the edges of the web CD shrinkage can occur. since there is no outward force preventing it. In the case when CD shrinkage is allowed, the CD modulus shown in Fig. 9 may not decrease with MD wet straining (18). Htun (20) has shown that the solids content is important in determining the magnitude of the wet straining effect. Only small increases in modulus are observed upon wet straining at solids above about 60%.

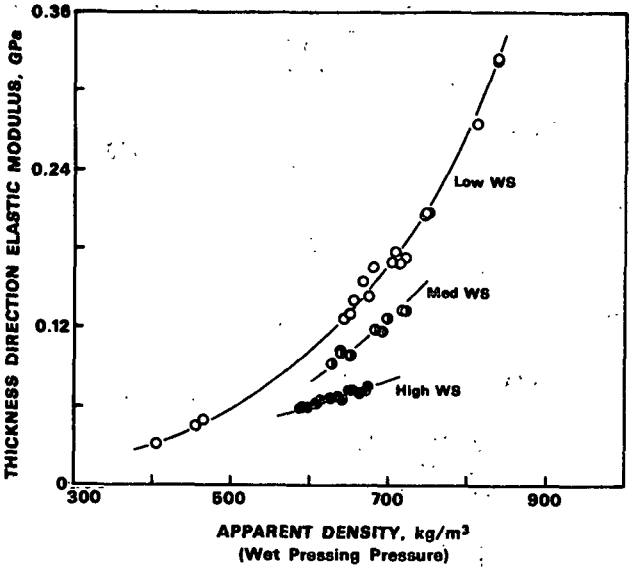

Fig. 10 E_{ZD} vs. density with changing fiber orientation and wet straining.

Of particular interest is the behavior of the out-of-plane stiffness, C_{33}. The in-plane fiber orientation has no impact on this out-of-plane parameter, but wet pressing and wet straining have very large influences. In Fig. 10 the magnitude of C_{33} increases by a factor of ten over the density range studied. On the other hand, wet stretching a small amount degrades this property very markedly.

Results similar to those shown in Fig. 8-10 are obtained for the tensile strengths or compressive strengths in these directions (19).

Figure 11 shows the behavior of the three anisotropy ratios R_{xy}, R_{xz}, and R_{yz} as functions of wet straining at two wet pressing levels (21). The anisotropy ratios are defined as $R_{xz} = C_{11}/C_{33}$, $R_{yz} = C_{22}/C_{33}$, and $R_{xy} = C_{11}/C_{22}$. The in-plane anisotropy, R_{xy}, increases with increasing wet strain, as expected, since C_{11} is increasing (in the direction of wet straining) while C_{22} is decreasing. Above about 3.5% wet strain the sample ruptures. Wet pressing should not produce any in-plane anisotropy. At nonzero wet strains, however, it may be that higher wet pressing pressures lead to a different value for R_{xy}. In these experiments the wet pressing operation was carried out prior to wet straining, just as on a paper machine. If there is an interaction between wet pressing and wet straining, it must be small, at least in the range of densities studied here.

For R_{xz} or R_{yz} at zero wet strain, however, the wet pressing pressure has quite a large effect on the anisotropy. Increasing the pressure from 25 psi (solid line) to 100 psi (dashed line) decreases R_{xz} ($=R_{yz}$ at zero wet strain) from about 75 to 55. Higher pressing pressures probably would decrease this ratio even more, although it is unlikely that the ratio would ever approach one, even with 100%

bonding, because of the inherent anisotropy of the collapsed ribbonlike fibers.

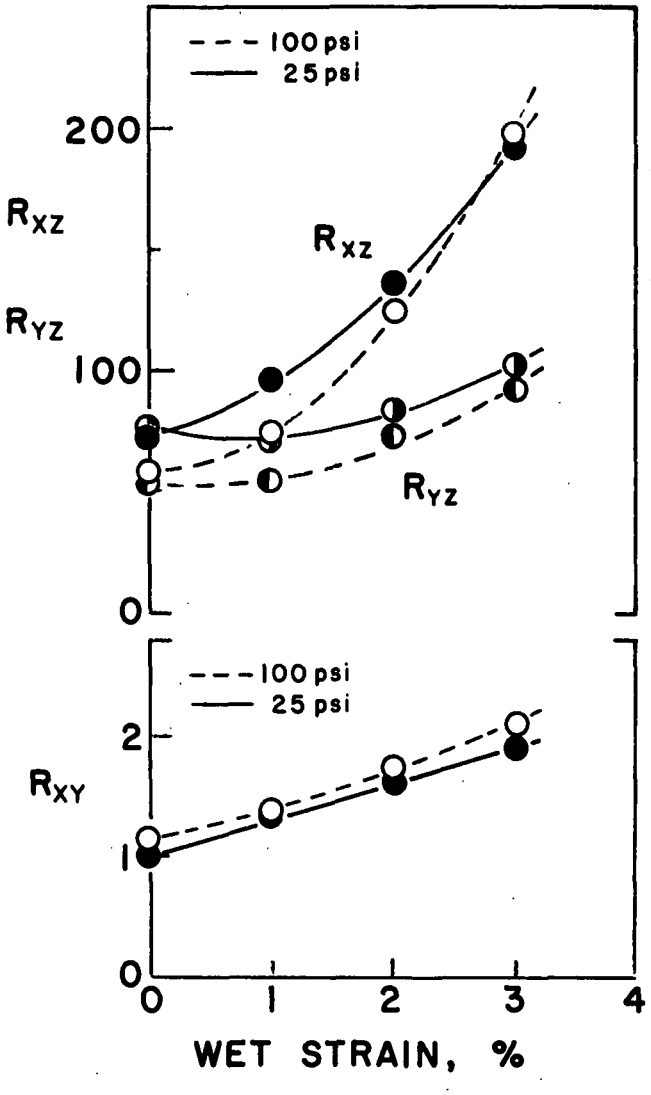

Fig. 11 The three anisotropy ratios as a function of wet straining and wet pressing.

Wet straining of the sample causes both R_{xz} and R_{yz} to increase. This happens even though C_{11} is increasing and C_{22} is decreasing (as in R_{xy}), because C_{33} is decreasing faster than C_{22}. It is apparent that a given level of R_{xz} (or R_{yz}) can be reached by different combinations of wet pressing and wet straining. The additional effects of refining and fiber orientation, both in and out of the plane, should also be included in the analysis. The implications of these anisotropy ratios on end-use performance need to be established.

The effects of fiber orientation, wet pressing, and wet straining on the shear stiffnesses are similar to those for the longitudinal stiffnesses. Table 2 summarizes how the stiffnesses behave with increases in the three variables if the experiments are carried out as described earlier.

Table 2. Effect of machine variables on elastic moduli[a]

Elastic Stiffness	Fiber Orientation (MD)	Wet Pressing	Wet[b] Straining (MD)
C_{11}	+	+	+
C_{22}	-	+	-
C_{33}	0	+	- (lg)
C_{66}	-	+	0
C_{44}	-	+	-
C_{55}	+ (sm)	+	- (sm)

[a](+) = increase, (-) = decrease, (0) = no change.
[b]These results are for the case where the sheets were wet strained at 35 to 40% solids and then dried under restraint in both MD and CD directions. Other drying conditions may give different results. See text.

The effect of these variables on the Poisson ratios has not been studied extensively. While ν_{MD-CD} and ν_{CD-MD} are functions of wet straining and fiber orientation, their product is not very sensitive to these variables (22). The quantity $(\nu_{MD-CD}\nu_{CD-MD})^{1/2}$, is a measure of how interrelated the tensions in the MD are to those in the CD.

Collectively, the results in Fig. 8-10 and Table 2 suggest that the elastic stiffnesses for paper are not independent but that process variables affecting a given parameter may affect related properties in predictable ways. An example of this is an empirical realtionship of the form $C_{66} = a(C_{11}C_{22})^{1/2}$ where a is a constant independent of machine variables, if C_{11}/C_{22} is less than about 3.5 (22). This result is similar to the relationship between the elastic properties of an isotropic material, discussed earlier. Htun and Fellers (18) showed that the geometric mean of MD and CD properties are often invariant under the action of increased fiber orientation and wet stretching of the web. In the case of elastic stiffnesses, it seems that the geometric mean of the longitudinal stiffnesses in any plane is highly correlated with the shear stiffness in that plane, since similar relationships exist in the other two symmetry planes as well. Thus $C_{55} = b(C_{11}C_{33})^{1/2}$ and $C_{44} = c(C_{22}C_{33})^{1/2}$, where b and c are constants. Taken together, a single relationship exists between the elastic stiffnesses, viz.

$$C_{11}C_{22}C_{33} = K(C_{44}C_{55}C_{66}).$$

The implication is that changes in paper machine variables change the relative magnitudes of the longitudinal and shear stiffnesses, but that changes in the furnish (species, pulping, yield, or refining) will change the slope of the line, K. This hypothesis is currently being tested.

Elastic Parameters and End-Use Performance

Most paper specifications involve tests which are taken to be descriptive of the end-use performance of the material. Such tests are usually destructive, and can only be made on samples taken at reel turnup. Changes in paper machine variables such as rush-drag, wet pressing, or wet straining,

however, often affect the elastic properties and strength properties in the same way. It is perhaps not surprising then, that values for many of the common paper tests often correlate with certain elastic parameters, at least over the ranges of values experienced in the paper mill. (The exceptions are apt to be changes in furnish or in formation.) This observation is significant, since it is possible to measure the three-dimensional elastic properties of most papers nondestructively using the ultrasonic methods. These can then be used to predict a number of the destructive test values. In this way it is possible to study the effect of process variables on end-use tests or to monitor product quality.

Figure 12 shows how MD or CD tensile strength varies with C_{11} or C_{22}. The data, covering a rather broad range of tensile strengths (either MD or CD), fall along a single line. The samples are those depicted in Fig. 8-10. Figure 13 shows how the ZD tensile strength (internal bond strength) varies with C_{33} for the same array of samples. Such results suggest that a given elastic stiffness might be used to predict tensile strength, or to monitor the changes in MD, CD, and ZD tensile strength with process changes. Measurements on only one specimen would be required to do this. Similar results are obtained if one compares density specific parameters, i.e., breaking length vs. C/ρ (or E/ρ). Such correlations have also been found to hold for machine-made papers.

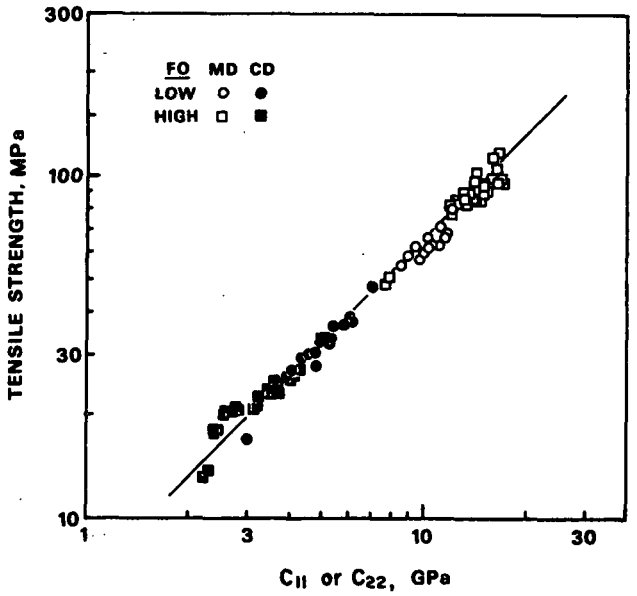

Fig. 12 MD and CD tensile strengths plotted against C_{11} and C_{22}, respectively.

Figure 14 shows MD and CD STFI compressive strength values plotted against the products of in-plane and out-of-plane elastic parameters. In this case a model has been developed which relates edgewise compressive failure with the product of elastic stiffnesses (23). It predicts that CD compressive strength, for example, should correlate with $(C_{22} \cdot C_{44})^{1/2}$. The experimental data give a best fit line with a slope of 0.49, in good agreement with the model.

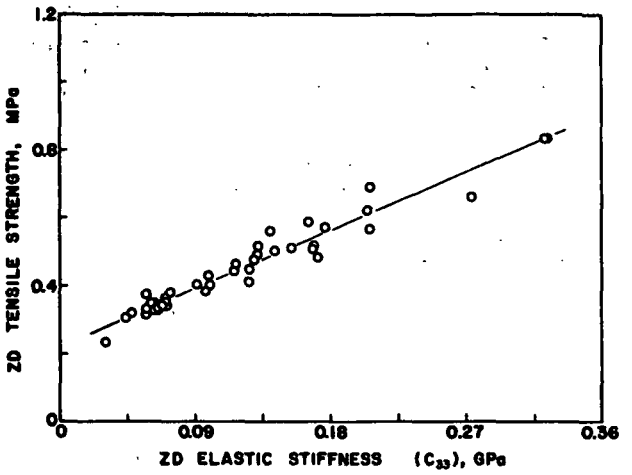

Fig. 13 ZD tensile strength plotted against the ZD elastic stiffness, C_{33}.

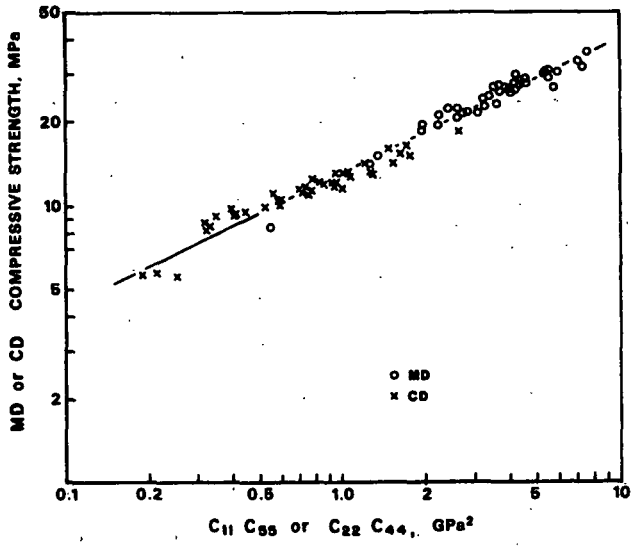

Fig. 14 MD and CD STFI compressive strength plotted against the products $C_{11}C_{55}$ and $C_{22}C_{44}$, respectively. The regression line coincides with the expected behavior (23).

Table 3 lists the relationships that have been studied relating the physical properties of paper with elastic stiffnesses (24). While such relationships may not be valid for all paper grades or basis weights, the use of elastic stiffnesses to evaluate end-use performance and to study the interactions between process variables and paper properties has so far been very productive. Work is continuing in this area.

On-Machine Measurements

A practical application of the relationships between elastic stiffnesses and paper quality factors has been made in a device which measures elastic stiffnesses on the paper machine. The first such sensors, tested on carton stock and more extensively

on linerboard, measured C_{11}/ρ and C_{66}/ρ (25,26). After correcting these values for moisture and temperature variations, they were used to predict the bursting strength, CD ring crush, and CD-STFI compressive strength of the linerboard on a continuous basis.

Table 3. End use tests and elastic parameters.[a]

Property	Elastic Parameters
MD tensile strength	C_{11} ($\sim E_{MD}$)
CD tensile strength	C_{22} ($\sim E_{CD}$)
ZD tensile strength	C_{33} ($\sim E_{ZD}$)
MD/CD tensile ratio	C_{11}/C_{22}
MD compressive strength	$C_{11}C_{55}$ ($\sim E_{MD}G_{MD-ZD}$)
CD compressive strength	$C_{22}C_{44}$ ($\sim E_{CD}G_{CD-ZD}$)
MD bending stiffness	$C_{11} \cdot T^3$
CD bending stiffness	$C_{22} \cdot T^3$
Internal bond strength	C_{33}
Bursting strength	$C_{11} + C_{22}$
Flutability	C_{11} and C_{55}
Combined board performance	C_{22} and C_{44}

[a] T = caliper, C_{ij} = elastic stiffness.

The real payoff for such a sensor, however, will probably be in paper machine control. Both C_{11} and C_{66} are sensitive to process and paper machine variables, but in different ways, and thus permit "tuning" the paper machine to provide optimum board properties. Eventually this capability could lead to automatic control of the papermaking process. Commercial instruments to monitor elastic properties on-machine are just now becoming available (27).

SUMMARY

In summary, the elastic properties of paper form a basic set of parameters which are useful for monitoring the effects caused by changes in process variables, capable of predicting end-use performance, and overall, helping us to better understand the fibrous network we call paper. Elastic parameters also are important in product design and modeling, e.g., in the construction of tubes, boxes, food containers, etc. Eventually their use will help us control the paper machine automatically. Because most of the elastic parameters needed to describe paper can now be determined easily and nondestructively using wave propagation methods, the opportunity exists to move forward in each of these areas.

REFERENCES

1. Jones, A. R., Tappi, 51(5): 203(1968).
2. Habeger, C. C., Mann, R. W., and Baum, G. A., Ultrasonics, 17: 57(1979).
3. Baum, G. A., and Bornhoeft, L. R., Tappi, 62(5): 87(1979).
4. Mann, R. W., Baum, G. A., and Habeger, C. C., Tappi, 62(8): 115(1979).
5. Mann, R. W., Baum, G. A., and Habeger, C. C., Tappi, 63(2): 63(1980).
6. Van Zummeren, M. L., Young, D. J., Habeger, C. C., Baum, G. A., and Treleven, R., Automatic determination of ultrasound velocities in planar materials, submitted to Ultrasonics.
7. Schulz, J. H., Tappi, 44(10): 736-744(1961).
8. Setterholm, V. C., and Chilson, W. A., Tappi, 48(11): 634-640(1965).
9. Meyers, G. C., Tappi, 50(3): 97-100(1967).
10. Parsons, S. R., Tappi, 55(10): 1516-1521 (1979).
11. Prud'homme, R. E., and Robertson, A. A., Tappi, 59(1): 145(1976).
12. Prusas, Z. C., Tappi, 25(5): 325(1963).
13. Gates, E. R., and Kenworthy, E. C., Paper Technol., 4(5): 485-494(1963).
14. Sauret, G., Chleq, J. P., and Lafabure, G., Techniques et Recherches Papetieres (6): 30-40(1965).
15. Craver, J. K., and Taylor, D. L., Tappi, 48(3): 142(1965).
16. Taylor, D. L., and Craver, J. K., Anisotropic elasticity of paper from sonic velocity measurements. In: F. Bolam's Consolidation of the Paper Web, Vol. 2, p. 852-72. London Tech. Section of the British Paper and Board Makers' Assoc., Inc. 1966.
17. Setterholm, V., and Kuenzi, E. W., Tappi, 53(10): 1915(1970).
18. Htun, M., and Fellers, C., Tappi 65(4): 113(1982).
19. Fleischman, E. H., Baum, G. A., and Habeger, C. C., Tappi, 65(10): 115(1982).
20. Htun, M. in Design Criteria for Paper Performance, Progress in Paper Physics Seminar, held at Swedish Forest Products Research Laboratory, Stockholm, Sweden, June 25-29, 1984, p. 173.
21. Baum, G. A., Pers, K., Shepard, D. R., and Ave-Lallemant, T. R., Tappi, 67(5): 100(1984).
22. Baum, G. A., Brennan, D. G., and Habeger, C. C., Tappi, 64(8): 97(1981).
23. Habeger, C. C., and Whitsitt, W. J., Fibre Science and Technology, 19: 215(1983).
24. Baum, G. A., Paper, March 19, 1984.
25. Baum, G. A., and Habeger, C. C., Tappi, 63(7): 63(1980).

26. Habeger, C. C., and Baum, G. A., Tappi, 69(6): 106(1986).

27. Baum, G. A., and Habeger, C. C., "On-line estimates of strength," presented at Control Systems 1986, Stockholm, May 26-30, 1986, to be published.

APPENDIX C
IPC Technical Paper Series - Number 190
July, 1986

ROUGHNESS ANISOTROPY IN PAPER

G. A. Baum and D. R. Waterman

ABSTRACT

The average or root mean square (rms) surface roughness of paper was measured using a stylus-type profilometer. Measurements in the machine direction (MD) and cross machine direction (CD) gave different roughness values. The roughness anisotropy, R_a, defined as R_{md}/R_{cd}, varies from about one to 1.6 and is greatest on the felt side of the paper. R_a increases with increasing levels of fiber orientation and MD wet straining of the sheet but is insensitive to the level of wet pressing pressure.

INTRODUCTION

The surface characteristics of paper are important in all grades that will be coated, printed, or laminated. Typically a "smooth" sheet is sought. This might be obtained by proper selection of furnish, paper making conditions, felt selection, calendering, or supercalendering. Most often paper smoothness (or roughness) is measured by one of a number of air leak methods. Such measurements are simple to carry out but suffer from a number of problems such as errors due to the porosity of the sheet or readings changing with changing pressure on the paper. Such measurements probably work best in rather narrow ranges of paper surface smoothness.

Stylus-type instruments are typically used in measuring the surface roughness of other engineering materials. In these devices a stylus with a small radius tip is pulled or pushed across the surface to be characterized and the vertical displacement of the stylus monitored with appropriate transducers. Such measurements have been made in paper (1-3). There are problems in applying these methods to paper because of the low stiffness of paper in the thickness direction. The local stress of the stylus could deform the paper, leading to erroneous results. In addition, the radius of the stylus determines the "quality" of the measurement. One could argue that in the case of paper it is not really possible to define a "surface" as we do for nonporous materials, since in paper the surface may actually go from one side of the paper to the other. These same difficulties also enter into the measurement of paper thickness (4).

This paper describes the surface roughness of paper as measured using a modern stylus-type instrument and describes how the roughness differs in the MD and CD as functions of paper machine operating variables.

EXPERIMENTAL

The surface analyzer used in this work was a Federal Products Surfanalyzer 4000. This device has a stylus tip radius of 100 microinches, with precisions in the horizontal and vertical positions of 6.1 and 50 microinches, respectively. The instrument had a digital output via a RS-232 serial port. Software was

developed to collect information from the surface analyzer, convert it from hexadecimal to digital format, check for data errors, and save it in a binary file for later data processing. Data processing software was written to provide a number of smoothness characteristics, including the average roughness, R_A, the root mean square roughness, R_{RMS}, the mean cube root roughness, RC, and the frequency and size of voids and segments in the profilometer trace. Voids are the areas of the measured surface profile that lie below the algebraic center line of the trace, and segments are the lengths along the center line between voids.

R_A and R_{RMS} are defined as

$$R_A = (1/L) \int | z | dx \quad \text{and}$$

$$R_{RMS} = [(1/L) \int z^2 dx]^{1/2},$$

where L is the scan length, x is the position along the profile, and z is the vertical coordinate of the profile, measured from the (algebraic) center line of the profile. Both R_A and R_{RMS} are widely used to characterize rough surfaces (5). R_{RMS} is the standard deviation of the surface height distribution and is more sensitive to large deviations from the mean line than R_A. For the results presented here, only the traditional RMS roughness results are discussed. For a description of the other statistics the interested reader is referred to reference 6.

The profilometer digital output has a dynamic range of 4,096 bits, with each bit representing 6.104 microinches. Thus the maximum vertical displacement is 0.25 inch. The horizontal position of the stylus is determined by multiplying the number of sample points times the distance between points. The latter is the ratio of drive speed (0.01 or 0.1 in/s) to sampling rate. Scan lengths typically ranged from 0.5 to 0.75 inch.

The paper samples used for the work reported here were from an earlier study (7). They were softwood kraft sheets prepared on an anisotropic sheet former with different levels of fiber orientation, and were wet pressed, wet strained, and dried under various conditions. Table I lists the preparation conditions and gives the MD/CD elastic stiffness anisotropy ratio for each sample. Surface profiles were obtained in the MD and CD on both felt and wire sides. Six traces were made for each direction or side.

When surface profile measurements are made in a soft material like paper, there is the possibility of damage, caused by the stylus cutting or tearing the paper surface as it is pulled across (3). The stylus force was 1.96 mN. Assuming that this was applied over the entire circular cross section of the stylus, a local pressure of 96.7 GPa (1.4x10 4 lb/in^2) results. To see if such pressures did, in fact, damage the surface, scanning electron photomicrographs were made in the scanned area. No evidence of damage was apparent in any of the SEM's.

RESULTS AND DISCUSSION

Table II presents the RMS roughness values as wet straining and fiber orientation are varied, at constant wet pressing pressure. The upper left corner of Table II gives the RMS values in the MD and CD as measured on the wire side of the sheet for the low wet straining (WS) situation. The effect of increasing

TABLE I

Experimental Sheets

Sample	FO	WP	WS	E_{MD}/E_{CD}
259	L	L	L	1.69
248	L	M	L	1.63
257	L	H	L	1.68
260	L	M	H	2.51
268	H	M	L	3.43
269	H	M	H	5.86

FO = fiber orientation, WP = wet pressing, and WS = wet straining. For wet pressing the L, M, and H values are 27, 53, and 89 psi, respectively. For wet straining the L and H values are 0 and 2.4%, respectively.

fiber orientation from low to high (FO-L to FO-H) causes a 17% increase in the roughness anisotropy RA, defined as the ratio of the MD and CD RMS roughness values. The upper right corner shows the data for the felt side of the sheet. The results are similar to those for the wire side. The RA is about 1.25 for either side of the sheet at low wet straining and high fiber orientation. The lower half of Table II gives the situation for high wet straining levels. At

TABLE II

RMS Roughness and Machine Variables at Medium Wet Pressing

	Wire Side			Felt Side		
	R-MD, µin	R-CD, µin	RA	R-MD, µin	R-CD, µin	RA
Low Wet Straining:						
FO-L	209	195	1.07	208	180	1.17
FO-H	210	168	1.25	219	178	1.23
Change, %	0	-14	+17	+5	-1	+6
High Wet Straining:						
FO-L	206	212	0.97	203	174	1.17
FO-H	243	197	1.33	226	156	1.45
Change, %	+18	-7	+37	+11	-10	+24

FO = fiber orientation, L = low, H = high, R = RMS roughness; RA = roughness anisotropy (= R-MD/R-CD).

low fiber orientation levels the results are similar to those for the low WS and low FO case. However, for high WS and high FO, the differences between MD and CD roughnesses give RA values of 1.33 on the wire side and 1.45 on the felt side. According to Table II, the effect of increasing MD fiber orientation on surface roughness is to increase MD roughness and to decrease CD roughness. The differences are more pronounced with increased wet straining. Wet straining by itself, at low FO levels, has little or no effect on roughness anisotropy.

Table III shows the RMS roughness values as wet pressing pressure is changed, at constant (low) levels of FO and WS. There appears to be no effect of pressing pressure on roughness or on roughness anisotropy. This is probably a consequence of pressing all three sheets against the same felt. Table III again shows that the surface anisotropy is greatest on the felt side of the sheet. It would be anticipated that changing the pressing or dryer felts could change the overall magnitude of the surface roughness but probably not the anisotropy in the surface roughness. Calendering or supercalendering would presumably level out differences between MD and CD roughness, but this was not studied.

TABLE III

RMS Roughness vs. Wet Pressing
at Low Fiber Orientation and Low Wet Straining

	Wire Side			Felt Side		
Wet Press	R-MD, μin	R-CD, μin	RA	R-MD, μin	R-CD, μin	RA
Low	216	206	1.05	218	183	1.19
Medium	209	195	1.07	208	180	1.16
High	202	200	1.01	205	180	1.14
Change, %	-6	-3	-4	-6	-2	-4

R = RMS roughness, RA = roughness anisotropy (= R-MD/R-CD).

The results presented in Table II are for samples 248, 260, 268, and 269 (see Table I) and had elastic anisotropy ratios of 1.63, 2.51, 3.43, and 5.86, respectively. The corresponding surface roughness anisotropy ratios are 1.17, 1.17, 1.23, and 1.45 (felt side). Surface roughness anisotropy values measured on commercial papers range from 0.7 to 1.1 for silicone release, one time carbonizing, MF, and MG papers, and around 1.6 for kraft sack papers. It is quite likely that large differences between the MD and CD could give problems during printing or other converting operations involving the surface. It is important to realize that the surface roughness anisotropy seems to be related primarily to the level of fiber orientation in combination with wet straining. In grades where the sheet is not calendered, it may be possible to alter the smoothness by changes in these variables.

The conclusions based on Tables II and III are supported by two-tailed t-tests at the 95% confidence level. Table IV gives the geometric mean values (the

square root of R-MD times R-CD) for the results shown in Tables II and III. These numbers should be related to the traditional air leak smoothness results, which also average over MD and CD directions. Table IV shows, in general, that the felt side is less rough than the wire side. Again, wet pressing pressure seems to have little effect, except possibly at very low levels. On the felt side of the sheets, the least rough samples are those that were highly wet strained, whereas the wire side of these same sheets are among the roughest. This latter result would be the expected one if the wet straining model proposed elsewhere is correct (8). More experiments will be required to clarify this point.

TABLE IV*

Geometric Mean Roughness Values, μin

	Wire Side	Felt Side
Low Wet Strain		
FO-L	202	193
FO-H	188	197
High Wet Strain		
FO-L	209	188
FO-H	219	188
Low Wet Strain and FO-L		
Low WP	211	200
Medium WP	202	193
High WP	201	192

*Based on results presented in Tables II and III. WP = wet pressing pressure.

CONCLUSIONS

Surface roughness is affected by machine process variables such as fiber orientation and wet straining. Together these can produce a surface roughness anisotropy as large as 1.5. The anisotropy is largest on the felt side of the sheet. It is not obvious how increasing MD fiber orientation increases MD roughness while decreasing CD roughness. It may be possible, however, to minimize the anisotropy effects if they are troublesome, by proper choice of machine operating conditions.

LITERATURE CITED

1. Cahierre, L., Papier, Carton et Cellulose 23(4):58(1974).

2. Setterholm, V. C., and W. L. James, Forest Product Laboratory Report 2130, September, 1958.

3. Murakami, K., R. Imamura, and T. Yamamoto, Japan Tappi 27(2):8(1973)

4. Wink, W. A., and G. A. Baum, Tappi 66(9):131(1983).

5. Thomas, T. R., Rough Surfaces, Longman Group Limited, Harlow, Essex, U.K., 1982.

6. Waterman, D. R., "The characterization of paper smoothness using a stylus type instrument", A190 Report, The Institute of Paper Chemistry, Appleton, WI, March 10, 1986.

7. Fleischman, E. H., "An investigation of the elastic and dielectric anisotropy of paper", Doctoral Dissertation. The Institute of Paper Chemistry, Appleton, WI, 1981.

8. Baum, G. A., K. Pers, D. R. Shepard, and T. R. Ave'lallemant, Tappi 67(5):100(1984).

ACKNOWLEDGMENTS

The authors are indebted to Thilmany Pulp and Paper Company who provided the use of the profilometer, and to Messrs. W. J. Whitsitt, J. F. Waterhouse, and D. Wahren who read the manuscript and offered useful suggestions. Portions of this work were used by D. R. Waterman as partial fulfillment of the requirements for the Master of Science degree at The Institute of Paper Chemistry.

THE INSTITUTE OF PAPER CHEMISTRY

Appleton, Wisconsin

Status Report

to the

PAPER PROPERTIES AND USES

PROJECT ADVISORY COMMITTEE

Project 3526

INTERNAL STRENGTH ENHANCEMENT

September 10, 1986

PROJECT SUMMARY

PROJECT NO. 3526: INTERNAL STRENGTH ENHANCEMENT

PROJECT STAFF: R. Stratton, J. Becher, K. Hardacker September 10, 1986

PROGRAM GOAL: Bring new attributes to fiber based products

PROJECT OBJECTIVE:

To improve internal strength and moisture tolerance in paper and paperboard. The short term goals are to establish those parameters fundamental to inter-fiber and intra-fiber bonding in conventional and ultra high yield pulps and to control these parameters, if possible, by chemical or mechanical treatments.

PROJECT RATIONALE, PREVIOUS ACTIVITY, AND PLANNED ACTIVITY FOR FISCAL 1986-87 are on the attached 1986-87 Project Form.

SUMMARY OF RESULTS LAST PERIOD: (October 1985 - April 1986)

(1) The duopolymer systems comprised of CMC/PAE and PAA/PAE were found to be effective bonding agents in a spruce chemimechanical pulp as had been found previously in softwood unbleached kraft and TMP pulps. Also, as previously noted, the duopolymer combinations were more effective (relative to the blank controls) in the classified pulp than in the whole pulp.

(2) A study of fines and polymer combinations in a softwood unbleached kraft pulp showed that re-addition of fines to the classified pulp failed to match the original whole pulp in dry and moist strength properties. This differs from the previously tested TMP in which case re-addition of fines produced dry breaking length, Et, and moist tensile properties which were roughly comparable to or greater than those of the whole pulp, when measured at the same moisture content. Once again, maximum strength was generally obtained when the polymers were added to the long fiber fraction. Although, in this case, the duopolymer systems were more effective than PAE in both the classified and whole pulps.

(3) Available results indicate that PAE is as effective as CMC/PAE and/or PAA/PAE in improving moist compressive strength.

(4) In a continuing study of bonding mechanisms in duopolymer systems, several series of tests were carried out using diffuse reflectance FTIR analysis. The results revealed that rather substantial strength improvements can be achieved in the absence of covalent bonding; more specifically, in the absence of ester formation. However, the maximum strength levels attained thus far under these conditions are notably lower than those produced by ester formation.

(5) New bonding and handling techniques were developed to permit the use of the FLER II for measurement of single fiber/fiber bond strengths.

(6) Better defined bond area measurements via Page's vertical polarized light method were obtained by bonding an undyed fiber to a fiber dyed black.

(7) Measurements of bond strength, bonded area, and locus of failure for an unrefined, loblolly pine springwood, kraft pulp revealed a broad distribution of the quantitative results. Poor correlation between bond failure load and bonded area, in agreement with previous workers, may suggest that Page's technique is not a valid measure of bonded area. SEM micrographs showed permanent deformation in the bonded area but little fiber wall tearing or disruption.

(8) The measurements were repeated on the same pulp which had been treated with the PAE/CMC additive combination found effective for conventional kraft pulps in the earlier handsheet studies. Increases in average load at failure, bonded area, and specific bond strength (load/area) of 150, 20, and 80%, respectively were found. In contrast to the untreated fibers, examination of the formerly bonded areas by SEM now showed extensive tearing and picking of the fiber walls.

(9) There has been little activity in development of the FLER II in the last six months. Nevertheless, a new differential lead screw has been obtained and installed. Operation of the instrument is now satisfactory.

Techniques are being developed for testing fiber/fiber bond strength by mounting a fiber on the edge of a microscope glass cover slip, placing two such mounted fibers in the FLER II at right angles to each other, wetting them, applying a small compacting load, then tensile testing the bond after it has dried. Early tests have been partially successful.

A small, 90-degree, glass prism has been mounted at the "fixed" specimen clamp of FLER I. One face forms a surface for fiber lateral compaction; another permits direct viewing of the fiber as it is being compacted. Compacting is done with a narrow flat ground on the edge of a razor blade mounted in the "movable" clamp. The technique is being further developed.

It will be desirable to photograph the fibers as they are being tested in the several possible modes. A video camera has been considered, but its resolution would not be adequate as it would have to be used. Consequently, we are looking at suitable photographic equipment.

During the next period we intend to bring the bond testing and the compaction techniques to working order and begin the investigation of fiber characteristics.

SUMMARY OF RESULTS THIS PERIOD: (April 1986 - September 1986)

(1) The effectiveness of the CMC/PAE and PAA/PAE bonding systems was expanded to include a wide range of pulps in whole and classified conditions including a softwood bleached kraft. The results show that these agents, particularly CMC/PAE, were effective in all pulps with some variations in the degree of success. Of the whole pulps, the bleached kraft and a) once-dried, average-yield southern pine unbleached kraft tended to be the most

responsive. Of the classified pulps, the TMP was the most responsive and a softwood CMP, the least responsive. Generally speaking, higher strength levels were attained with the whole pulps in the presence of the bonding agents but the greatest increases in strength due to the additives generally occurred in the classified pulps.

(2) The study of bonding agents was expanded to include carboxymethylated starch as an anionic polymer in combination with PAE. While anionic starch/PAE combinations did not quite match the overall performance of CMC/PAE, anionic potato starch/PAE approached or equalled CMC/PAE in some strength properties including moist Et and compressive strength.

(3) The incorporation of carboxymethylated fiber and PAE into a classified bleached kraft pulp failed to provide equivalent strength to that achieved by the addition of an equal amount of water-soluble CMC in the presence of PAE. In fact, the addition of up to 10% of carboxymethylated fiber failed to attain the same level of strength afforded by the external addition of 0.4/1.0 CMC/PAE. This is assumed to be due to lower accessibility of the reactive groups in the fibrous form of CMC.

(4) Diffuse reflectance/FTIR analysis indicated that covalent bonding (ester formation) occurred in the bleached kraft pulp whether the carboxymethyl group was included in the fibrous component or in an external treatment. FTIR analysis of papers treated with anionic potato starch/PAE also indicated the presence of covalent bonding. On the other hand, no evidence of covalent bonding was found in papers containing PEI or polydiallyl dimethyl ammonium chloride (a cationic polymer) alone or in combination with PAA in spite of the fact that several of these papers possessed strength properties approaching or equalling those containing PAE or PAE/PAA.

(5) A brief examination of the external treatment of unbleached kraft handsheets with polystyrene in solvent solution indicated that high levels of moist Et and compressive strength can be achieved while maintaining high tensile properties. It would appear, however, that high add-on levels would be required to achieve these desired effects.

(6) Work is continuing in the development of techniques for measuring the axial and transverse mechanical properties of single fibers and of Z-direction deformation of single fiber/fiber bonds using the FLER II.

(7) Measurements of bond strength, bond area, and locus of failure for a well-refined, classified southern pine provide a contrast to the unrefined sample reported previously. Frequent tearing of the fiber wall was now found for both untreated and chemically-treated fibers. However, extensive external fibrillation of the fibers make an unambiguous assessment of the damage due to bond failure difficult. Both breaking load and bond strength are considerably higher for the refined compared with the unrefined fibers.

PROJECT TITLE: Internal Strength Enhancement

PROJECT STAFF: R. Stratton/J. Becher/K. Hardacker

PRIMARY AREA OF INDUSTRY NEED: Properties related to end use

PROGRAM AREA: Moisture tolerant, superior strength paper and board

Date: 6/1/86
Budget: $230,000
Period Ends: 6/30/87
Project No.: 3526

PROGRAM GOAL: Bring new attributes to fiber based products

PROJECT OBJECTIVE:

To improve internal strength and moisture tolerance in paper and paperboard. The short term goals are to establish those parameters fundamental to inter-fiber and intra-fiber bonding in conventional and ultra high yield pulps and to control these parameters, if possible, by chemical or mechanical treatments.

PROJECT RATIONALE:

Major limitations of paper and board for many uses are low internal bond strength and poor moisture tolerance. Improved internal strength and enhanced moisture resistance would allow a number of present grades to be produced using less fiber and would also allow new end uses to be developed.

At present, commercial papers do not attain strength levels that realize the full potential of the wood fibers. Most paper mechanical properties are markedly degraded with increasing moisture content. We need to better understand the nature of the changes in fiber properties and fiber-to-fiber bonding with increasing moisture content if we are eventually to improve the moisture tolerance of paper.

RESULTS TO DATE:

PART ONE: Improved bonding via chemical additives.

Results presented in previous reports indicated that cationic/anionic duopolymer additives (primarily CMC/PAE and PAA/PAE) were very effective in improving the strength properties of several softwood unbleached kraft pulps as well as a softwood TMP. In addition to high levels of dry, moist, and wet tensile properties, these combinations significantly improved tensile energy absorption (TEA), extensional stiffness (Et), and stretch. The addition of these bonding agents to the softwood TMP revealed that superior results were generally obtained when added to the long (classified fiber) fraction. A subsequent study of fines and bonding agents in an average yield softwood unbleached kraft pulp showed that readdition of fines to the classified pulp failed to match the original whole pulp in any of the measured dry or moist tensile properties. This differs somewhat from the TMP where readditions of fines produced dry tensile and Et values roughly comparable to the whole pulp. As was found in the case of the TMP, maximum strength in the kraft pulp was generally achieved when CMC/PAE was added to the long fiber fraction.

CMC/PAE and PAA/PAE also proved to be effective bonding agents for a spruce chemimechanical pulp. One or both of these combinations has proved effective in all pulps tested thus far. This favorable result is somewhat tempered by the fact that their efficiency is generally lower in whole pulps than in classified pulps.

Diffuse reflectance FTIR analysis has indicated that covalent bonding occurs when the duopolymer systems are applied to cellulose, but it has not been established if the bonding occurs between the added polymers or between the polymers and cellulose. This work is being extended to include polymer systems where covalent bonding is not possible but where other forms of bonding may occur.

PART TWO: Fundamentals of bonding.

A literature search has been conducted. An instrument to measure axial or transverse fiber mechanical properties and fiber-fiber bond strength has been designed and constructed and is currently being readied for data gathering.

Techniques were developed to study the details of the fracture of the bond between two single fibers. They consisted of:

a) forming the fiber/fiber bond,
b) measuring the bond area using vertical polarized illumination,
c) determining the bond strength, and
d) determining the locus of failure of the bond using the scanning electron microscope.

Results on loblolly pine earlywood fibers revealed a normal distribution of bond areas and a bimodal distribution of bond breaking loads. Examination of the formerly bonded areas with the SEM showed permanent deformation where the fibers had been pressed together but little rupture (tearing) of the external fiber surfaces.

A vibrating reed instrument has been developed to measure the bending modulus of paper and board samples. A range of temperature from ambient to 200°C and a range of relative humidities from 0 to 95% at room temperature can be covered.

PLANNED ACTIVITY FOR THE PERIOD:

PART ONE:

(1) The study of bonding agents will continue. While several anionic/cationic polymers combinations have been found to be quite effective, other materials will be given consideration based on chemical structure and known properties.

(2) The utilization of duopolymer bonding agents will be expanded to include one or more bleached pulps.

(3) Means will be sought to improve the efficiency of polymer bonding agents in whole (fines-containing) pulps.

(4) The study of bonding mechanisms through chemical analysis will be continued in an effort to differentiate between polymer-to-polymer bonds and polymer-to-fiber bonds.

PART TWO:

(1) We plan to measure single fiber properties as functions of moisture content, refining, yield, and pulping method. The measurements will include both axial and transverse properties. The initial work will be with softwoods.

(2) Failure of single fiber/fiber bonds will be continued, with correlations expected among bonded area, bond strength, and locus of failure.

(3) Effective chemical additives identified in Part One will be used in forming single fiber/fiber bonds, whose failure will then be examined as above.

(4) Studies on the effects of pulp yield and refining on mode of bond failure will begin.

Status Report

INTERNAL STRENGTH ENHANCEMENT

Project 3526

PART ONE: Improved Bonding Via Chemical Additives

INTRODUCTION

Progress Report Two covering work in Part One of the program for the past 1½ - 2 years has been issued to the membership. In review, several anionic polymer/PAE combinations produced strength properties approaching or equalling those the "standard" CMC/PAE and PAA/PAE combinations. Of these, carboxymethylated corn and/or potato starch appear to offer the best balance of strength and feasibility. While these materials produced lower breaking length than CMC/PAE, they tended to produce relatively high moist Et and compressive strength.

In most cases, polymer additives and combinations were found to be more effective in improving strength in classified pulps than the whole (unclassified) pulps. This was supported in fines-bonding agent studies utilizing two widely differing pulps. In general, the results indicate that superior strength can be achieved by adding the bonding agents to the long fiber fraction rather than to the fines. A softwood TMP proved more sensitive to the presence of fines than a softwood unbleached kraft pulp.

Analysis of polymer - bonded papers using diffuse reflectance FTIR indicates that substantial improvements in strength over blank controls can be achieved in the absence of PAE and covalent (ester) bonds. Presumably ionic along with hydrogen bonds occur in systems containing cationic polymers such as polyethylenimine. In some cases, the ionic bonds were found to provide higher levels of moist Et and compressive strength but lower wet tensiles than were

afforded by the covalently bonded systems. The lower wet tensile would be expected to translate to improved repulpability. Overall, however, higher strength levels were generally attained in covalently bonded papers.

Finally, the external application of polystyrene to unbleached softwood kraft handsheets was found to provide high levels of Et and compressive strength while maintaining tensile and TEA levels roughly comparable to those achieved by the internal addition of PAE or CMC/PAE.

RESEARCH RESULTS

Some of the more interesting results (in Progress Report Two) obtained since the last Status Report are presented in the following sections. Work with duopolymer systems was extended to include several anionic carboxyl-bearing polymers in combination with PAE. Among these were two samples of carboxymethylated starch. Carboxymethylated cornstarch (CMCS) and potato starch (CMPS) dispersions were prepared by heating aqueous suspensions for 20 minutes at 95°C. These materials along with PAE were added to a classified softwood unbleached kraft pulp over a range in addition levels. PAE was stirred into 0.5% consistency pulp first followed by the starch and further agitation. Handsheets (2.5 g) were formed in a Noble & Wood mold at 0.04% consistency in tap water. The handsheets were pressed and dried in the manner previously described in the project, i.e., 5 minutes pressing at 50 psig and 7 minutes drying at 220°F. The handsheets were tested for the usual dry and moist tensile properties and for STFI compressive strength. Results are recorded in Table 1. Selected strength properties as a function of starch:PAE ratio at a constant PAE addition of 1% are presented in Fig. 1-5. While the starch/PAE combinations did not match the overall performance of CMC/PAE, several combinations approached or equalled the

reference controls in most strength properties. This would apply in particular to CMPS/PAE and to those properties which are of specific interest to this project, i.e. moist Et and compressive strength (Fig. 4 and 5). These anionic starches have a degree of substitution (DS) of approximately 0.11 - 0.12 compared to a D.S. of 0.7 for CMC and 1.0 for PAA. This may account for the greater amount of starch required to improve bonding strength relative to CMC and PAA.

Another series of interest is presented in Table 2 and Figs. 6-13. This series compares the effectiveness of PAE, CMC/PAE, and PAA/PAE in a classified and whole bleached softwood kraft and it also examines the effect of substituting carboxymethylated fiber (DS=0.7) for unmodified fiber. With respect to additive effectivness, the bleached kraft pulp responded to the bonding agents in about the same manner as previously tested pulps. In general, CMC/PAE was found to be the most effective followed by either PAA/PAE or PAE. Actually, the response of the whole pulp to CMC/PAE was the highest of all pulps tested thus far while the increase in the classified pulp was roughly comparable to the average-yield unbleached kraft pulps. Adding fibrous CMC in combination with PAE (Sets 25-28; Figs. 12 & 13) produced rather interesting results in that the fibrous form was not as responsive to PAE as CMC in aqueous solution. In fact, adding up to 10% of fibrous CMC failed to match the performance of 0.4% of water soluble CMC combined with 1% of PAE. Diffuse reflectance FTIR analysis of sets 23 and 25 indicates that a higher level of ester formation (covalent bonding) occurs with external addition. It is postulated that the carboxyl groups in the blended pulp are less accessible to covalent bonding compared with external addition or, alternatively, homocrosslinking plays an important role in the

Table 1. The effectiveness of carboxymethylated starch as a bonding agent in combination with PAE (once-dried classified softwood unbleached kraft).

Set No.	Additives % Based on Fiber	Basis Weight, g/m^2	Apparent Density, g/cc	Dry Strength Properties: Breaking Length, km Av.	SD	TEA, kgm/m^2 Av.	SD	Et, kg/cm Av.	SD	Stretch, % Av.	SD
1	Blank Control	62.9	0.447	3.83	0.284	4.51	0.563	316	33.5	2.6	0.26
2	PAE, 1.0	65.8	0.442	5.27	0.361	7.46	0.954	357	26.6	3.2	0.21
3	PAE, 1.5	61.4	0.447	5.38	0.368	7.64	1.236	313	5.7	3.5	0.36
4	PAE, 1.0; CMC, 0.4	64.9	0.484	7.27	0.531	12.2	1.41	409	22.2	4.0	0.22
5	PAE, 1.0; PAA, 0.2	64.7	0.466	6.14	0.380	10.4	1.01	368	24.9	3.9	0.27
6	PAE, 1.0; anionic starch[a] 1.5	65.4	0.477	5.87	0.368	8.93	0.867	339	32.7	3.5	0.26
7	PAE, 1.0; anionic starch[a] 1.0	68.3	0.456	6.10	0.176	10.1	0.94	367	16.4	3.7	0.27
8	PAE, 1.0; anionic starch[a] 0.5	69.9	0.462	5.99	0.605	10.7	1.32	361	36.9	3.8	0.13
9	PAE, 1.0; anionic starch[a] 0.2	66.7	0.461	5.90	0.293	9.14	0.962	360	25.3	3.5	0.33
10	PAE, 1.0; anionic starch[b] 1.0	73.2	0.492	6.32	0.350	12.3	1.07	407	40.8	3.9	0.16
11	PAE, 1.0; anionic starch[b] 0.5	65.6	0.461	6.38	0.302	10.3	0.54	368	25.4	3.7	0.13
12	PAE, 1.0; anionic starch[b] 0.2	67.2	0.460	5.91	0.521	9.08	1.674	369	20.8	3.4	0.37
13	Anionic starch[a] control, 1.0	60.7	0.423	3.51	0.124	4.06	0.288	272	14.4	2.6	0.10
14	Anionic starch[b] control, 1.0	60.3	0.427	3.61	0.213	4.14	0.530	274	11.5	2.6	0.17

[a]Corn starch -- Carboxymethyl content; 1.2% min.
[b]Potato starch -- Carboxymethyl content; 1.4% min.

Table 1 continued. The effectiveness of carboxymethylated starch as a bonding agent in combination with PAE (once-dried classified softwood unbleached kraft).

Set No.	Additives % Based on Fiber	Moisture Content, % at 91-93% RH	Moist Strength Properties: Breaking Length, km Av.	SD	TEA, kgm/m^2 Av.	SD	Et, kg/cm Av.	SD	Stretch, % Av.	SD
1	Blank Control	15.9	1.88	0.082	3.09	0.354	111	9.3	3.9	0.40
2	PAE, 1.0	15.2	3.64	0.336	7.74	1.03	129	5.1	5.1	0.35
3	PAE, 1.5	14.8	3.73	0.199	7.54	0.557	120	7.6	5.3	0.28
4	PAE, 1.0; CMC, 0.4	15.5	4.78	0.458	11.92	1.05	142	5.5	6.2	0.28
5	PAE, 1.0; PAA, 0.2	15.5	4.17	0.264	9.21	0.718	125	11.9	5.8	0.30
6	PAE, 1.0; anionic starch[a] 1.5	13.9	3.84	0.265	7.30	1.200	144	10.2	5.3	0.41
7	PAE, 1.0; anionic starch[a] 1.0	14.9	3.89	0.095	7.75	0.625	136	7.7	5.5	0.33
8	PAE, 1.0; anionic starch[a] 0.5	15.1	3.84	0.348	8.55	0.837	142	15.0	5.5	0.14
9	PAE, 1.0; anionic starch[a] 0.2	14.7	3.90	0.256	8.59	0.795	156	14.5	5.2	0.19
10	PAE, 1.0; anionic starch[b] 1.0	14.9	4.44	0.274	11.6	0.94	187	11.5	5.8	0.12
11	PAE, 1.0; anionic starch[b] 0.5	15.7	3.72	0.374	7.60	1.625	142	7.7	5.2	0.57
12	PAE, 1.0; anionic starch[b] 0.2	15.7	3.42	0.554	6.97	2.880	125	10.7	5.3	0.86
13	Anionic starch[a] control, 1.0	15.7	1.80	0.155	3.00	0.346	108	4.7	3.6	1.00
14	Anionic starch[b] control, 1.0	15.4	1.79	0.090	3.06	0.316	110	3.1	4.0	0.18

[a]Corn starch -- Carboxymethyl content; 1.2% min.
[b]Potato starch -- Carboxymethyl content; 1.4% min.

Table 1 continued. The effectiveness of carboxymethylated starch as a bonding agent in combination with PAE (once-dried classified softwood unbleached kraft).

Set No.	Additives % Based on fiber	Moist Tensile Factor	Wet Breaking Length, km Av.	Wet Breaking Length, km SD	Wet Tensile Factor	Compressive Strength lbf/in. Av.	Compressive Strength lbf/in. SD	Compressive Strength lbf/in. Av.	Compressive Strength lbf/in. SD	Compressive Strength Factor
1	Blank Control	1.0	0.129	0.008	1.00	7.13	0.777	2.89	0.208	1.00
2	PAE, 1.0	1.94	1.27	0.152	9.8	8.79	0.872	3.01	0.490	1.04
3	PAE, 1.5	1.98	1.66	0.095	12.9	8.36	0.777	3.02	0.291	1.04
4	PAE, 1.0; CMC, 0.4	2.54	2.30	0.138	17.8	10.12	0.813	3.75	0.326	1.30
5	PAE, 1.0; PAA, 0.2	2.22	1.73	0.112	13.4	8.97	0.641	3.41	0.388	1.18
6	PAE, 1.0; anionic starch[a] 1.5	2.04	1.41	0.116	10.9	9.21	0.903	3.33	0.314	1.15
7	PAE, 1.0; anionic starch[a] 1.0	2.07	1.61	0.096	12.5	9.22	0.931	3.45	0.323	1.19
8	PAE, 1.0; anionic starch[a] 0.5	2.04	1.53	0.155	11.9	9.90	0.819	3.72	0.403	1.29
9	PAE, 1.0; anionic starch[a] 0.2	2.07	1.67	0.128	12.9	8.92	0.675	3.87	0.451	1.34
10	PAE, 1.0; anionic starch[b] 1.0	2.36	1.84	0.121	14.3	11.03	1.024	3.95	0.477	1.37
11	PAE, 1.0; anionic starch[b] 0.5	1.98	1.73	0.130	13.4	8.93	0.926	3.39	0.314	1.17
12	PAE, 1.0; anionic starch[b] 0.2	1.82	1.66	0.161	12.8	8.37	0.624	3.94	0.362	1.36
13	Anionic starch[a] control, 1.0	0.96	0.0781	0.006	0.61	5.93	0.500	2.68	0.200	0.93
14	Anionic starch[b] control, 1.0	0.95	0.0847	0.002	0.66	6.05	0.519	2.89	0.247	1.00

[a]Corn starch -- Carboxymethyl content; 1.2% min.
[b]Potato starch -- Carboxymethyl content; 1.4% min.

Table 2. The effectiveness of polymer combinations in softwood bleached kraft.

Set No.	Additives, % Based on Fiber	Basis Weight, g/m^2	Apparent Density, g/cc	Dry Strength Properties: Breaking Length, km Av.	SD	TEA, kgm/m^2 Av.	SD	Et, kg/cm Av.	SD	Stretch, % Av.	SD
				Whole pulp							
15	Blank Control	65.2	0.516	4.35	0.220	6.49	0.806	340	12.4	3.2	0.25
16	PAE, 1.0	64.7	0.509	5.15	0.345	8.63	0.898	341	14.5	3.7	0.17
17	PAE, 1.5	64.7	0.520	5.53	0.290	8.72	0.906	359	13.3	3.5	0.22
18	PAE, 1.0; CMC, 0.4	67.9	0.537	6.88	0.147	13.43	1.158	396	22.3	4.3	0.35
19	PAE, 1.0; PAA, 0.2	65.1	0.519	5.73	0.304	9.68	1.034	363	10.2	3.8	0.21
				Classified pulp							
20	Blank Control	64.7	0.482	3.41	0.133	4.03	0.525	265	10.8	2.6	0.25
21	PAE, 1.0	65.6	0.485	4.66	0.247	7.61	0.511	307	16.4	3.6	0.09
22	PAE, 1.5	65.2	0.492	4.41	0.119	6.07	0.775	294	12.7	3.1	0.33
23	PAE, 1.0; CMC, 0.4	66.2	0.501	6.74	0.470	11.9	1.05	359	25.8	4.1	0.14
24	PAE, 1.0; PAA, 0.2	72.8	0.502	4.65	0.386	7.77	1.178	349	25.1	3.3	0.31
25	99.6:0.4 Bl. Kraft: CMC Fiber, PAE, 1.0	69.1	0.491	4.77	0.565	7.67	1.579	322	27.6	3.4	0.34
26	99:1 Bl. Kraft: CMC Fiber, PAE, 1.0	67.3	0.489	4.89	0.204	8.14	0.700	295	20.0	3.7	0.24
27	95:5 Bl. Kraft: CMC Fiber, PAE, 1.0	67.9	0.469	6.16	0.263	10.9	0.31	321	22.9	4.0	0.12
28	90:10 Bl. Kraft: CMC Fiber, PAE, 1.0	68.9	0.452	6.02	0.549	11.2	1.41	309	16.9	4.2	0.38

Table 2 continued. The effectiveness of polymer combinations in softwood bleached kraft.

Set No.	Additives, % Based on Fiber	Moist Strength Properties: Moisture Content, % at 91-93% RH	Breaking Length, km Av.	Breaking Length, km SD	TEA, kgm/m² Av.	TEA, kgm/m² SD	Et, kg/cm Av.	Et, kg/cm SD	Stretch, % Av.	Stretch, % SD	Moist Tensile Factor
					Whole Pulp						
15	Blank Control	13.6	2.44	0.122	4.65	0.672	149	7.0	4.3	0.47	1.0
16	PAE, 1.0	14.8	3.43	0.268	7.93	0.648	118	10.3	6.0	0.23	--
17	PAE, 1.5	14.0	3.73	0.341	7.64	1.308	137	6.4	5.4	0.45	1.53
18	PAE, 1.0; CMC, 0.4	14.0	4.91	0.144	11.5	1.01	157	8.8	6.1	0.31	2.01
19	PAE, 1.0; PAA, 0.2	13.3	3.80	0.176	8.50	0.479	145	13.9	5.7	0.17	1.56
					Classified pulp						
20	Blank Control	13.9	1.73	0.134	2.27	0.370	129	12.3	3.2	0.24	1.00
21	PAE, 1.0	14.7	2.91	0.243	5.82	0.807	110	4.9	5.1	0.26	1.68
22	PAE, 1.5	13.8	3.04	0.094	5.01	0.398	128	7.6	4.6	0.17	1.76
23	PAE, 1.0; CMC, 0.4	13.6	4.81	0.218	9.48	0.876	148	9.0	5.7	0.20	2.78
24	PAE, 1.0; PAA, 0.2	14.2	2.83	0.111	5.54	0.551	144	4.8	4.7	0.24	1.64
25	99.6:0.4 Bl. Kraft: CMC Fiber, PAE, 1.0	14.1	3.15	0.289	5.59	0.757	130	9.9	4.7	0.25	1.82
26	99:1 Bl. Kraft: CMC Fiber, PAE, 1.0	13.5	3.47	0.221	6.85	0.994	133	8.5	5.0	0.41	2.00
27	95:5 Bl. Kraft: CMC Fiber, PAE, 1.0	14.6	4.02	0.257	9.19	0.432	120	11.9	6.0	0.30	2.32
28	90:10 Bl. Kraft: CMC Fiber, PAE, 1.0	15.3	3.79	0.213	8.05	0.631	120	6.0	5.6	0.25	2.19

Table 2 continued. The effectiveness of polymer combinations in softwood bleached kraft.

Set No.	Additives, % Based on Fiber	Wet Breaking Length, km Av.	SD	Wet Tensile Factor	Brightness,[a] %	Dry STFI Compressive Strength, lbf/in. Av.	SD	Moist STFI Compressive Strength, lbf/in. Av.	SD	Moist Compressive Strength Factor
					Whole pulp					
15	Blank Control	0.109	0.033	1.00	82.2	7.84	0.311	3.03	0.193	1.00
16	PAE, 1.0	1.31	0.128	12.0	--	8.49	0.411	3.07	0.334	1.34
17	PAE, 1.5	1.36	0.091	12.48	72.8	8.66	0.406	3.06	0.226	1.01
18	PAE, 1.0; CMC, 0.4	1.97	0.039	18.07	75.2	9.69	0.508	3.31	0.114	1.09
19	PAE, 1.0; PAA, 0.2	1.16	0.054	10.64	79.8	8.59	0.488	3.33	0.180	1.10
					Classified pulp					
20	Blank Control	0.100	0.013	1.00	84.5	6.22	0.320	2.92	0.274	1.00
21	PAE, 1.0	1.03	0.070	10.3	--	6.65	0.358	2.97	0.228	1.02
22	PAE, 1.5	1.01	0.023	10.1	77.8	6.96	0.439	3.04	0.190	1.04
23	PAE, 1.0; CMC, 0.4	1.92	0.038	19.2	75.3	8.30	0.482	3.49	0.165	1.19
24	PAE, 1.0; PAA, 0.2	0.805	0.046	8.05	80.0	7.99	0.523	3.59	0.251	1.23
25	99.6:0.4 Bl. Kraft: CMC Fiber, PAE, 1.0	1.10	0.154	11.0	78.3	7.66	0.718	3.34	0.348	1.14
26	99:1 Bl. Kraft: CMC Fiber, PAE, 1.0	1.20	0.052	12.0	79.1	7.58	0.525	3.23	0.180	1.11
27	95:5 Bl. Kraft: CMC Fiber, PAE, 1.0	1.67	0.136	16.7	74.3	8.25	0.782	3.26	0.203	1.12
28	90:10 Bl. Kraft: CMC Fiber, PAE, 1.0	1.46	0.107	14.6	77.0	8.36	0.704	3.12	0.225	1.07

		Diffuse reflective FTIR analysis, absorbance peaks occurring at		
		1740 Ester	1650 Amide	A1740/A1650
		Classified pulp		
23	PAE, 1.0; CMC, 0.4	1.02	2.18	0.466
25	99.6:0.4 Bl. Kraft: CMC Fiber, PAE, 1.0	0.67	1.99	0.337

[a]Brightness was not measured immediately after handsheet preparation; hence values may be in error.

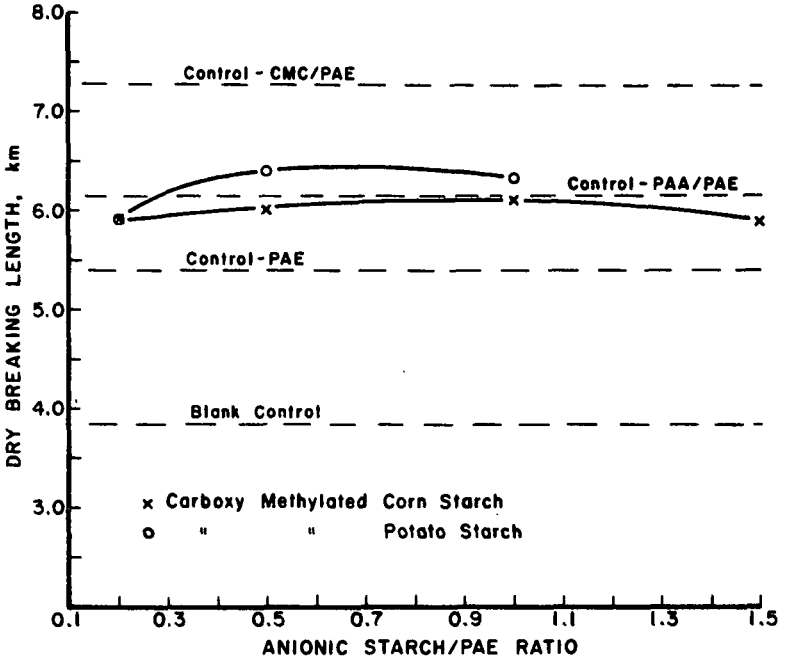

Figure 1. The effect of anionic starch/PAE ratio on dry breaking length (classified softwood unbleached kraft - pulp no. 4).

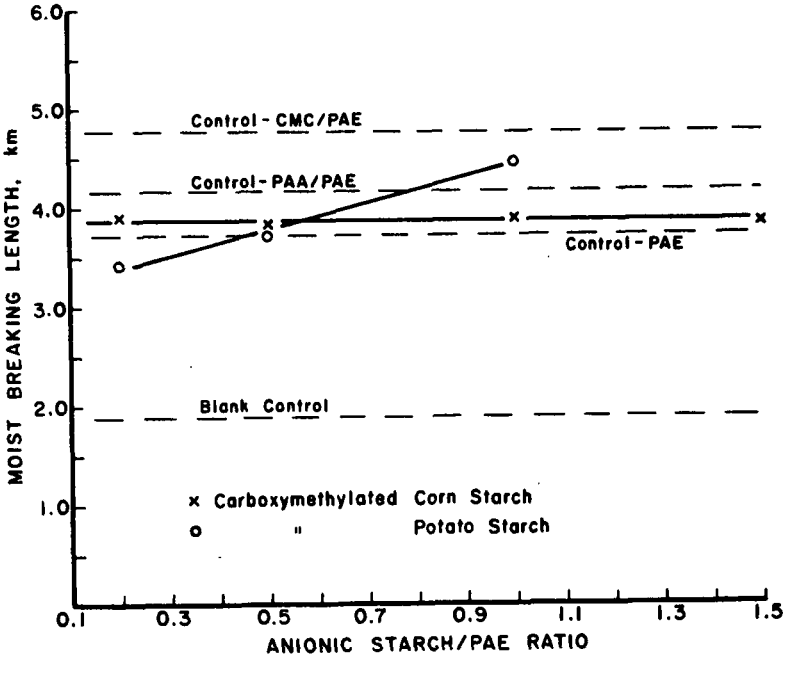

Figure 2. The effect of anionic starch/PAE ratio on moist breaking length (classified softwood unbleached kraft - pulp no. 4).

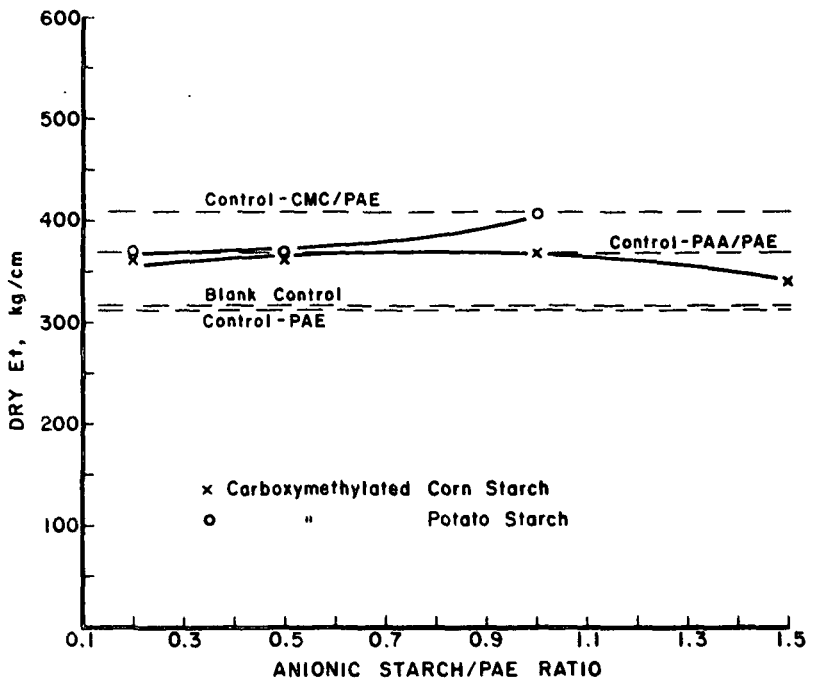

Figure 3. The effect of anionic starch/PAE ratio on dry Et (classified softwood unbleached kraft - pulp no. 4).

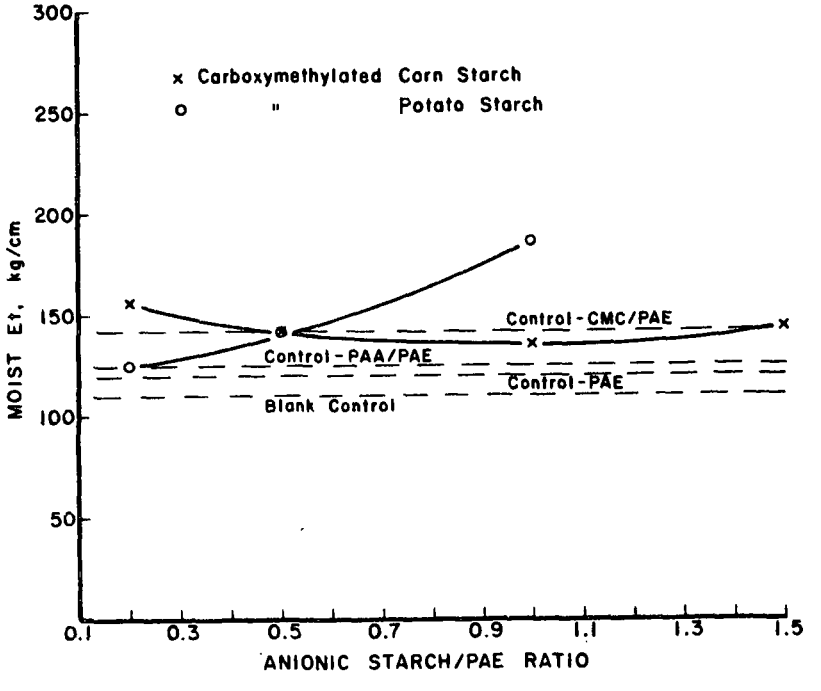

Figure 4. The effect of anionic starch/PAE ratio on moist Et (classified softwood unbleached kraft - pulp no. 4).

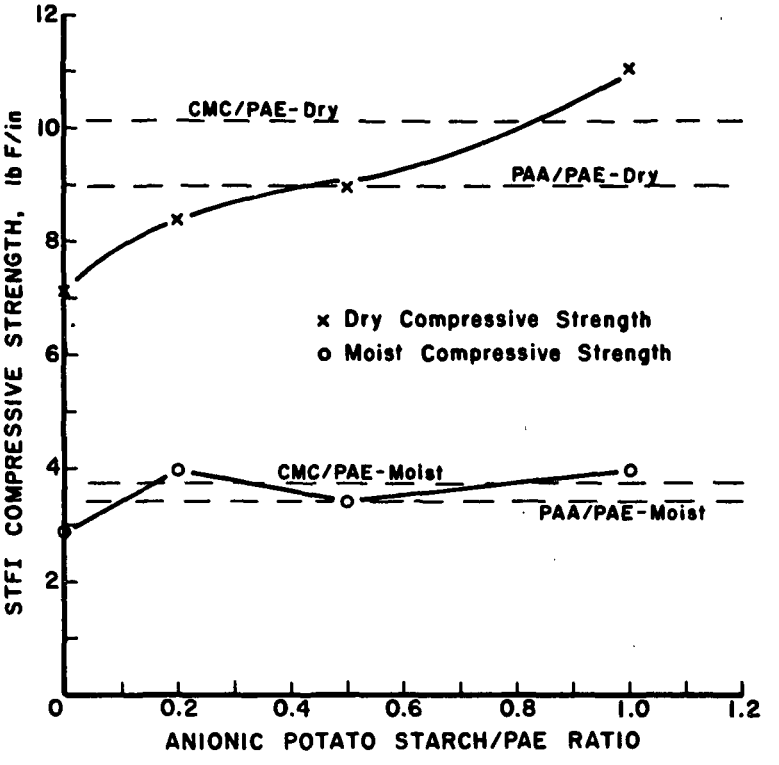

Figure 5. The effect of anionic potato starch/PAE ratio on STFI compressive strength (classified softwood unbleached kraft - pulp #4).

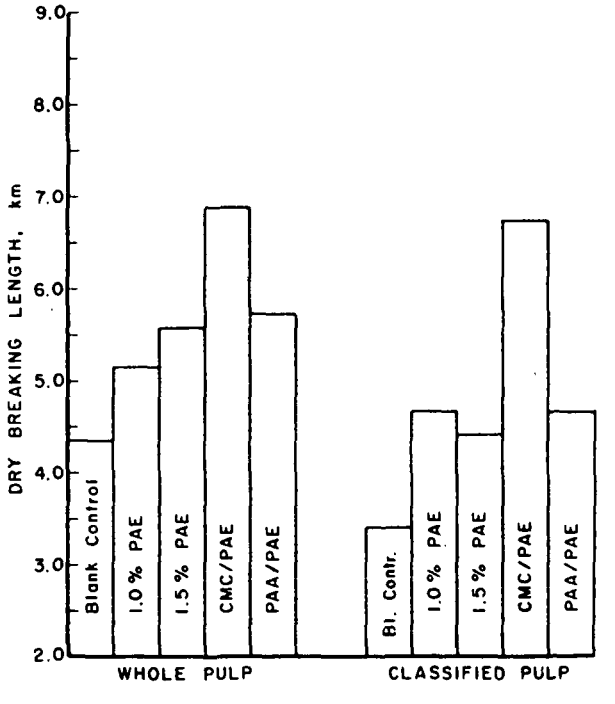

Figure 6. Dry breaking length - softwood bleached kraft.

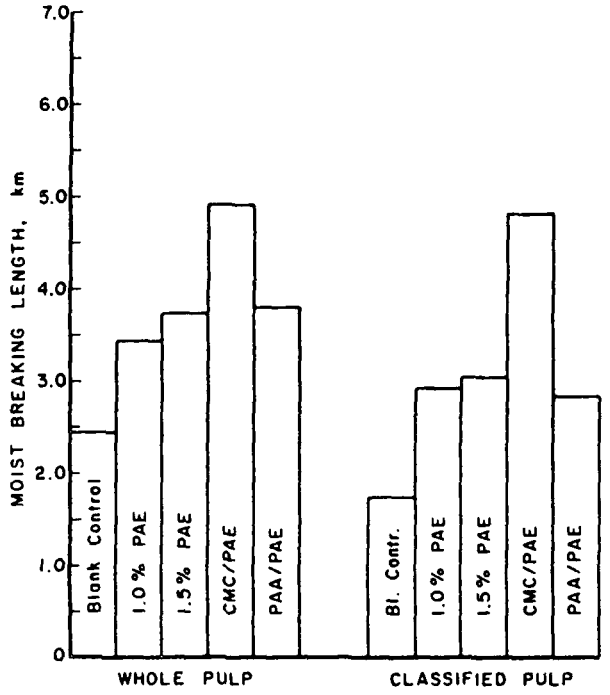

Figure 7. Moist breaking length - softwood bleached kraft.

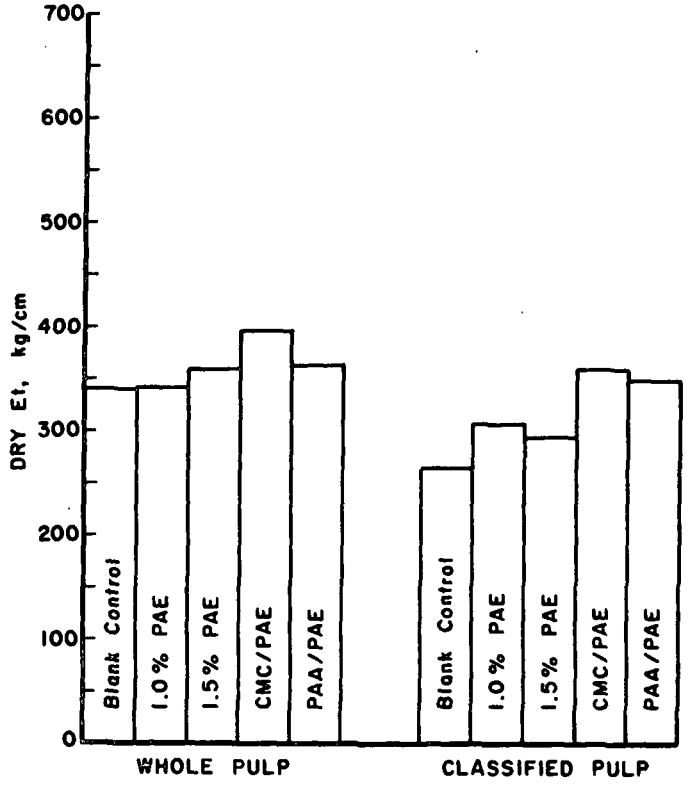

Figure 8. Dry Et - softwood bleached kraft.

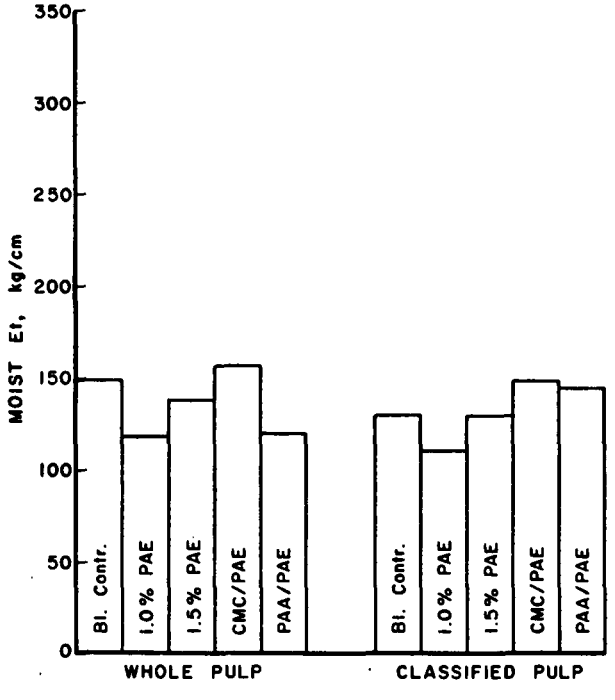

Figure 9. Moist Et - softwood bleached kraft.

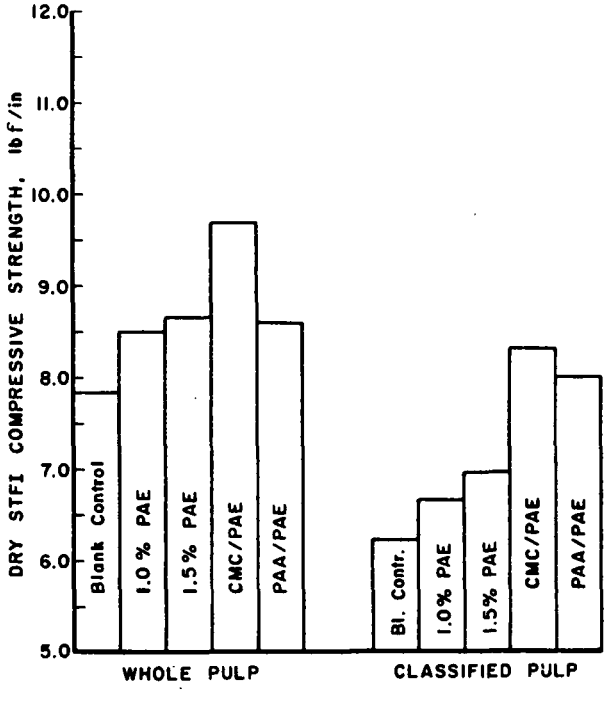

Figure 10. Dry STFI compressive strength - softwood bleached kraft.

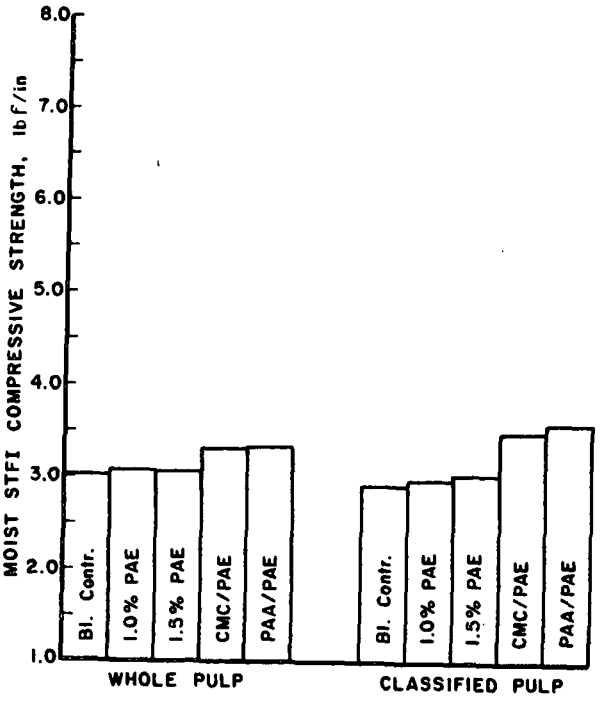

Figure 11. Moist STFI compressive strength - softwood bleached kraft.

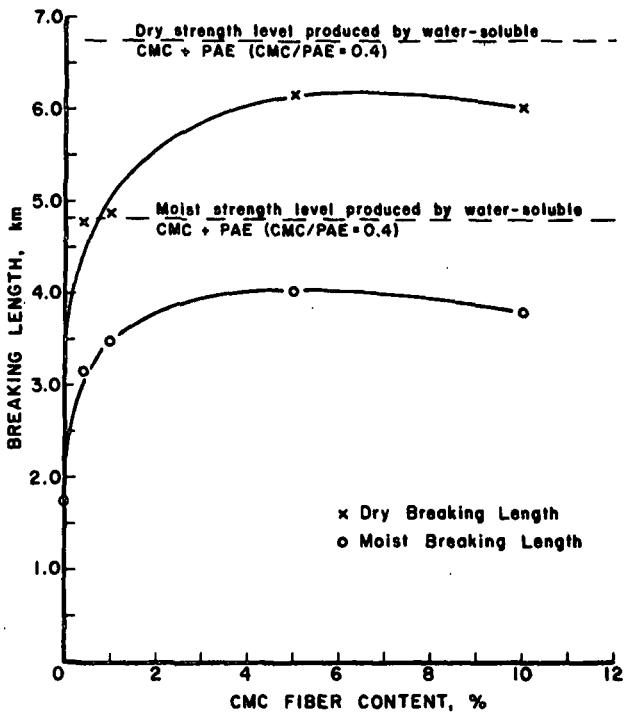

Figure 12. The effect of CMC fiber content on breaking length - bleached softwood kraft with 1% PAE added.

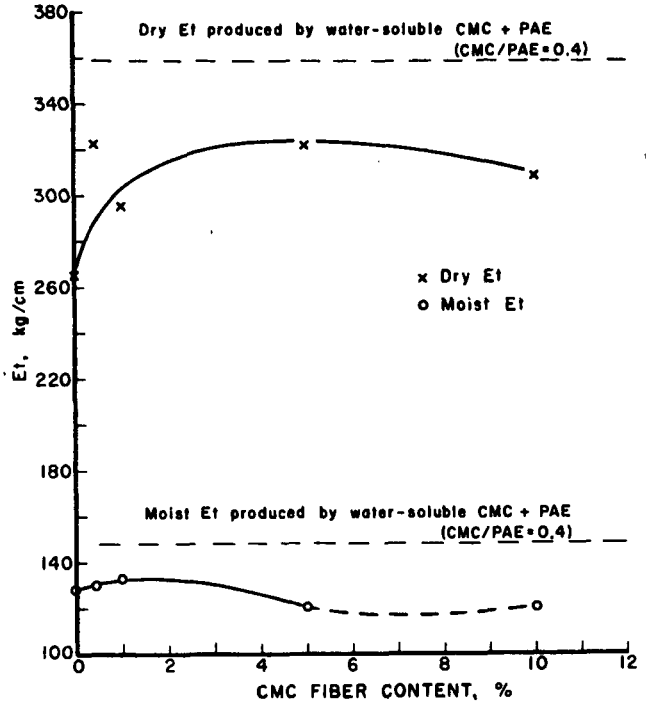

Figure 13. The effect of CMC fiber content on Et (bleached softwood kraft with 1% PAE added).

external addition of CMC/PAE as opposed to the inclusion of CMC fibers in the furnish where only co-crosslinking could occur.

In a continuing study of bonding mechanisms, tests were carried out using polymers which were capable or incapable of forming covalent bonds with cellulose or with themselves. For example, polyethylenimine (PEI) cannot form covalent bonds with cellulose but the combination of PEI/PAA could conceivably form covalent bonds with cellulose through the PAA part of the combination. The results of physical strength tests as well as FTIR analysis for sheets formed from a classified softwood unbleached kraft pulp incorporating PEI and various other polymers are presented in Table 3. These results revealed that rather substantial strength improvements can be achieved in the absence of covalent

bonding, more specifically in the absence of ester formation. However, maximum overall strength levels attained under these conditions were generally lower than those produced by ester formation. Nonetheless several noteworthy results were obtained under conditions where only ionic and hydrogen bonding could occur. For example, PEI alone or combined with polystryene sulfonic acid (PSFA) or PAA produced rather substantial increases in strength. Likewise, polydiallyl dimethylammonium chloride (PDDAC), a cationic polymer incapable of forming covalent bonds with cellulose) produced significant strength increases when combined with PSFA or PAA. Of particular interest are the high moist Et and compressive strengths produced by PEI, PEI/PAA, and several PDDAC combinations leading to the conclusion that ionic bonding may be adequate for the moist strength properties sought in this program.

In the final segment of work, a preliminary evaluation was made of the potential for treating paper externally with a high modulus material. To this end, handsheets formed from a whole unbleached softwood kraft pulp were treated with 10 and 20% polystyrene solutions in toluene. The sheets were immersed in the solvent solutions for 10 seconds and then blotted lightly to remove the excess solution. The treated papers were drum dried in the usual manner (7 min. at 220°F) and then subjected to the full range of physical tests. The results of these tests along with the results for handsheets treated internally with the usual reference agents (PAE, CMC/PAE etc.) are presented in Table 4. The results show that high moist Et and compressive strength were achieved while maintaining high levels of dry and moist tensile. It would appear, however that high add-on levels may be required to attain these properties. This unit of work was not intended to be of any immediate practical value but only to indicate the potential of external treatments for future consideration.

Table 3. Strength properties and bonding mechanisms (once-dried and classified softwood unbleached kraft)

Set No.	Additives, % Based on Fiber	pH in Sheetmold	Basis Weight, g/m^2	Apparent Density, g/cc	Dry Strength Properties: Breaking Length, km Av.	SD	TEA, kgm/m^2 Av.	SD	Et, kg/cm Av.	SD	Stretch, % Av.	SD
1	Blank Controls	7-9	62.9	0.447	3.83	0.284	4.51	0.563	316	33.5	2.6	0.26
2	PAE, 1.0	7-9	65.8	0.442	5.27	0.361	7.46	0.954	357	26.6	3.2	0.21
3	PAE, 1.5	7-9	61.4	0.447	5.38	0.368	7.64	1.236	313	5.7	3.5	0.36
4	PAE, 1.0; CMC, 0.4	7-9	64.9	0.484	7.27	0.531	12.2	1.41	409	22.2	4.0	0.22
5	PAE, 1.0; PAA, 0.2	7-9	64.7	0.466	6.14	0.38	10.4	1.01	368	24.9	3.9	0.27
29	PEI, 1.0	7-9	70.4	0.478	5.00	0.295	7.09	1.014	400	19.4	2.9	0.27
30	PEI, 1.0; PAA, 0.2	7-9	79.6	0.490	5.86	0.252	10.9	1.07	480	9.6	3.4	0.21
31	PDDAC, 0.5	7-9	67.4	0.461	3.89	0.142	5.22	0.372	308	11.8	2.8	0.12
32	PDDAC, 1.0	7-9	64.8	0.460	3.81	0.204	5.06	0.564	284	19.1	2.9	0.17
33	PDDAC, 0.5; PSFA, 0.2	7-9	67.8	0.454	4.06	0.212	5.16	0.709	325	17.0	2.6	0.25
34	PDDAC, 0.5; PSFA, 0.5	7-9	69.9	0.444	5.12	0.315	8.17	0.484	363	25.9	3.3	0.06
35	PDDAC, 1.0; PSFA, 0.2	7-9	69.3	0.455	3.85	0.197	5.80	0.754	312	17.0	3.0	0.24
36	PDDAC, 1.0; PSFA, 0.5	7-9	68.3	0.450	4.15	0.229	5.47	0.733	329	17.3	2.7	0.21
37	PDDAC, 0.5; PAA, 0.2	7-9	71.2	0.455	4.92	0.388	8.98	0.826	338	34.7	3.7	0.23
38	PDDAC, 0.5; PAA, 0.5	7-9	67.4	0.464	5.06	0.226	8.56	1.150	334	15.4	3.6	0.35
39	PEI, 1.0; PAA, 0.2	4.0	70.3	0.451	5.48	0.648	9.37	1.183	381	41.9	3.6	0.11
40	PDDAC, 0.2; PAA, 0.2	4.1	63.7	0.438	4.75	0.299	6.44	0.595	331	22.7	3.1	0.13
41	PDDAC, 0.5; PAA, 0.2	4.1	63.4	0.441	4.53	0.208	5.94	0.744	320	11.4	3.0	0.27
42	PDDAC, 0.5; PAA 0.5	4.1	68.7	0.443	5.23	0.111	8.32	0.355	370	8.0	3.3	0.12

Table 3 continued. Strength properties and bonding mechanisms (once-dried and classified softwood unbleached kraft).

Set No.	Additives, % Based on Fiber	Moisture Content, %	Moist strength properties: Breaking Length, km Av.	SD	TEA, kgm/m² Av.	SD	Et, kg/cm Av.	SD	Stretch, % Av.	SD	Moist Tensile Factor	Wet Breaking Length, km Av.	SD	Wet Tensile Factor	Dry Compressive Strength, lbf/in. Av.	SD
1	Blank Controls	15.9	1.08	0.082	3.09	0.354	111	9.3	3.9	0.40	1.00	0.129	0.008	1.0	7.13	0.777
2	PAE, 1.0	15.2	3.64	0.326	7.74	1.030	129	5.1	5.1	0.35	1.94	1.27	0.152	9.8	8.79	0.872
3	PAE, 1.5	14.8	3.73	0.199	7.54	0.557	120	7.6	5.3	0.28	1.98	1.66	0.095	12.9	8.36	0.777
4	PAE, 1.0; CMC, 0.4	15.5	4.78	0.458	11.92	1.050	142	5.5	6.2	0.28	2.54	2.30	0.138	17.8	10.12	0.813
5	PAE, 1.0; PAA, 0.2	15.5	4.17	0.264	9.21	0.718	125	11.9	5.8	0.30	2.22	1.73	0.112	13.4	8.97	0.641
29	PEI, 1.0	14.8	3.36	0.200	6.92	0.473	168	12.4	4.8	0.15	1.79	0.862	0.061	6.7	9.11	0.548
30	PEI, 1.0; PAA, 0.2	15.1	3.62	0.099	9.18	0.531	185	7.5	5.3	0.27	1.92	0.771	0.018	6.0	11.50	0.893
31	PDDAC, 0.5	15.7	1.80	0.137	3.11	0.422	117	6.1	3.8	0.24	0.89	0.104	0.10	0.82	7.47	0.527
32	PDDAC, 1.0	15.1	1.87	0.068	3.03	0.344	121	7.0	3.7	0.03	0.92	0.133	0.012	1.05	7.30	0.525
33	PDDAC, 0.5; PSFA, 0.2	15.5	1.91	0.064	3.36	0.335	118	7.7	4.0	0.27	0.94	0.179	0.009	1.41	7.67	0.503
34	PDDAC, 0.5; PSFA, 0.5	15.2	2.57	0.156	5.14	0.482	139	5.7	4.5	0.20	1.27	0.353	0.015	2.78	8.97	0.627
35	PDDAC, 1.0; PSFA, 0.2	14.9	2.00	0.070	3.53	0.539	148	10.1	3.8	0.40	0.99	0.115	0.009	0.91	8.10	0.521
36	PDDAC, 1.0; PSFA, 0.5	15.6	2.00	0.086	3.69	0.113	119	5.0	4.2	0.16	0.99	0.177	0.008	1.39	7.77	0.571
37	PDDAC, 0.5; PAA, 0.2	15.6	2.22	0.176	4.28	0.361	131	11.7	4.3	0.23	1.10	0.128	0.009	1.00	8.62	0.635
38	PDDAC, 0.5; PAA. 0.5	15.1	2.51	0.207	4.72	0.561	131	8.6	4.7	0.28	1.24	0.087	0.006	0.68	8.62	0.487
39	PEI, 1.0, PAA, 0.2	15.0	2.89	0.285	6.73	0.615	151	7.5	4.9	0.23	1.54	0.599	0.064	4.6	9.14	1.051
40	PDDAC, 0.2, PAA, 0.2	15.1	2.36	0.171	4.46	0.306	135	9.7	4.3	0.20	1.26	0.111	0.011	0.86	7.54	0.774
41	PDDAC, 0.5, PAA, 0.2	14.9	2.31	0.098	4.47	0.255	127	5.2	4.4	0.13	1.23	1.23	0.006	0.95	7.35	0.79
42	PDDAC, 0.5, PAA, 0.5	15.2	2.55	0.171	5.41	0.322	146	8.9	4.6	0.14	1.36	0.110	0.010	0.85	8.44	0.708

Table 3. continued. Strength properties and bonding mechanisms (once-dried and classified softwood unbleached kraft).

Set No.	Additives, % Based on Fiber	Moist Compressive Strength, lbf/in. Av.	SD	Moist Compressive Strength Factor	Diffuse Reflectance Absorbance Peaks Occurring at 1740 (Ester)	1650 (Amide)	A1740/A1650	Comments
1	Blank Controls	2.89	0.208	1.00	--	--	--	------
2	PAE, 1.0	3.01	0.490	1.04	0.573	2.00	0.287	Band in Ester range 1767-1696 cm^{-1}
3	PAE, 1.5	3.02	0.291	1.04	--	--	--	------
4	PAE, 1.0; CMC, 0.4	3.75	0.326	1.30	--[a]	--[a]	--[a]	------
5	PAE, 1.0; PAA, 0.2	3.41	0.388	1.18	--[a]	--[a]	--[a]	------
29	PEI, 1.0	3.79	0.324	1.31	--	--	--	------
30	PEI, 1.0; PAA, 0.2	4.10	0.512	1.42	--	--	--	------
31	PDDAC, 0.5	3.10	0.282	1.07	--	--	--	No evidence of Ester formation; broad band at 1740-1516 cm^{-1}
32	PDDAC, 1.0	2.96	0.238	1.02	--	--	--	No evidence of Ester formation; broad band at 1740-1516 cm^{-1}
33	PDDAC, 0.5; PSFA, 0.2	3.21	0.183	1.11	--	--	--	No evidence of Ester formation; broad band at 1740-1516 cm^{-1}
34	PDDAC, 0.5; PSFA, 0.5	3.62	0.321	1.25	--	--	--	No evidence of Ester formation; broad band at 1740-1516 cm^{-1}
35	PDDAC, 1.0; PSFA, 0.2	3.33	0.232	1.15	--	--	--	No evidence of Ester formation; broad band at 1740-1516 cm^{-1}
36	PDDAC, 1.0; PSFA, 0.5	3.62	0.302	1.25	--	--	--	No evidence of Ester formation; broad band at 1740-1516 cm^{-1}
37	PDDAC, 0.5; PAA, 0.2	3.23	0.307	1.11	--	--	--	No evidence of Ester formation; Peaks <1600 cm^{-1}
38	PDDAC, 0.5; PAA. 0.5	3.30	0.278	1.14	--	--	--	No evidence of Ester formation; Peaks <1720&1600 cm^{-1}
39	PEI, 1.0, PAA, 0.2	3.28	0.354	1.13	--	--	--	No Ester; Peaks at 1723 & 1661 cm^{-1}
40	PDDAC, 0.2, PAA, 0.2	2.94	0.249	1.02	--	--	--	No Ester; one peak at 1720 cm^{-1}
41	PDDAC, 0.5, PAA, 0.2	2.93	0.295	1.01	--	--	--	No Ester; one peak at 1727 cm^{-1}
42	PDDAC, 0.5, PAA, 0.5	3.31	0.166	1.15	--	--	--	No Ester; one peak at 1720 cm^{-1}

[a]Previously tested and found to contain covalent (ester) bonds.

Table 4. *The effects of externally applied polystyrene on strength properties (whole softwood unbleached kraft handsheets).*

Set No.	Treating Agent	Pickup, % Based on Sheet Wt.	Basis Weight, g/m^2	Apparent Density, g/cc	Dry Strength Properties: Breaking Length, km Av.	SD	TEA, kgm/m^2 Av.	SD	Et, kg/cm Av.	SD	Stretch, % Av.	SD
					External Treatments							
43	Toluene Control	--	64.8	0.483	5.36	0.348	8.02	1.137	379	12.4	3.3	0.29
44	10% Polystyrene solution in toluene	3.87	59.9	0.459	6.70	0.569	10.5	2.11	414	15.0	3.6	0.44
45	20% Polystyrene solution in toluene	12.02	71.6	0.538	7.08	0.268	13.7	1.46	496	16.8	3.8	0.34
					Internal Treatments							
46	Blank Control	--	63.9	0.484	5.20	0.196	7.93	0.939	385	6.4	3.3	0.25
47	PAE, 1.0	--	64.7	0.494	6.14	0.322	8.83	1.354	412	10.9	3.2	0.34
48	PAE, 1.5	--	62.8	0.485	6.31	0.268	9.47	0.757	395	16.0	3.5	0.22
49	PAE, 1.0; CMC, 0.4	--	61.8	0.501	7.35	0.085	13.05	0.745	397	15.3	4.3	0.24
50	PAE, 1.0; PAA, 0.2	--	61.2	0.506	6.97	0.280	11.0	1.09	410	6.7	3.8	0.24

Set No.	Treating Agent	Moisture Content, % (at 91-93% RH)	Moist Strength Properties: Breaking Length, km Av.	SD	TEA, kgm/m^2 Av.	SD	Et, kg/cm Av.	SD	Stretch, % Av.	SD	Moist Tensile Factor	Wet Breaking Length, km Av.	SD	Wet Tensile Factor
							External Treatments							
43	Toluene Control	15.3	3.21	0.117	6.60	0.394	151	9.1	5.0	0.26	1.00	0.157	0.008	1.00
44	10% Polystyrene solution in toluene	14.1	4.12	0.160	8.06	0.737	174	5.1	5.1	0.29	1.28	0.631	0.068	4.02
45	20% Polystyrene solution in toluene	11.6	4.94	0.375	12.7	1.67	232	11.2	5.7	0.31	1.54	1.20	0.213	7.64
							Internal Treatments							
46	Blank Control	15.3	2.84	0.224	5.52	0.706	141	4.7	4.7	0.37	1.00	0.141	0.010	1.00
47	PAE, 1.0	15.9	4.42	0.277	9.76	1.33	135	7.4	6.0	0.39	1.56	1.81	0.137	9.48
48	PAE, 1.5	15.4	4.48	0.188	8.95	0.429	132	8.6	5.8	0.20	1.58	2.13	0.197	11.15
49	PAE, 1.0; CMC, 0.4	15.3	5.17	0.244	11.39	0.856	140	3.3	6.4	0.20	1.82	2.19	0.090	11.47
50	PAE, 1.0; PAA, 0.2	15.8	4.60	0.152	9.77	0.763	135	11.0	6.2	0.28	1.62	1.91	0.070	10.00

Table 4 continued. The effects of externally applied polystyrene on strength properties (whole softwood unbleached kraft handsheets).

Set No.	Treating Agent	Dry STFI Compressive Strength, lbf/in. Av.	SD	Moist STFI Compressive Strength, lbf/in. Av.	SD	Moist Compressive Strength Factor
			External Treatments			
43	Toluene Control	8.82	0.567	3.28	0.218	1.00
44	10% Polystyrene solution in toluene	10.27	1.025	5.02	0.467	1.53
45	20% Polystyrene solution in toluene	14.44	1.280	7.31	0.944	2.23
			Internal Treatments			
46	Blank Control	8.92	0.707	3.97	0.352	1.0
47	PAE, 1.0	10.56	1.280	--	--	--
48	PAE, 1.5	10.54	1.060	4.41	0.476	1.11
49	PAE, 1.0; CMC, 0.4	10.07	0.545	4.37	0.302	1.10
50	PAE, 1.0; PAA, 0.2	10.11	0.875	3.78	0.454	0.95

FUTURE WORK

Information accumulated within the past 12 months indicates that covalent bonding may not be required to provide high levels of moist Et and compressive strength as sought in this program. Future work will include further examination of ionically bonded systems as viable alternatives to covalently bonded paper which is presumably difficult to repulp. Cationic polymers other than PEI and PDDAC will be sought to replace PAE in duopolymer systems and comparisons will be made of the repulpability of ionically and covalently-bonded papers. Means will be sought to improve the efficiency of polymer bonding agents in whole pulps. The study of bonding mechanisms through chemical analysis will be continued in an effort to differentiate between polymer-to-polymer and polymer-to-fiber bonds[1]. Finally consideration will be given to external treatments which are more amenable to practical mill operations than the solvent applications described in this report.

LITERATURE CITED

1. Westfelt, L. Cellulose Chem. Technol. 13:813-25 (1979).

Status Report

INTERNAL STRENGTH ENHANCEMENT

Project 3526

PART TWO: Fundamentals of Bonding.

A. DEVELOPMENT OF TECHNIQUES FOR FLER II

We have been able to pursue the development of techniques for the use of the FLER II at only a minimum level during this period.

Bond strength measurements made by gluing fibers to the edges of microscope cover - glass slips were tried for a few fibers. These were unsuccessful because the fractured edges of the slips were not flat and perpendicular to the plane of the slips, resulting in glass-glass or glass-fiber contact rather than fiber-fiber contact during the initial compressive preloading for bonding. Careful selection of slip edges will be needed when further tests are made.

The electronic balance used for load sensing has enough compliance that the movable clamp is not held extremely rigidly. As a consequence, it is not possible to install pin-mounted fibers for tensile testing without breaking them during the installation. It has been found that this difficulty can be overcome by cementing only one end of a fiber to a pin, clamping that pin in the movable clamp, and then pushing the free end of the fiber into a bit of molten hot-melt adhesive on the fixed clamp. Cooling the hot melt completes the preparation for testing. We are still looking for a suitable hot melt, since those we have tested so far either wick into the fiber wall and lumen, suffer brittle fracture in the joint area, or do not adequately grip the fiber. Adhesive and hardness/toughness characteristics similar to those of the epoxy resin used are needed.

A 35-mm camera has been purchased for attachment to the microscope on the FLER II to enable use to photograph the individual fibers as they are being tested. This is a necessary adjunct for lateral compaction tests, where it will be used to record the fiber area under compaction.

B. SINGLE FIBER/FIBER BONDS

Van den Akker[1] has reviewed the parameters that are important to the strength of paper. Both experimentally and theoretically[2] tensile failure is found to depend on a) individual fiber strength and b) the extent and strength of fiber/fiber bonding. A specific objective of this project is to improve the strength of the individual fiber/fiber bond. This bond depends upon (a) the strength of the interaction between the two fibers and (b) the area over which these interactions occur (or the bonded area). In absence of additives the interactions are thought to be hydrogen bonds plus the ubiquitous van der Waals bonds. Chemical additives can supplement these interactions to produce improved wet or dry strength. If the fiber/fiber interactions are strong enough, the locus of failure may be between the S1 and S2 layers of one of the fibers. It is important that we know the location of the failure so that we may direct the chemical additives to this weak spot. Our research is focused on characterizing the strength of the fiber/fiber bond and on its dependence on bonded area and locus of failure.

We form the bonds by crossing two wet fibers at right angles in a sandwich between two teflon-faced rubber disks. The sandwich is then placed under a static load (nominal pressure 17 psi) in an oven at 105°C for one hour. The now-bonded fiber pair is then cemented to a jig for subsequent measurements.

The vertical polarized light method to measure the bond area optically was developed by Page and associates[3-5]. Page[3] has argued that the areas of optical contact do indeed represent bonded areas but see below.

After measurement of the bond area, the sample is mounted in the FLER II instrument. Strain in the bond is produced by pulling on the end of one of the fibers while holding the ends of the other fiber fixed. This results in a nominal shear strain in the fiber/fiber bond region. In practice the second fiber experiences some deformation in the direction of the extension as well as some rotation about its axis. Thus the geometry of the strain in the bonded region is a combination of shear and peeling. The relative contributions of these two strains likely varies from sample to sample and may partly account for the wide distribution of breaking loads observed for a given sample population. The load at which failure occurs is noted and can be converted to a bond strength by dividing by the bond area determined previously.

It might be expected that breaking load should vary directly with the bond area. However, both for the present data and that of earlier workers[6], no correlation between the two parameters exists. This is probably a result of the variability in strain geometry noted above and also to the basic heterogeneity of wood fibers. Cell wall thickness, S2 fibrillar angle, and pit architecture are among the important factors which vary within a fiber population. Button[7] has shown that cellophane strips apparently follow linear elastic theory where breaking load decreases with increasing bond area due to stress concentration effects. Application of this concept to the present data did not produce any clear trend, again perhaps due to the variable fiber population and strain geometry.

Observation of the formerly bonded areas was carried out in a scanning electron microscope (SEM) after coating the samples with gold/palladium to eliminate electrostatic charging effects.

Results have been obtained from two sets of fibers to date. The first is a loblolly pine conventional kraft cook using only springwood chips. After they were washed, the chips were gently defibered to yield individual fibers, probably with the S1 layer intact. Fiber/fiber bonds from this population (denoted "untreated") were formed and tested. The averages from 34-45 bonds are given in the second column of the upper half of Table 5. A slurry of a portion of the same fibers was treated with the combination PAE/CMC found to be an effective strength aid in Part One of this project. The dosage was 1% PAE followed by 0.4% CMC based on fiber weight. A series of fiber/fiber bonds from this population (denoted "treated") was likewise formed and tested. The average values are given in the third column of Table 5. The ratio of the results for the treated to the untreated are presented in the last column. As previously alluded to, the parameters of the individual bonds vary widely. Bond area shows a normal distribution while breaking load gives a skewed distribution on both the normal and log normal scales. In spite of the broad distribution the effect of the polymer treatment is significant at a 98% confidence level. The table shows that the breaking load, bond area, and bond strength increase by 159, 17, and 77%, respectively, when the chemical treatment is applied. These improvements are in line with those found in the handsheet studies of Part One of this project. The increase in bond area suggests the polymer may bring about closer contact along the periphery of the bond.

The SEM results were quite revealing. For the untreated fibers almost no fiber wall damage was observed. Formerly bonded areas were easily identified

Table 5. Average values for single fiber/fiber bond properties.

Property	Arithmetic Mean Untreated	Arithmetic Mean Treated	Treated/ Untreated
Unrefined Fibers			
Breaking Load, g	0.44	1.14	2.59
Bond Area, μm^2	2530	2970	1.17
Bond Strength, $\mu g/\mu m^2$	220	390	1.77
Refined Fibers			
Breaking Load, g	0.75	1.47	1.96
Bond Area, μm^2	1350	1600	1.19
Bond Strength $\mu g/\mu m^2$	600	1030	1.72

by the impressions (permanent deformations) each had left in the other along the edges of the crossover area. The bond areas, however, for the most part were smooth and unfractured.

Dramatically different results were found for the treated fibers. Here the majority of the fibers showed picking and tearing of their walls. Apparently, the chemical additive shifted the locus of failure, thereby increasing the strength.

We next looked at the effect of refining. The second set of fibers was a conventional kraft cook of a southern pine which was then beaten to 370 mL CSF. This pulp was then classified on a 65 x 35 mesh twill wire followed by washing of the long fibers in a Britt drainage jar fitted with a 60 mesh bronze wire. Few fines should remain. Fiber bonds were formed and tested as before. Fibers were either "untreated" or "treated" with the same levels of PAE/CMC as

was the first set. The results are presented in the lower half of Table 5. Again, significant improvements in breaking load, bond area, and breaking strength are achieved when the strength additives are used. Note that although the breaking load and bond strength of the refined fibers are greater than the values for the unrefined fibers, the bond areas for the latter are much less. This is likely due to the refined fiber population being comprised of both springwood and summerwood.

Although the SEM work showed clear differences between treated and untreated fiber bonds for the unrefined samples, this was not the case with the refined fibers. Formerly bonded areas of the latter showed extensive picking and tearing of both treated and untreated fibers. In addition there was a great deal of loosened fibrillar material (S1 layer?) along the fiber. It was not possible to unambiguously conclude that the additives changed the locus of failure. Further work with less heavily refined fibers may clarify the situation.

From the results to date we can conclude that additives have a strong effect on individual fiber/fiber bonds. In the case of unrefined fibers the increase in bond strength is apparently (at least in part) a result of a shift in the locus of failure. For the refined fibers the additives produce a similar enhancement in strength, but a possible shift in the locus of failure is unclear.

Future studies on bond strength will examine:

- the effect of light refining,
- the difference between summerwood and springwood,
- the effect of additives on a high yield (TMP or other) pulp, and
- the effect of "all-ionic" bonding agents as used in Part One of this project.

LITERATURE CITED

1. Van den Akker, J. A., Tappi 53(3):388(1970).

2. Page, D. H., Tappi 52(4):674(1969).

3. Page, D. H. Paper Tech. 1:407(1960).

4. Page, D. H., and Tydeman, P. A., Paper Tech. 1: 519(1960).

5. Page, D. H., Tydeman, P. A. and Hunt, M. In Bolam's Formation and Structure of Paper, Tech. Sec. BPBMA, London, Vol. I, p. 171 (1962).

6. Mayhood, Jr., C. H., Kallmes, O. J., and Cauley, M. M., Tappi 45(1):69(1962).

7. Button, A. F., Doctoral Dissertation. Appleton, Wisconsin. The Institute of Paper Chemistry, 1979

THE INSTITUTE OF PAPER CHEMISTRY

Appleton, Wisconsin

Status Report

to the

PAPER PROPERTIES AND USES

PROJECT ADVISORY COMMITTEE

Project 3571

BOARD PROPERTIES AND PERFORMANCE

September 10, 1986

PROJECT SUMMARY

PROJECT NO. 3571: BOARD PROPERTIES AND PERFORMANCE September 10, 1986

PROJECT STAFF: W. J. Whitsitt, R. A. Halcomb

PROGRAM GOAL:

Develop relationships between critical paper and board property parameters and how they are achieved in terms of raw material selection, principles of sheet design, and processing conditions.

PROJECT OBJECTIVE:

- To develop relationships between container performance, combined board and component properties.
- To improve the performance/cost ratios of combined board (including medium).
- The short term goals are directed to (1) using structural models to assess the impact of papermaking factors on combined board and box performance and (2) improving medium end-use and converting performance properties.

PROJECT RATIONALE, PREVIOUS ACTIVITY AND PLANNED ACTIVITY FOR FISCAL 1986-87 are on the Project Form that follows.

SUMMARY OF RESULTS LAST PERIOD: (October 1985 - March 1986)

Section 1 - ECT/Box Compression

(1) Experimental linerboards were made to test the effects of changing linerboard compressive strength-to-flexural stiffness ratios on combined board and box performance. These linerboards were made into C-flute combined boards on the Institute's pilot corrugator. In other work we have experimentally varied medium properties.

(2) Our results indicate that ECT is primarily dependent on the compressive strengths of the liners and medium. The flexural stiffness of the liners plays a minor role.

(3) ECT can be satisfactorily related to the elastic stiffnesses of the linerboard and medium.

(4) We have also related the elastic stiffnesses of the components to the flexural stiffnesses of the combined board, taking into account flute geometry.

(5) Box compression predictions indicate that top load compressive strength increases as the linerboard and medium are densified by wet pressing. Making a squarer linerboard also increases box compressive strength.

Section 2 - Process Research

(1) Fracture speeds predicted with our runnability model decrease with increasing basis weight of medium. This is the same trend as is obtained experimentally.

(2) The stress ratios calculated from the model are correlated with the occurrence of high-lows for mediums of different basis weights.

(3) Work is underway to make mediums with various combinations of fiber orientation, refining, pressing, and weight. In terms of end-use the results will show how to balance flat crush and ECT demands. They will also provide information on some of the parameters entering into our runnability model.

(4) The strength degradation of the medium as speed is increased is under study. Preliminary results show that the tensile strength of the formed medium decreases with increasing speed. The reductions in strength are related to the applied stresses and changes in draw factor.

SUMMARY OF RESULTS THIS PERIOD: (April 1986 - September 1986)

Section 1 - ECT/Box Compression

(1) Models are being developed to evaluate the impact of papermaking improvements on ECT strength per unit weight of fiber in the components.

(2) Preliminary results suggest that the following papermaking factors can improve strength-to-weight ratios.
a) Increased fiber-to-fiber bonding of the liners and medium.
b) Decreased MD/CD ratios (directionality).

Section 2 - Medium Improvement

(1) For a given Concora, CD STFI strength can vary over a wide range. Higher CD STFI strengths are favored by increased wet pressing, refining, and less directionality.

(2) For heavy weight mediums at least, it should be possible to reduce flat crush levels but increase ECT strengths.

Section 3 - Runnability Modeling

(1) Our runnability model shows that flute fracture speeds and high-lows depend on four properties of the medium. They are MD tensile, MD stretch, hot coefficient of friction and thickness.

(2) Linear and curvilinear relationships between stress ratios calculated from the model and high-lows have been developed. Both forms show high correlations.

(3) At a constant high-low level, a sensitivity analysis shows that changes in stretch and thickness have the greatest effect on operating speeds. Friction and MD tensile have slightly lower effects than the other two properties.

Section 4 - Periodicites in high-low flute formation.

(1) Activities during this period have concentrated on spectral analysis techniques. A significant periodic component with a period of about 5-6 flutes continues to be observed.

Section 5 - Flat crush modeling.

(1) The use of different medium physical properties (E_{MD}, G_{MD-ZD} and caliper) produced significant changes in the load-deflection curves generated by the finite element analysis. Knowledge of the fluted medium physical properties, both before and during loading, will determine the accuracy of the flat crush finite element analysis.

(2) A finite element program capable of material and geometric nonlinear analysis will be necessary to conduct extensive studies of paper materials.

PROJECT TITLE: Board Properties and Performance

PROJECT STAFF: W. Whitsitt/R. Halcomb

PRIMARY AREA OF INDUSTRY NEED: Properties related to end uses.

PROGRAM AREA: Performance and Properties of Paper and Board

Date: 6/1/86
Budget: $150,000
Period Ends: 6/30/87
Project No: 3571

PROGRAM GOAL:

Develop relationships between critical paper and board property parameters and how they are achieved in terms of raw material selection, principles of sheet design, and processing conditions.

PROJECT OBJECTIVE:

- To develop relationships between container performance, combined board and component properties.
- To improve the performance/cost ratios of combined board (including medium).
- The short term goals are directed to (1) using structural models to assess the impact of papermaking factors on combined board and box performance and (2) improving medium end-use and converting performance properties.

PROJECT RATIONALE:

There are many aspects of container and component performance which have not been adequately related to board properties through structurally sound models. Such structural models identify the critical board properties needed for end use performance. They can then be used to select papermaking approaches to maintain or improve box performance at less cost. An important step is to incorporate the elastic stiffnesses of the board into such models if possible. This will allow us to use our developing knowledge on how papermaking factors affect the elastic stiffnesses to make board improvements.

RESULTS TO DATE:

Rayleigh-Ritz methods have been used to analyze container failure under several types of load. Finite element techniques have been used to model the bending behavior of container board. Analysis of present ECT vs. component local buckling models indicates they fail to predict ECT performance when the liner or medium density is changed. Therefore new models have been developed which show that combined board ECT is primarily dependent on the compressive strength and/or elastic stiffnesses of the liners and medium. The bending stiffness of the liners appears to have only a minor effect on ECT. These results have been experimentally validated and are being extended to box compression. In the case of medium we have shown that the compressive strength is lowered by high bending and shear stresses imposed during forming. These losses in strength lower flat crush and ECT. The losses are inversely related to the density and Z-direction elastic stiffness of the medium. Densification via wet pressing is one way to improve end-use performance of medium.

Our current forming models indicate that satisfactory high speed runnability on the corrugator is dependent on at least four medium properties as well as nip geometry and medium web tension.

PLANNED ACTIVITY FOR THE PERIOD:

The relationships being developed will show how the elastic stiffnesses and compressive strengths of the components will affect combined board ECT and box compression strength. The analysis will help us assess the relative importance of compressive strength and the bending stiffnesses of the liners and medium in determining box performance. We will confirm and validate the relationships using components made under various papermaking conditions as well as commercial boards.

We plan to use finite element techniques to model flat crush load-deformation characteristics in relation to medium properties and flute geometry. This work will better define how crushing of board during conversion and end-use degrades box performance. The same technique will be considered as a way to improve our understanding of the bending stresses during fluting.

Our research on medium shows that densification via wet pressing improves strength retention during fluting and gives higher ECT and flat crush in the combined board. We will continue and extend this research to consider other ways to improve formability and performance. This will include work on sheet directionality, pressing, and refining.

As an outgrowth of this and related work for FKBG, we will investigate ways to show what properties of the linerboard and medium are required for high-speed runnability on the corrugator. Runnability refers to the critical speeds associated with strength retention, the development of high-lows and flute fracture.

We are also considering initiating work in fracture mechanics as related to flute fracture and the application of power spectral density techniques to flute uniformity.

POTENTIAL FUTURE ACTIVITIES:

Application of similar techniques to end-use failures involving flexure, shear and combined tension, flexure and shear.

Status Report

BOARD PROPERTIES AND PERFORMANCE

Project 3571

The objectives of this program are to: (1) develop relationships between container performance, combined board and component properties, and (2) determine ways to improve the cost/performance ratios of medium and linerboard. To fulfill these objectives we must consider both end-use performance and processing runnability on the corrugator. Therefore our current work is divided into several parts, namely, (1) ECT and box compression performance, (2) medium improvement, (3) runnability modeling, (4) high-low periodicity, and (5) flat crush modeling.

ECT and Box Compression Relationships

An important part of our past work has been directed to developing relationships between combined board ECT and the properties of the linerboard and medium which will be valid under most papermaking conditions. A specific goal is to incorporate the elastic stiffnesses of the components in such relationships. This will allow us to use nondestructive ultrasonic techniques to characterize board and box performance. It also enables us to use our developing knowledge on how papermaking factors affect elastic stiffnesses to assess ways to improve performance.

After study of alternatives we modeled ECT in the same way as the Institute top load box compression formula. This is termed the miniature plate approach. Conceptually ECT is set equal to the sum of the maximum strengths of the individual liner and medium plate elements. Following this approach the contributions of the liners and medium are formulated as the product of two terms:

Liner: $(\text{compressive strength})^{b} \times (\text{mean flexural stiffness of liner})^{1-b}$

Medium: $(\text{compressive strength})^{c} \times (\text{mean flexural stiffness of medium})^{1-c}$

The constants b and c must be experimentally determined and their magnitudes will reflect the relative importance of the two properties. For compressive strength we employ either short span compressive strength values or the in-plane and out-of-plane elastic stiffnesses.

As discussed in the last status report we obtained good predictive accuracies using this approach. The magnitudes of the exponents indicated that ECT is primarily dependent on the compressive strength characteristics of the liners and medium. The flexural stiffness of the medium has a negligible effect; the flexural stiffness of the liners appears to have only a small effect on combined board ECT.

To validate these results experimental linerboards were made wherein we varied the ratio of CD compressive strength to flexural stiffness. This was accomplished by varying the density via wet pressing, directionality and incorporating additives. Good agreement was obtained between observed and predicted ECT values. Thus we are now able to relate ECT to either short span compressive strength or the elastic stiffnesses of the liners and medium. For the last meeting combined board flexural stiffness was also modeled. Good agreement was obtained with experimental results. Use of these models on box compression predictions was begun.

Currently we are studying ways to optimize ECT and box strength-to-weight ratios. As an initial step in developing optimization procedures we have considered the effects of selected papermaking changes to improve liner and/or medium properties on ECT strength-to-combined board weight ratios.

We used the following equation:

$$ECT = 1.375 \times STFI_L + 1.101 \times STFI_M + 1.212 \qquad (1)$$

where ECT is combined board edge crush (lb/in.) and $STFI_L$ and $STFI_M$ are the CD short span compressive strengths (lb/in.) for the liner and the medium respectively. This equation was determined from the experimental data base, reported on at the last meeting, which included combined boards made with liners and mediums of varying basis weights, densities and MD/CD ratios. This equation may be written in the form:

$$ECT = 1.375 \times BW_L \times SS_L + 1.101 \times BW_M \times SS_M + 1.212 \quad (2)$$

BW_L = basis weight of liner (lb/1000 sq ft)

BW_M = basis weight of medium (lb/1000 sq ft)

SS_L = CD liner specific compressive strength ((lb/in.)/(lb/1000 sq ft))

SS_M = CD medium specific compressive strength ((lb/in.)/(lb/1000 sq ft)).

In Eq. 2 the STFI strengths in Eq. 1 have been reformulated as the product of basis weight times specific compressive strength, i.e. compressive strength per basis weight.

In this form it is possible to investigate how improved specific compressive strengths will influence the amount of fiber required. It is assumed in Eq. 2 that the basis weights may be changed independently of the specific strength values. For the purpose of the current study the specific strength properties of the three liners and two mediums from our past experimental data base were selected. Table 1 below gives the specific compressive strengths for the five components, their codes and an explanation of how the enhanced strength were experimentally achieved.

Three discrete liner and medium basis weights (26, 29 and 32 lb/1000 sq ft) were chosen to illustrate the dependence of ECT on component basis weights for the component specific compressive strength given in Table 1. Each

Table 1. Component specific compressive strengths.

Component	Specific Compressive Strength (lb/in.)/(lb/10000 sq ft)	Code	Comment
Liner	0.4975	NL	"Normal" liner
Liner	0.5648	HL	High density liner achieved by wet pressing
Liner	0.6558	1L	Low ratio E_x/E_y liner achieved by controlling fiber alignment
Medium	0.5918	NM	"Normal" medium
Medium	0.6569	HM	High density medium

of the three liner basis weights was combined with each of the three medium basis weights in the calculations giving a total of nine different combined boards as shown in Table 2.

Table 2. Basis weight combinations.

	Basis Weight, (lb/1000 sq ft).								
Liner	26.0	26.0	26.0	29.0	29.0	29.0	32.0	32.0	32.0
Medium	26.0	29.0	32.0	26.0	29.0	32.0	26.0	29.0	32.0
Combined Board	89.4	93.8	98.1	95.4	99.8	104.1	101.4	105.8	110.1

In Fig. 1 we have plotted predicted ECT (using Eq. 2) versus combined board basis weight for the 9 basis weight combinations shown in Table 2. The specific strengths used for the points plotted in Fig. 1 were those of the "normal" liner (NL) and "normal" medium (NM) in Table 1. As an illustration the data Point 1 in Fig. 1 is the predicted ECT of 41.9 lb/in. for a 29-32-29 combined board (total basis weight 104.1). (Note: these 9 points represent the

base case where the increase in ECT has been obtained by adding component basis weights only without enhancing the component specific strengths).

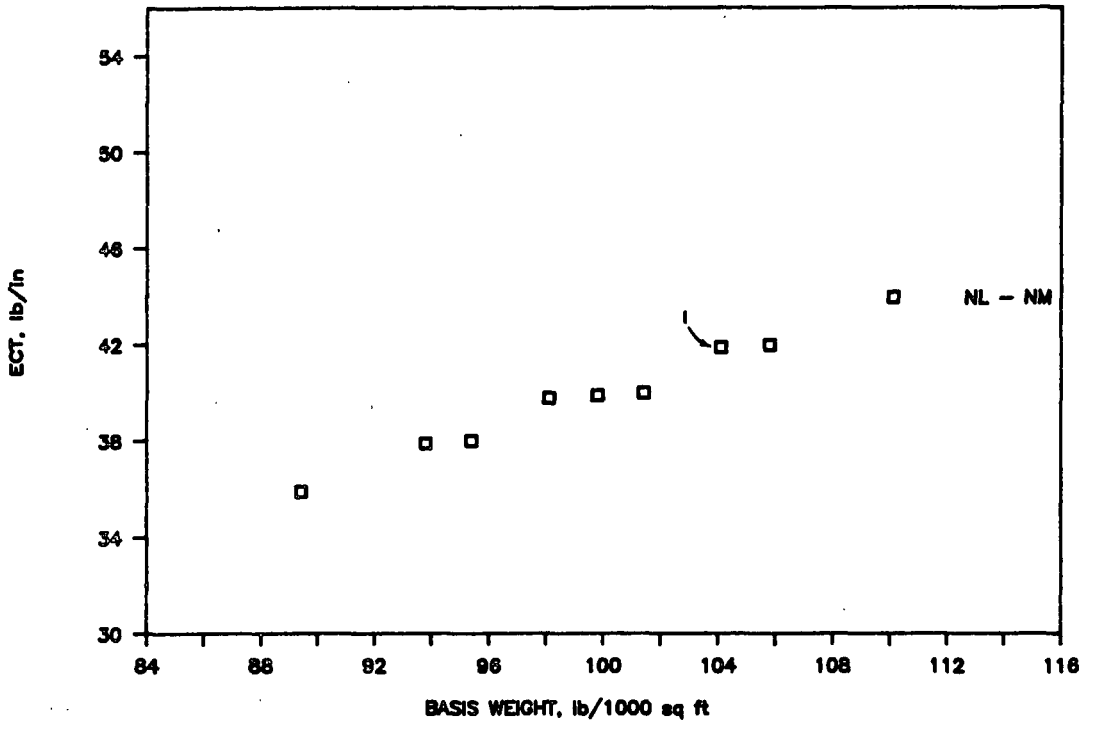

Figure 1. Predicted ECT vs. combined board basis weight. For explanation of numbered data point see text.

Figure 2 shows ECT vs. weight values for the case where "normal" liners are combined with a higher density medium (NL-HM). As would be expected using a stronger medium results in higher ECT values at a given basis weight than for the base case using "normal" components. For about the same ECT value (42 lb/in.) as Point 1 of the base case, Point 2 of the NL-HM case uses about 6 lb/1000 sq ft less basis weight.

Figure 3 shows the ECT data points plotted in Fig. 2 together with the predicted ECT values for two more cases. In one case the high density liner is combined with the normal medium (HL-NM) and in the other case the high density

liner is combined with the high density medium (HL-HM). For about the same ECT value (42 lb/in.) as Point 1 of the base case, Point 3 of the HL-HM case uses 93.8 lb of fiber suggesting a savings of about 10 lb over Point 1.

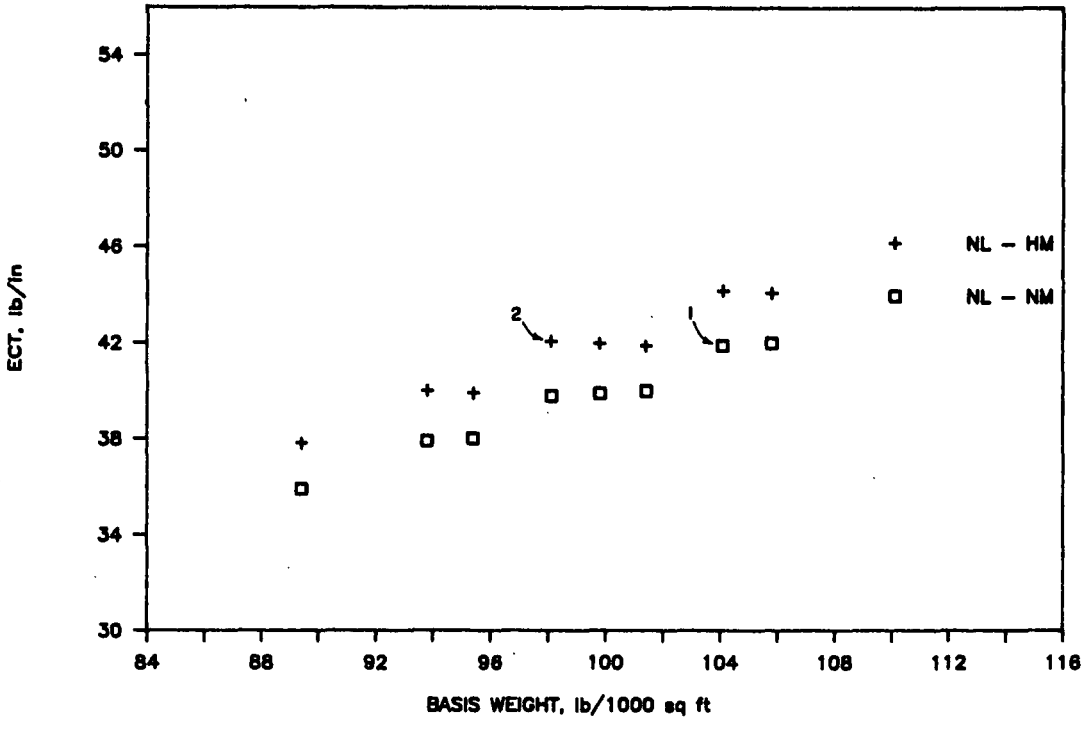

Figure 2. Predicted ECT versus combined board basis weight. For explanation of numbered data points, see text.

Figure 4 shows how the predicted ECT for base case (NL-NM) compares against the case where the low directionality liner is combined with the normal medium (1L-NM) and the case where the low directionality liner is combined with the high density medium (1L-HM). For about the same ECT value (42 lb/in.) as Point 1 of the base case, Point 4 of the 1L-NM case uses 89.4 lb of fiber suggesting a savings of about 14 lb.

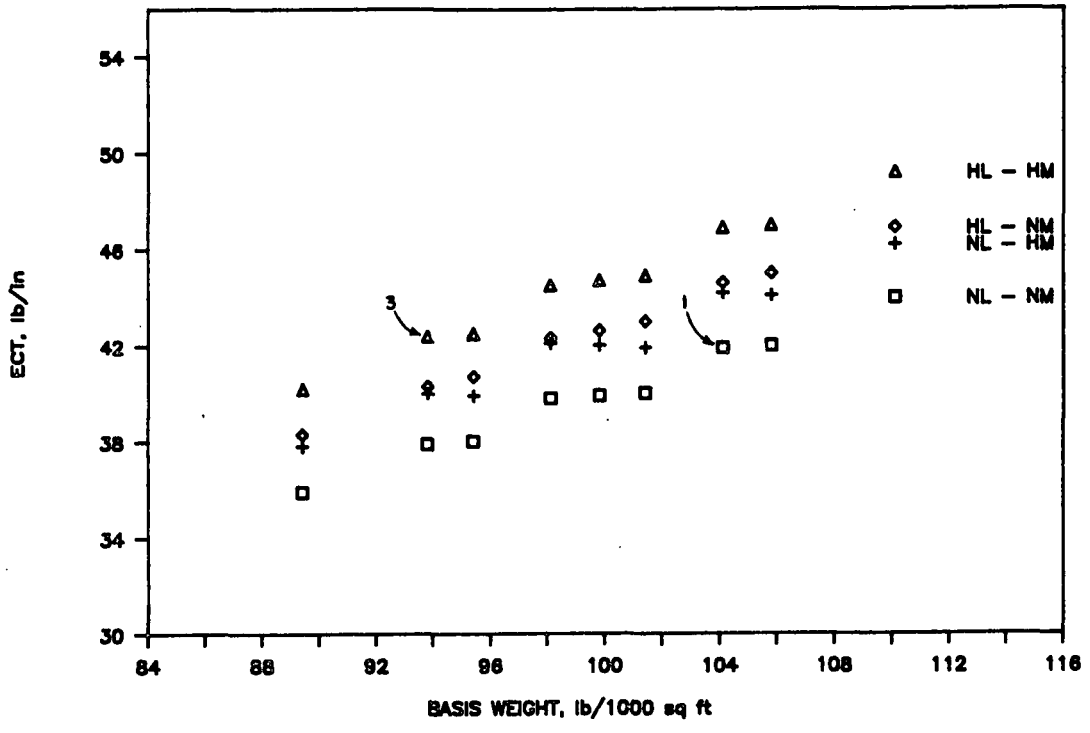

Figure 3. Predicted ECT versus combined board basis weight. For explanation of numbered data points, see text.

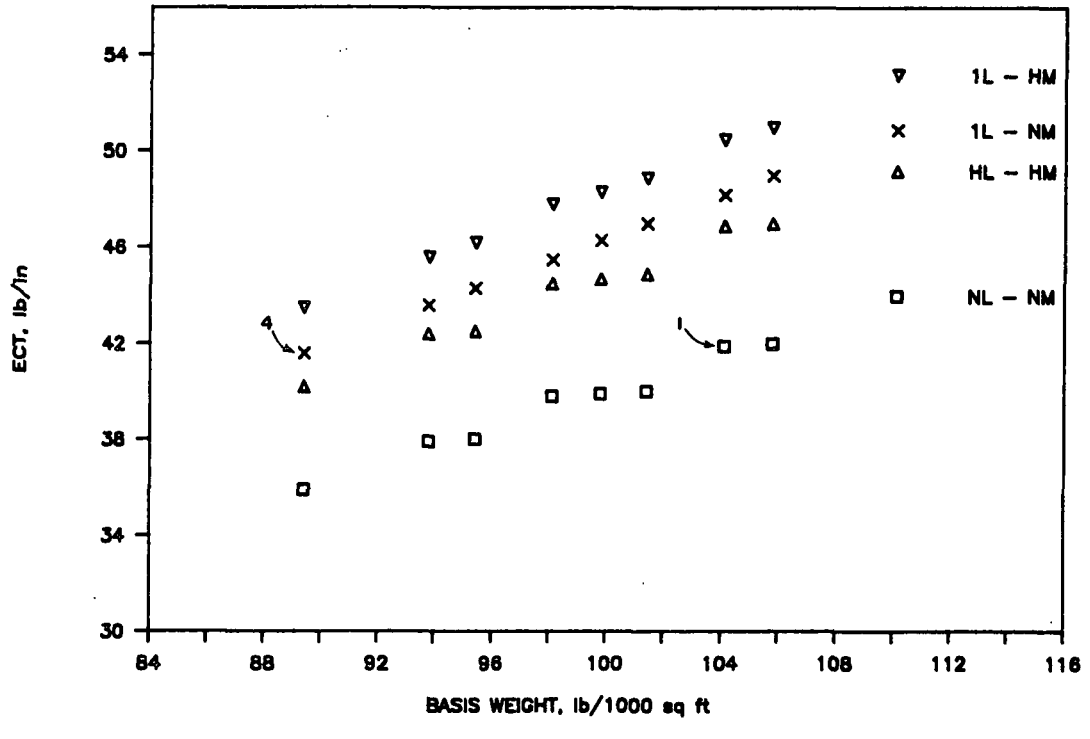

Figure 4. Predicted ECT versus combined board basis weight. For explanation of numbered data points, see text.

As indicated by the above preliminary results, the strength models can be used to look at ways to optimize ECT strength for a given weight of fiber. The examples shown suggest that the following papermaking changes would give the same ECT values for less basis weight:

1. increased wet pressing of the liner and/or medium to give high CD compression strength,
2. decreased MD/CD ratio of the liner.

In our future work several alternative ways of optimizing the selection of the components to achieve a given ECT are being considered. Another possibility is to determine what ECT levels can be achieved for components having a given basis weight.

Medium Improvement

Medium requirements include both MD and CD strengths for end use. Good runnability requires consideration of MD strength, coefficient of friction and thickness. As papermaking changes are made to increase medium strength it should be possible to square up the sheet to improve CD strength for improved ECT while maintaining reasonable levels of flat crush and good runnability.

We have begun to develop information on papermaking ways to optimize medium properties considering both flat crush and CD compressive strength as well as runnability. As an initial step experimental mediums have been made on the Formette former using combinations of pressing, refining, directionality and basis weight.

The furnish is comprised of 75% NSSC pulp with 25% softwood kraft. The following experimental combinations have been made and tested at this time.

1) Refining: Low and high refining (about 400 and 475-550 CSF).

2) Wet pressing: Low and high levels.

3) Fiber orientation (elastic stiffness ratios of about 1.0+, 2.0+, and 2.5+.

4) Basis weights: 26 and 40-lb/1000 ft^2.

Presently this corresponds to a partial factorial design; we will expand on the design and add other factors as is appropriate.

After preparation of the Formette sheets they were fabricated into corrugated board on the Institute's pilot corrugator. Corrugating speeds ranged from 400 - 800 fpm depending on the basis weight and other characteristics of the medium.

Table 3 summarizes selected compression properties of the mediums and the combined board made therefrom. In Fig. 5 the 40-lb CD STFI results are plotted vs. Concora Index results for the several conditions; Fig. 6 shows the corresponding combined board properties of ECT vs. flat crush. For these 40 lb mediums the graph configurations are somewhat similar but not identical. In general, however, increasing directionality reduces CD STFI or ECT while increasing Concora or flat crush. On the other hand increased fiber-to-fiber bonding via refining or wet pressing increases both ECT and flat crush or CD STFI and Concora strengths.

For a given minimum Concora level in Fig. 5, say 1.9 Nm^2/g, CD STFI strengths can vary widely depending on the pressing, refining and directionality levels. For this furnish and conditions employed, CD STFI strengths could vary between about 16 to 30 Nm/g. If minimum values for both Concora and CD STFI are prescribed, say Concora and CD STFI indexes of 1.9 and 21 respectively, then the acceptable operating conditions for these conditions would lie in an upper right quadrant above the respective minimums.

Table 3. Physical characteristics of experimental mediums.

Lot. No.	Test Factors: Wet Pressing	MD/CD	Refining	Basis Weight, g/m2	Density IPC kg/m3	MD STFI lb/in.	CD STFI lb/in.	MD Tensile lb/in.	CD Tensile lb/in	MD Stretch, %	CD Ring Crush, lb/6 in.	Concora, lb	Flat Crush lb/sq-in.	ECT, lb/in.
3761-43	High	Low	Low	125.80	742	21.8	21.0	42.9	34.0	2.13	51.6	58.0	35.51	55.1
3761-45	High	Medium	Low	130.10	759	29.9	16.6	57.7	22.5	1.83	50.0	81.2	47.88	53.0
3761-46	High	High	Low	131.70	755	32.5	15.1	63.7	19.6	1.74	50.0	89.3	56.04	51.5
3761-34	Low	Low	Low	125.00	524	17.9	17.3	33.8	28.4	1.76	47.6	47.8	27.68	49.1
3761-36	Low	Medium	Low	127.00	540	25.1	12.4	45.4	18.1	1.48	41.2	64.2	37.77	46.5
3761-37	Low	High	Low	133.20	550	29.2	11.2	52.7	16.0	1.44	40.4	75.7	42.97	44.6
3761-24	Low	Low	High	141.00	560	22.1	20.8	41.0	31.7	1.72	62.2	67.2	38.94	53.9
3761-27	Low	Medium	High	133.60	586	29.5	15.2	54.3	22.0	2.05	52.2	81.8	47.94	48.5
3761-28	Low	High	High	128.60	589	29.2	12.8	54.4	17.7	1.51	43.8	81.2	51.16	47.2
3761-48	High	Low	Low	197.40	703	33.9	32.3	62.5	53.4	2.28	109.2	90.8	54.99	68.0
3761-50	High	Medium	Low	201.80	729	46.3	27.5	84.1	38.5	1.96	101.6	107.8	68.35	62.9
3761-51	High	High	Low	204.40	735	50.2	25.1	97.6	33.6	2.02	101.6	136.0	83.34	60.2
3761-39	Low	Low	Low	193.60	526	28.4	26.9	50.9	44.6	1.78	82.2	62.7	31.82	58.5
3761-41	Low	Medium	Low	197.00	553	37.9	21.1	74.2	29.8	1.74	72.8	81.7	35.11	52.7
3761-42	Low	High	Low	205.70	563	45.5	19.5	83.8	28.7	1.61	76.2	97.2	40.41	53.0
3761-29	Low	Low	High	187.90	545	30.0	26.4	53.1	41.8	1.93	89.6	79.8	46.24	59.7
3761-31	Low	Medium	High	191.80	562	38.7	21.7	72.7	32.0	1.92	87.4	105.7	58.93	56.5
3761-33	Low	High	High	197.00	580	44.2	20.7	81.7	29.0	1.62	82.6	125.8	62.49	53.7

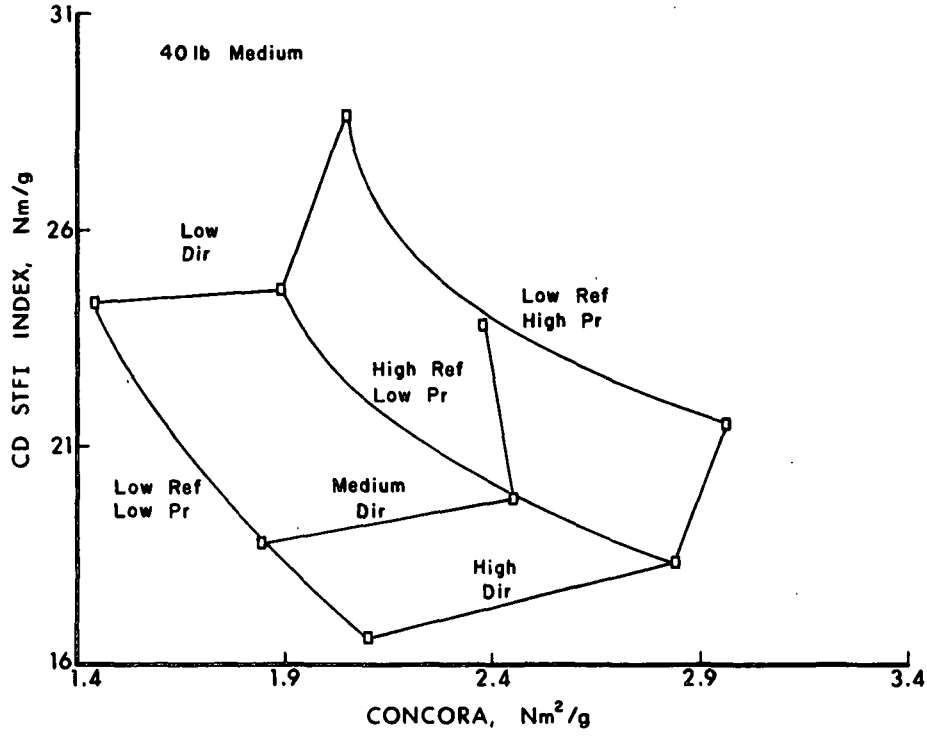

Figure 5. Relationships between CD STFI compressive strength and Concora for 40-lb mediums.

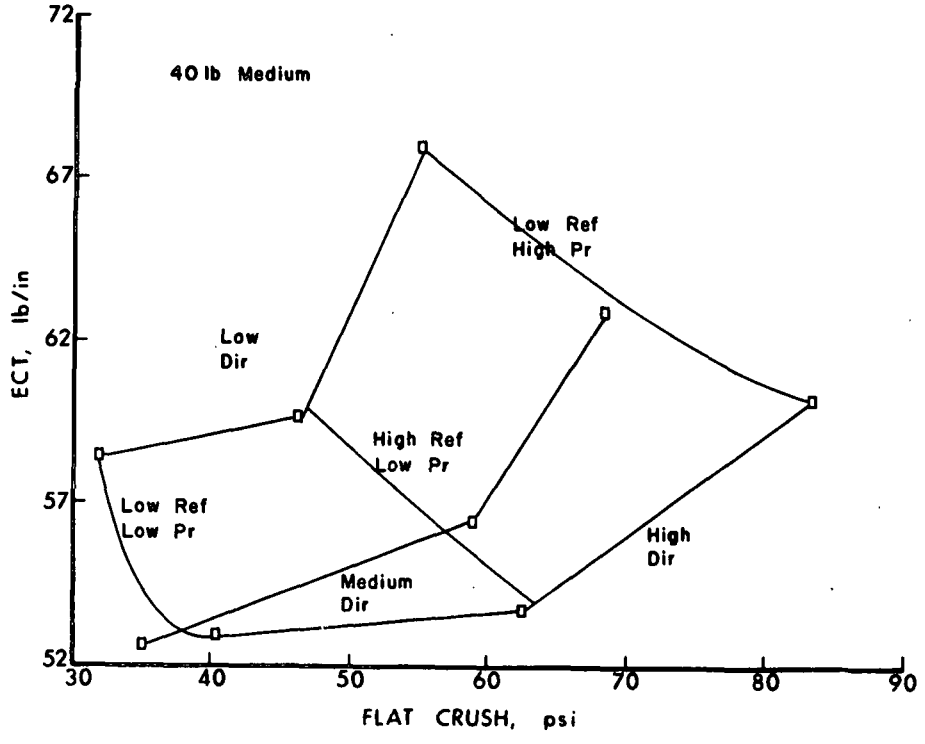

Figure 6. Relationships between ECT and flat crush for 40-lb medium combinations (42-lb liners).

Figure 6 can be interpreted in the same manner. It directly shows how changes in medium papermaking conditions affect flat crush and ECT strengths. In general higher ECT strengths at a given flat crush level are favored by papermaking conditions resulting in better fiber bonding and less sheet directionality. For heavy weight mediums it may be quite possible to reduce flat crush target levels if this makes it possible to maintain ECT strengths more economically.

Figure 7 and 8 show the corresponding results for the 26-lb mediums. The STFI vs. Concora Index results in Fig. 7 are esentially similar to the 40-lb medium results in Fig. 5 because basis effects are removed. As in the case of 40 lb results, there may be opportunities to shift the balance between Concora and CD compressive strengths by adjustment of papermaking conditions.

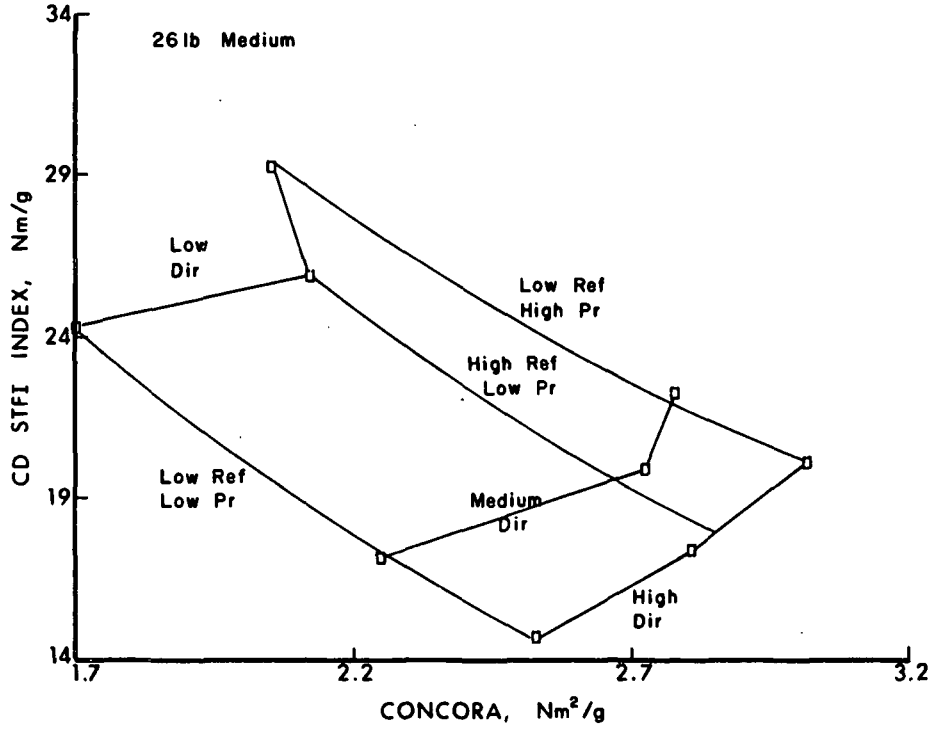

Figure 7. Relationships between CD STFI compressive and Concora strengths for 26-lb medium.

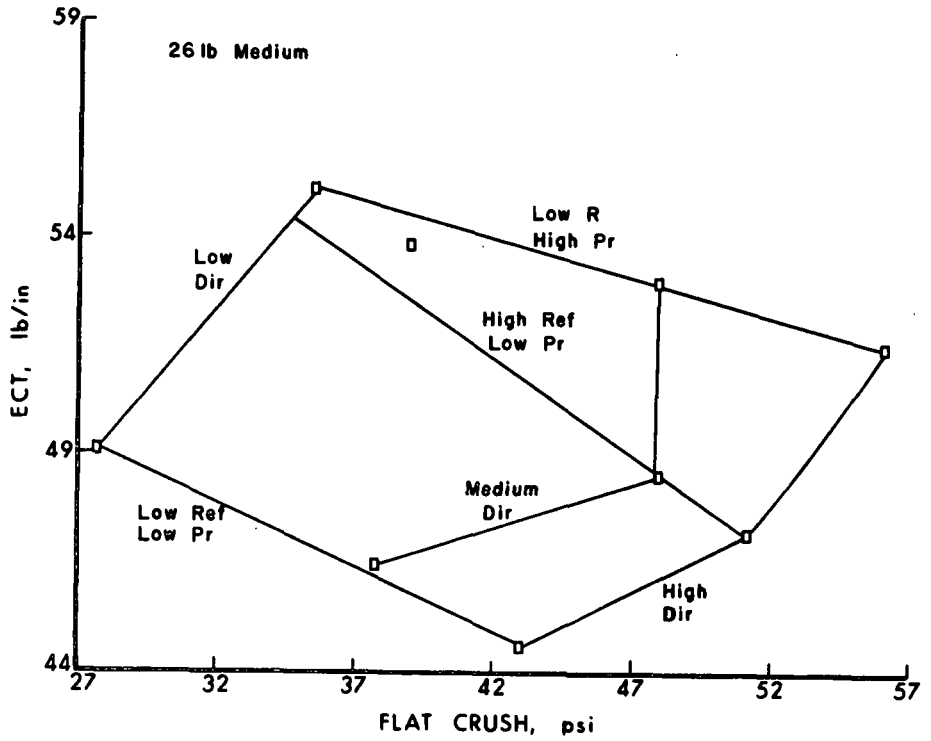

Figure 8. Relationships between ECT and flat crush for 26-lb medium combinations (42-lb liners).

Figure 9 shows that the CD STFI results increase with density in the expected manner as refining and wet pressing were changed. Separate curves are obtained depending on the directionality induced during forming.

The CD ring crush results show more complex trends with density because of the buckling mode of failure on thinner sheets (Fig. 10). This probably accounts for the lower strengths per unit weight of the 26-lb mediums and their tendency to exhibit a maximum as density was increased.

We plan to expand our data base to include other papermaking ways to enhance medium strength. At the same time we will analyze the results to show how runnability on the corrugator would be affected by changes in Concora/CD STFI short span compression strength balance. Our current results show that

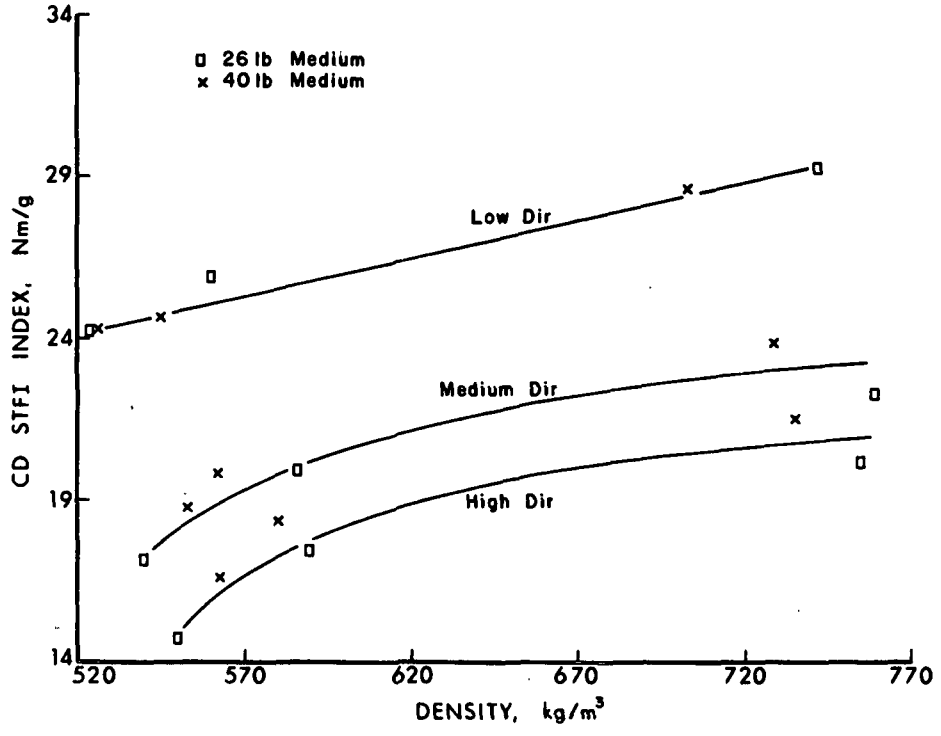

Figure 9. STFI short span compressive strength vs. density.

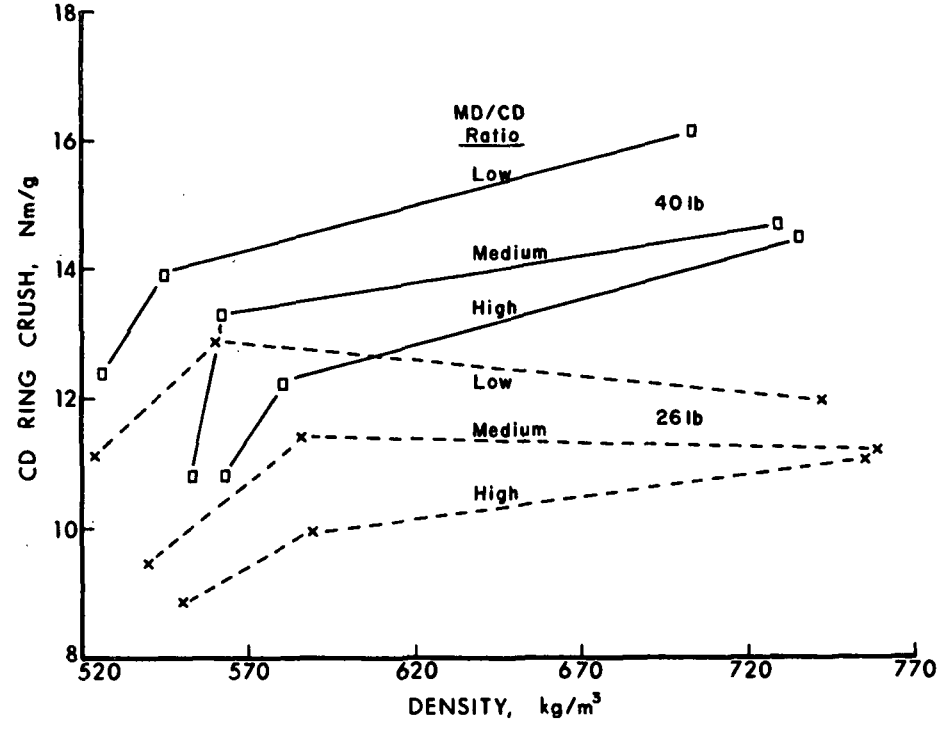

Figure 10. CD ring crush vs. density for varius MD/CD ratios.

1) For a given Concora, CD STFI strengths can vary over a wide range. Higher CD STFI strengths are favored by increased wet pressing and refining and less directionality.

2) For heavy weight mediums at least, it should be possible to reduce flat crush levels but increase ECT strengths. Savings in medium fiber can result from this approach, depending on papermaking factors.

Runnability Modeling

To supplement our research on high speed runnability for the FKBG we are developing models which will explain how critical corrugating speeds are dependent on medium properties, nip geometry, and operational factors. The models are based on physical analysis of the corrugating process but are empirical at this time. We believe the model has application to high-low flute formation, flute fracture, and to strength losses during fluting. A discussion of the model concepts is contained in previous status reports.

Applied Stresses and Flute Fracture

The following equation is being used to predict the speed at which flute fracture is observed.

$$(T_o + k_1 S_f)e^{\mu\theta} + k_2 T_b = T_f \qquad (3)$$

where T_o = brake tension

S_f = fracture speed

θ = total wrap angle in labyrinth $\doteq$ 3.09 rad.

μ = coefficient of friction

T_b = tension in outer layer induced by bending

T_f = tensile strength of medium

k_1 = empirical constant $\doteq$ 1/297

k_2 = empirical constant $\doteq$ 0.0979

At present the bending strain T_b is being estimated as follows.

$$T_b = 50\ T_f t/[\varepsilon(R + t/2)] \quad (4)$$

where T_f = tensile strength of medium

t = thickness of medium

ε = medium stretch, %

R = radius of curvature of flute tip

Equation 1 gives the following relationship for the fracture speed S_f:

$$S_f = (370/e^{\mu\theta})[T_f - k_2 T_b - T_o e^{\mu\theta}] \quad (5)$$

Based on average results for 26, 33 and 40-lb mediums Fig. 11 shows that estimated fracture speeds decrease with basis weight and web tension in the expected way. We expressed these as relative speeds because some allowance for the decreased flank clearance in the corrugating nip or shear effects may be necessary for very thick mediums.

Figure 12 shows that observed and predicted fracture speeds are in good agreement for 26-lb mediums. Most of the predictions for 33-lb mediums were also in good agreement with the observed fracture speeds. These results lend credence to the model. Thus flute fracture appears to be dependent on the four properties incorporated in the model, namely, friction, MD tensile, MD stretch, and thickness.

If S is given some value less than the fracture speed, then the left side of Eq. 3 is an estimate of the total applied tensile stresses at that speed. As speed is increased the total stress increases. Fracture occurs when the applied stress exceeds the tension stress. Dividing the applied stress at a given speed by the tensile strength provides an estimate of the applied stress intensity ratio at the given speed.

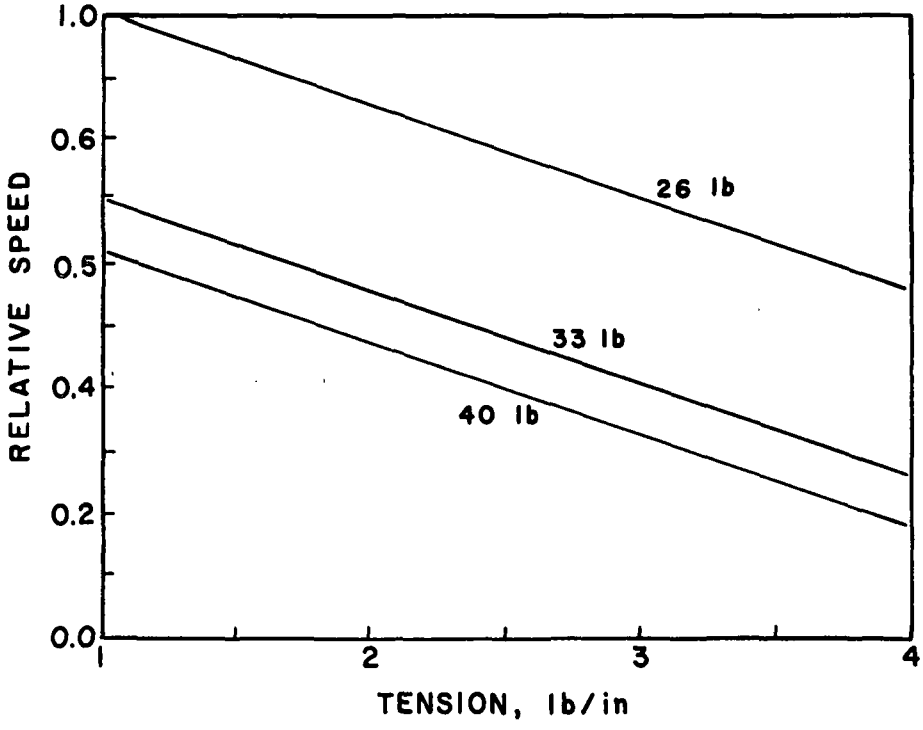

Figure 11. Estimated average relative speeds to flute fracture for 26, 33 and 40-mediums.

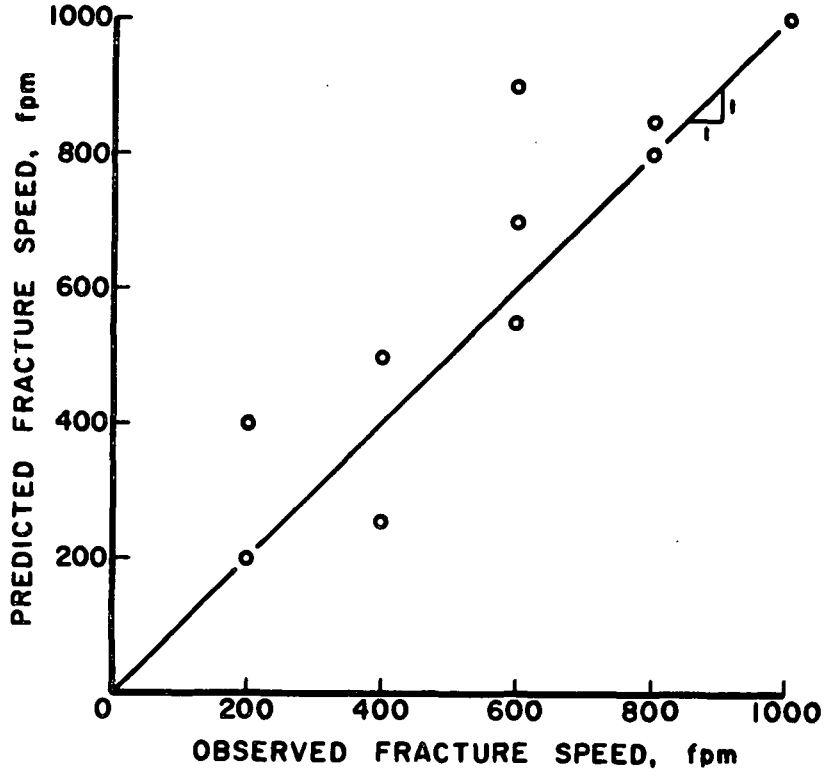

Figure 12. Predicted and observed fracture speeds are in good agreement.

High-lows are a manifestation of form instability, i.e. the medium attempts to relax back to a flat shape but in a non-uniform way. A portion of the strain applied during forming will be non-recoverable, the remaining portion will be recoverable and contribute to form changes. In general, both components should increase as the applied stress increases. This would explain why high-lows become more pronounced as speed increases. Also as the stresses increase toward fracture, local variations in stress and strain which are associated with paper machine formation should become more pronounced. These local variations in strain would manifest themselves as differences in recoverable and non-recoverable stretch (or TEA) in localized regions.

From this viewpoint high-low flute formation should depend on the applied stress intensity. The latter will depend on the material and process factors associated with the model.

In Fig. 13 the average high-lows greater than four mils for 26, 33 and 40-lb mediums are plotted vs. stress ratio. As expected the occurrence of high-lows decreases with medium basis weight at a given speed. When the stress ratios exceed about 0.85 the occurrence of high-lows increases rapidly. Thus mediums with combinations of friction tensile, stretch and thickness which yield lower stress ratios at a given speed should exhibit less high-lows.

For prediction purposes high-lows were correlated with the applied stress ratio in two ways. Initially two straight lines were fit to the data in Fig. 13, one line for stress ratios (R) less than 0.85 and a second line for ratios greater than 0.85. The resulting equations for high-lows > 4 mil were:

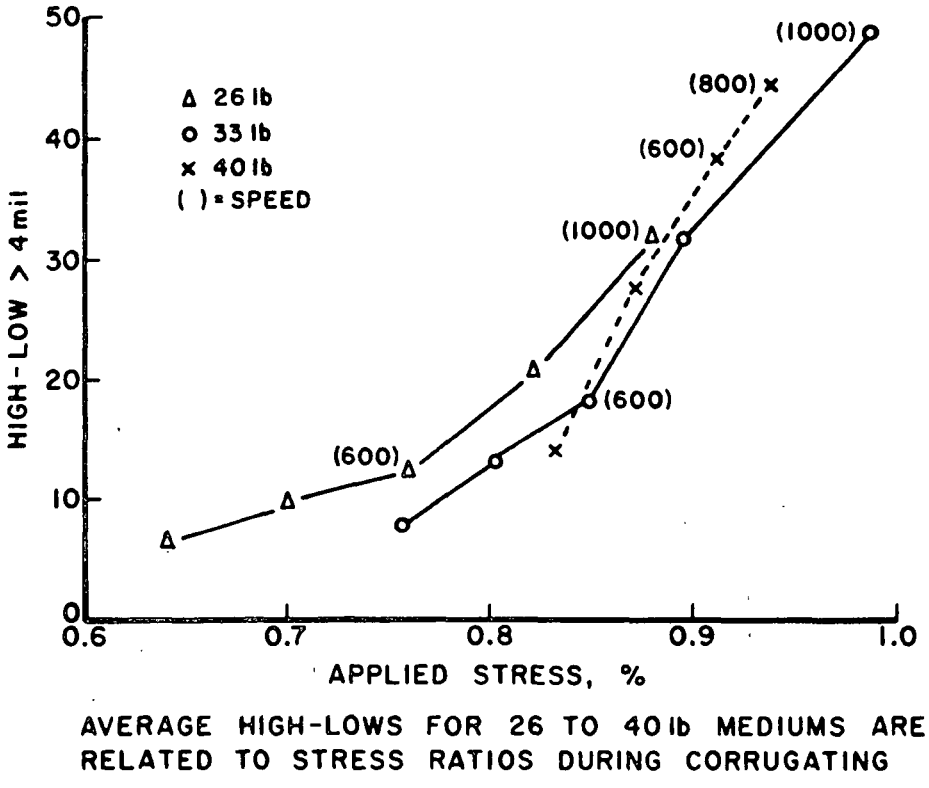

Figure 13. High-lows increase greatly as the stress ratio approaches unity and fracture occur.

Stress ratio < 0.85

$$\text{High-low, \%} = 56\ R - 31;\ r = 0.83 \quad (6)$$

Stress ratio > 0.85

$$\text{High-low, \%} = 215\ R - 160;\ r = 0.96 \quad (7)$$

Generally these equations give predictions which are in good agreement with results on our corrugator under normal steaming and tension conditions.

However, for sensitivity purposes analysis it appeared desirable to fit a curvilinear function to the data in Fig. 13. The following equation was obtained.

$$\text{High-low, \%} = -3.30 + 59.63\ R^5;\ r = 0.96 \quad (8)$$

Figure 14 illustrates that the power function fits the data quite well.

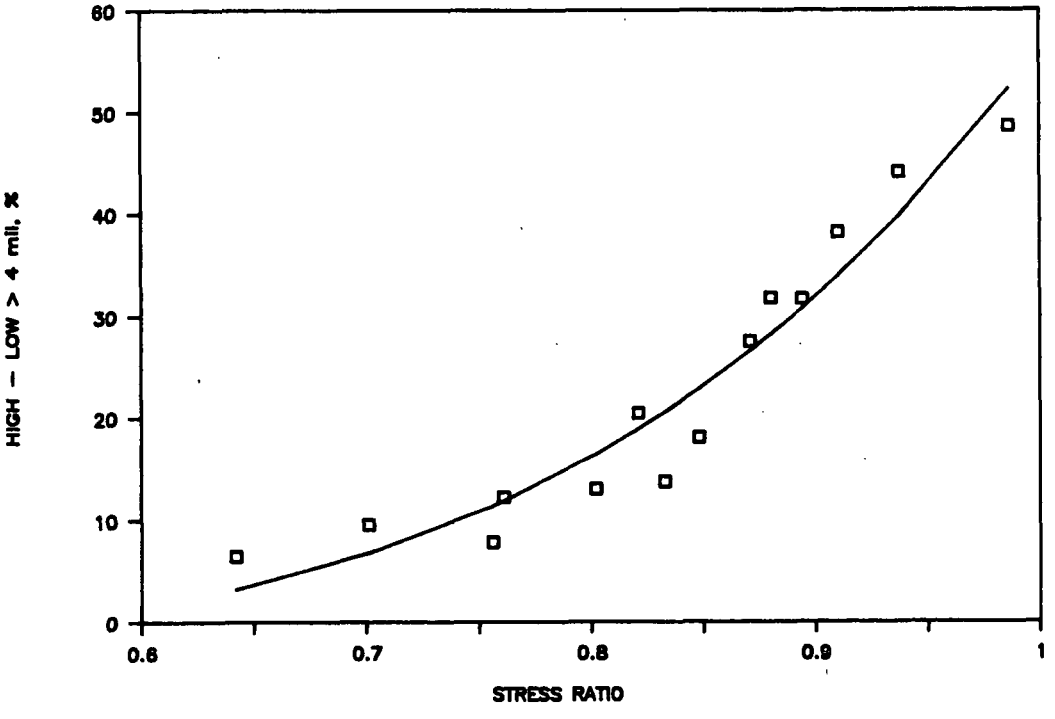

Figure 14. Curvilinear relationship between high-lows and the applied stress ratio. (High-low = -3.3 + 59.6 R^5, R = stress ratio.)

The effects of changes in medium properties on high-lows were estimated using Eq. 8 in conjunction with the runnability model equation. Each of the four properties was varied over a range of ±30% about the following average values.

1) Hot coefficient of friction, = 0.3
2) MD tensile strength, T_f = 40 lb/in.
3) MD stretch, = 1.3%
4) Thickness (IPC soft platen), t - 0.008 in.

Figure 15 shows how changes in test properties affects speed for a constant high-low percentage of 10%. The base medium with average properties had a speed of 800 fpm. Figure 15 indicates that at a constant high-low level, changes in stretch and thickness have the greatest effect on operating speed. Friction and tensile strength have significant but lesser effects than the other two properties.

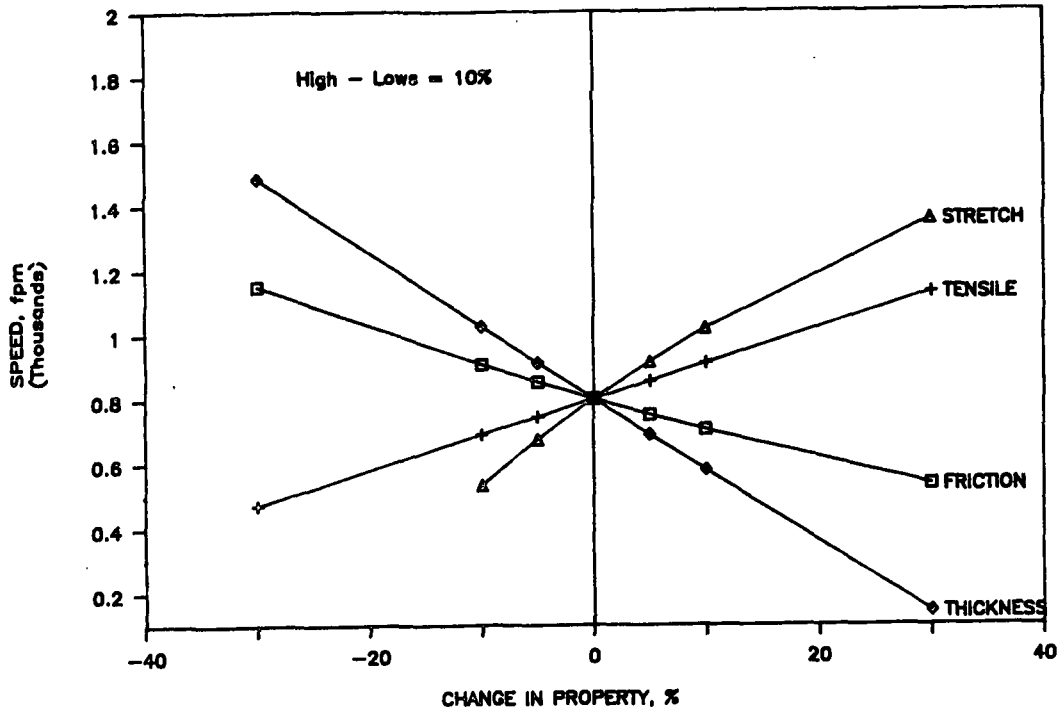

Figure 15. Effects of changes in medium properties on the speed at which high-lows equal 10%.

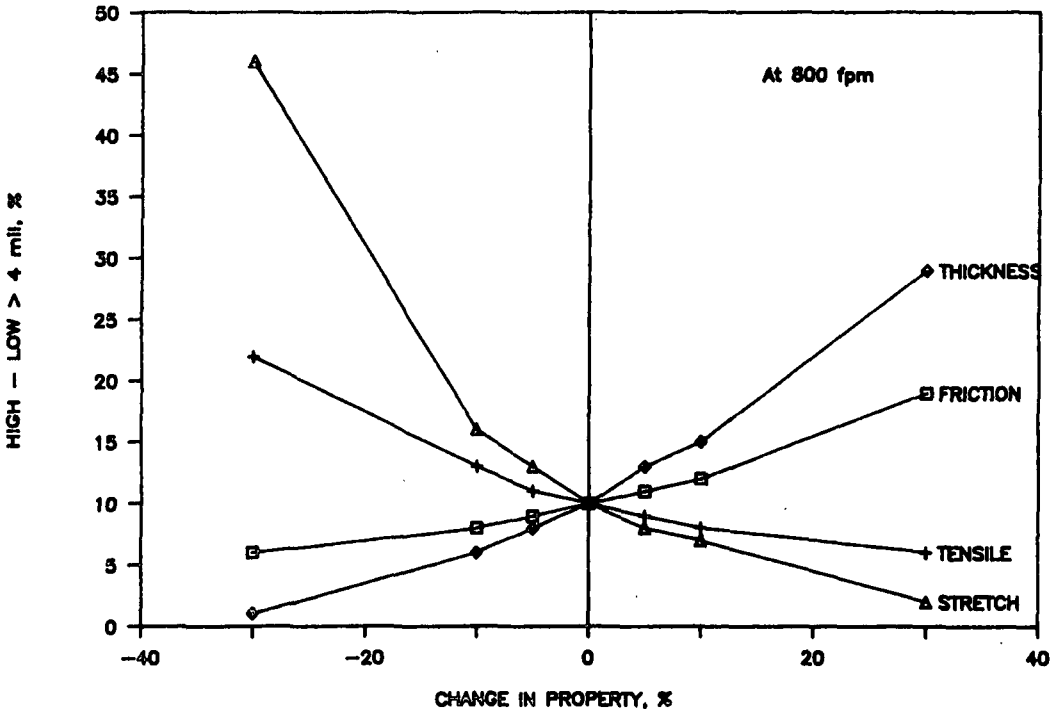

Figure 16. Effects of changes in medium properties in high-low magnitudes at a constant speed of 800 fpm.

We also estimated the effects of changes in properties on high-low magnitudes, keeping speed constant at 800 fpm (Fig. 16). The property rankings remain the same, i.e. stretch and thickness have somewhat larger effects than friction and tensile strength.

These results illustrate that papermaking factors which give higher stretch and tensile strength and lower friction and thickness will promote operation at higher speed with less high-lows. Many papermaking changes will affect more than one of these properties. Changes which simultaneously improve tensile and stretch and reduce friction or thickness will be particularly beneficial.

In addition we are developing further information on other flute profiles to test and expand our modeling. For this purpose flute profile casts have been obtained as follows:

1) A-flute,
2) B-flute,
3) special C-flute, larger diameter rolls.

The profile data is being analyzed to compare with our present Langston C-flute rolls.

Periodicities in High-low Flute Formation

Our goal is to identify periodicities in high-low flute formation using power spectral analysis techniques and to determine what machine elements cause these periodicities. Using a microcomputer statistical software package called Statgraphics, we obtained the periodogram shown in Fig. 17 of 1000 consecutive flute height differences produced at 1000 fpm on the corrugator. The

periodogram indicates that there are important cyclic components with periods near 5 - 6 flutes, 10 flutes, and others with longer periods. Similar patterns are obtained at other speeds. While we can see definite frequency components present, the software is limited in the amount of analysis it can perform. For this reason we switched to the more advanced BioMedical Computer Programs (BMDP) statistical software package on our mainframe computer. It is capable of univariate and bivariate spectral analysis using data tapering, spectral smoothing, and a feature which allows us to magnify a small section of the spectrum.

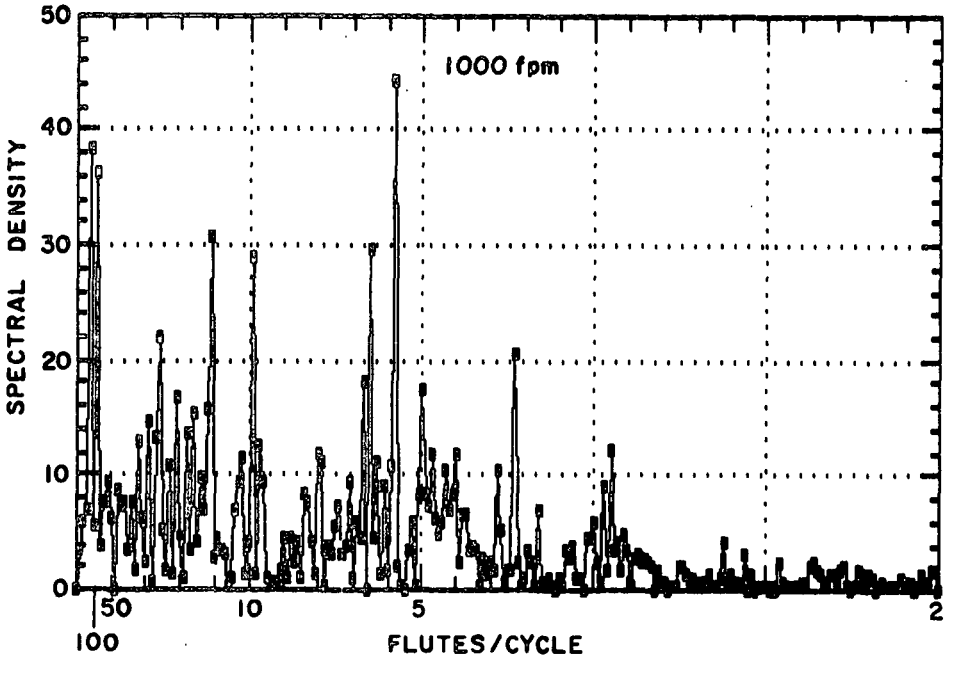

Figure 17. Power spectrum for flute height differences at 1000 fpm suggests that a number of long-period components may be present.

Confidence intervals, necessary for the interpretation of spectra, are calculated manually and depend on the following items: the amount of data tapering, the shape and width of the smoothing function, and the desired level of confidence. Data tapering refers to tapering both ends of the data sequence

to reduce errors in the spectra. We tapered 10% of each end of the sequence, or a total of p = 20% of the data. The correction due to tapering is

$$T = \frac{1}{2} \frac{128 - 93p}{(8 - 5p)^2} = 1.116 \quad (9)$$

To smooth the periodogram we used a cosine bell smoothing function encompassing 5 periodogram ordinates. The correction due to smoothing is

$$S = \sum_{i=1}^{5} c_i^2 = 0.3 \quad (10)$$

where the c_i's are the individual weights of the smoothing function. The equivalent degrees of freedom is then $\nu = 2/ST = 6$. Next, for a 90% confidence interval with 6 degrees of freedom, the Chi-Square (X^2_ν) distribution table gives the points 1.64 and 12.59. Finally, the confidence interval about a spectral estimate g(w) is given by log g(w) + log (ν/X^2_ν); log g(w) + 0.563 (upper limit) and log g(w) - 0.322 (lower limit). Note that to narrow the confidence interval it is necessary to increase the amount of smoothing, but this results in a loss of detail in the spectra.

Using the BMDP software on the same data we produced the power spectrum shown in Fig. 18, essentially a smoothed version of the periodogram in Fig. 17. Figure 18, plotted on a log scale, highlights the same frequency components but with less detail. Again the dominant peak is around 5-6 flutes/cycle. The area of the spectrum around this peak is shown enlarged in Fig. 19, complete with confidence bands. The single peak in Fig. 18 is now resolved into two closely spaced peaks. The confidence bands indicate only two peaks: the left peak cannot be resolved into smaller components. Analysis of a different section of the same board shows these peaks in the same area, though not as dominant. We plan on testing other samples from our pilot corrugator to

ensure that these peaks are real, then looking at the corrugator for the cause of these and other peaks.

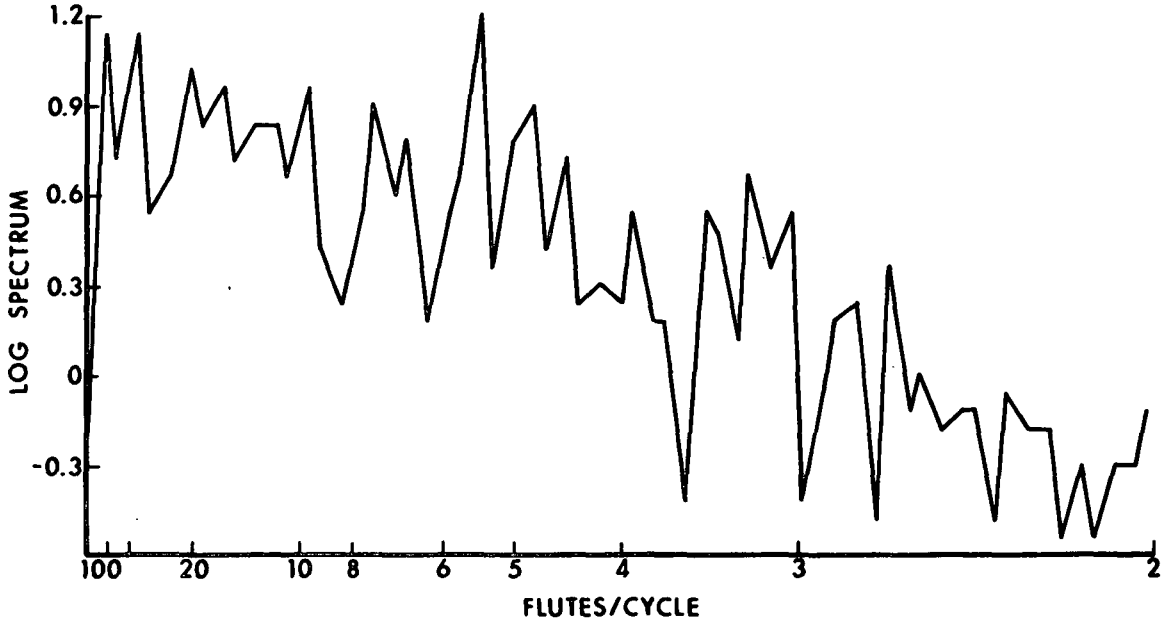

Figure 18. Power spectra of flute-bright-difference difference data of Fig. 1, using data tapering and spectral smoothing.

A full corrugator width sample of commercial single-face board produced at a speed of 600 fpm has been cut into 12-inch wide strips and corresponding groups of 1000 flutes have been measured on the middle, drive side, and operator side of the board. The analysis of this data is in process.

Our plan for future work includes the following:

1. Frequency spectra. In this phase we plan to identify the significant vibrational frequencies influencing high-lows using single-faced boards fabricated on our pilot corrugator and on commerical board. Among the variables to be studied are speed, liner and medium web tension, idler roll balance, parent roll condition, flute size and medium weight or type. Concurrently we are conducting a literature search on possible machine vibration causes.

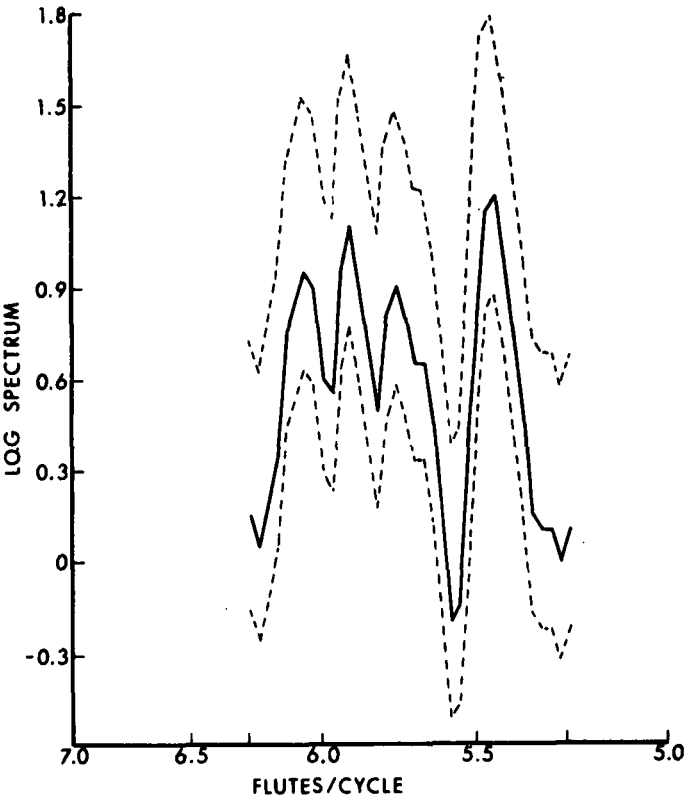

Figure 19. Detailed closeup of largest peak in Fig. 2 with 90% confidence limits (dashed lines).

2. Instrumentation. The second step will be to instrument the corrugator with vibration sensors to experimentally identify machine elements which cause high-lows.

Flat Crush Modeling

Corrugated board must be able to resist compressive forces in the thickness direction because if it is crushed during fabrication or end-use, box compressive strength will suffer. The maximum resistance of the fluted structure to thickness direction compression forces is termed flat crush strength. This is a commonly measured property of combined board. However the entire compression load vs. deformation curve can be of importance to performance

The medium is the primary element in corrugated board resisting compressive forces in the thickness direction. A typical flat crush load -

deflection curve for single-faced board is shown in Fig. 20. The curve normally has three distinct regions described as follows: 1) Initially the curve is nearly linear and the corrugated board behaves elastically. In this region the board resists compression forces with a relatively small decrease in thickness. The first yield point occurs as the top arch-shaped portion of the flute flattens. 2) The compression resistance increases to a second yield point associated with a flattening of the bottom flute tip which is adhered to the liner. 3) Further increases in compression resistance occur until the third yield point is reached. At the third yield point the straight-leg portion of the flute rotates to a vertical position. Final failure results from a buckling of the straight-leg portion of the flute.

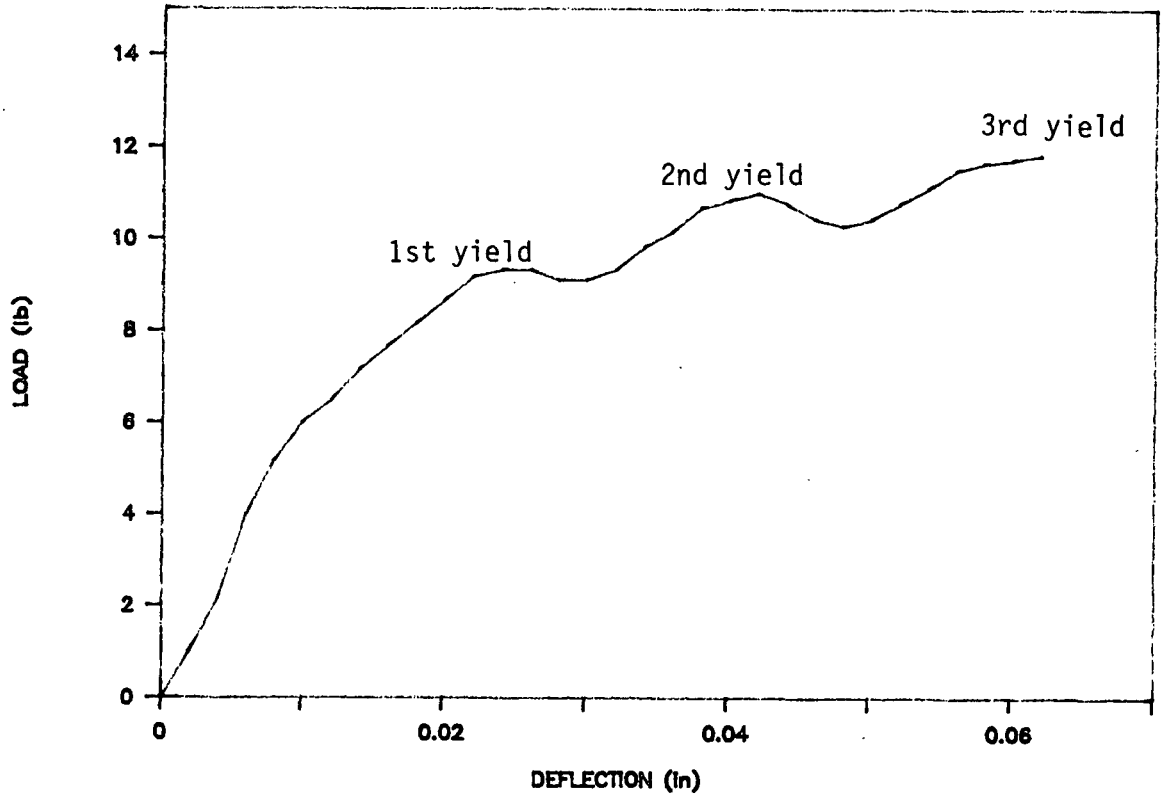

Figure 20. Typical flat crush load-deflection curve. (Load values equivalent to a 1-inch wide section of one C flute.)

In flat crush test results the maximum load applied to reach the third yield point portion of the load-deflection curve is normally reported. However,

the corrugated board undergoes irreversible damage before the maximum flat crush load is reached. If compression forces exceed the first yield point, permanent damage occurs to the board. Thus the initial portion of the curve is more critical than the maximum load in assessing whether a given amount of crushing will damage the board. The initial portion of the curve is presently under study using finite element analysis techniques.

The finite element method is a numerical analysis technique based on classical mechanics principles. The method assumes that a system can be modeled as an assembly of parts called elements. The elements are connected only at discrete points called nodes. A finite element structure resembles the actual structure. Using the finite element method, a structure of arbitrary geometry can be modeled with elements of various types, sizes and shapes. Arbitrary support conditions and loading may be applied to the structure. Composite structures made up of materials with different properties can also be modeled.

The most common finite element analysis assumes that displacement of the structure is extremely small and that the material is linearly elastic. A second class of finite element analysis involves non-linear behavior of a structure. Non-linear behavior may occur due to time-dependent and time-independent material non-linearity or because of large displacements which alter the shape of the structure so that applied load change their distribution or magnitude. Analysis of paper structures quickly enter the non-linear range from both large deflections and material reasons.

The accuracy of a finite element analysis depends on knowledge of the basic material properties. If the structure being modeled remains within the linear elastic range, only one set of elastic properties needs to be determined.

Non-linear analysis requires the knowledge of the entire stress-strain curve. Present knowledge of the stress-strain relationship for paper materials is quite limited, especially in compression and shear. Also, the state of stress in the fluted medium prior to flat crush loading is not well established. The elastic properties of the medium can be determined prior to corrugating. However, the corrugating operation which stretches and bends the medium in the machine direction and compresses portions in the thickness direction probably reduces the elastic properties. It is also likely that the elastic properties vary along the flute. The lack of extensive knowledge of the medium properties, both before and during flat crush loading make the finite element analysis extremely difficult.

The finite element modeling of flat crush has been conducted using a program called MSC/PAL. This program is capable of analyzing structures comprised of materials which remain in the linear elastic/small deflection range. An estimate of the non-linear effects due to large deflection can be obtained though an iterative loading approach. The MSC/PAL program recalculates the system equations after each load increment. However, the program was not capable of keeping track of the total nodal deflections or element forces. A scheme was developed in which the results from each iteration were imported into a spreadsheet program and added to previous results.

An initial flat crush finite element model comprised of 36 beam elements was developed as shown in Fig. 21. The fluted shaped was assumed to be sinusoidal. A 1-inch wide section of a C-type flute was used in the initial model. The flat crush test apparatus was modeled as a moveable steel beam above the flute and a fixed base below. The flute was loaded by moving the steel beam downward in increments of 0.002 inches. The load resistance of the fluted shape was determined from the reactions at the ends of the steel beam.

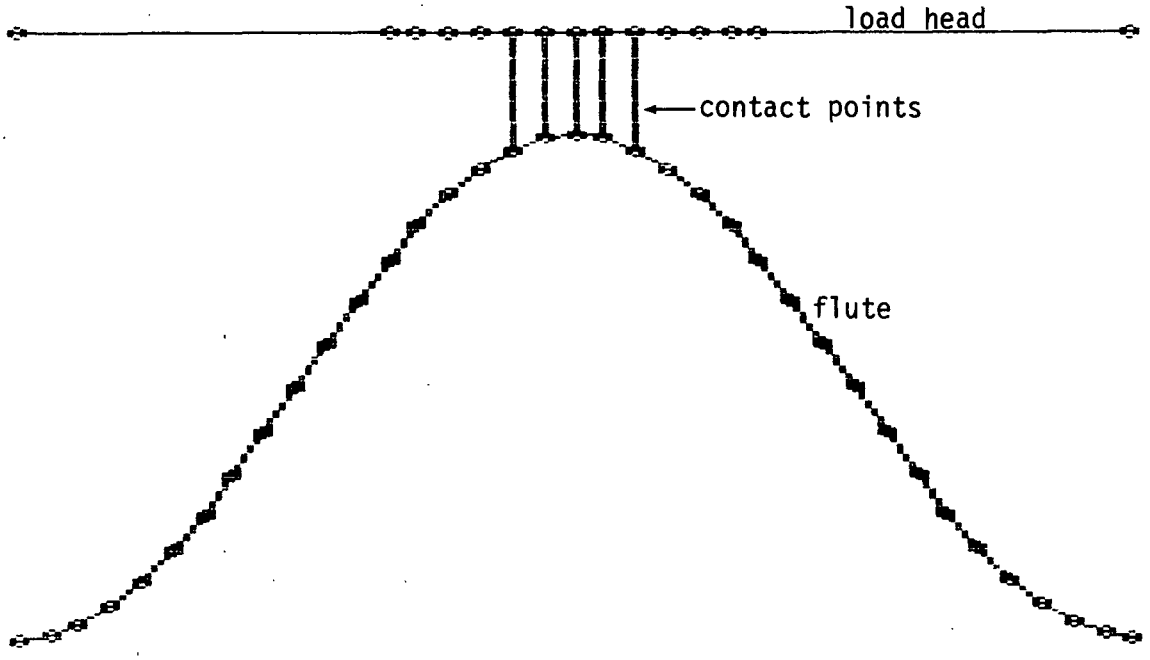

Figure 21. Flat crush finite element model.

Medium physical properties which affect the accuracy of the finite element model are as follows:

1) Compressive elastic modulus in the machine direction (E_{MD})

2) Out-of-plane shear modulus (G_{MD-ZD})

3) Thickness

The effect of changes in the three parameters were studied initially.

The first set of finite element analyses involved three different elastic modulus values. The shear modulus (G_{MD-ZD}) was set at 5×10^3 psi and the medium caliper at 0.010 inches. The results of the three runs are shown on Fig. 22. After a load-head deflection of 0.010 inches the following flat crush compression forces were obtained:

E_{MD} (psi)	Flat Crush Load (lb)
10×10^5	23.4
5×10^5	16.7
2.5×10^5	9.4

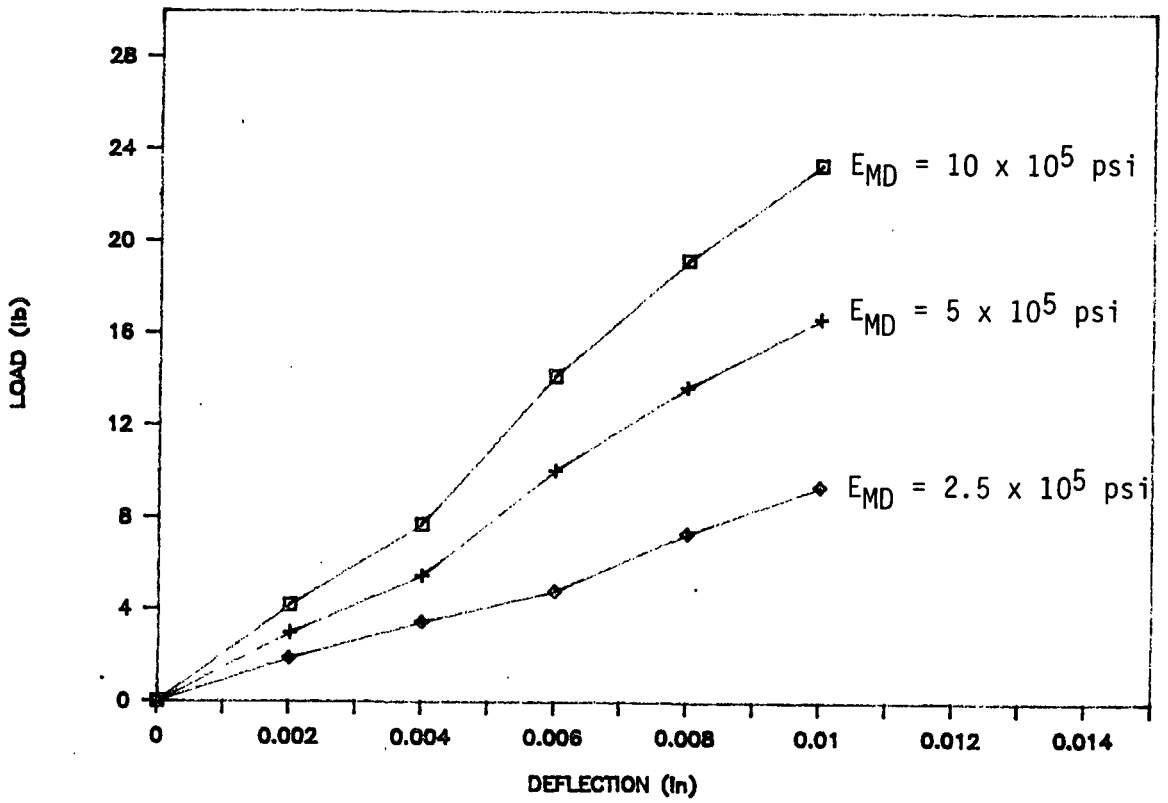

Figure 22. Load-deflection results from finite element analysis with 3 different values of E_{MD}.

A second set of runs was conducted to determine the effect of different shear modulus (G_{MD-ZD}) values on the flat crush load-deflection curve. Three different shear modulus values were used and also an additional case where the shear deflection was eliminated ($G_{MD-CD} = \infty$). The elastic modulus (E_{MD}) was set at 5×10^5 psi and the caliper at 0.010 inches. The load-deflection results from the finite element analysis are presented in Fig. 23. The results of the four runs are as follows:

G_{MD-ZD} (psi)	Flat Crush Load (lb)
∞	26.4
10×10^3	21.2
5×10^3	16.7
2.5×10^3	11.7

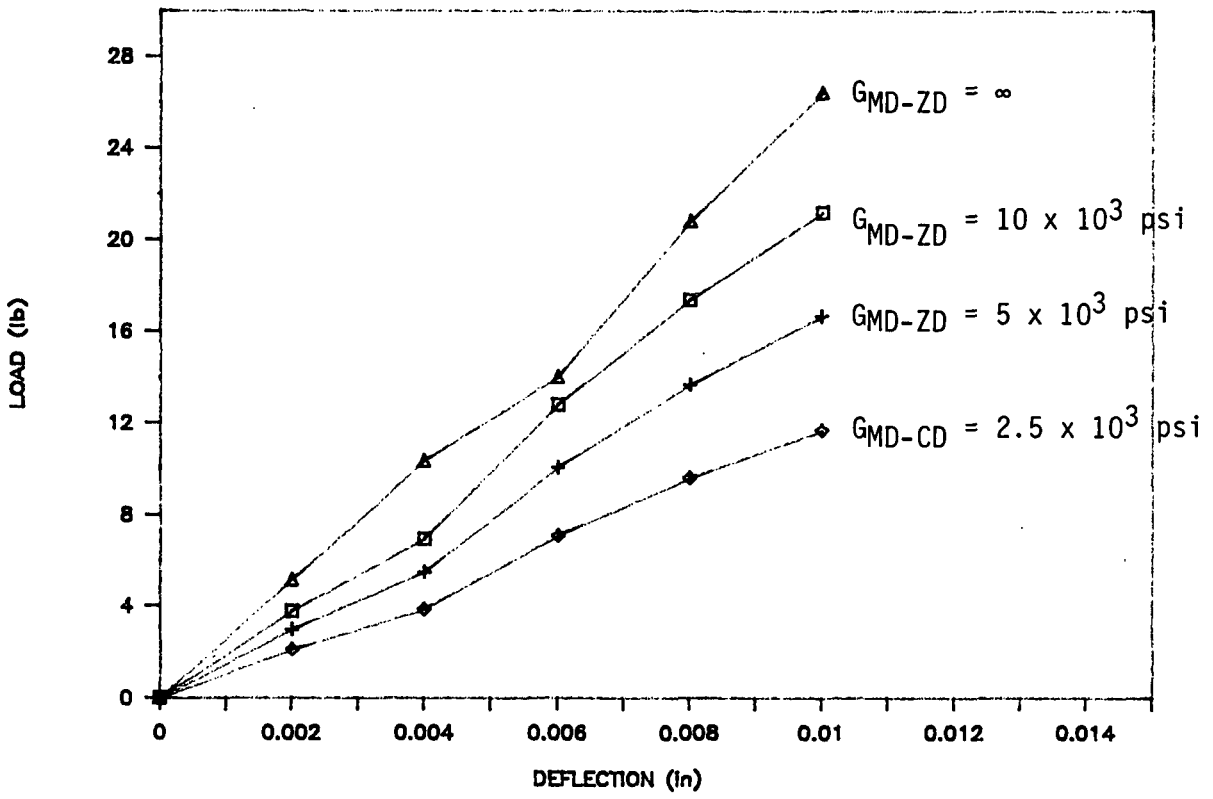

Figure 23. Load-deflection results from finite element analysis with 4 different values of G_{MD-ZD}.

A third set of finite element runs was conducted to assess the effect of caliper on the initial portion of the flat crush curve. Three calipers (0.012, 0.010, and 0.008 inches) where used in the analysis. The elastic modulus (E_{MD}) was set at 5 times 10^5 psi and the shear modulus (G_{MD-ZD}) set at 5×10^3 psi. The results of this analysis are plotted in Fig. 24. The results of the flat crush load after a 0.010 inch deflection are as follows:

Caliper (in.)	Flat Crush Load (lb)
0.012	23.9
0.010	16.7
0.008	10.6

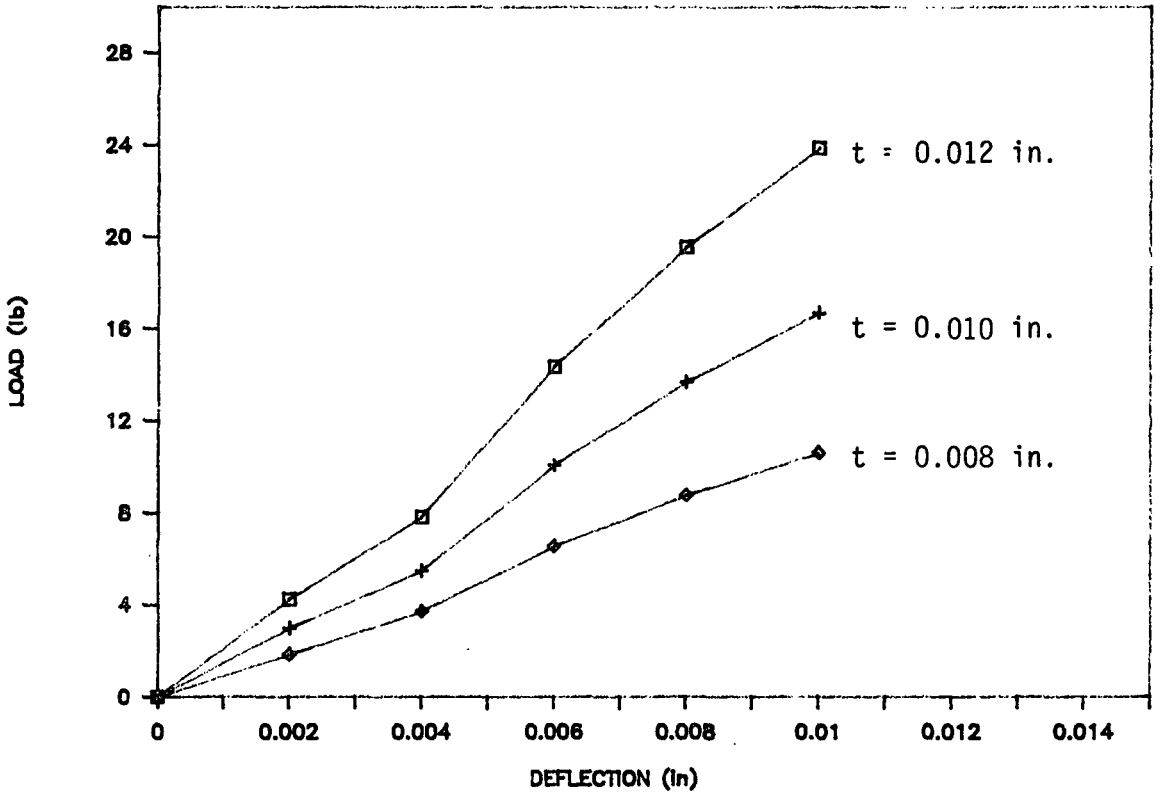

Figure 24. Load-deflection results from finite element analysis with 3 different values of caliper (t).

Significant changes were observed in the flat crush load resistance when different values of E_{MD}, G_{MD-ZD} and caliper were used in the finite element analysis. Knowledge of the level of these parameters will be necessary for an accurate analysis.

Presently an assessment of the elastic properties in the fluted medium is being conducted. The best estimates of the properties will be made and the finite element analysis compared with actual test data. Future work will

include an analysis of the effects of various flute geometries. Also, a search for a finite element program which would have the capacity for geometric and material non-linearities is being conducted. This may allow the analysis to proceed beyond the first yield portion of the flat crush curve.

THE INSTITUTE OF PAPER CHEMISTRY

Appleton, Wisconsin

Status Report

to the

PAPER PROPERTIES AND USES

PROJECT ADVISORY COMMITTEE

Project 3332

ON-LINE MEASUREMENT OF PAPER MECHANICAL PROPERTIES

September 10, 1986

PROJECT TITLE: On-Line Measurement of Paper Mechanical Properties

Date: 6/1/86
Budget: $100,000
Period ends: 6/30/87
Project No.: 3332

PROJECT STAFF: C. Habeger/G. Baum

PRIMARY AREA OF INDUSTRY NEED: Properties related to end uses

PROGRAM AREA: Control of manufacturing processes

PROGRAM GOAL: Develop ways to measure and control manufacturing processes

PROJECT OBJECTIVE:

To develop the capability to measure elastic parameters on a moving paper web. Current emphasis is on out-of-plane measurements.

PROJECT RATIONALE:

The ability to measure mechanical properties on the paper machine is valuable from several standpoints. It provides a potential means for control of process variables. It also provides a non-destructive way to assess product quality on a continuous basis.

RESULTS TO DATE:

Developed theory of ultrasound propagation in paper, and developed devices for measuring paper and board in-plane elastic parameters on-machine. Successfully tested devices in mill environments. Constructed and tested a version useful for light weight grades which is also self-calibrating. Developed cross correlation technique for use with in-plane velocity measurements, and initiated work relating to on-line measurements of z-direction properties. Developed a high-frequency, low impedance out-of-plane transducer using a plastic film piezo-electric material which is superior to commercial ceramic transducers. Developed superior in-plane "bender" transducer. Developed equipment for measuring moisture and temperature effects on paper elastic properties.

PLANNED ACTIVITY FOR THE PERIOD:

We intend to continue studies to explore the possibility of making out-of-plane ultrasonic measurements on a moving paper web. We will build high frequency, broad banded, and low impedance transducers that are mounted in wheels. We plan to look at both ceramic and plastic piezoelectric transducer constructions. Hardware and software for a high speed data acquisition system will be designed and built. On-line caliper measurements techniques will be investigated to be used with the ZD measurement system.

RELATED ACTIVITIES:

The proposal submitted to the Department of Energy to investigate possible control strategies on the paper machine and to develop a sensor to measure out-of-plane properties has been approved. Work should be underway by March, 1986.

STUDENT RELATED RESEARCH: Bernie Berger, Ph.D.-1988.

PROJECT SUMMARY

PROJECT NO. 3332: ON-LINE MEASUREMENT OF PAPER MECHANICAL PROPERTIES

PROJECT STAFF: C. C. Habeger, G. A. Baum September 10, 1986

PROGRAM GOAL: Develop ways to measure and control manufacturing processes.

PROJECT OBJECTIVE:

To develop the capability to measure elastic parameters on a moving paper web. Current emphasis is on out-of-plane measurements.

PROJECT RATIONALE, PREVIOUS ACTIVITY, AND PLANNED ACTIVITY FOR FISCAL 1986-87 are on the attached 1986-87 Project Form.

SUMMARY OF RESULTS LAST PERIOD (October 1985 - March 1985)

(1) New broadband plastic (PVDF) ZD transducers for use in wheels are being designed for use in an out-of-plane measurement on a moving paper web.

(2) Implementation of a high speed signal processing system for use with on-machine ZD measurements is underway using a LeCroy transient recorder and related equipment. The LeCroy system will be integrated with an IBM-XT.

(3) The above will also be incorporated into a laboratory system which will make ZD measurements at low web speeds.

(4) The study of transient effects in the mechanical properties vs. changing moisture content continues on both theoretical and experimental levels.

(5) The DOE project concerned with an in-plane and out-of-plane sensor for on-machine measurements and subsequent machine control is expected to be funded by April 1, 1986.

SUMMARY OF RESULTS THIS PERIOD: (April 1986 - September 1986)

(1) Several preliminary PVDF wheel transducers have been built and tested. Development of improved models continues.

(2) A high speed data acquisition system has been developed for ZD operation. This is described in the report for Project 3467 but most of the work is directly applicable to on-line measurements of ZD properties.

(3) A paper "On-line Estimates of Strength" (IPC Technical Paper Series 187) was presented at the 1986 Control Symposium in Stockholm and will be published in the proceedings of that meeting. It is attached as an Appendix.

(4) The DOE project, concerned with combined in-plane and out-of-plane measurements on the paper machine is expected to be initiated in the near future.

Status Report

ON-LINE MEASUREMENT OF PAPER MECHANICAL PROPERTIES

Project 3332

During the last six months we have focused on the development of ZD wheel transducer for eventual on-line application. These are modeled after the low-impedance, broadband, disc transducers which we recently built for laboratory testing.

Figure 1 is a drawing of a disc transducer. The active piezoelectric elements are polarized polyvinylidene fluoride (PVDF or Kynar) films. Compared to standard ceramic piezoelectrics, the films have a very low mechanical impedance (making them more efficient in coupling energy into paper) and a very low quality factor (making broadband transducer construction practical). A stack of four films, each 110 μm thick were used. The polarization direction of the two layers on the top is opposite the two on the bottom of the stack. The transducer electrode is the stack center and the two outer surfaces are ground. To reduce backside reflections (and increase bandwidth) one end of the stack is epoxied to an unpolarized Kynar disc. The front of the stack is a polystrene disc. It has low acoustic loss and improves the impedance match to the soft neoprene front face. The soft neoprene conforms to the sample surface giving good acoustic coupling and a resemble value for caliper. The thickness of the Kynar, polystyrene, and neoprene are all greater than one wavelength of sound at 1.0 MHz, the excitation frequency. This means that a single pulse can be isolated in the received signal and that this pulse has no interference from multiple reflections between transducer interfaces. Cross-correlation techniques can then be used to establish a delay time difference between a sample and a thin aluminum foil.

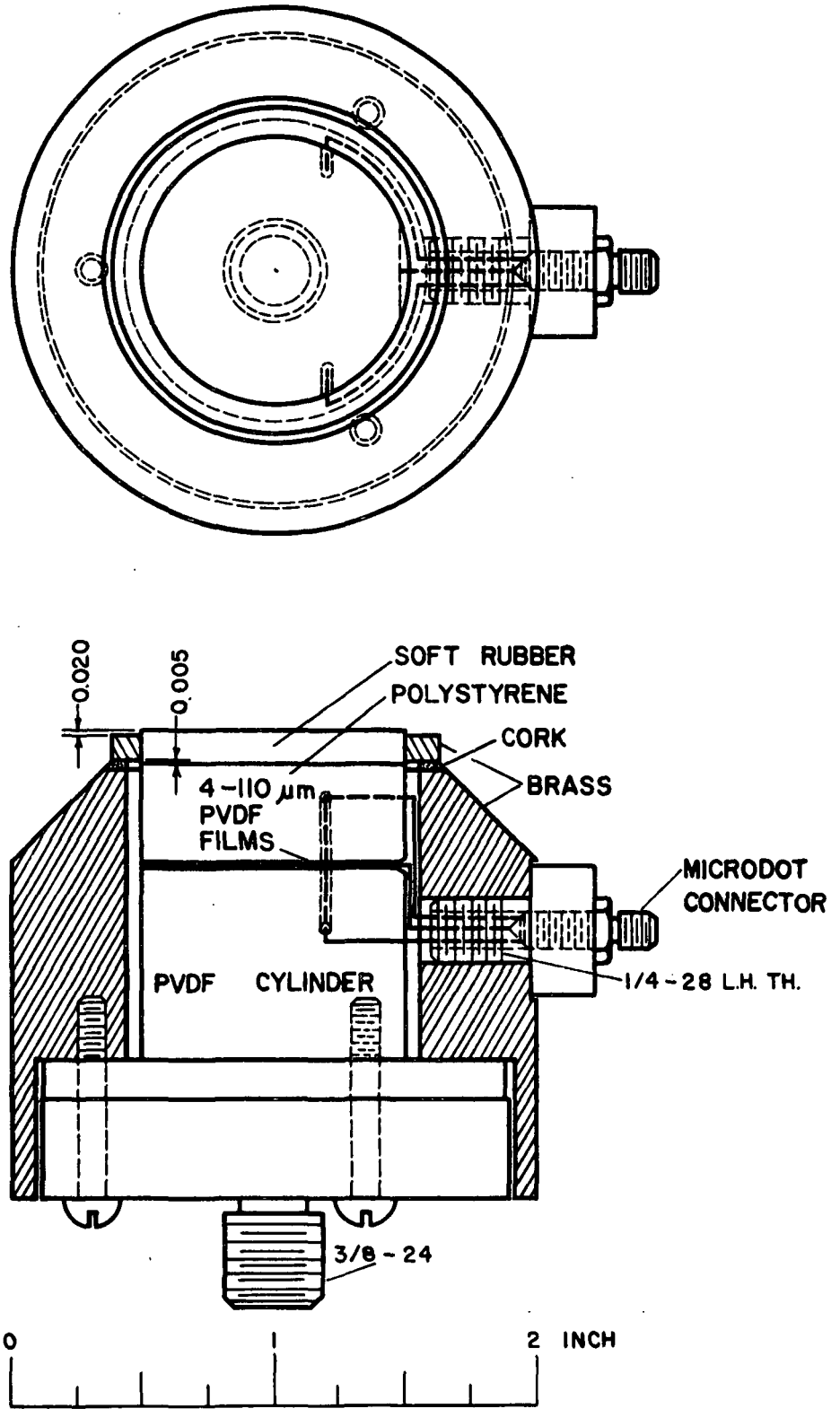

Figure 1. Kynar disc transducer.

The aim of the present work is to adapt this design to a wheel transducer. The wheels should be equally active over their circumference They will make rolling contact on opposite sides of the paper and transmit signal through the paper. Initially we hope to use this in the laboratory. Here, the wheels would be motor driven, and a sample would be fed through the nip. This would give us experience with dynamic caliper and delay time measurements, and perhaps provide a useful instrument for profiling soft caliper and ZD longitudinal velocity.

Our first attempt was an axially symmetric transducer with the same layering as the discs. A Kynar disc 2 3/8" in diameter and 1/2" thick is the base of the transducer. A small v-shaped notch was cut across the disc at one point on the circumference. The films were cut and conductive epoxy was used to secure them to the Kynar disc one at a time. To achieve the intimate contact necessary for acoustic coupling, the films are wrapped around the disc and placed in a circular vise made of teflon. The vise was tightened, extruding epoxy around the periphery. Pressure was maintained until the epoxy has cured. A polystyrene ring about 1/4" thick was epoxied to the outer flum. To get good contact, the ring which was undersized a few thousands of an inch, was heated and carefully placed around the core. As the ring contracted a bead of epoxy was extruded at the interface. After the final layer of conductive epoxy had cured, the edges of the layered film ring were machined to remove excess epoxy. Electrical contact to the ground planes at the inner and outer surfaces of the film ring was achieved as in the disc transducers. That is bare copper wire was inserted in a small hole drilled through the plastic to the surface. Conductive epoxy was forced into the holes making electrical contact when the curing load was applied. The electrical contact to the film center was made at the notch in

the inner Kynar wheel. A hole was drilled through the wheel to the notch. A copper wire was threaded through this hole. During film stack assembly the ends of the two inner films were bent to the sides of the notch while the two outer films were attached to the polystyrene ring. The end of the wire was fixed with conductive epoxy to the stack center in the notch gap. Finally a 1/8" thick layer of soft neoprene was glued to the rim of the wheel.

Transducers constructed in this manner were promising, but had some distinct limitations. Compared to the disc transducers, they had fair sensitivity, and they were slightly less broadbanded. We had hopes that the wheels would be of uniform sensitivity over their circumference; however, we encountered a factor of two variability. This was due not only to inhomogenities in the electrode contact regions, but also to nonuniform epoxy thickness at film interfaces. Perhaps the conductive epoxy is too viscous to form uniform film and perhaps uniform pressure is not applied by the ring clamp. At any rate it was unacceptable. Another problem resulted from the physical properties of the polystyrene. It is a brittle plastic with a lower thermal expansivity than the Kynar. This made fitting of the undersized, heated ring to the cool core difficult and stress fractures were often observed in the polystyrene after assembly. Any heating of the competed wheel increased the chance of fracture.

The second wheel design was modified to eliminate these shortcomings. We decided to sacrifice the better impedance match and transmission coefficient realized from the polystyrene ring and make both plastic pieces from Kynar. Kynar is very tough and has a large thermal expansivity. This allowed us to machine a smaller inner diameter to the outer ring and produce a tighter wheel. The tougher Kynar did not fracture and (as the design was all Kynar) stresses

were not increased by temperature changes. To achieve circumferential sensitivity uniformity, we made radical changes in the acoustic coupling of the films and in the method of electrode attachment. Instead of using conductive epoxy. We metered a thin film of silicone grease onto the film surface. Electrical contact was achieved by inserting copper wire flattened to a thickness of 10 μm in the appropriate interfaces. The ring clamp was unnecessary as coupling at all interfaces was established as the outer ring cooled. The main concern in this design is that the silicone does not interfere with electrical contact between wire and films.

The initial wheels built in this manner were circumferentially uniform. The improved acoustic coupling compensated for the poorer impedance match, and the sensitivity was approximately equal to that of the sensitive regions of the first wheels. Some contact difficulty was encountered on one of the leads. If necessary, we think we can assure good contact by applying a small amount of silver paint to the flattened electrode. We could also make electrical contact by leaving tabs on the films; however, this would be a less rugged design and increase changes on the films shorting.

From experience building disc transducers of different radii, we think that increasing wheel thickness would lead to a more broadbanded transducer. This would also increase sensitivity to what we feel is an acceptable level for practical transducers. Our present plan is to build the first serviceable transducers to a one-inch thickness and with silicone grease coupling. We are still experimenting to determine is film tabs are necessary.

APPENDIX

ON-LINE ESTIMATES OF STRENGTH

Gary A. Baum
Director,
Paper Materials Division

Charles C. Habeger, Jr.
Research Associate,
Paper Materials Division

The Institute of Paper Chemistry
P.O. 1039
Appleton, Wisconsin 54912

Virtually all paper products must meet mechanical property specifications. This usually requires destructive testing that cannot be performed on the paper machine. It is possible, however, to measure other properties on-line which are also indicators of product quality or can be correlated with the strength properties. The elastic stiffnesses of paper are such properties.

The elastic stiffnesses* of any material are the ratios of stress to strain in the limit of small strain. For a material which has three mutually perpendicular symmetry planes, such as paper, nine independent elastic parameters are required to describe the three dimensional elastic response. The elastic properties of paper are very sensitive to paper machine operating variables (1) and also can be correlated with many of the usual strength tests (2).

Seven of the nine elastic properties of paper can be routinely measured nondestructively using ultrasound velocity techniques (3). The velocity of sound in a material depends upon the elastic properties and the material density. Using the appropriate propagation directions and wave polarizations, mass specific elastic properties of paper can easily be determined by measured ultrasound velocities. The square of the velocity (for a particular mode) is an elastic property divided by density, i.e., a mass specific elastic stiffness. Details of such measurements may be found elsewhere (3). At present, only three of the seven elastic stiffnesses have been measured on a moving paper web. These are the longitudinal planar stiffnesses in the machine direction, MD, and cross machine direction, CD, C_{11} and C_{22}, respectively, and the shear modulus, C_{66}. Poisson's ratio, ν_{MD-CD}, could be determined from on-machine measurements, but this has not been done yet.

Our first on-line instrument, tested about six years ago (4), used piezoelectric transducers mounted inside of wheels which rolled along the paper (see Fig. 1). The piezoelectric element in each wheel was coupled to a section of the rim of the wheel by an aluminum "button". Three such wheels were used, one serving as a transmitter and two as receivers. The receivers were positioned relative to the transmitter, with one about 20 cm away in the MD and the other about 20 cm away in the CD. All three wheels were synchronized so the buttons contacted the web at the same time. At web contact, the transmitter was excited with a burst of sine waves, so that it vibrated and created a mechanical disturbance in the paper. This disturbance propagated away from the transmitter in all directions. The MD receiver detected the longitudinal displacements of the disturbance after a time delay Δt_L. This time was corrected for nonpaper delays (determined during calibration) and the longitudinal velocity in the MD, V_{L-MD}, was calculated as the transducer separation distance divided by the corrected delay time. The value of C_{11}/ρ is $(V_{L-MD})^2$. C_{11} is the elastic stiffness which is closely related to the MD Young's modulus, E_{MD}. E_{MD} is typically 95% of C_{11}. The CD receiver detected a shear component of the initial mechanical disturbance, allowing C_{66}/ρ (or G_{MD-CD}/ρ), the specific shear stiffness, to be determined. From the two measured specific elastic stiffnesses, it is possible to predict C_{22}/ρ (approximately E_{CD}/ρ) (5).

Another instrument, developed later for application to lower basis weight sheets, has its transducers mounted in a cylindrical shell. To avoid cross-talk through the cylinder, the transducers are acoustically isolated from the shell of the cylinder. Laboratory tests with the cylinder have been made on a variety of coated and uncoated paper grades. Basis weights from about 12 g/m^2, to 500 g/m^2, at web speeds up to 650 m/min, have been studied. The cylinder device has improved the performance by using two receivers for each velocity measurement. These are spaced at different distances from the transmitter so that two delay times are determined. The velocity is then computed by finding the ratio of the difference in separation distances between receivers and transmitter to the difference in delay times. This procedure reduces the sensitivity of the measurement to the environment or to coupling variables between the transducers and the web, and eliminates the need for separate calibration to eliminate nonpaper delay times.

Figure 2 shows a typical output obtained during an extended mill trial (6,7) using a wheel type system. The NOW column is updated approximately every 40 seconds. The first two entries in this column are C_{11}/ρ and C_{66}/ρ. These were corrected for moisture content and temperature variations in the web, using moisture and temperature measurements taken from the scanning (Measurex) sensor. The third and fourth entries are the first two, respectively, multiplied by the basis weight (BW) at the location of the sensor. Next is (C_{22}/ρ) BW, computed as noted above. Squareness is the ratio, C_{11}/C_{22}. CD ring crush, Mullen (bursting strength), and CD STFI compressive strength are estimated from the measured values using empirical relationships established in the laboratory on samples taken from many reel turn-ups. The two columns on the right are the running reel averages and twice their standard deviations.

All of the work described thus far has been carried out by The Institute of Paper Chemistry, in part sponsored by the Fourdrinier Kraft Board Group of the American Paper Institute. The technology described has been licensed to two instrument manfacturers, AccuRay and Measurex. Both companies have prototypes and are negotiating with customers. I will discuss them in alphabetical order.

The AccuRay device uses the roll approach with a transmitter and two receivers. The transducers may be oriented to measure either shear or longitudinal waves in the paper. That is, C_{66}/ρ and C_{22}/ρ are measured. C_{11}/ρ can be determined from the two measured values.

*We avoid the use of elastic "constant", because for paper these parameters are seldom constant because of their extreme sensitivity to machine variables.

Figure 3 shows the sensor mounted on a corrugating medium machine during a mill test.

The Measurex system, shown in Fig. 4, apparently measures E_{MD} and E_{CD}. This device has been tested in several mills, as outlined in Fig. 5, including linerboard, multiwall sack, specialty kraft, and newsprint grades. Fig. 6 shows CD profiles of MD tensile strength for weights of linerboard. The agreement between the laboratory results and the predictions from on-machine measurements is good. The decrease in mechanical properties at the edges of the profile is commonly observed, even though the basis weight and moisture profiles may be flat. Figure 7 is a plot of CD tensile, as measured in the laboratory, versus CD tensile as estimated from on-machine measurements. Figure 8 is a similar graph showing laboratory MD STFI compressive strength vs. values estimated from on-machine measurements. Figure 9 shows end of reel data for bursting strength in a newsprint grade. Note the change in Mullen with time (or reel number), and the good agreement between lab and on-machine estimates.

All of the systems discussed so far are capable of continuously monitoring product quality in real time. The operators can immediately determine when product quality fluctuates. At the same time, the effects of changes made on the machine on mechanical integrity can be rapidly monitored (6). In this way the paper machine can be "fine-tuned" to give optimum product quality at the lowest possible cost.

The next step will be to use the sensor in automatic process control. For this purpose the basic measured parameters, the elastic properties, should be used to control setpoints. An important question to ask is, "What should be controlled on the machine?". You know the old papermaker said "Paper is made in the beater.", but the old papermaker was not completely right. Today's grades, whether commodity or specialty grade, require careful adjustment of the machine. In addition to refining, paper machine variables which should be considered include jet-to-wire speed differentials, wet pressing pressure levels, wet straining, and drying restraints. Of course, we cannot neglect furnish variables, yield or bleaching levels, HW to SW ratios, etc. We are now in a position, however, to monitor the impact of these process variables on sheet properties and to provide real time input for process control.

If more than one elastic parameter is measured on the machine, it should be possible to separate the effects of some of the papermaking variables. Measurements of in-plane shear stiffness, C_{66} or G_{MD-CD}, are sensitive to changes in density due to refining or wet pressing. They are less sensitive to those factors which affect directionality, such as jet-to-wire speed differentials, wet straining, and drying restraints. C_{11} and C_{22} are sensitive to all of the above machine variables. C_{33}, on the other hand, is independent of fiber orientation effects, but is extremely sensitive to wet straining (or draws), and is considerably more sensitive to refining than either C_{11}, C_{22}, or C_{66}. Thus the three measurements, C_{11}, C_{66}, and C_{33} would allow three of the machine variables, viz., refining, fiber orientation, and wet straining (assuming other variables are not changing) to be monitored separately.

It is conceivable that these three paper machine variables could be controlled automatically. However, CD control of mechanical properties on the machine will be considerably more difficult than for the MD case. Remember that CD profiles of mechanical properties can vary even though basis weight and moisture content are constant across the web. Since CD variations are primarily caused by local changes in fiber orientation and nonuniform CD shrinkage, it will be a challenge to control them. Bell-shaped profiles, like those in Fig. 6, might be flattened by a spreader roll that resisted the normal CD shrinkage near the edges.

As on-machine measurements of elastic properties become more widespread and our experience grows, there will be more emphasis on their use as inputs for control purposes. Prior to that time, they will find immediate application as product quality monitors. Ultimately, these devices will lead to increases in machine productivity, more efficient use of raw materials and energy, and better product uniformity.

References

1. Fleischman, E. H., G. A. Baum, and C. C. Habeger, Tappi 65(10):115(1982).

2. Baum, G. A. "Paper testing and end use performance", Paper, March 19, 1984.

3. Mann, R. W., G. A. Baum, and C. C. Habeger, Tappi 62(8):115(1979).

4. Baum, G. A., and C. C. Habeger, Tappi 63(7): 63(1980).

5. Baum, G. A., D. G. Brennan, and C. C. Habeger, Tappi 64(8):97(1981).

6. Habeger, C. C., and G. A. Baum, Tappi 69(6):106 (1986).

7. Baum, G. A., and C. C. Habeger, "On-line Measurement of Paper Mechanical Properties", Project 2692-4 Progress Report One. Fourdrinier Kraft Board Group, The American Paper Institute, May 15, 1985.

Acknowledgements

We are indebted to AccuRay Corporation for providing Fig. 3 and to Measurex Corporation for providing Figs. 4-9.

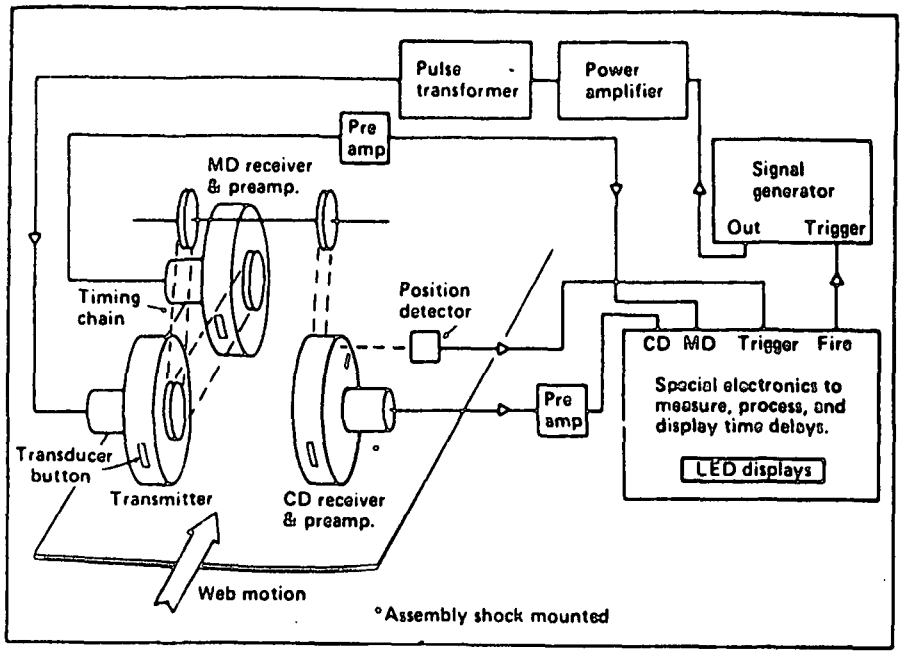

Figure 1. Schematic of the first on-line ultrasonic velocity gage.

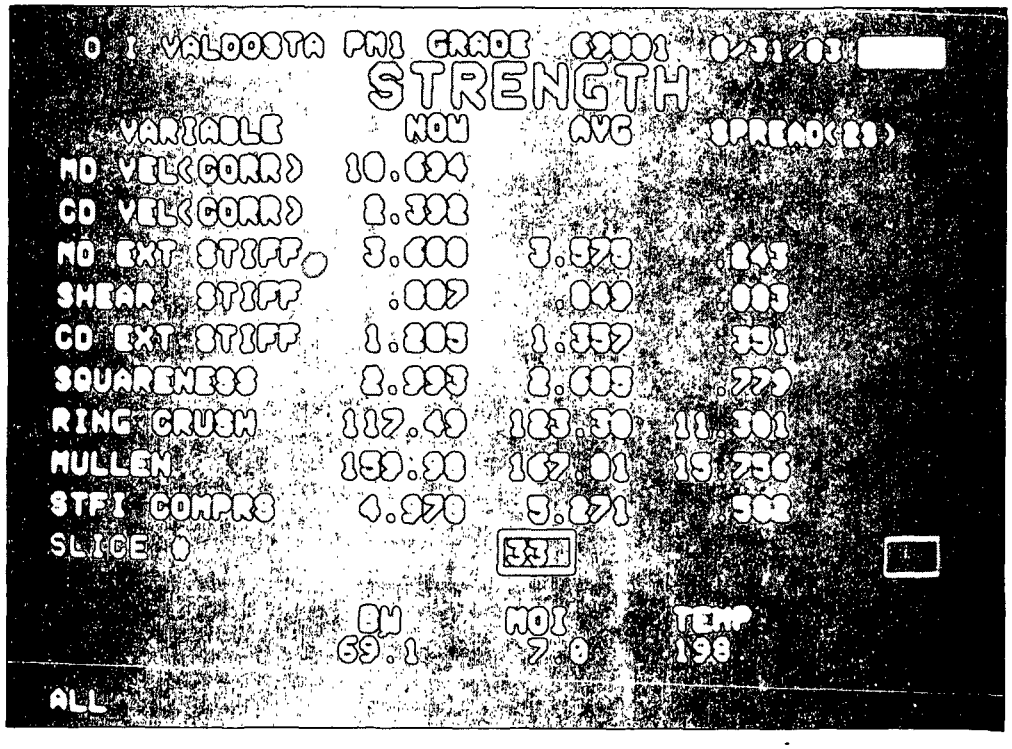

Figure 2. CRT display for IPC field trials.

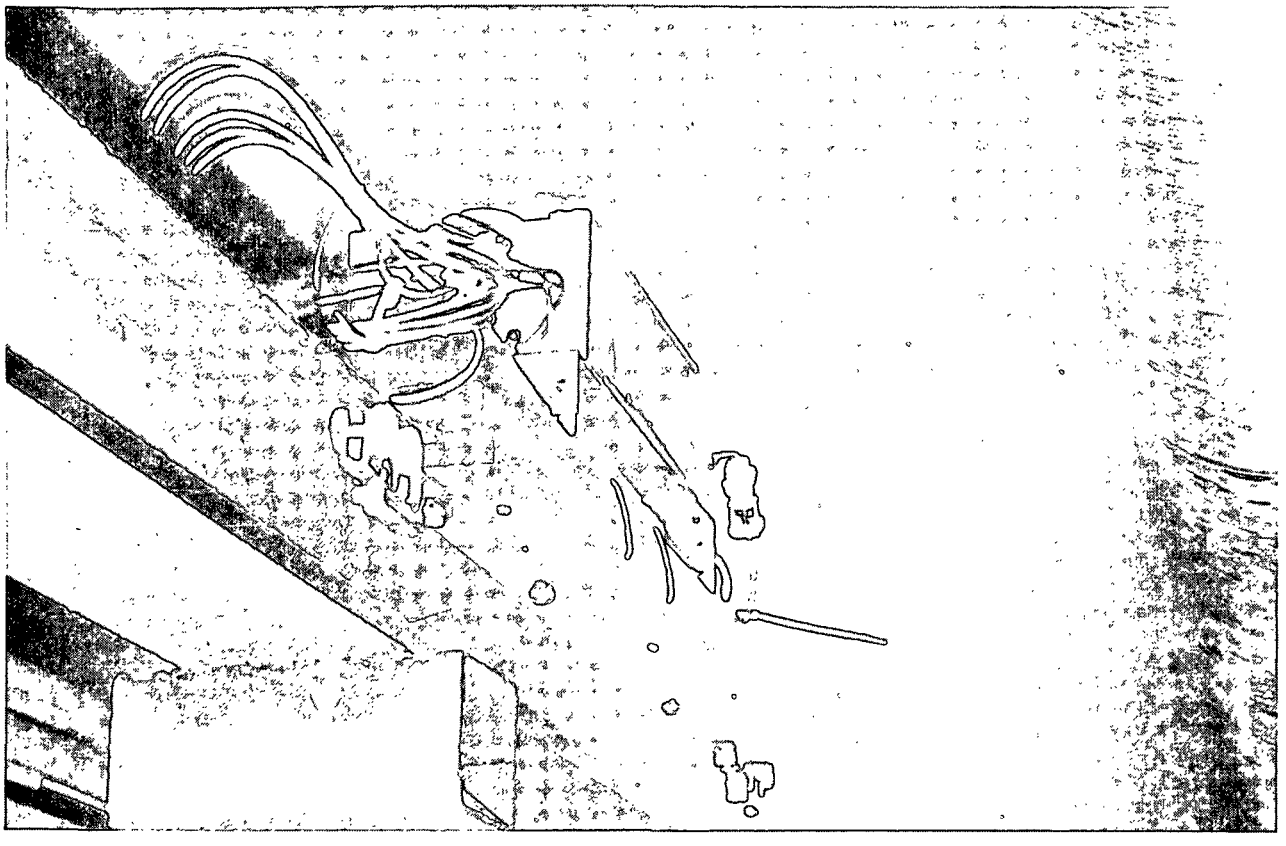

Figure 3. AccuRay prototype during field trials.

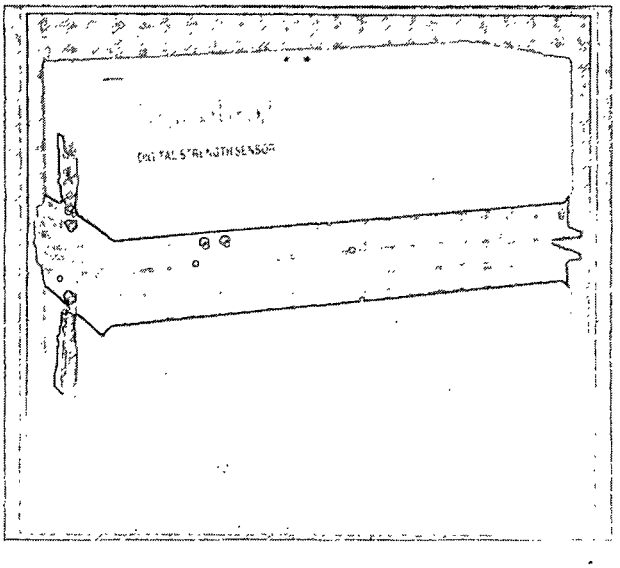

Figure 4. Measurex digital strength sensor.

DIGITAL STRENGTH SENSOR INSTALLATIONS

CUSTOMER	LOCATION	PRODUCTS	MEASUREMENTS
1. Longview Fibre	Longview, WA	26-33# Linerboard (127-161 GSM) 50-75# Multi-Wall Bag (81-122 GSM) 50-65# Gumming Paper (81-106 GSM) 21# Specialty Kraft (103 GSM)	Mullen, MD & CD Tensile, MD & CD STFI
2. U.S. Confidential	Confidential	26-61# Linerboard (127-298 GSM)	Mullen, MD & CD Tensile, MD & CD STFI
3. Consolidated Bathurst	Shawinigan, QUE	30# Newsprint (48 GSM)	Mullen, MD & CD Tensile, MD & CD TEA
4. Consolidated Bathurst	Shawinigan, QUE	30# Newsprint (48 GSM)	Mullen, MD & CD Tensile, MD & CD TEA

Figure 5. Measurex field trials.

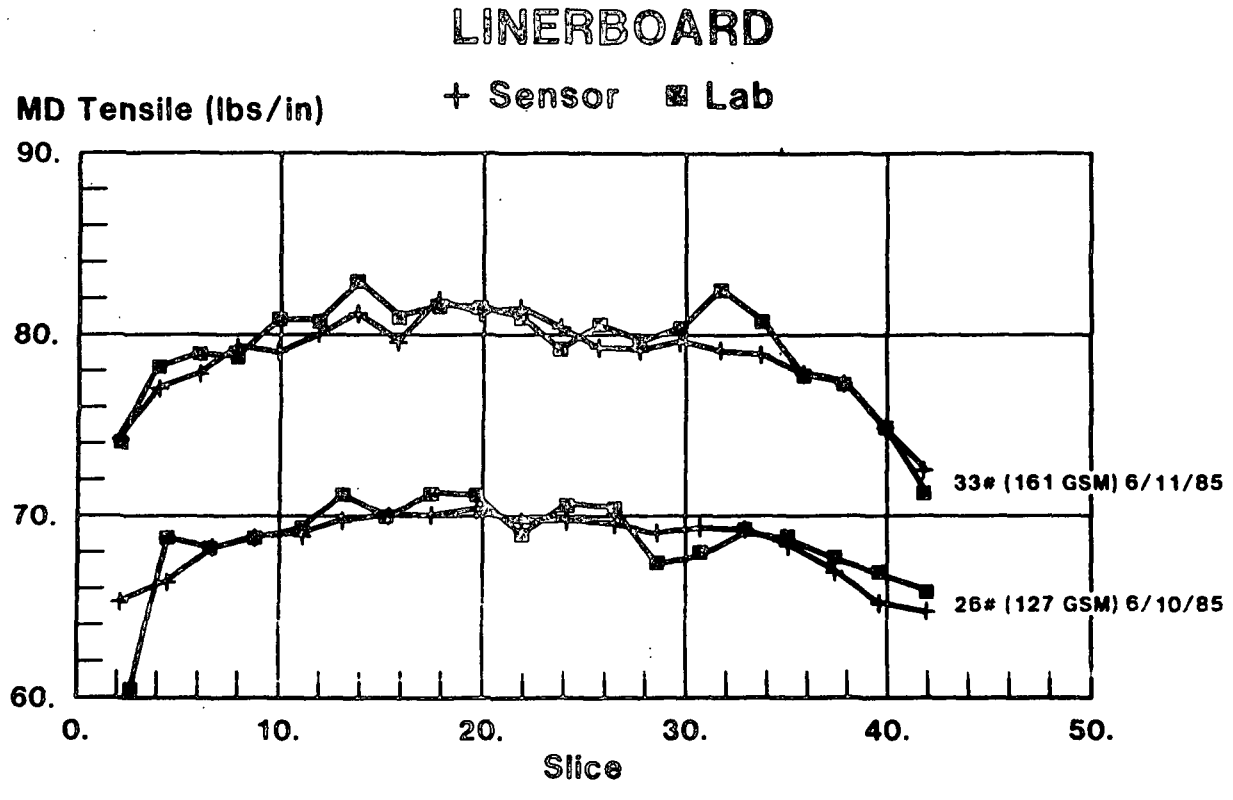

Figure 6. Linerboard CD profiles.

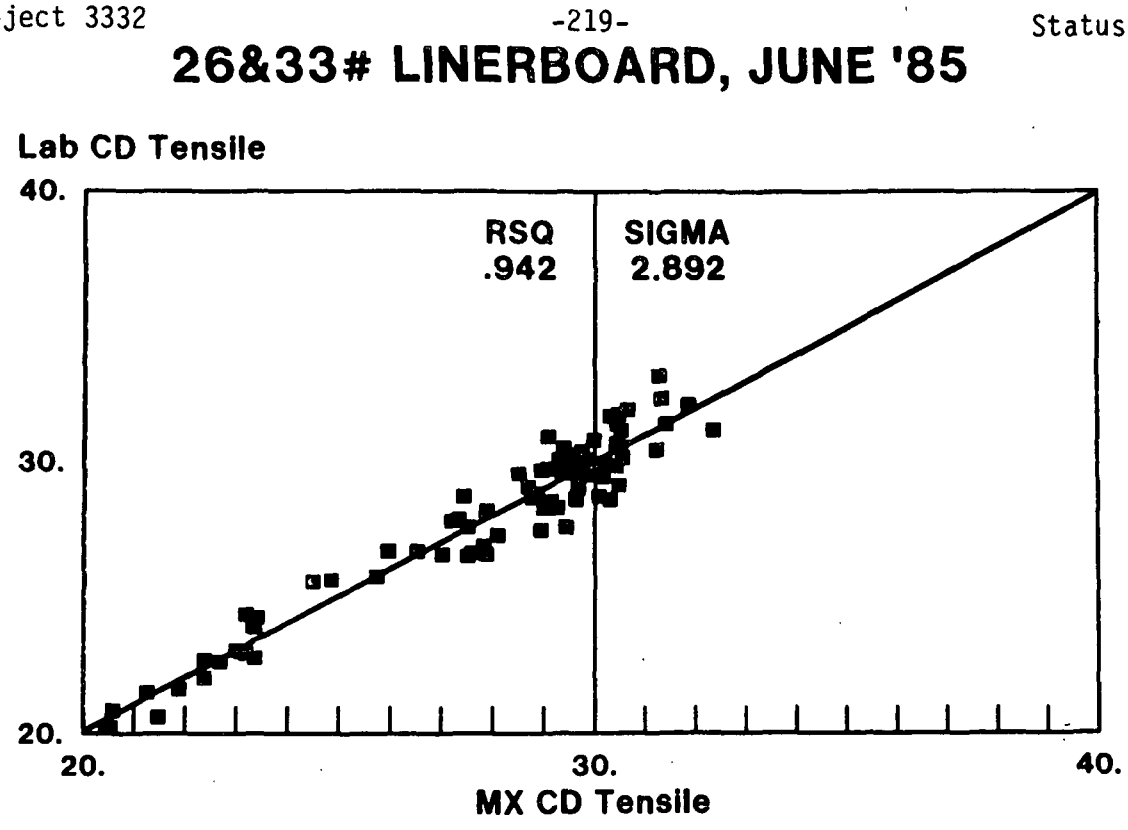

Figure 7. Comparison of laboratory measurements and on-machine estimates of CD tensile strength.

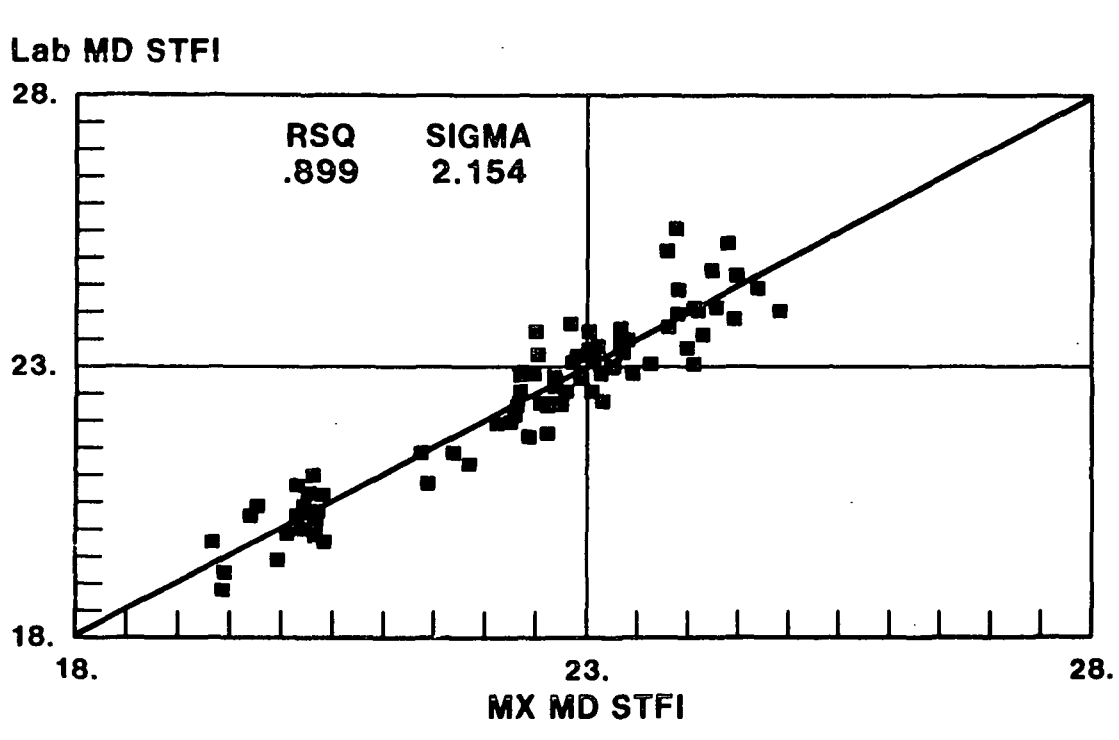

Figure 8. Comparison of laboratory measurements and on-machine estimates of STFI compressive strength in the MD.

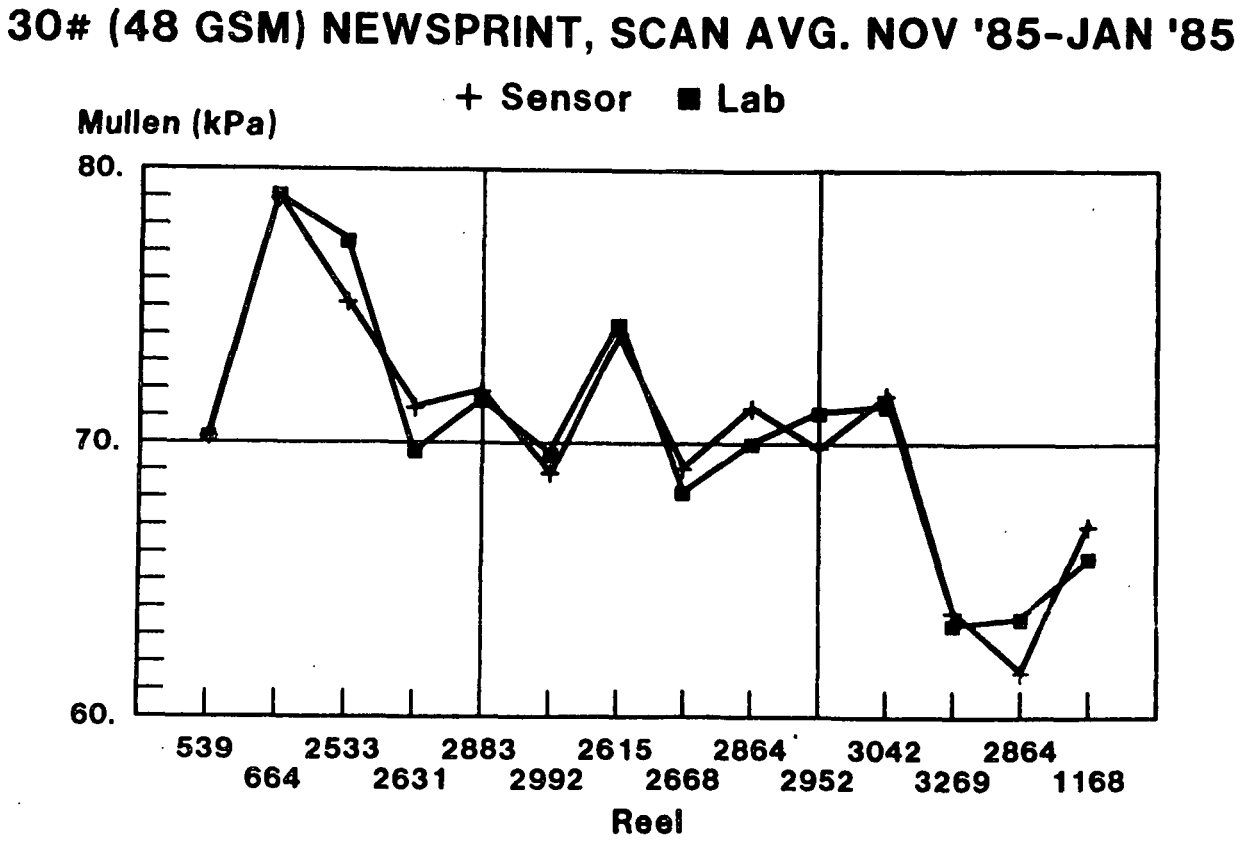

Figure 9. Changes in bursting strength plotted against reel number. Laboratory measurements compared with on-machine estimates.

GLOSSARY

GLOSSARY

acid-chlorite delignification	H_2O + glacial acetic acid and sodium chlorite.
breaking load	Force in grams to cause failure of a single fiber/fiber bond in the quasi-shear deformation geometry.
bond area	Optical contact area in the crossed fiber region determined by Page's vertical polarization technique.
bond strength	For single fiber/fiber bonds, the ratio of breaking load to bond area.
classified pulp	Pulp with fines removed.
CMC	Carboxymethyl cellulose.
CMCS	Carboxymethyl cornstarch.
CMPS	Carboxymethyl potato starch.
co-crosslinking	Bonding between fiber and added polymer.
combined out-of-plane stresses	Stresses which act together e.g. normal stress σ_{33}/ρ and shear stresses τ_{12}/ρ or τ_{23}/ρ.
Concora flat crush or CMT:	Refers to flat crush strength of medium fluted in the Concora fluter.
conversions	Pressure: $lbs/in^2 \times 6.895 \times 10^3$ = Pascals Pa.
	Specific elastic constants: E/ρ or c/ρ $(km/sec)^2 \times 10^3$ = Nm/g.
	Specific strength: σ/ρ or σ_c/ρ breaking length K.M. x 9.80 = Nm/g
corrugating medium	Paperboard used in forming the fluted portion of corrugated board.
diffuse reflectance	Reflectance in all directions.
distribution of mass density	Small scale basis weight or gramage variation.
DS	Degree of substitution - in this case, the number of carboxyl groups per monomer unit.
earlywood	Thin walled fibers.
ECT	Edge Crush Test, an edgewise compressive test made on combined board.

effective stiffness — The effective stiffness is the radius of a circle having the same area as that enclosed by a polar diagram.

engineering constants — The set of elastic constants including Young's moduli, shear moduli, and Poisson ratios.

elastic and engineering constants

C_{ij}: Elastic stiffnesses with units of force/area (GPa). i and j range from 1 to 6. For paper, considered to be an orthotropic material, the only non-zero elastic stiffnesses are C_{11}, C_{22}, C_{33}, C_{44}, C_{55}, C_{66}, C_{12}, C_{13}, and C_{23}.

E_i: Young's modulus in the i direction, where i is either 1, 2, or 3 (or x, y, or Z, or MD, CD, or ZD). E_i is considered an "engineering" elastic constant having stress units.

G_{ij}: Shear modulus in the ij plane. G is an engineering constant.

S_{ij}: Elastic compliances with units of inverse stress (area/force). In general, i and j range from 1 to 6. For paper the only possible values for i and j are those combinations listed under C_{ij}.

ν_{ij}: Poisson ratio in the ij plane. ν is an engineering constant. In a uniaxial stress test, it is the ratio of the lateral contraction to the axial extension. It is therefore unitless.

ε_i: Strain (dimensionless). i goes from 1 to 6.

σ_i: Stress (force/area). σ_i has a range from 1 to 6.

elastic stiffnesses — The C_{ij} defined above. The specific elastic stiffnesses are measured in ultrasonic tests.

extensional stiffness — The product of elastic stiffness and caliper or an engineering stiffness and caliper. In an Instron test, plotting load/width vs. elongation, it is the initial slope of the load-elongation curve.

flat crush: — The force required to crush the corrugations in a specimen of corrugated board.

FLER II — Fiber Load-Elongation Recorder, Model II.

flexural rigidity — A measure of bending stiffness, define as EI, where E is Young's modulus and I is the second moment of the cross-section.

fixed clamp — Specimen-holding clamp of FLER which remains fixed in position during a test.

FTIR analysis	Fourier transform infrared analysis.
geometric mean	The square root of the product of an MD and CD property, e.g. geometric mean stiffness would be $(C_{11}*C_{22})^{**1/2}$.
high-lows	In single faced combined board, a term denoting flutes that are greater than or less than the average. Most often a "high" is followed by a "low".
latewood	Thick walled fibers.
linerboard	Paperboard used for the flat facings of corrugated fiberboard.
medium	See corrugating medium.
MD, CD, ZD	Machine direction, cross machine direction, and thickness direction, respectively, in a commercial paper. Other notations used include x, y, and z or 1, 2, and 3.
MC	Moisture content, %.
mini-handsheets	19 mm diameter made in centrifuge tubes on a 200 mesh screen.
"moist"	Refers to papers conditioned at 91-93% RH usually resulting in a moisture content of 14-16%.
Moist compressive strength factor	The moist breaking length of the treated handsheet divided by that of the untreated control.
moist tensile factor	The moist breaking length of the treated handsheet divided by that of the untreated control.
movable clamp	Specimen-holding clamp of FLER to which a push or pull force is applied and which moves as the specimen deforms.
NSSC	Neutral sulfite semichemical medium.
PAA	Polyacrylic acid.
PAE	Polyamide polyamine epichlorohydrin.
PDDAC	Polydiallyldimethyl ammonium chloride.
PEI	Polyethyleneimine.
polar diagram	A polar graph plotting longitudinal or shear stiffness as a function of angle from the MD.
PSFA	Polystyrene sulfonic acid (sodium salt of).

PVDF	Polyvinylidene fluoride, a plastic material which can be polarized to be made piezoelectric.
ring crush	One of several methods in use for measuring the ultimate compressive strength of paperboard.
soft x-rays	Low energy x-rays.
specific elastic stiffnesses	Elastic stiffnesses divided by sheet density or C_{ij}/density. These are the quantities determined in ultrasonic measurements. They are equal to a square of a sound velocity.
STFI	Swedish Forest Products Laboratory
STFI short span compressive strength test	A test devised by the Swedish Forest Products Laboratory to measure the ultimate compressive strength of paperboard.
wet tensile factor	The wet breaking length of the treated handsheet divided by that of the untreated control.
Whitsitt/Habeger compressive strength correlation	$\sigma_c/\rho \propto E/\rho^{0.75} E_z/\rho^{0.25}$.
wood coupon	16 mm x 16 mm tangential wood sections.
WRV	Water retention value, the water remaining in fiber mat after centrifuging (gms of water/gm of fiber).